# UC Irvine

## UC Irvine Electronic Theses and Dissertations

### Title

Spatiotemporal Analysis of Particulate Matter Chemical Composition: Liquid Water Impacts over the United States

### Permalink

https://escholarship.org/uc/item/2d47550f

### Author

Christiansen, Amy Elizabeth

### Publication Date

2020

Peer reviewed|Thesis/dissertation

eScholarship.org Powered by the California Digital Library
University of California

UNIVERSITY OF CALIFORNIA,
IRVINE

# Spatiotemporal Analysis of Particulate Matter Chemical Composition: Liquid Water Impacts over the United States

DISSERTATION

submitted in partial satisfaction of the requirements
for the degree of

DOCTOR OF PHILOSOPHY

in Chemistry

by

Amy Elizabeth Christiansen

Dissertation Committee:
Associate Professor Ann Marie Carlton, Chair
Professor Sergey Nizkorodov
Professor James N. Smith

2020

Chapter 2 © 2019 American Chemical Society
Chapter 4 © 2020 American Chemical Society, unpublished work
All other materials © 2020 Amy Elizabeth Christiansen

# DEDICATION

To my parents, Grant and Mary,

who have encouraged me from the day I was born

and from whom the bad jokes never cease.

Thanks for putting up with me. I love you.

“Mama said:
‘Burn your biographies, rewrite your history, light up your wildest dreams!’
…
Mama said:
‘Don’t give up, it’s a little complicated.’”

---

“Well, this calls for a toast, so pour the champagne!”

---

-Panic! At The Disco

# TABLE OF CONTENTS


Page

LIST OF FIGURES v

LIST OF TABLES viii

ACKNOWLEDGMENTS ix

CURRICULUM VITAE xiii

ABSTRACT OF THE DISSERTATION xvi

CHAPTER 1: INTRODUCTION 1
1.1 Background 1
1.1.1 Atmospheric Aerosol 1
1.1.2 Inorganic Fraction of Aerosol 2
1.1.3 Organic Fraction of Aerosol 2
1.1.3.1 Long-term particulate OC measurement 4
1.1.4 Aerosol Liquid Water 6
1.1.4.1 Contribution to ALW from Organics 8
1.2 Motivation 8
1.2.1 Impacts on Health 8
1.2.2 Impacts on Radiation 9
1.3 Key Knowledge Gaps 13
1.4 Research Questions 14
1.5 Specific Aims 14
1.6 Structure of Dissertation 15

CHAPTER 2: AEROSOL OPTICAL THICKNESS: ORGANIC COMPOSITION, ASSOCIATED PARTICLE WATER, AND ALOFT EXTINCTION 17
2.1 Abstract 17
2.2 Introduction 18
2.3 Experimental 22
2.4 Results and Discussion 27
2.5 Conclusions 37

CHAPTER 3: DIFFERENCES IN FINE PARTICLE CHEMICAL COMPOSITION ON CLEAR AND CLOUDY DAYS 39
3.1 Abstract 39
3.2 Introduction 40
3.3 Data and Methods 43
3.4 Results and Discussion 48
3.4.1 Hygroscopicity and Chemical Composition 48
3.4.2 $PM_{2.5}$ Mass Concentrations 57

3.4.3 Case Study: The Mid South 58
3.5 Conclusions 60

CHAPTER 4: THE CHANGING NATURE OF ORGANIC CARBON OVER THE UNITED STATES 62
4.1 Abstract 62
4.2 Introduction 63
4.3 Materials and Methods 66
4.3.1 Surface Measurements and Estimates 66
4.3.2 GEOS-Chem Modeling 70
4.4 Results and Discussion 72

CHAPTER 5: SUMMARY AND FUTURE DIRECTIONS 81
5.1 Summary 81
5.1.1 Aerosol Optical Thickness: Organic Composition, Associated Particle Water, and Aloft Extinction 81
5.1.2 Differences in Fine Particle Chemical Composition on Clear and Cloudy Days 82
5.1.3 The Changing Nature of Organic Carbon over the United States 83
5.1.4 Key Knowledge Gaps Identified 84
5.2 Future Directions 85
5.2.1 Effects of Changing Salt Molality on Organic Partitioning into Aerosols and Cloud Droplets 85
5.2.2 Identifying the Role of Chemical Composition in Health Endpoints 89

REFERENCES 93

APPENDIX A: SUPPORTING INFORMATION FOR CHAPTER 2 119

APPENDIX B: SUPPORTING INFORMATION FOR CHAPTER 3 132

APPENDIX C: SUPPORTING INFORMATION FOR CHAPTER 4 149

APPENDIX D: R CODE FOR CHAPTER 2 163

APPENDIX E: R CODE FOR CHAPTER 3 201

APPENDIX F: R CODE FOR CHAPTER 4 241

# LIST OF FIGURES

Page

Figure 2.1 Seasonal average aerosol compositional mass by year integrated through the PBL for each region from 2007 to 2016 using PM measurements and estimated inorganic and organic water content. In each stacked bar, green corresponds to TOM, red corresponds to $SO_4^{2-}$, dark blue to $NO_3^-$, light blue to inorganic ALW, and turquoise to organic ALW. Seasonal average MODIS AOT (dotted yellow line) and PBL height (solid orange line) over time is overlaid for each region and season. 30

Figure 2.2 Monthly dry $PM_{2.5}$ and total (inorganic + organic) ALW mass integrated through the PBL and MODIS AOT from 2007 to 2016 for all focus sites in (a) Appalachia and (b) the CO Plateau summer (red) and winter (blue). Note that the axes are not equal between panels. The horizontal error bars indicate the potential range of water contributed by organics, with the left-hand side representing low $\kappa_{org}$ values (0.01-0.04) and right-hand side representing high $\kappa_{org}$ values (0.17-0.20). Note some horizontal bars are smaller than the marks. 31

Figure 2.3 Vertical profiles of 2007-2016 average total (inorganic + organic) water and CALIPSO-measured extinction coefficients for (a) Appalachia and (b) the CO Plateau. In both panels, red lines indicate summer ALW content, blue lines indicate winter ALW content, and brown lines indicate summertime (solid) and wintertime (dashed) CALIPSO-retrieved extinction at 532 nm. 32

Figure 2.4 Seasonal average OM mass from each OC fraction by year integrated from the surface through the PBL for each region from 2007 to 2016. In each stacked barchart, OM1 is the lightest green (bottom stack), and OM4 is the darkest green (top stack). 34

Figure 3.1 ALW mass concentrations are significantly different between Clear Sky and Cloudy time periods beyond what would arise from changes solely in meteorology (e.g., RH). Monthly median estimated ALW distributions at each IMPROVE monitor in the eastern US during Clear Sky times (yellow, Clear Sky scenario), Cloudy times (blue, Cloudy scenario), and Cloudy times employing Clear Sky particle chemical composition (green, Mixed scenario). The black asterisk in (a) indicates the only situation where Clear Sky and Cloudy scenarios differ significantly. The red asterisk in (a) indicates the only situation where the Cloudy and Mixed scenarios do not differ significantly. The midline in the box is the median, the box boundaries are the 25th and 75th percentiles, and the whiskers are the 10th and 90th percentiles. Potential outliers are not shown but are used in calculations. 49

Figure 3.2 Box plots of $PM_{2.5}$, RH, $NO_3^-$, and $SO_4^{2-}$ during clear sky times (yellow) and cloudy times (blue) across the eastern US. Note that potential outliers are not shown but are used in calculations. The width of the box plot is proportional to the number of observations. Red asterisks denote Cloudy and Clear Sky differences that are significant ($p<0.05$) by the Mann-Whitney U Test. 50

Figure 3.3 Maps of the difference in ALW mass concentration medians (Cloudy-Clear Sky) for all regions from 2010-2014 for (a) winter, (b) spring, (c) summer, and (d) fall. The color of the point corresponds to the magnitude of the difference. Triangles indicate that median differences are significant by the Mann-Whitney U Test. Note that the difference in wintertime medians for daily ALW concentrations in the Ohio River Valley (denoted with asterisk) is substantially larger than other regions (Cloudy median value is 4.6 μg $m^{-3}$ larger than Clear Sky). 52

Figure 3.4 Maps of the difference in $PM_{2.5}$ mass concentration medians (Cloudy-Clear Sky) for all regions from 2010-2014 for (a) winter, (b) spring, (c) summer, and (d) fall. The color of the point corresponds to the magnitude of the difference. Triangles indicate that median differences are significant by the Mann-Whitney U Test. 53

Figure 3.5 Maps of the difference in $SO_4^{2-}$ mass concentration medians (Cloudy-Clear Sky) for all regions from 2010-2014 for (a) winter, (b) spring, (c) summer, and (d) fall. The color of the point corresponds to the magnitude of the difference. Triangles indicate that median differences are significant by the Mann-Whitney U Test. 54

Figure 3.6 Maps of the difference in $NO_3^-$ mass concentration medians (Cloudy-Clear Sky) for all regions from 2010-2014 for (a) winter, (b) spring, (c) summer, and (d) fall. The color of the point corresponds to the magnitude of the difference. Triangles indicate that median differences are significant by the Mann-Whitney U Test. Note that the difference in medians for daily $NO_3^-$concentrations in winter for the Central Great Plains (denoted with asterisk) is substantially larger than other regions (Cloudy median value is 1.07 μg $m^{-3}$ larger than Clear Sky). 56

Figure 3.7 Maps of the difference in TOC mass concentration medians (Cloudy-Clear Sky) for all regions from 2010-2014 for (a) winter, (b) spring, (c) summer, and (d) fall. The color of the point corresponds to the magnitude of the difference. Triangles indicate that median differences are significant by the Mann-Whitney U Test. 57

Figure 3.8 Box plots of cloudy and clear sky distributions of $PM_{2.5}$ and chemical constituent mass concentrations (μg $m^{-3}$) and RH in the Mid South for each season from 2010-2014. The width of the box plot is proportional to the number of observations. Note that potential outliers are not shown but are used in calculations. Red asterisks denote Cloudy and Clear Sky differences that are significant ($p<0.05$) by the Mann-Whitney U Test. 59

Figure 4.1 Maps of relative decadal trends (2005-2015) in a) TOC, b) OC1, c) OC2, d) OC3, e) OC4, and f) PC mass concentrations for each chemical climatology region. Size corresponds to the magnitude of the percent change. Red indicates an increasing trend, blue indicates a decrease, a colored circle indicates that the increase or decrease is significant ($p<0.05$) by the Mann-Kendall test, and an unfilled circle indicates the change is insignificant. 73

Figure 4.2 Decadal trends across the CONUS for a) TOC, OC fraction, and PC mass concentrations and b) fractional contribution of OC fractions and PC to TOC. Error bars represent the standard error of the medians. 74

Figure 4.3 IMPROVE TOM and GEOS-Chem predictions of TOA across the CONUS from 2005-2015. Standard errors are represented via error bars. 76

Figure 4.4 Decadal decreases in ALW, GEOS-Chem predicted ISOAAQ, and OM2 for a) Appalachia and b) Great Basin. Note the y-axes are different between panels. 78

Figure 5.1 Annual average (a) $SO_4^{2-}$ molality, $NO_3^-$ molality, and ALW mass concentrations in the eastern US, and annual average (b) temperature and RH in the eastern US from 2005-2016. 85

# LIST OF TABLES

Page

Table 2.1 Correlation ($R^2$) and significance values from linear trend analyses for seasonal annual surface particle chemical component mass concentrations, MODIS AOT, CALIPSO AOT, and IMPROVE-estimated extinction over time from 2007 to 2016. Bolded values indicate significant correlations. 28

Table 3.1 Particle chemical constituent concentrations, meteorology, and growth factors during Cloudy (Cl) and Clear Sky (CS) times in the Mid South. 59

# ACKNOWLEDGMENTS

As I prepare this dissertation in isolation due to COVID-19 pandemic, I have had the time and space to reflect without distraction on the people who have helped me on my journey to my PhD. If someone had told me everything I would do and experience during my PhD when I applied, I would never have believed them. I never anticipated that I would start at one institution and end at another, or that I would meet so many incredible people along the way. I can confidently say that I would not have been able to do this without everyone around me. This has especially been true in these past couple months. I am incredibly grateful and forever indebted to so many people who have encouraged and believed in me. It is emotionally difficult to defend without having everyone here in person as I have been imagining throughout my entire graduate career, but I know that it is the everyday encouragement that has made the difference all along.

First and foremost, I would like to thank Ann Marie Carlton, my advisor and friend, who has never stopped believing in me once these past five years. When I started graduate school at Rutgers University in New Jersey, I never anticipated being asked by my advisor to move across the country and complete graduate school at a different institution. When Ann Marie asked me to move with her to California, I had no idea what to say. I was filled with so many doubts, but Ann Marie never was. Even though I had only completed one year of graduate school and still had so much to learn, she never doubted my ability to be successful. I decided to accept her offer after I realized that I had a rare and special advisor, one who was not going to give up on me. I am so very glad I made that move almost four years ago now. I am incredibly grateful for her guidance and patience throughout my graduate career. Ann Marie, thank you for learning how to “read”

me and how to interpret my odd Midwestern communication tendencies. I had no idea at the time what a good choice in an advisor I had made back when I started graduate school. I admire you so much, and I look forward to staying in touch.

Of course, I am also incredibly grateful to the members of my lab – past, present, and honorary – who have encouraged me along the way. From reading over my writing to reminding me that I am capable, this experience would have been much harder and sadder without them. Thank you all for being a captive audience as I have prepared for my defense. I am grateful to my lab members at Rutgers, especially Khoi Nguyen for all the help she gave me as I was starting out. I must also thank Madi Flesch and Mooji Boldbaatar for being great sounding boards and providing me with delicious snacks. I'm going to miss your baking almost as much I'll miss you. I am also grateful to Jonathon Babila for asking me critical science questions and keeping me well-informed on the political state of America. Of course, this shoutout would not be complete without including Alicia Hoffman and Cynthia Wong, our honorary lab members, for providing valuable outside input and reminding me that life is bigger than the lab.

I also thank my collaborators, Virendra Ghate, Will Porter, Barron Henderson, and Chris Hennigan for their incredible insights and help. I would never have been able to think as deeply and critically about satellites, atmospheric models, and experiments without their assistance. I am grateful for their patience and scientific expertise. Chris, it was such an awesome experience to be able to do Journal Club with you and to perform experiments in your lab.

I would also like to thank Sergey Nizkorodov and Jim Smith, both of whom served on my advancement committee and are now on my dissertation committee. They have both been very supportive of me during my time at UCI. Jim, thank you for being so welcoming to me when I first arrived, giving me a space to exist while my office was being constructed, and serving as a mentor during that time. It was fun to TA Kinetics for you as well. Sergey, thank you for being supportive of my teaching ambitions and setting me up with Chem 1X during Fall 2019. I learned so much from that experience and am grateful that you gave me that opportunity.

I am also grateful to the entire Smith group, who took me into their lab space when I had just arrived here from Rutgers. They were so welcoming while I transitioned to life at UCI, and I am happy and lucky to be able to call them my friends. Sabrina, our coffee support chats, your constant friendship, and your unmatched heroism have kept me going these past few years.

I am very grateful for my family and friends who have supported me along the way. I am deeply in debt to my parents, who have always supported me regardless of what I do, even though it meant helping me move across the country one and a half times. I am thankful for the time I get to spend with them and the time they take to visit me. Mom and Dad, it hasn't been easy to be so far apart, but I am grateful that you have been so supportive of my goals and ambitions. You have been behind me 100% for as long as I can remember, and I will always be grateful to you for your support and encouragement. I miss you both every day and can't wait until you are able to come visit me in my new stomping grounds in Montana.

I am so incredibly grateful for Brian Rosney and his outstanding support and patience during my graduate career. Thank you for always listening to me and being understanding. It's been difficult these past few months between my dissertation and world events, and your FaceTimes and Snapchats of cats have been instrumental in the completion of my degree. Thank you for your flexibility and for supporting me, even when it took me away for weeks at a time. And most of all, thank you for being open-minded and making the move with me to Montana. It's hard to leave everything behind (trust me, I know!), but I'm so excited to start our lives together.

I also acknowledge my funding sources. Chapter 2 was supported by NSF Grants AGS-1242155 and AGS-1445831. Chapter 3 was supported by NSF Grant AGS-1242155 and NASA Grant #80NSSC19K0987. Chapter 4 was supported by NOAA Grant #17OAR4310103 and NSF Grant #171945.

Lastly, I thank the American Chemical Society for permission to reuse my published and submitted work in my dissertation. Chapter 2 was originally published in *ACS Earth and Space Chemistry* in February 2019, and Chapter 4 has been submitted to *Environmental Science and Technology* for publication.

# CURRICULUM VITAE

**Amy Elizabeth Christiansen**

## *EDUCATION*

Ph.D. **Chemistry, University of California, Irvine, Irvine, CA** *June 2020*
Thesis Advisor: Dr. Annmarie Carlton
Program: Chemistry, Overall GPA: 3.99, Advanced to Candidacy 04/04/2018
**Atmospheric Science, Rutgers University, New Brunswick, NJ** *September 2015 –*
Thesis Advisor: Dr. Annmarie Carlton *August 2016*
Program: Atmospheric Science, Overall GPA: 4.0

B.A. **Chemistry & Environmental Studies, Gustavus Adolphus College, St. Peter, MN**
Overall GPA: 3.95, *Summa cum laude* *May 2015*

## *PUBLICATIONS*

*In review*. **Christiansen, A.E.**; Carlton, A.G.; Henderson, B.H.: Differences in Fine Particle Chemical Composition on Clear and Cloudy Days. *Open for discussion in Atmospheric Chemistry and Physics Discussions in March 2020,* doi: 10.5194/acp-2020-184

*In review*. Carlton, A.G.; **Christiansen, A.E.;** Flesch, M.; Hennigan, C.J.; Sareen, N.: Liquid Water and the Tropospheric Particulate Matter Burden: An Uncertain Chemical Continuum Across Phase States and Impacts. *Submitted to Chemical Accounts in February 2020.*

*In review*. **Christiansen, A.E.**; Carlton, A.G.; Porter, W.C.: The Changing Nature of Organic Carbon over the United States. *Submitted to Environmental Science and Technology in January 2020.*

*Submitted*. Lance, S.; Zhang, J.; Schwab, J.; Brewer, M.; Minder, J.; Casson, P.; Brandt, R.; Fitzjarrald, D.; Schwab, J.; Lu, C.-H.; Chen, S.-P.; Yun, J.; Freedman, J.; Shrestha, B.; Min, Q.; Joseph, M.B.E.; Crandall, B.; Orlowski, D.; **Christiansen, A.**; Carlton, A.G.; Barth, M.: Overview of the CPOC Pilot Study at Whiteface Mountain, NY: Cloud Processing of Organics within Clouds. *Submitted to the Bulletin of the American Meteorological Society in November 2019.*

[2019] **Christiansen, A.E.**; Ghate, V.P.; Carlton, A.G.: Aerosol Optical Thickness: Organic Composition, Associated Particle Water, and Aloft Extinction. *ACS Earth Space Chem*, **3**, 3, 403-412, doi: 10.1021/acsearthspacechem.8b00163

[2016] Anderson, S.C.; **Christiansen, A.**; Peterson, A.; Beukelman, L.; Nienow, A.M.: Statistical Analysis of the Photodegradation of Imazethapyr on the Surface of Extracted Soybean (Glycine max) and Corn (Zea mays) Epicuticular Waxes. *Environ. Sci.: Processes Impacts*, doi: 10.1039/c6em00401f.

[2015] **Christiansen, A.**; Peterson, A.; Anderson, S.C.; Lass, R.; Johnson, M.; Nienow, A.M.: Analysis of the Photodegradation of the Imidazolinone Herbicides Imazamox, Imazapic, Imazaquin, and Imazamethabenz-methyl in Aqueous Solution. *J. Agric. Food Chem.*, **63,** 50, 10768–10777, doi:10.1021/acs.jafc.5b04663.

## *PRESENTATIONS*

**Christiansen, A.E.**; Carlton, A.G.; Davis, J.M.; Porter, W.C. (2019) ***Poster:*** "Decadal Trends in Particulate Organic Carbon Volatility Fractions" at the American Chemical Society National Meeting & Expo, San Diego, CA, August 27, 2019

***Invited:*** **Christiansen, A.E.** (2019) ***Oral:*** "The Clear Sky Bias: A Perspective from a Girl with Her Head in the Clouds" at the UCI Southern California Undergraduate Research Symposium, Irvine, CA, August 3, 2019

**Christiansen, A.E.**; Carlton, A.G.; Henderson, B.H.; Srivistava, D.; Daniels, J. (2019) ***Oral:*** "The Clear Sky Bias: Reconciling Satellite and Surface Measurements of Atmospheric Aerosol Burden" at the AirUCI Internal Symposium, Irvine, CA, March 28, 2019

**Christiansen, A.E.**; Ghate, V.P.; Carlton, A.G. (2018) ***Poster:*** "Aerosol Optical Thickness: Organic Volatility and Associated Particle Water" at the American Geophysical Union Fall Meeting, Washington, DC, December 13, 2018

**Christiansen, A.E.**; Ghate, V.P.; Carlton, A.G. (2018) ***Oral:*** "Aerosol Optical Thickness: Regional Variation in Organic Composition and Associated Particle Water" at the Lake Arrowhead AirUCI Retreat, Lake Arrowhead, CA, September 25, 2018

**Christiansen, A.E.** and Carlton, A.G. (2017) ***Poster:*** "Spatial Differences in Summertime Enhancement of Aerosol Optical Thickness: Organic Carbon Fractionation and Particle Size" at the American Association for Aerosol Research Annual Conference, Raleigh, NC, October 17, 2017

*Awarded Student Poster Award*

**Christiansen A.**; Peterson, A.; Nienow, A.M. (2014) ***Poster:*** "Photodegradation of Imidazolinone Herbicides and Pesticides in Aqueous Solution and on Plant Surfaces" at the American Chemical Society National Meeting, San Francisco, CA, August 2014

**Christiansen A.**; Peterson, A.; Nienow, A.M. (2013) ***Poster:*** "Imidazolinone Herbicides: Photodegradation in Aqueous Solution and on Waxes" at the Midstates Consortium Undergraduate Research Symposium in the Physical Sciences, Math, and Computer Science at the University of Chicago, Chicago, IL, October 25, 2013

## *TEACHING EXPERIENCE*

**Instructor of Record, General Chemistry Plus (Chem 1X)** *September – December 2019*
University of California, Irvine, Chemistry Department

**Graduate-Level Chemical Kinetics Teaching Assistant** *April – June 2018*
University of California, Irvine, Chemistry Department

**General Chemistry Teaching Assistant, Lab and Lecture** *September 2016 – June 2017*
University of California, Irvine, Chemistry Department

**Introduction to Climate Science Teaching Assistant** *January – May 2016*
Rutgers University Meteorology Department

**Environmental Chemistry Teaching Assistant** *February – May 2015*
Gustavus Adolphus College Chemistry Department

**General Chemistry Teaching Assistant** *September – December 2014*
Gustavus Adolphus College Chemistry Department

**Chemistry Tutor** *September 2014 – May 2015*
Gustavus Adolphus College Chemistry Department

## *HONORS AND AWARDS*

**Student Poster Award at the 2017 American Association for Aerosol Research Annual Conference**

**School of Environmental and Biological Sciences Excellence Fellowship at Rutgers University**

**Phi Beta Kappa Society,** *inducted Spring 2014*

**2014 American Chemical Society Division of Environmental Chemistry Undergraduate Student Award**

**2014 Barry Goldwater Scholarship Nominee**

**2014 Knock Scholarship at Gustavus Adolphus College**

## *ACADEMIC AND PROFESSIONAL SERVICE*

**American Association for Aerosol Research Student Chapter at UCI** *December 2018-*
**Founding Member, Undergraduate Liaison, and Secretary** *Present*
In charge of engaging undergraduate students in chapter events such as Q&A panels and workshops, as well as responsible for chapter meeting minutes.

**University of California, Irvine, Chemistry Graduate Recruitment Events** *Spring 2018*
Participated in tours, Q&A panels, and dinners to recruit prospective graduate students.

# ABSTRACT OF THE DISSERTATION

Spatiotemporal Analysis of Particulate Matter Chemical Composition: Liquid Water Impacts over the United States

By

Amy Elizabeth Christiansen

Doctor of Philosophy in Chemistry

University of California, Irvine, 2020

Associate Professor Annmarie Carlton, Chair

Organic compounds and aerosol liquid water (ALW) are two poorly-characterized components of fine particulate matter ($PM_{2.5}$), a criteria pollutant that negatively impacts human health and affects Earth's radiation budget. Organic compounds influence particle hygroscopicity, yet this is not well-constrained because of the difficulties inherent to characterizing the complex organic matrix, which is composed of hundreds of thousands of individual species. ALW impacts aerosol radiative properties, and aerosol growth due to water affects the formation of clouds, which are important drivers of weather and climate. Despite this, the influence of atmospheric water is minimized in field studies, laboratory experiments, and routine measurements. A quantitative understanding of organic speciation, ALW, and interactions between particle chemical components is necessary for accurate prediction of future air quality and climate. My dissertation aims to increase understanding of interactions between water and particle chemical components, especially organics. Specifically, I 1) investigate the potential of routinely-measured organic carbon (OC) and associated hygroscopicity to reconcile discrepancies between surface-measured $PM_{2.5}$ and remotely-sensed aerosol optical thickness (AOT), 2) investigate differences in

chemical composition, particle hygroscopicity, and ALW between cloudy and clear sky days, and 3) analyze decadal trends in organic aerosol by combining measurements and model output to lend insights into changing organic speciation or formation pathways. I find that ALW qualitatively explains patterns in satellite-measured vertical extinction within the planetary boundary layer. Routinely-measured OC is unable to reconcile $PM_{2.5}$ and AOT measurements, largely due to organic hygroscopicity uncertainties and extinction aloft, which cannot be extrapolated from surface measurements. I also find that ALW mass concentrations are significantly altered between cloudy and clear sky days. In a case study of the Mid South region, aerosol growth due to water is highest during cloudy times, when current techniques are least able to characterize particle mass and impacts. Finally, I find that organic aerosol chemical composition in both humid and arid regions across the US has been changing over time in ways related to ALW chemistry. This work highlights the need for a quantitative understanding of water-mediated chemistry in order to accurately characterize atmospheric aerosol burden and impacts.

# CHAPTER 1

## INTRODUCTION

Organic compounds compose a substantial fraction of atmospheric fine particulate matter ($PM_{2.5}$), a criteria pollutant which negatively impacts public health and affects Earth's radiation budget. Temporal and geospatial trends in the organic fraction and subsequent impacts are not well described by models, possibly due, in part, to poorly understood multiphase liquid water-mediated chemistry.

## 1.1 Background

### 1.1.1 Atmospheric Aerosol

Atmospheric aerosol impacts public health, visibility, and regional and global climate. The matrix of aerosol is complex and chemically diverse, comprising extremely low-volatility species, which are major contributors to aerosol mass (Ehn et al., 2014; Tröstl et al., 2016), low-volatility components, and semi-volatile compounds, including water, which partition between the gaseous and condensed phases (Pöschl, 2005). Aerosols are either emitted directly (e.g., biomass burning, fossil fuel combustion, dust suspension) or formed via chemical reactions of gaseous precursor species (Finlayson-Pitts and Pitts, 2000; McNeill, 2017). Generally, aerosols that are directly emitted tend to be in the coarse mode, with aerodynamic diameters between 2.5 and 10 μm, referred to as coarse particulate matter ($PM_{10}$). Particles formed through secondary processes are typically fine mode, with aerodynamic diameters less than 2.5 μm ($PM_{2.5}$). $PM_{2.5}$ poses a larger risk to human health than $PM_{10}$ due to its ability to enter the bloodstream and is linked to cardiovascular disease, respiratory illnesses, and premature mortality (Pope et al., 2015;

Pope and Dockery, 2006). Major chemical constituents of $PM_{2.5}$ include inorganic species such as sulfate, nitrate, and ammonium, as well as organic species and water.

### 1.1.2 Inorganic Fraction of Aerosol

Gaseous inorganic precursor species of atmospheric particles include $SO_2$ and $NO_x$ ($NO + NO_2$), which originate mainly from combustion (Finlayson-Pitts and Pitts, 2000). Other sources of $SO_2$ include volcanic eruptions and the oxidation of dimethyl sulfide (DMS) near oceans (Liao, 2003; McNeill, 2017). $NO_x$ can also originate from lightning and microbial activity in soils (Zhang et al., 2012). Another common inorganic precursor species is $NH_3$, which is emitted from agriculture, wildfires, and biological sources (Zhang et al., 2012). Atmospheric oxidation of $SO_2$ and $NO_x$ leads to the secondary formation of $SO_4^{2-}$ and $NO_3^-$, two dominant particle-phase species. These species can be neutralized by excess $NH_3$ to form ammonium sulfate and ammonium nitrate, although $NH_3$ is not often in excess.

### 1.1.3 Organic Fraction of Aerosol

Across the contiguous US (CONUS), and especially in the southeast US, the organic fraction of aerosol comprises an increasing majority of aerosol mass as sulfate concentrations decrease due to air quality regulations (Attwood et al., 2014; Malm et al., 2017). Organic components of aerosol can be emitted into the atmosphere directly via combustion processes (Hodzic et al., 2010), although this accounts for only about 20% of total organic aerosol (OA) mass (Kanakidou et al., 2005; Spracklen et al., 2011). The rest of the organic mass is formed in the atmosphere as secondary organic aerosols (SOA) through condensational and aqueous-phase pathways (McNeill, 2017). Carbon-14 analysis at rural locations shows that most organic carbon is non-

fossil and derived from the biosphere (Bench et al., 2007; Schichtel et al., 2008). Biogenic volatile organic carbon (VOC) interacts with anthropogenic emissions to enhance formation of SOA and thus is controllable via regulations targeting $SO_2$ and $NO_x$ (Carlton et al., 2018a).

Organic aerosol (OA) composition is currently not well characterized due to its complex matrix containing thousands of chemical species. As part of large field campaigns representing the efforts of dozens of PIs and hundreds of measurements, high mass closures between total measured organic aerosol and characterized particle-phase organic chemical composition are able to be obtained at specific locations, but this level of detailed measurement is not able to be obtained routinely by monitoring networks. For example, during the Southern Oxidant and Aerosol Study (SOAS), ~74% of total OA mass was characterized using gas chromatography and various mass spectrometry techniques (Zhang et al., 2018b). Aerosol mass spectrometers (AMS) are also used in field campaigns to characterize the organic fraction of aerosol. In conjunction with factor analysis methods, AMS measurements can be used to break down the organic fraction into different categories, such as oxygenated OA, hydrocarbon-like OA, low-volatility OA, semi-volatile oxygenated OA, and biomass burning OA (Zhang et al., 2011). These categories are useful since each factor corresponds to hundreds of individual OA constituents that have similar chemical composition and behavior, which is indicative of various sources and processes. While these techniques offer a wealth of information about the organic fraction, routine monitoring networks are unable to perform measurements at this level of detail, and thus organic aerosol composition is largely unknown at most locations and times.

#### 1.1.3.1 Long-term particulate OC measurement

The longest record of routine organic carbon (OC) measurements in a wide variety of locations, representing over 30 years of data, is taken by the Interagency Monitoring of PROtected Visual Environments (IMPROVE) network. This represents a wealth of information on OC concentrations over a long period of time, and thus offers unique insight to decadal trends. The IMPROVE network measures total organic carbon (TOC) and volatility fraction mass concentrations, which do not provide chemical composition information. To measure TOC mass concentrations, a 0.5-$cm^2$ punch is removed from a $PM_{2.5}$ filter sample and placed in the heating zone of a DRI Model 2001 thermal/optical carbon analyzer. The temperature is increased stepwise under a helium environment to avoid oxidation of the species on the filter (Chow et al., 2007). The carbonaceous material is converted to $CO_2$ via a heated $MnO_2$ oxidizer and then reduced to $CH_4$ with a hydrogen-enriched nickel catalyst. The $CH_4$ is detected via a flame-ionization detector to yield organic carbon (OC) mass concentrations (Chow et al., 2007). OC mass is measured in four categories based on volatility: OC1 (140 ºC), OC2 (280 ºC), OC3 (480 ºC), and OC4 (580 ºC) (Chow et al., 2007), referred to as the OC fractions. As the filter is heated in the absence of oxygen, some carbon pyrolyzes, especially above 300 ºC, and combusts upon the introduction of oxygen at the start of the subsequent elemental carbon measurement. The carbon that combusts upon introduction of oxygen is measured in the category “pyrolyzed carbon” (PC). Dividing the analysis into several temperature steps (i.e., the OC fractions) reduces the amount of pyrolysis (Chow et al., 1993; Rau, 1986). PC is measured in a separate category and cannot be assigned to a particular step in the temperature-ramp. Hence, reported mass concentrations for the OC fractions are lower mass bounds because some of each fraction may be lost to charring and counted as PC. TOC mass measurements are the sum of OC1, OC2,

OC3, OC4, and PC. Recently, Malm et al. (2020) demonstrated that PC and EC co-evolve from the filter, causing lower-temperature oxidation of EC. This may bias TOC mass concentrations high because they include some EC. The OC fractions are also subject to some uncertainties, including the loss of volatile species before and during analysis and interferences from metal salts, carbonate, KCl, and NaCl (Baumgardner et al., 2012; Chow and Watson, 2002; Dillner et al., 2009; Malm et al., 2011; Wang et al., 2010).

The OC fractions do not identify individual species or functional groups, but they potentially lend insight to chemical composition and formation processes. A laboratory analysis of individual organic compounds found widely in the atmosphere (e.g., oxalic acid, levoglucosan, azelaic acid, and humic-like substances) found that as the molecular weight of an organic species increases, higher temperatures are needed for carbon evolution (Miyazaki et al., 2007). Field campaigns in locations around the world associate OC1 and OC2 with biomass burning and fossil fuel combustion, and OC3 and OC4 with cooking emissions and dust (Aswini et al., 2019; Cao et al., 2005; Chow et al., 2004). Meier and Schwab (2011) investigated individual organic compounds and mixtures that are prevalent in aerosols to determine which compounds may evolve in each OC fraction. Several organic species evolve in multiple fractions, although most evolve primarily in OC2 (Meier and Schwab, 2011). Other efforts to identify functional groups via Fourier-transform infrared spectroscopy of IMPROVE filters find evidence of carbonyls, alcohols, carboxylic acids, organonitrates, amines, and aromatics in $PM_{2.5}$ samples analyzed for TOC content (Dillner and Takahama, 2015; Kamruzzaman et al., 2018; Weakley et al., 2016).

### 1.1.4 Aerosol Liquid Water

Aerosol liquid water (ALW), a ubiquitous component of the aerosol matrix, makes up, on average, from 3.7% (Riverside, CA) to 85% (Hyytiala, Finland) of aerosol mass in areas sampled around the world (Nguyen et al., 2016a). ALW is a function of RH, chemical composition, temperature, and particle number concentration. It plays an important role as a facilitator of SOA formation by providing a medium for the partitioning and reaction of water-soluble gases (Carlton and Turpin, 2013). Traditionally, SOA formation has been thought to occur via semi-volatile gas-phase oxidation products partitioning onto dry organic aerosol (Odum et al., 1996; Pankow, 1994), a mechanism conceived because most laboratory experiments are performed under dry conditions. For over 30 years, it has been well-established that small water-soluble organic gases are taken up by water in aerosols, cloud droplets, or fog and undergo aqueous chemistry to form lower volatility products that remain in the aerosol phase (Munger et al., 1984), and this has been shown to occur worldwide (Blando and Turpin, 2000). Chemical reactions continue to occur in the aqueous phase of aerosol and contribute to SOA mass, leading to oxygenated species, functionalization, oligomerization, and accretion (Ervens et al., 2011). Cloud processing of organic species is also an important source of SOA globally (Liu et al., 2012). Organic species oxidize and form water-soluble compounds, such as aldehydes, that can partition into cloud droplets and continue to oxidize into carboxylic acids and oligomers (Altieri et al., 2006, 2008; Boone et al., 2015; Carlton et al., 2006, 2007; Sorooshian et al., 2006).

Despite the prevalence and importance of ALW in modulating particle chemical constituents, such as providing a medium for the formation of SOA, it is rarely measured. Measurements of ALW under ambient conditions have been made previously, but only as part of intensive field

studies (Khlystov, 2005; Nguyen et al., 2014b). ALW is not measured as a part of routine monitoring networks. Routine surface networks (e.g., IMPROVE, CSN) measure $PM_{2.5}$ and chemical constituents after equilibration of filters typically at a standardized RH of 30-40% and temperature of 20-23 ºC (Chow et al., 2015; US EPA, 1998). These standards are often not representative of the ambient conditions when sampling took place. In humid places such as the southeast US, this results in the loss of water, nitrate, and dissolved and semi-volatile organic compounds (El-Sayed et al., 2016). Characterization of these filters thus lacks some condensed-phase chemical information, especially with regard to ALW (Babila et al., 2020). Studies of ALW have traditionally focused on visibility issues and estimating particle growth factors (Ahlm et al., 2016; Malm et al., 1996; Pitchford and McMurry, 1994; Sorooshian et al., 2008). Lack of information on ALW concentrations and trends hinders understanding of the fate and transport of trace species in the atmosphere and adversely affects control strategies aimed at reducing aerosol impacts on climate, visibility, air pollution, and public health.

To overcome this measurement challenge, ALW content is typically estimated using applications such as the aerosol inorganic ($K^+$-$Ca^{2+}$-$Mg^{2+}$-$NH_4^+$-$Na^+$-$SO_4^2$-$NO_3$-$Cl^-$-$H_2O$) thermodynamic equilibrium model ISORROPIA (Fountoukis and Nenes, 2007). It is important to note that ISORROPIA considers only inorganic components in its calculations, as organic contributions to water uptake are not well quantified and organic aerosol hygroscopicity is poorly constrained. Other aerosol thermodynamic models such as E-AIM (Clegg et al., 1998) incorporate organic components and are most useful when the precise chemical identity of the organic species are known, which is not the case for ambient OC measurements at routine networks.

#### 1.1.4.1 Contribution to ALW from Organics

Historically, organic hygroscopicity data is not routinely measured. Organic aerosol constituents can impact ALW (Saxena et al., 1995), although quantitative amounts remain uncertain. Typical hygroscopicity ($\kappa_{org}$) values for the organic fraction of aerosols are low ($\kappa_{org}$~0.1) (Engelhart et al., 2011; Pierce et al., 2012; Prenni et al., 2007), although individual compounds may have a larger impact based on polarity (Suda et al., 2012). Polarity in organic compounds generally increases as particles age via oxidation reactions, and thus hygroscopicity also tends to increase with age (Li, 2019; Tritscher et al., 2011). Aerosol water due to the organic fraction can be estimated according to κ-Kohler theory and the Zdanovskii-Stokes-Robinson (ZSR) mixing rule (Petters and Kreidenweis, 2007; Kreidenweis et al., 2008) (Eqn 1.1):

$$V_{w,o} = V_o \kappa_{org} \frac{a_w}{1-a_w} \quad (1.1)$$

In this equation, $V_{w,o}$ and $V_o$ are the volumes of water and organic matter, respectively, $\kappa_{org}$ is the organic hygroscopicity parameter, and $a_w$ is water activity, which can be estimated as equivalent to RH when particle diameter information is not available. The difference between RH and $a_w$ is ~0.01-0.02 (Tang, 1996), which may result in an overestimate in water volume up to 11% (Nguyen et al., 2014b). $V_o$ is determined by dividing organic mass by a standard organic density of 1.4 g $cm^{-3}$ (Turpin and Lim, 2001).

## 1.2 Motivation

### 1.2.1 Impacts on Health

$PM_{2.5}$ is a major contributor to air pollution, and elevated levels are associated with increased morbidity and mortality (Pope et al., 2015). There is currently no agreement amongst experts as to a safe level of $PM_{2.5}$ exposure for regulatory purposes (Pope et al., 2015; Samet et al., 2000;

Smith et al., 2000). $PM_{2.5}$ is absorbed deep in the lungs and is linked to negative health endpoints such as cardiovascular and respiratory diseases, increased cancer risk, and premature death (Burnett et al., 2014; Pope et al., 2015; Turner et al., 2011). Atmospheric $PM_{2.5}$ is the fifth-ranking mortality risk factor globally, causing an estimated 4.2 million deaths in 2015 (Cohen et al., 2017). There is an extensive historical record of extreme air pollution negatively impacting public health. One of the most famous examples is the Great London Smog of 1952, which led to estimated premature deaths numbering from 4000 (Logan, 1953) to 12,000 (Bell et al., 2004). Other air pollution events include episodes in Meuse Valley, Belgium, in 1930 and Donora, PA, in 1948 that led to 60 and 20 deaths, respectively, with thousands more stricken with respiratory problems (Fletcher, 1949; Nemery et al., 2001).

While $PM_{2.5}$ alone is linked to adverse health impacts, its chemical composition likely plays a role in modulating these effects (Atkinson et al., 2015; Lippmann, 2014). When PM deposits in the lungs, metals (e.g., Cu, Fe, Zn, As, Mn, and Ni) and organic components (e.g., organic hydroperoxides and peroxides, aromatic oxidation products, and black carbon) react with antioxidants and form reactive oxygen species (ROS) (Pöschl and Shiraiwa, 2015; Shiraiwa et al., 2017a). ROS triggers inflammation and leads to oxidative stress, cell death, and disease. Understanding the sources and composition of $PM_{2.5}$ can help regulators and legislators enact appropriate control measures to safeguard public health.

### 1.2.2 Impacts on Radiation

$PM_{2.5}$ imparts radiative impacts and affects visibility and climate via light extinction. Depending on chemical composition, aerosols can scatter and absorb incoming solar radiation and (if aloft)

diffuse backscatter from clouds (McNeill, 2017). Both scattering and absorption contribute to decreased visibility and aerosol optical thickness (AOT), a measure of the extinction of a ray of light as it travels through the atmosphere. Light scattering by fine particles proceeds largely via Mie scattering, which occurs when the diameter of a particle is approximately equal to the wavelength of radiation. Incident light is scattered primarily in the forward direction, causing a hazy appearance and limiting visual range (Finlayson-Pitts and Pitts, 2000).

Light scattering and absorption of aerosol impacts regional and global climate via direct and indirect effects (Boucher et al., 2013). In the direct effect, aerosols reflect incoming shortwave radiation back to space, increasing Earth's albedo and resulting in a cooling effect. Absorbing aerosols such as black carbon (BC) absorb visible and near-IR radiation and reduce albedo when deposited on snow and ice, resulting in a warming effect (Ramanathan and Carmichael, 2008). Indirect effects occur because aerosols serve as cloud condensation nuclei (CCN). A greater number concentration of aerosols results in an increase in cloud droplet number concentration and causes each droplet to be smaller in size when liquid water content is held constant (Boucher et al., 2013; Twomey, 1977). This leads to an increase in cloud albedo since the total droplet surface area is increased when many small droplets are present (Boucher et al., 2013; Twomey, 1977). In addition, a decrease in cloud droplet size results in suppression of precipitation and increases the atmospheric lifetime of clouds (Albrecht, 1989), although this effect may not hold true for certain types of clouds (Ackerman et al., 2004; Jiang and Feingold, 2006; Xue and Feingold, 2006). Currently, aerosols and clouds are the areas of largest uncertainty in climate models (Boucher et al., 2013). The best estimate of the effective radiative forcing of aerosols is -0.95 to +0.05 W $m^{-2}$ (Boucher et al., 2013). The complex chemical nature of aerosols and

incomplete understanding of their impacts on radiative forcings and cloud processes contributes to this large uncertainty.

Organic aerosol composition affects particle intensive properties and may substantially impact the Earth's radiation budget, but this is not well characterized. Model estimates of radiative forcings by organic aerosols tend to predict negative (cooling) forcings (Penner et al., 2001; Xu and Penner, 2012), and OA is generally treated as a scattering species (Flores et al., 2014; Kim et al., 2012; Lang-Yona et al., 2010; Ma and Thompson, 2012; Nakayama et al., 2010; Redmond and Thompson, 2011; Schnaiter et al., 2005). The effects of organic composition on particle scattering are complex, as some studies find that increasingly oxidized OA increases scattering (Cappa et al., 2011; Flores et al., 2014; Moise et al., 2015), while others find the opposite (Lambe et al., 2013; Nakayama et al., 2010). Coatings of certain organic species, such as succinic and glutaric acids, have been found to increase light scattering of aerosols by up to 3.8-fold (Xue et al., 2009).

Some chemical constituents, such as those in black and brown carbon, absorb radiation and thus impart a positive (warming) radiative forcing (McNeill, 2017). Black carbon (BC) absorbs strongly in a wide range of wavelengths from the UV to the IR regions. Sources of BC include fossil fuel combustion and biomass burning. While BC is a powerful climate forcer, it is short-lived in the atmosphere and is often co-emitted with scattering aerosols (Bond et al., 2013). Brown carbon (BrC) absorbs efficiently in the near-UV and visible ranges (Zhang et al., 2013), although not as strongly as BC. The chemical composition of BrC is largely uncharacterized but determines its optical properties. Primary BrC is emitted from fossil fuel combustion and

biomass burning (Zhang et al., 2013). Secondary BrC is produced in the atmosphere via aging processes, and laboratory studies suggest that this is often a result of reactions with nitrogen (Bones et al., 2010; Updyke et al., 2012). Photooxidation of anthropogenic aromatics has been shown to lead rapidly to BrC formation under high-$NO_x$ conditions, and while biogenic VOCs can also form BrC, they tend to form relatively less than aromatic VOCs (Jaoui et al., 2008; Nakayama et al., 2010; Zhong and Jang, 2011). Both the absorption and scattering of radiation by organic aerosol affects remotely sensed products such as AOT in ways that are not well constrained.

ALW, which is influenced by chemical composition, efficiently scatters visible light, impacting local visibility and remotely sensed variables such as AOT (Christiansen et al., 2019; Malm et al., 1994; Nguyen et al., 2016b; Pitchford et al., 2007). Particle size is a determining factor in light scattering by particles, and this is modulated by chemical composition via particle hygroscopicity and water uptake. Further, aerosol hygroscopic growth impacts cloud formation, storm morphology, and precipitation patterns (Kawecki et al., 2016; Kawecki and Steiner, 2018). Clouds play a dominant role in the Earth's radiation budget (Trenberth et al., 2009) and are the primary drivers of vertical transport. Pollutants are transported by clouds from the boundary layer to the free troposphere, where their radiative impacts are amplified and the distance over which they are transported is increased (Barth, 2003). Aerosol-cloud interactions are a key uncertainty in climate model projections.

## 1.3 Key Knowledge Gaps

Laboratory studies, ambient sampling, modeling, and analysis strategies are often designed in ways that minimize the influence of atmospheric water, despite its prevalence and the important role it plays in Earth's radiation budget and aerosol burden. For example, during atmospheric chemistry field campaigns, aircraft typically avoid clouds. Remotely sensed variables such as AOT often do not include retrievals from cloudy times in the final data product, as error increases when clouds are present (Martin, 2008). Validation of satellite-derived AOT occurs primarily through comparison to surface observations such as those from sun photometers, which also include only cloud-free measurements (Liu et al., 2018). Further, air quality model evaluations are often conducted using cloud-free satellite retrievals (van Donkelaar et al., 2010; Guo et al., 2017; de Hoogh et al., 2016; Song et al., 2014; Tian and Chen, 2010) and cloud-free aircraft samples (Bray et al., 2017; McKeen et al., 2009). This biases model development toward cloud-free conditions and induces a persistent, implicit clear-sky bias in our understanding of tropospheric chemical composition. Further, laboratory experiments performed to understand particulate matter formation have historically been conducted under dry conditions (e.g., Lamkaddam et al., 2017; Ng et al., 2007) atypical of cloudy time periods and of ambient conditions in most locations in the CONUS. Current approaches are limited in their ability to quantitatively assess ambient aerosol physicochemical properties in all conditions, and this is a key knowledge gap. Given the prevalence of atmospheric water in the form of clouds, fog, and areas of high RH, and that atmospheric water is expected in increase in a warming climate (Boucher et al., 2004; Lavers et al., 2015), it is imperative to understand aqueous processes that impact aerosol chemical composition and subsequent radiative, meteorological, and climate impacts. Quantitative understanding of interactions between atmospheric water and particle

chemical components, especially organics, is essential to understanding the fate of trace species, resolving model uncertainty, and accurately predicting atmospheric aerosol burden and subsequent impacts. It remains a key knowledge gap.

## 1.4 Research Questions

The studies in this dissertation were guided by the following questions:

- How does surface particle chemical composition influence ALW and its associations with surface-based extinction and remotely sensed AOT in climatologically different areas over the United States?
- How does particle chemical composition change between cloudy and clear sky conditions?
- How are ALW concentrations modulated by different meteorological conditions, emissions, and *in situ* chemical reactions?
- How and why has the chemical speciation of organic aerosol changed over time across the CONUS?

## 1.5 Specific Aims

I address these questions via spatiotemporal analysis of large environmental $PM_{2.5}$ composition datasets, satellite information, and model output over the CONUS. In my dissertation, I 1) investigate the potential of thermally-defined OC fractions and associated hygroscopicity to explain discrepancies between surface-measured $PM_{2.5}$ and remotely-sensed AOT, 2) investigate differences in fine particle chemical composition, especially ALW, between cloudy and clear sky days as defined by satellite cloud flags, and 3) analyze decadal changes in organic aerosol

composition through a combination of routine measurements and atmospheric modeling to understand changing organic speciation, formation pathways, and associated implications for particle viscosity.

## 1.6 Structure of Dissertation

Chapter 2 aims to reconcile differences in seasonality between surface measurements of $PM_{2.5}$ and remotely sensed AOT trends. Over the CONUS, the strongest remotely sensed AOT is observed in the east, where ALW and extinction per unit $PM_{2.5}$ dry mass are highest. However, surface measurements of $PM_{2.5}$ do not show the same seasonality as remotely sensed AOT in the southeast US. This discrepancy is partly explained through water uptake from the inorganic chemical components $SO_4^{2-}$ and $NO_3^-$ calculated by the thermodynamic equilibrium model ISORROPIA. To explore if this discrepancy can be better reconciled, organic water uptake is estimated using κ-Kohler theory in two areas of the CONUS that exhibit differing patterns in AOT seasonality. Particle chemical constituent concentrations are taken from the IMPROVE network, and OC volatility fractions are used to estimate κ values for organic water uptake. Particle mass and ALW concentrations are integrated from the surface to the top of the planetary boundary layer (PBL). Integrated $PM_{2.5}$ + ALW concentrations at two groups of four sites are compared to AOT derived from the Moderate Resolution Imaging Spectroradiometer (MODIS) and vertically resolved extinction from the Cloud-Aerosol Lidar and Infrared Pathfinder Satellite Observation (CALIPSO) from 2007 to 2016.

Chapter 3 investigates the ways in which chemical composition differs between cloudy and clear sky conditions, with a particular focus on differences in particle hygroscopicity and ALW.

Surface $PM_{2.5}$ chemical constituent concentrations from the IMPROVE network are examined from 2010 to 2014 across the CONUS during cloudy and clear sky times defined using MODIS cloud flags. The Mid South region, which encompasses large swaths of Oklahoma, Arkansas, and Missouri, as well as the location of the Atmospheric Radiation Measurement Southern Great Plains (ARM SGP) site, is used as a case study to investigate how chemical composition exerts a controlling effect on ALW concentrations in ways that cannot be explained solely through meteorology (e.g., RH).

Chapter 4 investigates decadal trends in routine measurements of OC fractions taken from the IMPROVE network from 2005 to 2015 to determine which OC fractions are driving overall changes in total organic carbon (TOC). The measurements are paired in space and time with GEOS-Chem simulations of organic aerosol to assess species and formation pathways that may be changing in ways that impact the organic carbon budget. Results from this study lend insight to changing chemical regimes and controlling processes, with implications for particle phase state, viscosity, and oxidation state.

Chapter 5 focuses on future investigative directions. This includes 1) the examination of the effect of salt concentrations on organic partitioning, a mechanism that may help to further explain decadal trends in organic aerosol, and 2) the assessment of potential health impacts of organic species for which partitioning is affected by atmospheric salts.

# CHAPTER 2

## AEROSOL OPTICAL THICKNESS: ORGANIC COMPOSITION, ASSOCIATED PARTICLE WATER, AND ALOFT EXTINCTION

Reproduced with permission from *ACS Earth and Space Chemistry.* Christiansen, A.E.; Ghate, V.P.; Carlton A.G., Aerosol Optical Thickness: Organic Composition, Associated Particle Water, and Aloft Extinction. *ACS Earth and Space Chemistry* **2019** *3* (3), 403-412, DOI: 10.1021/acsearthspacechem.8b00163. © 2019 American Chemical Society.

## 2.1 Abstract

Over the contiguous U.S., the strongest remotely sensed aerosol optical thickness (AOT) is observed in the east, where aerosol liquid water (ALW) and extinction per unit $PM_{2.5}$ dry mass are highest. Positive associations between ALW due to sulfate and nitrate with remotely sensed AOT offer a contributing explanation for geospatial patterns in AOT seasonality. We seek to further resolve patterns in ALW-AOT relationships by investigating organic mass (OM) fractionation, converted from organic carbon (OC) measurements using regionally specific OM:OC ratios, and the associated impacts on ALW. ALW is integrated from the surface through the boundary layer and estimated from measured particle chemical composition using ISORROPIAv2.1 and κ-Kohler theory at eight Interagency Monitoring of PROtected Visual Environments (IMPROVE) sites in areas of contrasting AOT seasonality. Two groups of four sites each, clustered by chemical climatology, are compared to AOT derived from the Moderate Resolution Imaging Spectroradiometer and vertically resolved extinction retrieved from Cloud-Aerosol Lidar and Infrared Pathfinder Satellite Observation (CALIPSO) from 2007-2016.

Estimated ALW within the planetary boundary layer (PBL) differs between the regions. Spatial patterns and vertical profiles are qualitatively similar to CALIPSO patterns. However, inclusion of volatility-based organic speciation from routine surface networks and the associated ALW do not improve correlation with satellite-derived AOT. CALIPSO-measured extinction is enhanced above the PBL, and may partly explain discrepancies. This work suggests that the effects of intrinsic physicochemical properties are remotely sensed, but approaches to link AOT to current surface measurements are limited in detail and their ability to assess aloft phenomena.

## 2.2 Introduction

Surface measurements of particle mass are insufficient to fully explain multi-year analyses that demonstrate summertime enhancement of aerosol optical thickness (AOT) over the southeast United States (U.S.), as observed by the Moderate Resolution Imaging Spectroradiometer (MODIS), the Multi-angle Imaging SpectroRadiometer (MISR) (Goldstein et al., 2009), and the Cloud-Aerosol Lidar with Orthogonal Polarization (CALIOP) (Nguyen et al., 2016b). During 2013, summer and winter MODIS AOT measurements in the southeast U.S. differed up to a factor of 4, while seasonal change in surface fine particle mass ($PM_{2.5}$) show negligible differences (Kim et al., 2015). Poor agreement between AOT and surface $PM_{2.5}$ arises for multiple reasons such as complex vertical structure, background spectral properties, and poorly constrained distribution in aerosol intensive properties such as those that affect volumetric growth due to particle hygroscopicity (van Donkelaar et al., 2006, 2010; Hersey et al., 2015; Jin et al., 2019; Kaku et al., 2018; Li et al., 2015; Liu et al., 2004; Martin, 2008; Wang and Christopher, 2003). Surface $PM_{2.5}$ mass is partially decoupled from satellite retrievals of AOT because aerosol liquid water (ALW) is removed from particles upon collection, and surface

measurements do not capture a vertical column. Nguyen et al. 2016b suggest that ALW, a substantial component of tropospheric aerosol volume that is acknowledged to reduce visibility (i.e., scatter solar radiation in visible region) (Khan et al., 2011; Malm et al., 1996; Pitchford and McMurry, 1994; Volkamer et al., 2015) and increase surface extinction (Garland et al., 2007; Pitchford et al., 2007), is a plausible contributing factor to spatial and seasonal differences in AOT-surface $PM_{2.5}$ mass relationships. ALW affects light extinction and is not directly captured by surface mass measurements of $PM_{2.5}$ (Jefferson et al., 2017; Nguyen et al., 2016b; Pitchford et al., 2007; Volkamer et al., 2015; Ziemba et al., 2013).

Reliable evaluation of policies to manage air quality requires an accurate understanding of the controlling chemical and physical mechanisms (Mao et al., 2018) that determine atmospheric composition measured at the surface and from satellite-derived estimates. Remotely sensed satellite data records dramatic improvements in air quality over the U.S., in particular the eastern U.S., in response to environmental regulations that reduce anthropogenic emissions (Attwood et al., 2014; Duncan et al., 2014; Kaku et al., 2018). Over the contiguous U.S. (CONUS), the strongest AOT and highest extinction-to-dry mass ratios are observed over the east (Li et al., 2013), where ALW mass concentrations are predicted to be most abundant (Carlton and Turpin, 2013; Nguyen et al., 2016b), particularly when the vertical column is considered (Carlton and Turpin, 2013). Aerosol chemical constituents such as sulfate ($SO_4^{2-}$) and nitrate ($NO_3^-$) facilitate water uptake and contribute to ALW mass with a controlling effect on particle size, the predominant property that determines particle scattering (Tang, 1996). These species also contribute to biogenic secondary organic aerosol (SOA) formation (Carlton and Turpin, 2013; McNeill, 2015; Pye et al., 2013). Biogenic SOA is more pronounced in forested locations such as

the southeast U.S., where ALW is abundant and precursor emissions increase with temperature. Remote AOT measurements in that region also increase in magnitude with temperature (Mielonen et al., 2018). Over the past decade, decreasing trends in particle inorganic chemical constituents that largely control ALW (e.g., $SO_4^{2-}$) (Nguyen et al., 2015) are linked to regional observations of changes in climate-relevant aerosol optical properties and impacts such as summertime surface measurements of visibility, particle extinction, and ground-based and satellite-derived AOT (Attwood et al., 2014; Leibensperger et al., 2012; Li and Martin, 2018). These trends are also linked to changes in the diurnally averaged surface radiative effect and large-scale changes coincident with the disappearance of the southeast U.S. warming hole (Meehl et al., 2015; Yu et al., 2014).

Model estimates of radiative forcings by organic aerosols generally predict negative (cooling) forcings (Penner et al., 2001; Xu and Penner, 2012), and organic aerosol from both biogenic and anthropogenic sources is largely treated in the literature as a scattering species (Flores et al., 2014; Kim et al., 2012; Lang-Yona et al., 2010; Ma and Thompson, 2012; Nakayama et al., 2010; Redmond and Thompson, 2011; Schnaiter et al., 2005). Some studies linking organic aerosol composition to refractive index (RI), the real part of which is a measure of particle scattering, find a positive correlation between increasing RI and increasing O:C ratios from various precursor volatile organic carbon (VOC) species (Cappa et al., 2011; Flores et al., 2014; Moise et al., 2015), while others find the opposite trend (Lambe et al., 2013; Nakayama et al., 2010). Atmospheric processing may increase light absorption by secondary organic species, but this depends on specific molecular identity, concentration, pH, and relative humidity (Moise et al., 2015). Such detailed ambient measurements are usually episodic and associated with an

intensive observing period (Carlton et al., 2018b; Docherty et al., 2011; Toon et al., 2016) and are not a part of routine monitoring network data.

In the southeast US, ALW derived from surface measurements of inorganic particle chemical composition exhibits positive associations with AOT that differ by season (Nguyen et al., 2016b). A possible explanation for these seasonal differences is the hygroscopic and chromophoric properties of the constituent organic species in aerosols that affect extinction (Brock et al., 2016), which are not considered in that analysis. Substantial uncertainties persist in regards to the effects of organic carbon composition and its influence on climate-relevant aerosol optical and hygroscopic properties (Moise et al., 2015). Previous studies demonstrate that inclusion of organic species is critical to understand and predict water uptake, which is dominated by organic species at certain times and locations (Mircea et al., 2005; Mochida et al., 2006; Novakov and Penner, 1993).

The Interagency Monitoring of PROtected Visual Environments (IMPROVE) network provides surface-based chemical speciation measurements at locations across the U.S. from 1988 to present. Ambient $PM_{2.5}$ samples are analyzed for OC using thermal optical OC/EC analyzers (Khan et al., 2012; Meier and Schwab, 2011). Mass concentrations in four categories of OC (OC1, OC2, OC3, and OC4), pyrolyzed OC (OCP), and three categories of elemental carbon (EC1, EC2, and EC3) are measured based on volatilization at various temperatures, where OC1 is the most volatile fraction and EC3 is the least (Chow et al., 2007). While these measurements provide information related to volatility of the organic $PM_{2.5}$ constituents, they do not provide chemical identity or specific functional group information, though this is an active research area

(Dillner and Takahama, 2015; Kamruzzaman et al., 2018; Weakley et al., 2016). Generally, these data are only used for total OC and EC measurements, with the temperature ramp-based categories receiving relatively less attention in the literature. Studies have attempted to link thermal fractions to specific compounds, molecular weight, and refractory behavior, but variety in thermal protocols, matrix effects within aerosols, and the fact that some compounds evolve in multiple thermal fractions complicate interpretation (Meier and Schwab, 2011; Miyazaki et al., 2007). Sources have been linked to thermal behavior, and positive matrix factorization analysis facilitates estimation of carbonaceous aerosol sources (Gilardoni et al., 2011), although this has not been directly linked to IMPROVE OC fractions.

Here, we explore the potential of OC fractions, converted to organic mass (OM) using regionally specific values that account for oxygen and hydrogen, to further reconcile satellite-measured AOT and surface $PM_{2.5}$ measurements through their hygroscopic effects. We test the hypothesis that differences in IMPROVE-measured organic chemical composition are important for water uptake and influence remotely sensed light extinction. To do so, we analyze regional and temporal trends in OC fractions, AOT, and ALW in the Appalachia and Colorado (CO) Plateau regions defined by chemical climatology that coincide with contrasting seasonal AOT patterns. For the first time, we compare surface $PM_{2.5}$ to AOT accounting for OC categories defined and reported by IMPROVE and their contributions to ALW.

## 2.3 Experimental

IMPROVE data are downloaded from public archives (IMPROVE Network, 2019) on 26 May 2016 for eight unique locations with complete data records in the continental U.S. from January

2007 to August 2016. These sites are grouped into two regions, Appalachia and CO Plateau, defined by IMPROVE as having similar chemical climatology (Hand et al., 2011). We choose four Appalachia sites, Cohutta, GA (COHU1), Great Smoky Mountains National Park, TN (GRSM1), Linville Gorge, NC (LIGO1), and Shining Rock Wilderness, NC (SHRO1), and four CO Plateau sites, Bryce Canyon National Park, UT (BRCA1), Canyonlands National Park, UT (CANY1), Capitol Reef National Park, UT (CAPI1), and Mesa Verde National Park, CO (MEVE1) (Figure A1). Appalachia exhibits summertime enhancement of AOT over wintertime values, while the CO Plateau does not (Figure A1). Here, we use summer definitions of June, July, and August (JJA) and winter definitions of December, January, and February (DJF). We use IMPROVE surface mass concentration data of $PM_{2.5}$, and $SO_4^{2-}$, $NO_3^-$, and OC constituents for ALW estimates, which are available every three days. The OC fractions are differentiated by temperature using the IMPROVE thermal protocol, which changed fraction-temperature definitions beginning in 2005 (Chow et al., 2007). We analyze the years 2007-2016 to ensure consistent organic fractional comparisons among the years. This time period coincides with measurements from both MODIS and Cloud-Aerosol Lidar and Infrared Pathfinder Satellite Observation (CALIPSO). The mass concentration of OM is calculated by multiplying OC mass concentrations by regionally specific OM:OC ratios, 1.58 for sites within the CO Plateau and 2.01 for sites within Appalachia (El-Zanan et al., 2005). In the absence of additional organic speciation information, we assume the same OM:OC for each OC fraction within an individual region, and this adds some uncertainty to our analysis.

Mass concentrations of particle-phase liquid water at all sites are estimated using the inorganic aerosol thermodynamic equilibrium model ISORROPIAv2.1 (Fountoukis and Nenes, 2007). The

method application, species, and meteorology input data (from the North American Regional Reanalysis (NARR) model (https://www.esrl.noaa.gov/psd/)) are described in detail elsewhere (Nguyen et al., 2016b). Briefly, we assume metastable particles. Ammonium and dust are collected by surface monitors and contribute to the unspeciated $PM_{2.5}$ dry mass used in this analysis, but their contribution to ALW is not included due to a lack of relevant speciation data at all sites for all years and uncertainties regarding water uptake by dust (Metzger et al., 2018). This introduces uncertainty and the net impact of this approach results in lower bound estimates of ALW mass concentrations. Water volume from organic species ($V_{w,o}$) is estimated using κ-Kohler theory and the Zdanovskii-Stokes-Robinson (ZSR) mixing rule (Kreidenweis et al., 2008; Petters and Kreidenweis, 2007) (Eqn 2.1)

$$V_{w,o} = V_o \kappa_{org} \frac{a_w}{1-a_w} \quad (2.1)$$

Here, $a_w$ is water activity, $V_o$ is the volume of organic matter, and $\kappa_{org}$ is the hygroscopicity parameter of the organic components. Activity is assumed to be equivalent to RH because particle diameter data is not readily available at IMPROVE monitoring stations. $V_o$ is determined by dividing OM by a typical organic density of 1.4 g $cm^{-3}$ (Turpin and Lim, 2001). Species that volatilize at lower temperatures are most susceptible to loss during field latency, transport, and storage, especially at warm ambient temperatures (40 ºC) and storage times >3 hours (Dillner et al., 2009). OC1, carbon that evolves at T <300 ºC, is associated with low molecular weight (MW) (<180 g $mol^{-1}$) and water-insoluble compounds (Miyazaki et al., 2007). We expect OC1 to be made up of primary emissions and interpret reported mass concentrations as a lower bound. Conversely, OC4 is less volatile and is expected to be composed of water-soluble, high-MW compounds associated with high volatilization temperatures (>300 ºC) (Miyazaki et al., 2007). We do not consider pyrolyzed OC, organic carbon that chars during heating, or EC in our

analysis. Sensitivities for assigned $\kappa_{org}$ values are performed encompassing the full range observed for organic species in laboratory studies ($0.01 \leq \kappa_{org} \leq 0.20$) and $V_{w,o}$ estimates can vary up to a factor of four (Nguyen et al., 2015; Petters and Kreidenweis, 2007). Because the chemical composition of the OC fractions is largely unknown, we assign $\kappa_{org}$ values of 0.08 for organic mass from OC1 (OM1), 0.10 for OC2 (OM2), 0.12 for OC3 (OM3), and 0.13 for OC4 (OM4). Lower-bound organic water contributions are estimated by assigning $\kappa_{org}$ values of 0.01 to OM1, 0.02 to OM2, 0.03 to OM3, and 0.04 to OM4, and upper-bound contributions are estimated using $\kappa_{org}$ values of 0.17 for OM1, 0.18 for OM2, 0.19 for OM3, and 0.20 for OM4. These $\kappa_{org}$ assignments preserve differences in OC fractions, even when TOC does not change, and encompass the full range of typical values given in Petters and Kreidenweis (Petters and Kreidenweis, 2007). Additionally, surface extinction was calculated using the IMPROVE algorithm as described in Pitchford et al. 2007, which predicts measured median values better than extremes (Pitchford et al., 2007).

Monthly AOT values from the MODIS onboard the Terra satellite, available as a Level-3 monthly gridded product at a 1x1 degree resolution, across the CONUS were obtained from public archives (National Aeronautics and Space Administration, 2018b) on 28 September 2018 for evaluation in the Appalachia and CO Plateau focus regions (Figure A1). The combined AOT at 550 nm closest to each site was used, calculated using the daily average corrected AOT over land. We investigate seasonal MODIS-derived AOT measurements (Levy et al., 2013; Remer et al., 2005) from January 2007 to August 2016. Monthly aggregates of single overpass MODIS AOT and of daily average particle speciation measurements are used for comparison (Figure A2). Previous analysis suggests monthly aggregation is suitable to resolve temporal mismatches

in sampling due to cloud cover (Christopher and Gupta, 2010). Additionally, publicly available (National Aeronautics and Space Administration, 2018a) daytime, cloud-free Level-3 monthly average CALIPSO-derived extinction coefficients and AOT from the CALIOP lidar (Tackett et al., 2018), available at the 5-degree longitude, 2-degree latitude, and 60 m vertical resolution, were obtained on 16 February 2018 at 532 nm by taking the pixel closest to each site. Quality control for MODIS and CALIOP data follow the algorithms by Platnick et al. 2015 and Tackett et al. 2018, respectively (Platnick, 2015; Tackett et al., 2018). CALIPSO data are used to examine AOT vertical profiles and to supplement MODIS AOT observations. Differences between 532 nm and 550 nm AOT are minimal, especially over the long-term timescales used here. MODIS AOT is primarily used for quantitative analysis, as MODIS Terra overpass is at 10:30 local time each day, while CALIPSO overpass is at 13:32 local time every 16 days. AERONET AOT (Holben et al., 1998) at 500 nm is used to confirm spatial representativeness of MODIS in these regions. The root mean square error is small (<0.1) when comparing monthly averages for both regions and seasons (Figure A3 and Table A1).

Seasonal differences in particle-phase species mass concentrations and AOT data are analyzed between summer and winter. In both the Appalachia and CO Plateau regions, a well-mixed boundary layer is assumed (Jin et al., 2019; Wagner et al., 2015). ALW is calculated using layer-specific temperature and relative humidity and daily average species mass concentrations. Layer meteorological data is obtained from the NARR and the limits of integration are applied at each site individually from the surface to the top of the NARR-derived PBL. Overestimates of PBL height can arise with the NARR in areas of increased elevation (Lee and De Wekker, 2016). ALW concentrations in each layer are calculated thermodynamically and with the ZSR mixing

rule using the methods described above and previously (Nguyen et al., 2015, 2016b). Column values are estimated as a Riemann sum. All regression statistics are calculated using the lm function in R statistical software (R Core Team, 2013).

## 2.4 Results and Discussion

Decadal changes in aerosol chemical composition relevant to particle radiative effects (Alston and Sokolik, 2018; Jin et al., 2019) qualitatively match remotely sensed trends in Appalachia during summer. Statistically significant decreases over time (2007-2016) are found in Appalachia during summer for $PM_{2.5}$, inorganic ALW, $SO_4^{2-}$, total organic mass (TOM) driven by OM2, AOT, and IMPROVE-estimated surface extinction (Table 2.1 and Figures 2.1, A4). During this time period, summertime $PM_{2.5}$ mass that includes ALW decreases by 73%. MODIS and CALIPSO AOT decrease by 55% and 52%, respectively. In Appalachia during winter, statistically significant decreases are found for $PM_{2.5}$, inorganic ALW, $SO_4^{2-}$, $NO_3^-$, total organic mass (TOM) driven by OM1 and OM2, and IMPROVE-estimated surface extinction but not in remotely sensed AOT. Correlations between MODIS-derived AOT and IMPROVE-estimated extinction at the surface are robust during the summer in both Appalachia ($R^2$=0.76) and the CO Plateau ($R^2$=0.69) (Table A2). Wintertime correlations are low in both regions. Over the CO Plateau there is no statistically significant change in either satellite-retrieved AOT for the time period, and the only significant decadal change in surface-derived observations is for wintertime TOM driven by OM2 (Table 2.1). There is no statistically robust trend in organic ALW over time for either region or season.

**Table 2.1.** Correlation ($R^2$) and significance values from linear trend analyses of species trends over time for seasonal annual surface particle chemical component mass concentrations, MODIS AOT, CALIPSO AOT, and IMPROVE-estimated extinction over time from 2007 to 2016. Bolded values indicate significant correlations.

| Species, Season, and Region | $R^2$ (Species vs. Time) | p-value |
|---|---|---|
| ***Appalachia Summer*** | | |
| **$PM_{2.5}$** | **0.66** | **<0.01** |
| **Inorganic ALW** | **0.92** | **<0.01** |
| Organic ALW | 0.21 | 0.10 |
| **Sulfate** | **0.82** | **<0.01** |
| Nitrate | -0.12 | 0.95 |
| **TOM** | **0.38** | **0.03** |
| OM1 | 0.30 | 0.06 |
| **OM2** | **0.72** | **<0.01** |
| OM3 | 0.09 | 0.20 |
| OM4 | 0.21 | 0.10 |
| **MODIS AOT** | **0.47** | **0.02** |
| **CALIPSO AOT** | **0.43** | **0.02** |
| **Extinction** | **0.84** | **<0.01** |
| ***Appalachia Winter*** | | |
| **$PM_{2.5}$** | **0.77** | **<0.01** |
| **Inorganic ALW** | **0.41** | **0.03** |
| Organic ALW | 0.15 | 0.15 |
| **Sulfate** | **0.68** | **<0.01** |
| **Nitrate** | **0.37** | **0.04** |
| **TOM** | **0.45** | **0.02** |
| **OM1** | **0.41** | **0.03** |
| **OM2** | **0.58** | **0.01** |
| OM3 | 0.08 | 0.21 |
| OM4 | 0.22 | 0.10 |
| MODIS AOT | <0.01 | 0.34 |
| CALIPSO AOT | <0.01 | 0.87 |
| **Extinction** | **0.65** | **<0.01** |
| ***CO Plateau Summer*** | | |
| $PM_{2.5}$ | -0.03 | 0.41 |
| Inorganic ALW | -0.02 | 0.39 |
| Organic ALW | 0.03 | 0.28 |
| Sulfate | 0.29 | 0.06 |
| Nitrate | 0.01 | 0.32 |
| TOM | 0.02 | 0.30 |
| OM1 | 0.20 | 0.11 |
| OM2 | 0.40 | 0.03 |
| OM3 | -0.12 | 0.94 |
| OM4 | -0.08 | 0.60 |
| MODIS AOT | -0.08 | 0.57 |

| | | |
|---|---|---|
| CALIPSO AOT | 0.10 | 0.19 |
| Extinction | 0.10 | 0.19 |
| ***CO Plateau Winter*** | | |
| $PM_{2.5}$ | 0.19 | 0.12 |
| Inorganic ALW | 0.12 | 0.17 |
| Organic ALW | -0.05 | 0.47 |
| Sulfate | 0.14 | 0.15 |
| Nitrate | 0.03 | 0.28 |
| **TOM** | **0.35** | **0.04** |
| OM1 | -0.003 | 0.35 |
| **OM2** | **0.53** | **0.01** |
| OM3 | -0.001 | 0.35 |
| OM4 | 0.26 | 0.08 |
| MODIS AOT | -0.03 | 0.41 |
| CALIPSO AOT | <0.01 | 0.45 |
| Extinction | 0.20 | 0.11 |

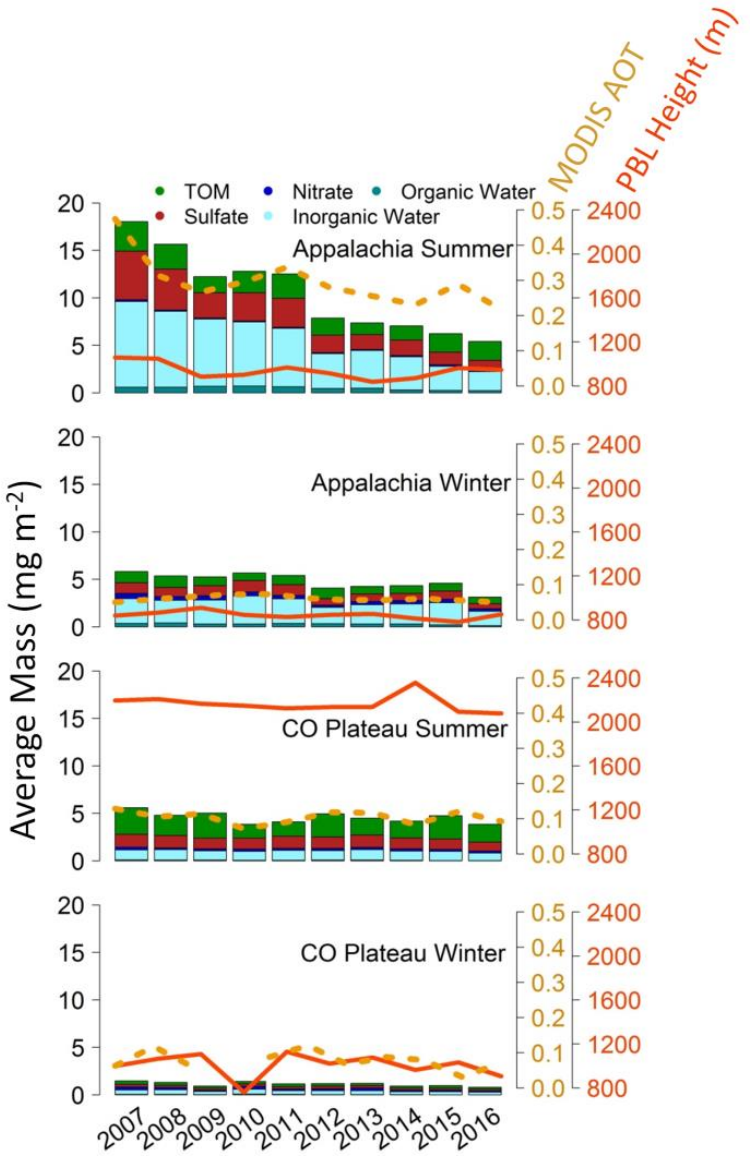


**Figure 2.1.** Seasonal average aerosol compositional mass by year integrated through the PBL for each region from 2007 to 2016 using PM measurements and estimated inorganic and organic water content. In each stacked bar, green corresponds to TOM, red corresponds to $SO_4^{2-}$, dark blue to $NO_3^-$, light blue to inorganic ALW, and turquoise to organic ALW. Seasonal average MODIS AOT (dotted yellow line) and PBL height (solid orange line) over time is overlaid for each region and season.

Monthly averaged column-integrated MODIS AOT and $PM_{2.5}$ mass correlations over Appalachia and the CO Plateau are consistently low ($R^2 < 0.2$), with the exception of Appalachia summer (Figures 2.1, 2.2, and Table A3). Daily (24-hour) integrated surface measurements of particle

mass, chemical constituents and the related extinction change over a day (Guo et al., 2015; Nguyen et al., 2014c). However, AOT values are calculated from a single overpass for sun-synchronous satellites such as Terra and CALIOP. Further, CALIPSO-retrieved extinction coefficients increase with height and are enhanced above the PBL during the summer in Appalachia, consistent with other findings for the southeast U.S. (Ford and Heald, 2013; Wagner et al., 2015). Aloft (>1200m) extinction is enhanced during winter in the CO Plateau (Figure 2.3). Differences in temporal resolution and aloft extinction contribute to discrepancies between remotely sensed aerosol and integrated fine particle mass.

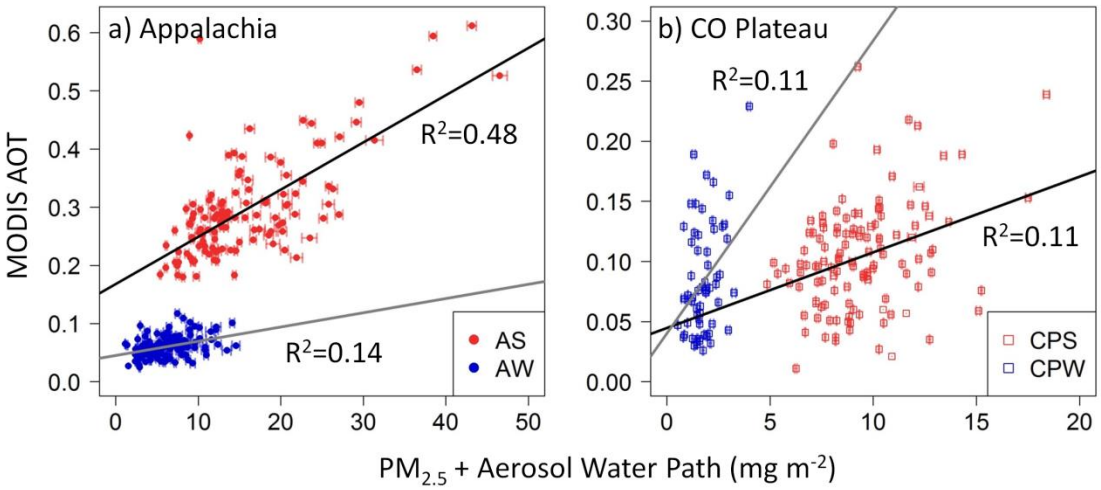


**Figure 2.2.** Monthly dry $PM_{2.5}$ and total (inorganic + organic) ALW mass integrated through the PBL and MODIS AOT from 2007 to 2016 for all focus sites in (a) Appalachia and (b) the CO Plateau summer (red) and winter (blue). Note that the axes are not equal between panels. The horizontal error bars indicate the potential range of water contributed by organics, with the left-hand side representing low $\kappa_{org}$ values (0.01-0.04) and right-hand side representing high $\kappa_{org}$ values (0.17-0.20). Note some horizontal bars are smaller than the marks.

Patterns in CALIPSO-retrieved extinction coefficients qualitatively match ALW trends (Figures 2.3, A5). Within the boundary layer, both CALIPSO extinction and ALW estimates exhibit strong seasonal differences in Appalachia. ALW differs on average by a factor of 2 from winter to summer, and CALIPSO extinction by a factor of 4 in Appalachia. CALIPSO-measured extinction increases with height within the boundary layer in Appalachia, as does ALW (Figure 2.3). Estimates of radiative forcings in the southeast US at the top of the atmosphere and at the surface are more similar in winter than in summer (Alston and Sokolik, 2018). ALW mass concentrations and vertical change in ALW are substantially less in winter than in summer, consistent with boundary layer CALIPSO patterns and independent radiative transfer calculations (Alston and Sokolik, 2018). There is no statistically discernible seasonality in CALIPSO extinction or ALW over the CO Plateau.

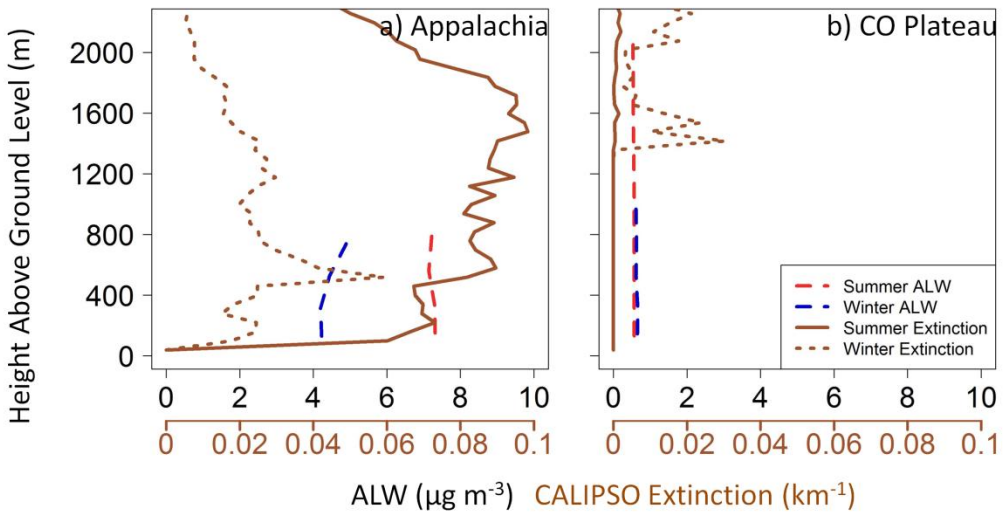


**Figure 2.3.** Vertical profiles of 2007-2016 average total (inorganic + organic) water and CALIPSO-measured extinction coefficients for (a) Appalachia and (b) the CO Plateau. In both panels, red lines indicate summer ALW content, blue lines indicate winter ALW content, and brown lines indicate summertime (solid) and wintertime (dashed) CALIPSO-retrieved extinction at 532 nm.

Seasonal differences in particle chemical constituents and AOT are noted in Appalachia, but only particle composition in the CO Plateau (Figures 2.1, 2.4). MODIS AOT is highest over Appalachia in summer when both PBL and aerosol mass concentrations are highest in the region (Figure 2.1). Seasonal change in both AOT and total $PM_{2.5}$ mass (dry + wet) is greatest in Appalachia. In the CO Plateau, seasonal PBL change is substantial (Figure 2.1). The highest PBL and surface mass are both observed in summer, but neither column-integrated AOT nor surface extinction coefficients (Figure A4) are enhanced relative to winter values in this region. In the CO Plateau, seasonal differences are greatest for OM. Spatial and seasonal differences in organic matter are enhanced over OC seasonality when region-specific OM:OC ratios are applied to measured OC mass (Figures 2.4, A6-A8). From 2007-2016, integrated TOM in the CO Plateau is 1.9 mg $m^{-2}$ higher in summer over winter on average, and fluctuations in Appalachia average 1.2 mg $m^{-2}$. Integrated OM seasonality fluctuates most in OM2 and OM3 over both the CO Plateau and Appalachia. On average, OM2 and OM3 decrease by 0.52 and 0.83 mg $m^{-2}$ from summer to winter in the CO Plateau, and by 0.54 and 0.31 mg $m^{-2}$ in Appalachia, respectively.

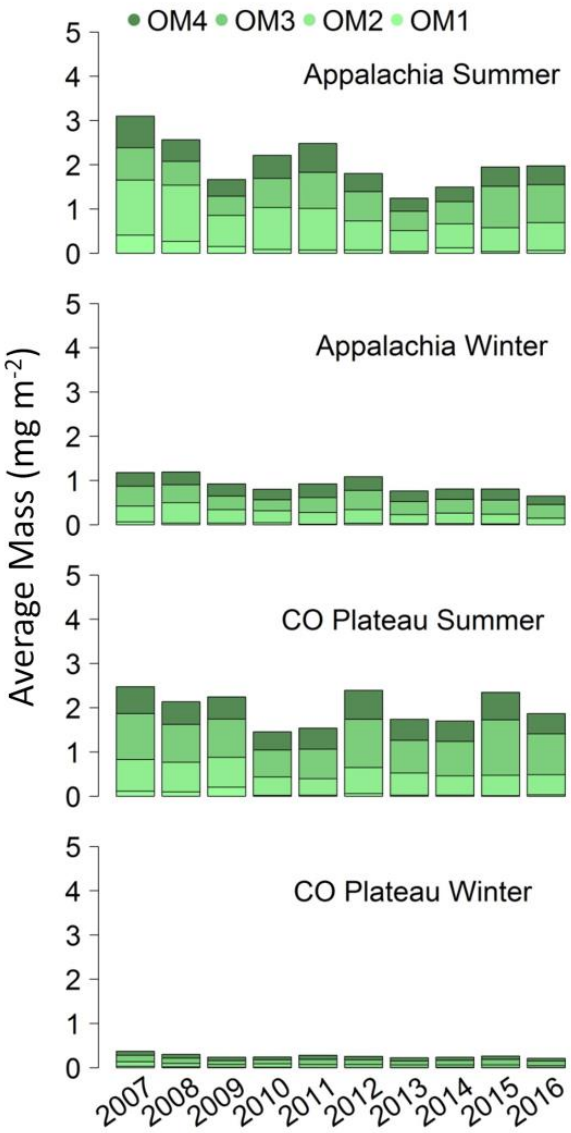


**Figure 2.4.** Seasonal average OM mass from each OC fraction by year integrated from the surface through the PBL for each region from 2007 to 2016. In each stacked barchart, OM1 is the lightest green (bottom stack), and OM4 is the darkest green (top stack).

In Appalachia, seasonal differences in $PM_{2.5}$, inorganic ALW, $SO_4^{2-}$, $NO_3^-$, OM2, and estimated surface extinction decrease over the past decade (Table A4). From 2007 to 2016, seasonality in $PM_{2.5}$ over Appalachia that includes ALW decreases by 81%, and MODIS and CALIPSO AOT decrease by 62% and 54%, respectively (Table A4). In the Southeast U.S., annual trends of seasonal differences in surface visibility and ground-based measured extinction have decreased

(Attwood et al., 2014; Li and Martin, 2018). Alston and Sokolik 2018 estimate radiative transfer for the southeast U.S. and find summertime radiative forcings at the surface are greater than in wintertime (Alston and Sokolik, 2018). That seasonality resembles seasonal patterns for ALW estimates in the region described here. Seasonality in the CO Plateau does not change from 2007-2016 significantly for any surface-measured or estimated variable, nor remotely sensed AOT considered in this work (Table A4).

ALW mass contributions dominate over $PM_{2.5}$ dry mass in Appalachia in summer and winter. Yet, correlations between monthly average MODIS-derived AOT and integrated $PM_{2.5}$ mass improve only slightly from dry mass only correlations when ALW is considered (Table A3), and the changes are not statistically significant. On average in Appalachia, inorganic ALW is a factor of 10 larger than organic ALW in summer and a factor of 8 in winter. Although ALW from organic aerosol constituents is typically less than from inorganic constituents, organic contributions can contribute substantially to uncertainty in ALW mass (Nguyen et al., 2015). Sensitivities to explore potential impacts of changes in particle organic chemical composition do not significantly change associations between integrated $PM_{2.5}$+ALW and MODIS AOT (Table A3). This range of potential organic ALW is shown as error bars in Figures 2.2 and A9 and demonstrates that correlations with MODIS AOT are not improved by consideration of organic species contribution to ALW as estimated using routine air quality monitoring network data. A lack of chemically specific detail in aerosol OM speciation is a large source of uncertainty. However, the large uncertainties in OM and related ALW uptake have a negligible effect on satellite AOT-surface $PM_{2.5}$ associations, similar to recent findings by Jin et al. 2019.

Changing atmospheric composition in the Southeast U.S. is linked to reductions in anthropogenic emissions, in particular for those that contribute to particle hygroscopic species (Carlton et al., 2018b; Nguyen et al., 2015; Tosca et al., 2017), and these findings are consistent with the decadal and seasonal trends for the atmospheric burden of $PM_{2.5}$+ALW over Appalachia presented here. The effects of intrinsic chromophoric and hygroscopic properties of individual compounds present in aerosol that directly and indirectly affect extinction may be observed by satellite-based systems but are poorly described in current approaches to link to surface measurements of routinely available data. Emissions and particulate chemical composition vary seasonally and spatially, in particular for organic species (Goldstein et al., 2009; Hand et al., 2012, 2013; Schichtel et al., 2017). This is not reflected in surface measurements of particulate TOC (i.e., total organic carbon only) mass. Fourier-transform infrared spectroscopy (Kamruzzaman et al., 2018; Ruthenburg et al., 2014; Weakley et al., 2016) of IMPROVE filters describes the presence of diverse organic species such as carbonyls, alcohols, carboxylic acids, organonitrates, amines, and aromatics. Light-absorbing carbon may affect remote AOT measurements, such as primary brown carbon from forest fires and residential coal combustion (Alexander et al., 2008; Andreae and Gelencsér, 2006; Bond and Bergstrom, 2006), and oxidation of biogenic gas-phase compounds exposed to reduced nitrogen compounds (Bones et al., 2010; Laskin et al., 2010; Updyke et al., 2012), the hydroxyl radical, or direct photolysis (Hems and Abbatt, 2018; Zhao et al., 2015). Xue et al. 2009 find aerosol coatings of succinic and glutaric acids increase light scattering up to 3.8-fold. Routinely available individual OC fractions provide an indication of volatility, which is suggestive of chemical differences but not identity. Seasonal and spatial differences are pronounced in OM when measurement of organic fractions and non-carbon organic mass are considered. OM2 varies substantially between Appalachia and

the CO Plateau and by season (Figures A6, A7). Dicarboxylic salts are hygroscopic, evolve in OM2 (Kawamura and Bikkina, 2016), and may be important for overall ALW and subsequently extinction and AOT. However, dicarboxlyic compounds also co-evolve in other IMPROVE OC fractions (Meier and Schwab, 2011). Detailed particle chemical composition and size measurements improve understanding of the properties and controlling factors that determine subsequent radiatively important aerosol impacts (Brock et al., 2016; Jin et al., 2019). The chemical detail and knowledge needed to adequately describe subsequent impacts on aerosol extinction are lost in the context of volatility-defined TOC measurements (Meier and Schwab, 2011). Development and application of methods that chemically identify individual compounds in different OC volatility fractions is a critical open area and may improve understanding of $PM_{2.5}$-AOT relationships over long time periods and large spatial scales to better reconcile satellite- and surface-based measurements.

## 2.5 Conclusions

Decadal, seasonal, and spatial change in $PM_{2.5}$ that includes ALW is positively associated with AOT most closely in Appalachia during summer. Correlations are low elsewhere and not significantly changed upon consideration of organic and inorganic contributions to ALW. However, within the boundary layer, spatial trends, seasonal patterns, and vertical profiles of remotely sensed extinction qualitatively match patterns in integrated ALW. Discrepancies between surface measurement integrations and satellite-derived AOT arise from poorly described particle chemical composition and limits on approaches to quantitatively extrapolate surface measurements to elevations aloft. Long-term trends of the atmospheric $PM_{2.5}$ burden are limited in data availability to routine measurements, which lack chemical detail for organic species.

Organic speciation is a major source of uncertainty for aerosol chemical composition and is an area for future study.

# CHAPTER 3

## DIFFERENCES IN FINE PARTICLE CHEMICAL COMPOSITION ON CLEAR AND CLOUDY DAYS

Reproduced under the Creative Commons Attribution 4.0 License from Christiansen, A.E.; Carlton, A.G.; Henderson, B.H., Differences in Fine Particle Chemical Composition on Clear and Cloudy Days. *Atmospheric Chemistry and Physics Discussions* **2020**, DOI: 10.5194/acp-2020-184.

## 3.1 Abstract

Clouds are prevalent and alter fine particulate matter ($PM_{2.5}$) mass and chemical composition. Cloud-affected satellite retrievals are subject to higher uncertainty and are often removed from data products, hindering quantitative estimates of tropospheric chemical composition during cloudy times. We examine surface $PM_{2.5}$ chemical constituent concentrations in the Interagency Monitoring of PROtected Visual Environments (IMPROVE) network in the United States during Cloudy and Clear Sky times defined using Moderate Resolution Imaging Spectroradiometer (MODIS) cloud flags from 2010-2014 with a focus on differences in particle hygroscopicity and aerosol liquid water (ALW). Cloudy and Clear Sky periods exhibit significant differences in $PM_{2.5}$ mass and chemical composition that vary regionally and seasonally. In the eastern US, relative humidity alone cannot explain differences in ALW, suggesting emissions and *in situ* chemistry exert determining impacts. An implicit clear sky bias may hinder efforts to quantitatively understand and improve representation of aerosol-cloud interactions, which remain dominant uncertainties in models.

## 3.2 Introduction

At any given time, visible clouds cover over 60% of the Earth's surface (King et al., 2013), and a warming climate causes cloud cover to change (Norris et al., 2016). Average cloud fraction values over the contiguous US (CONUS) are ~40% year-round with higher values in winter (44-54%) than summer (26-34%) (Ju and Roy, 2008; Kovalskyy and Roy, 2015). Clouds act as atmospheric aqueous phase reactors, and their condensed phase oxidative chemistry generates particle mass aloft, such as sulfate (Zhou et al., 2019), water-soluble organic carbon (Carlton et al., 2008; Duong et al., 2011), and organo-sulfur compounds (Pratt et al., 2013). Clouds are the primary drivers of vertical transport in the atmosphere, moving trace species from the boundary layer to the free troposphere (FT) (Ervens, 2015). The radiative impacts of aerosols in the FT are substantial, especially when located above clouds where they scatter and absorb both incoming solar radiation and diffuse back scatter from clouds (Seinfeld, 2008). Aerosol-cloud interactions are complex and a critical uncertainty in model projections (Fan et al., 2016).

Atmospheric chemistry laboratory studies, ambient sampling, modeling, and analysis strategies are often designed in ways that minimize cloud and water influences. This leads to an implicit, yet persistent clear sky bias in the quantitative understanding of tropospheric composition. During atmospheric chemistry field campaigns, aircraft typically avoid clouds, and direct measurement of in-cloud particle chemical composition is rare (Wagner et al., 2015). There is increased error in remotely sensed aerosol optical thickness (AOT) retrieval techniques during cloudy times (Martin, 2008), and impacted retrievals are screened from final data products to avoid measurement artifacts. Most validation of satellite-derived AOT through comparison to surface measurements, such as those from sun photometers used to retrieve AOT from the

ground up, is conducted for cloud-free periods (Liu et al., 2018). Air quality models are often evaluated with cloud-free satellite retrievals (van Donkelaar et al., 2010; Guo et al., 2017; de Hoogh et al., 2016; Song et al., 2014; Tian and Chen, 2010) and cloud-free aircraft samples (Bray et al., 2017; McKeen et al., 2009). This biases model development and predictive skill toward cloud-free conditions and hinders accurate prediction of trace species during cloudy time periods. Laboratory experiments to understand particulate matter formation are conducted under dry conditions (e.g., Lamkaddam et al., 2017; Ng et al., 2007) atypical of cloudy time periods. Should differences in aerosol physicochemical properties exist between cloudy and clear sky time periods, current approaches are limited in their ability to quantitatively assess those differences. This is a key knowledge gap.

Characterization of fine particulate matter ($PM_{2.5}$) mass and chemical composition in the US primarily relies on surface measurements from relatively sparsely spaced monitors. At various locations across the CONUS, the Interagency Monitoring of PROtected Visual Environments (IMPROVE) network samples every 3 days, and the Chemical Speciation Network (CSN) samples every 3 or 6 days (US Environmental Protection Agency, 2008). To improve upon surface network spatial and temporal limitations, data can be interpolated to describe particle mass (Li et al., 2014; Zhang et al., 2018a) and chemical composition over larger areas (Liu et al., 2009; Tai et al., 2010). Satellite information can also be used (van Donkelaar et al., 2015b), such as the Moderate Resolution Imaging Spectroradiometer (MODIS) instruments aboard the Aqua and Terra satellite platforms. These view the entire Earth surface every 1 to 2 days and are used to impart information for use in air quality applications (van Donkelaar et al., 2015b; Gupta et al., 2006; Kloog et al., 2011; Sorek-Hamer et al., 2016). Many advanced satellite AOT models

translate space-based radiation measurements to surface $PM_{2.5}$ (van Donkelaar et al., 2010, 2015b, 2015a; Gupta et al., 2006; Kessner et al., 2013; Kloog et al., 2011; Kumar et al., 2007; Liu et al., 2011; Schaap et al., 2009; Wang et al., 2012; Wang and Christopher, 2003) and employ sophisticated techniques that account for aerosol size and type, vertical extinction, mass, and relative humidity (RH) (van Donkelaar et al., 2010). Evaluation of AOT-to-$PM_{2.5}$ techniques finds that monthly aggregated AOT can robustly estimate relationships spanning five years of daily mean values over North America ($R>0.77$) (van Donkelaar et al., 2010). While temporal and geospatial satellite AOT is useful for understanding trends in $PM_{2.5}$ concentrations (van Donkelaar et al., 2015b; Sorek-Hamer et al., 2016; Wang and Christopher, 2003), an implicit constraint for this and other similar findings is that such agreement is for clear sky conditions.

Surface networks record $PM_{2.5}$ mass and chemical composition during clear sky and cloudy time periods alike. The difference between spatially and temporally aggregated $PM_{2.5}$ mass concentrations in the CONUS for cloudy and all sky (cloudy + clear sky) conditions is estimated to be $\pm 2.5$ μg $m^{-3}$ (Christopher and Gupta, 2010). Less attention has been given to clear sky and cloudy differences in $PM_{2.5}$ chemical composition, especially with regards to particle hygroscopicity and water uptake. Aerosol mass concentrations and chemical speciation including aerosol liquid water (ALW) influence AOT (Christiansen et al., 2019; Malm et al., 1994; Nguyen et al., 2016b; Pitchford et al., 2007), cloud microphysics, and mesoscale convective systems (Kawecki and Steiner, 2018), including storm morphology and precipitation patterns (Kawecki et al., 2016). Particle chemical composition modulates particle size via water uptake. Particle size is a determining factor in light scattering by particles, which is important for aerosol radiative calculations. An implication of this work is that if particle hygroscopicity changes from clear sky

to cloudy time periods, when aerosol-cloud interactions are most important, a quantitative understanding remains unclear.

In this work, we test the hypothesis that there are quantitative differences in $PM_{2.5}$ chemical composition between cloudy and clear sky time periods in ways important for water uptake. We employ a combination of satellite products, surface measurements, and thermodynamic modeling to analyze annual and seasonal trends in chemical climatology regions across the CONUS. We assess and quantify seasonal statistical significance (Kahn, 2005) for differences in distributions of RH, $PM_{2.5}$, and chemical speciation during cloudy and clear sky times using surface measurements from the IMPROVE network from 2010-2014 within the context of MODIS cloud flag values. Further, we examine one chemical climatology region in detail, the Mid South, as a case study. This region encompasses the location of the Atmospheric Radiation Measurement Southern Great Plains (SGP) site in an area of the CONUS that experiences varied weather patterns, a broad range of cloud conditions, and distinct seasonal variations in temperature and humidity (Sisterson et al., 2016).

## 3.3 Data and Methods

Cloudy and clear sky classifications are determined using publicly available data (National Aeronautics and Space Administration, 2018b) from MODIS on the Aqua and Terra satellites. Pairing of satellite and surface $PM_{2.5}$ mass measurements typically works best in rural and vegetated locations, where the spectral properties of the background tend to be dark and vary little over the space of a satellite grid cell (Hauser, 2005; Jones and Christopher, 2010). For this reason, we use rural IMPROVE network sites that are located primarily in national parks,

although improvements have been made for retrievals over bright surfaces (Hauser, 2005; Hsu et al., 2004, 2006, 2013; Zhang et al., 2016). We use 500 m resolution pixels that contain the IMPROVE sites. Retrievals are flagged as cloudy if QA flags specifically identified clouds as preventing retrieval, or if 2.1-micrometer reflectance was too high (r>0.35) and the fraction of 500 m sub pixels that were cloudy was greater than 44.4%. We choose 44.4% because it is a fundamental limit of the algorithm (Remer et al., 2013). IMPROVE monitors are frequently under a MODIS swath with valid retrievals even if the pixel containing the IMPROVE station is not successfully retrieved. As an alternative to the IMPROVE pixel, we employ a method for quality assurance, a 17x17 grid. This allows for any retrieval within a 50 km x 50 km area to represent the IMPROVE station. If all 17x17 pixels are not retrieved, then the state over the monitor is determined to be cloudy. The 17x17 grid approach is much more likely to attribute non-retrieved data to clouds (98.5%) than the containing pixel approach, which attributes 89.8% of non-retrieved data to clouds. Misidentifying non-retrievals as cloudy is unlikely to substantially affect interpretation, as the sample size is large (N>70,000 total observations, and N>1500 for an individual region).

IMPROVE network data were downloaded on 13 July 2015 and 26 May 2016 from public archives (IMPROVE Network, 2019) for 132 unique sites across the CONUS with complete data records for the years 2010-2014 (Figure B1a). IMPROVE data are collected every 3 days. We investigate 24-hour average $PM_{2.5}$ mass, ALW, RH, sulfate ($SO_4^{2-}$), nitrate ($NO_3^-$), and total organic carbon (TOC) mass concentrations. Other species affect particle hygroscopic properties but are not widely measured in routine networks. For example, we investigate TOC as a whole even though primary and secondary species affect water uptake differently. There is no direct

measurement of either in routine monitoring network operations, although fractionation can sometimes be used to infer information about sources and formation processes (Aswini et al., 2019; Cao et al., 2005; Chow et al., 2004). We group IMPROVE sites across the CONUS into 22 chemical climatology regions defined by the IMPROVE network (Figure B1b) (Hand et al., 2011; Malm et al., 2017). $PM_{2.5}$ mass and composition are provided directly from the IMPROVE database, while ALW is estimated.

ALW is a function of RH, particle concentration, and chemical composition. We estimate ALW using a metastable assumption in the inorganic ($K^+$–$Ca^{2+}$–$Mg^{2+}$–$NH_4^+$–$Na^+$–$SO_4^{2-}$–$NO_3^-$–$Cl^-$–$H_2O$) aerosol thermodynamic equilibrium model ISORROPIAv2.1 (Fountoukis and Nenes, 2007). The metastable state, in which the aerosol is in the aqueous phase and can be supersaturated with respect to dissolved salts, has been observed in field studies in different regions of the United States (Nguyen et al., 2014b; Rood et al., 1989). We use the reverse, open-system problem because only aerosol measurements are available. Particle mass concentration inputs of $SO_4^{2-}$ and $NO_3^-$ are taken from IMPROVE measurements. Ammonium ion is not considered due to limited measurement availability. Dust and organic species are also not considered because water uptake properties are not well constrained (Jathar et al., 2016; Metzger et al., 2018), and there is large spatial heterogeneity in dust. Our approach to employing ISORROPIA introduces uncertainties (e.g., pH estimates would be unreliable (Guo et al., 2015)), but neglect of dust does not affect overall interpretation of ALW mass (Figure B2), consistent with an earlier sensitivity using this technique that included organic species (Nguyen et al., 2015). The temperature and RH were extracted from the North American Regional Reanalysis (NARR) model (Kalnay et al., 1996) similar to Nguyen et al. 2016b.

Cloudy and Clear Sky differences in ALW are investigated in two ways. First, we compare ALW estimated using 24-hour average chemical composition and meteorology and group results into Clear Sky and Cloudy bins using the MODIS cloud flag. We use these daily values when comparing ALW within chemical climatology regions. Second, we investigate trends across the eastern US to isolate the effect of chemical composition. We select the eastern US since ALW concentrations are largest in this region (Figure B3) and it is in cloud often and consistently (cloud fraction 30-50% year-round) (Figure B4). This makes statistical comparisons between Cloudy and Clear Sky times more robust than in the western US, where ALW concentrations and cloud fraction are low in most seasons. We group 24-hour average chemical composition and meteorology into Clear Sky and Cloudy bins and take monthly medians. We perform ALW estimations using the medians via three ISORROPIA calculation scenarios: 1) Clear Sky chemical composition and Clear Sky meteorology ("Clear Sky" scenario), 2) Cloudy chemical composition and Cloudy meteorology ("Cloudy"), and 3) Clear Sky chemical composition and Cloudy meteorology ("Mixed") (Table B1 and Figure B5). We use monthly medians to avoid complications that arise from differing numbers of Cloudy and Clear Sky days in the Mixed scenario. To investigate meteorology and chemical composition impacts separately, we perform the Mixed scenario in order to reproduce studies in which cloud free growth factors (Brock et al., 2016) are eventually applied to models that contain cloudy meteorological conditions (Bar-Or et al., 2012). When the Mixed scenario is significantly different than Cloudy, we can reject the hypothesis that RH and temperature alone explain the difference. Wet deposition is unconstrained in this analysis, but cloud droplets typically evaporate (Pruppacher and Klett, 2010).

Growth factors used in the Mid South region are estimated from a modified Kohler equation (Brock et al., 2016; Jefferson et al., 2017) (Eqn 3.1). We use RH from the NARR and estimate $\kappa_d$, the particle hygroscopicity, from IMPROVE-measured chemical composition mass concentrations and individual species κ values ($\kappa_{SO4}$=0.5, $\kappa_{NO3}$=0.7) (Petters and Kreidenweis, 2007). Here, $gf(D)$ is the hygroscopic diameter growth.

$$gf(D) = (1 + \kappa_d \frac{RH}{100-RH})^{1/3} \quad (3.1)$$

Statistical significance for differences in measurement distributions of $PM_{2.5}$ chemical composition and properties between Cloudy and Clear Sky time periods from 2010-2014 is determined using the Mann-Whitney U Test in R statistical software (R Core Team, 2013). The Mann-Whitney U Test is a non-parametric test that compares two samples to assess whether population distributions differ (McKnight and Najab, 2010). 2010-2014 encompasses typical conditions and coincides with several intensive observation periods including the Southeast Atmosphere Studies (SAS) (Carlton et al., 2018b), the Studies of the Emissions and Atmospheric Composition, Clouds, and Climate Coupling by Regional Surveys ($SEAC^4RS$) (Toon et al., 2016), and the California Research at the Nexus of Air Quality and Climate Change (CalNex) (Ryerson et al., 2013) field campaigns. We define cloud fraction for each region as the number of MODIS-flagged cloudy IMPROVE sampling days over the total number of IMPROVE sampling days. Further, we define winter as December, January, and February (DJF), spring as March, April, and May (MAM), summer as June, July, and August (JJA), and fall as September, October, and November (SON).

## 3.4 Results and Discussion

### 3.4.1 Hygroscopicity and Chemical Composition

Distributions in monthly particle chemical composition across the eastern US in 2010-2014 are sufficiently changed between MODIS-defined Cloudy and Clear Sky times to affect hygroscopicity and alter predicted ALW mass concentrations beyond differences that would arise from changes in meteorology alone (Figure 3.1). These findings are consistent with an analysis in the desert southwest US that shows that chemical composition is an essential factor for improving cloud condensation nuclei predictions (Crosbie et al., 2015). The only difference between the Mixed and Cloudy ALW calculations is that the Mixed scenario employs Clear Sky chemical composition (rather than Cloudy chemical composition) extrapolated to Cloudy meteorology. This type of scenario can occur in model development or satellite validation applications when $PM_{2.5}$-AOT relationships or growth factors remain unmeasured for Cloudy periods (Brock et al., 2016; van Donkelaar et al., 2010; de Hoogh et al., 2016; Tian and Chen, 2010). Previous work using climate models shows that application of ALW uptake that is influenced by incorrect chemical composition significantly affects top of atmosphere radiative forcing estimates and attribution of anthropogenic climate impacts (Rastak et al., 2017). When Clear Sky chemical composition is extrapolated to Cloudy period meteorology ("Mixed"), monthly median ALW concentrations in the eastern US, in all seasons except winter, are significantly different from our best estimate, which employs the actual chemical composition during cloudy periods ("Cloudy"). Interestingly, monthly median Clear Sky and Cloudy scenario ALW concentrations do not differ significantly except during winter despite higher Cloudy RH (Figure 3.2). This is consistent with chemical composition as a determining factor in ALW

(Carlton and Turpin, 2013; Liao and Seinfeld, 2005), CCN (Crosbie et al., 2015), and extinction (Pitchford et al., 2007) on cloudy days because the pattern in ALW is opposite the pattern in RH.

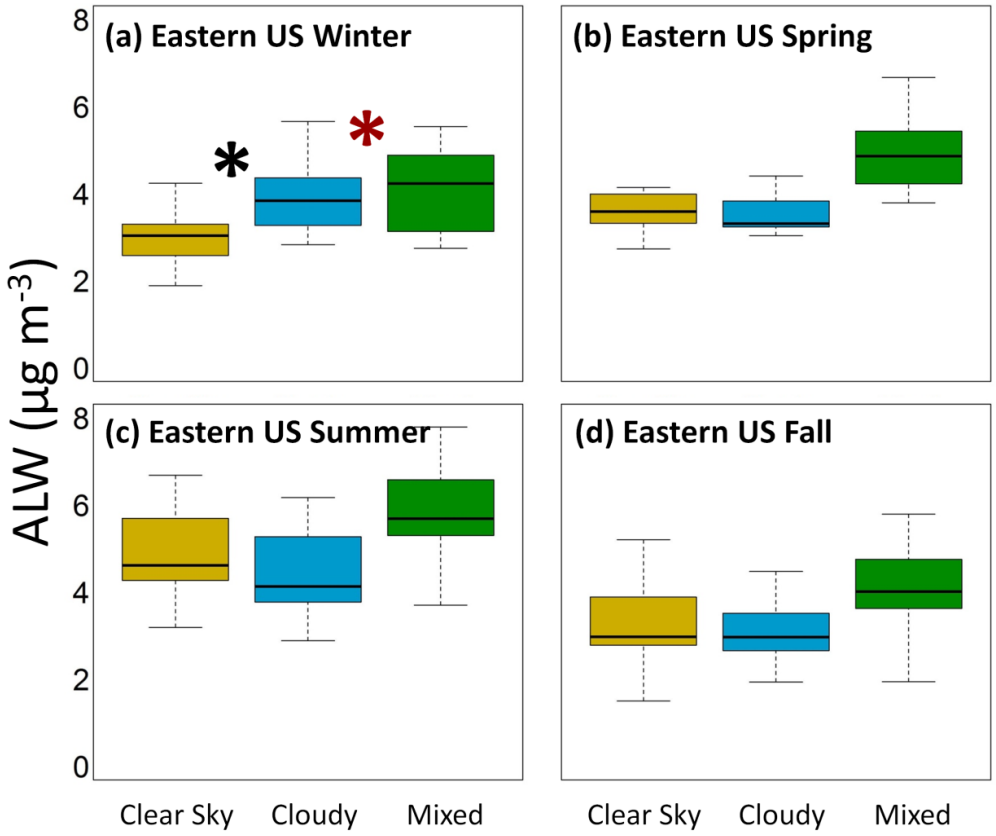


**Figure 3.1.** ALW mass concentrations are significantly different between Clear Sky and Cloudy time periods beyond what would arise from changes solely in meteorology (e.g., RH). Monthly median estimated ALW distributions at each IMPROVE monitor in the eastern US during Clear Sky times (yellow, Clear Sky scenario), Cloudy times (blue, Cloudy scenario), and Cloudy times employing Clear Sky particle chemical composition (green, Mixed scenario). The black asterisk in (a) indicates the only situation where Clear Sky and Cloudy scenarios differ significantly. The red asterisk in (a) indicates the only situation where the Cloudy and Mixed scenarios do *not* differ significantly. The midline in the box is the median, the box boundaries are the 25th and 75th percentiles, and the whiskers are the 10th and 90th percentiles. Potential outliers are not shown but are used in calculations.

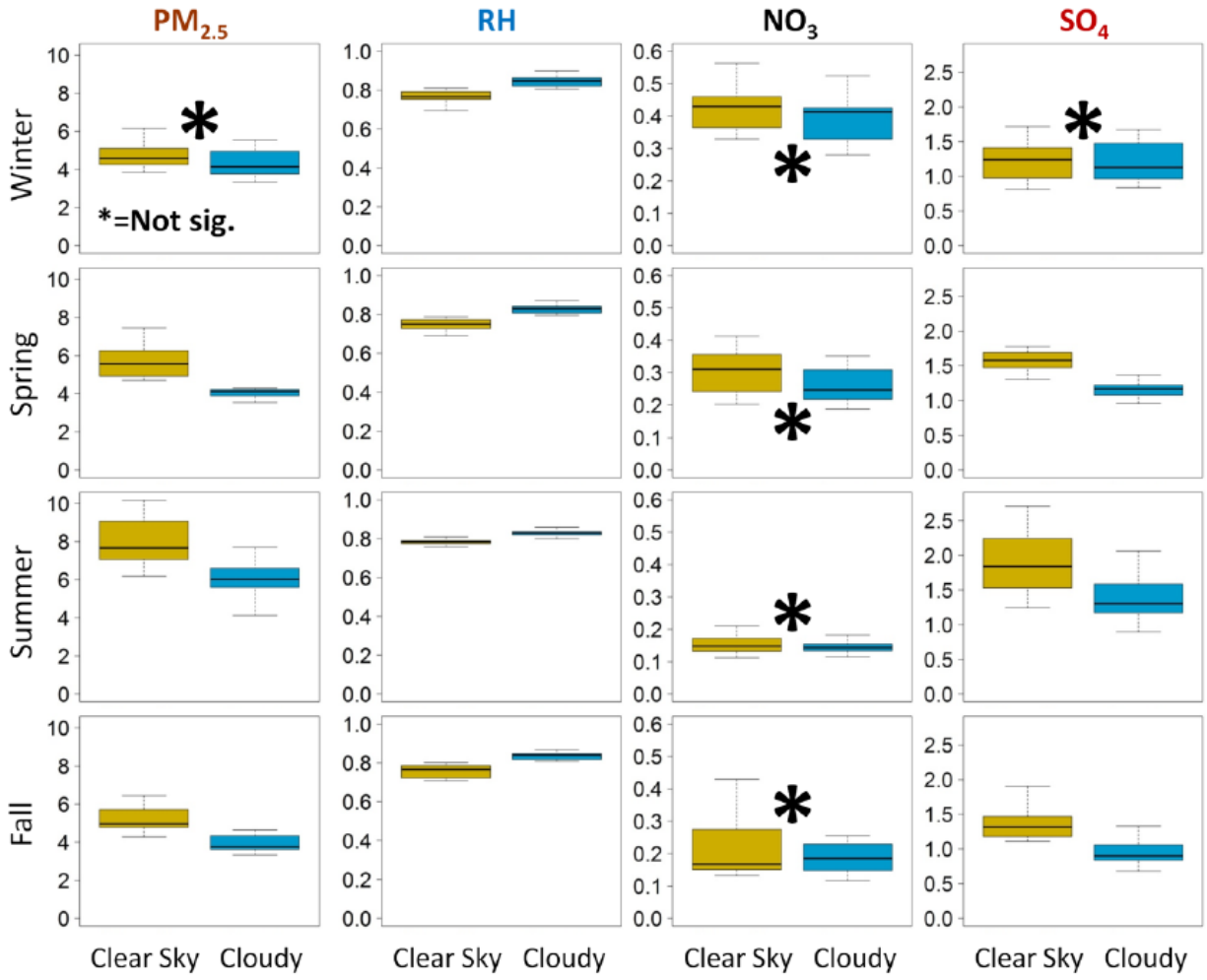


**Figure 3.2.** Box plots of $PM_{2.5}$, RH, $NO_3^-$, and $SO_4^{2-}$ during clear sky times (yellow) and cloudy times (blue) across the eastern US. Note that potential outliers are not shown but are used in calculations. The width of the box plot is proportional to the number of observations. Asterisks denote Cloudy and Clear Sky differences that are *not* significant ($p<0.05$) by the Mann-Whitney U Test.

Clear Sky/Cloudy patterns in $SO_4^{2-}$ and $NO_3^-$ mass concentrations, which affect particle hygroscopicity, vary regionally and seasonally. When aggregated over the eastern US, ALW estimates for the Mixed case are largest during summer and spring and can be explained by elevated Clear Sky $SO_4^{2-}$ and $NO_3^-$ concentrations and high Cloudy RH (Figure 3.2). Generally, Mixed ALW concentrations in the eastern US are higher than for the Cloudy scenario because Clear Sky chemical composition facilitates greater hygroscopicity and Cloudy RH is elevated

(Table B2). A notable exception is the Ohio River Valley during winter, where Cloudy $SO_4^{2-}$, $NO_3^-$, and RH are higher than Clear Sky. In this case, Cloudy period ALW concentrations are higher than for the Mixed scenario. These findings highlight that a changing $PM_{2.5}$ chemical composition has a determining effect on ALW mass concentrations (Nguyen et al., 2016b), a critical element in the estimation of aerosol-cloud interactions and particle radiative impacts. During cloudy periods, when the accurate prediction of ALW and aerosol-cloud interactions is most critical, *in situ* knowledge of $PM_{2.5}$ chemical composition is required.

Differences in daily mass concentrations of fine particle chemical constituents between Cloudy and Clear Sky periods across the CONUS are spatially and temporally different among $PM_{2.5}$ mass and its chemical constituents except in the Northwest region (Figures 3.3-3.7, B6, and Tables B3-B7). These patterns cannot be adequately described as a function of MODIS cloud fraction (Figures B6-B7). If meteorological processes and physical transport are the only controlling factors, then patterns in mass concentrations among $PM_{2.5}$ and constituents should not vary. However, they do, suggesting differences in emissions and/or *in situ* chemical production of $PM_{2.5}$ during Cloudy and Clear Sky time periods. Where differences are significant for ALW, Cloudy ALW is higher than Clear Sky in all seasons, with few exceptions (Figure 3.3 and Table B3). Water uptake contributes to particle growth with a determining impact on particle size and radiative properties. $PM_{2.5}$ mass, greater during Clear Sky times in most regions and seasons, has nearly an opposite pattern to ALW spatial and seasonal trends (Figure 3.4). The largest ALW differences are observed in the central and eastern US during winter. Wintertime Cloudy $SO_4^{2-}$ mass concentrations are greater than Clear Sky (Figure 3.5 and Table B5), and the highest $NO_3^-$ mass concentration differences are observed during Cloudy times in winter when

temperatures are coldest (Figure 3.6 and Table B8). This promotes thermodynamic stability of nitrate in the condensed phase, increasing particle hygroscopicity and facilitating ALW.

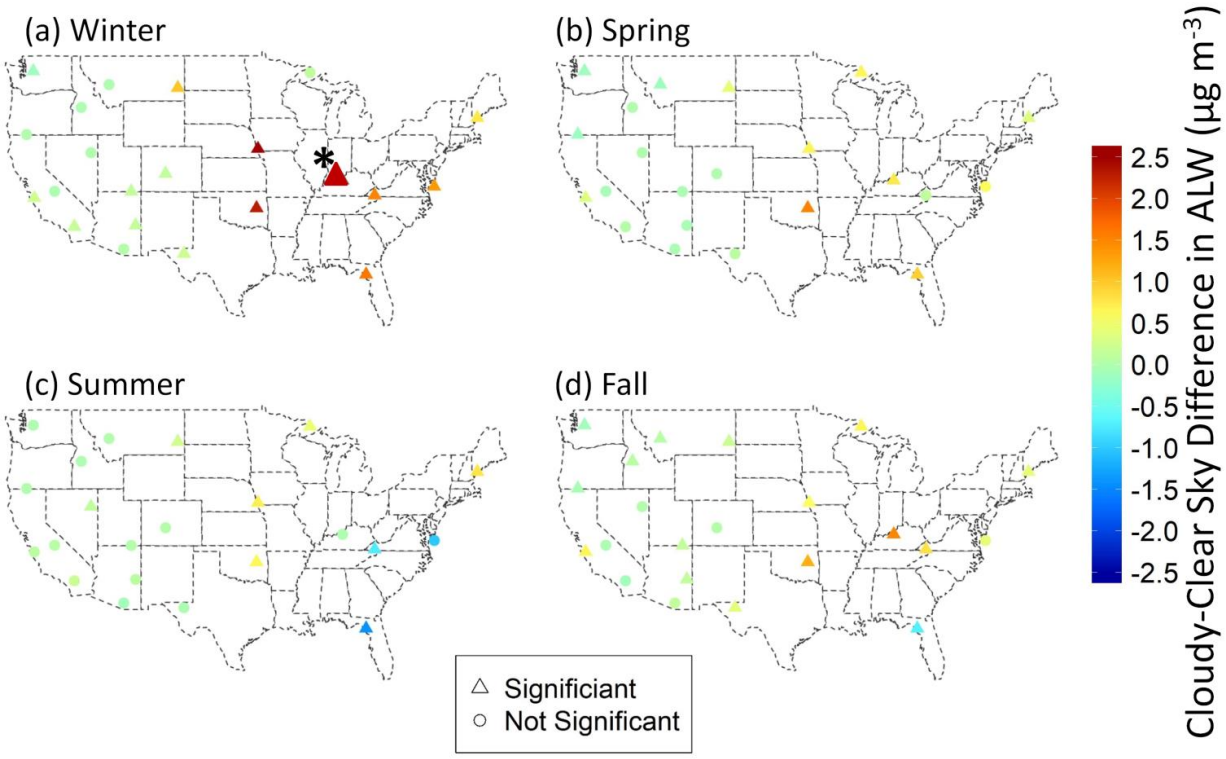


**Figure 3.3.** Maps of the difference in ALW mass concentration medians (Cloudy-Clear Sky) for all regions from 2010-2014 for (a) winter, (b) spring, (c) summer, and (d) fall. The color of the point corresponds to the magnitude of the difference. Triangles indicate that median differences are significant by the Mann-Whitney U Test. Note that the difference in wintertime medians for daily ALW concentrations in the Ohio River Valley (denoted with asterisk) is substantially larger than other regions (Cloudy median value is 4.6 µg $m^{-3}$ larger than Clear Sky).

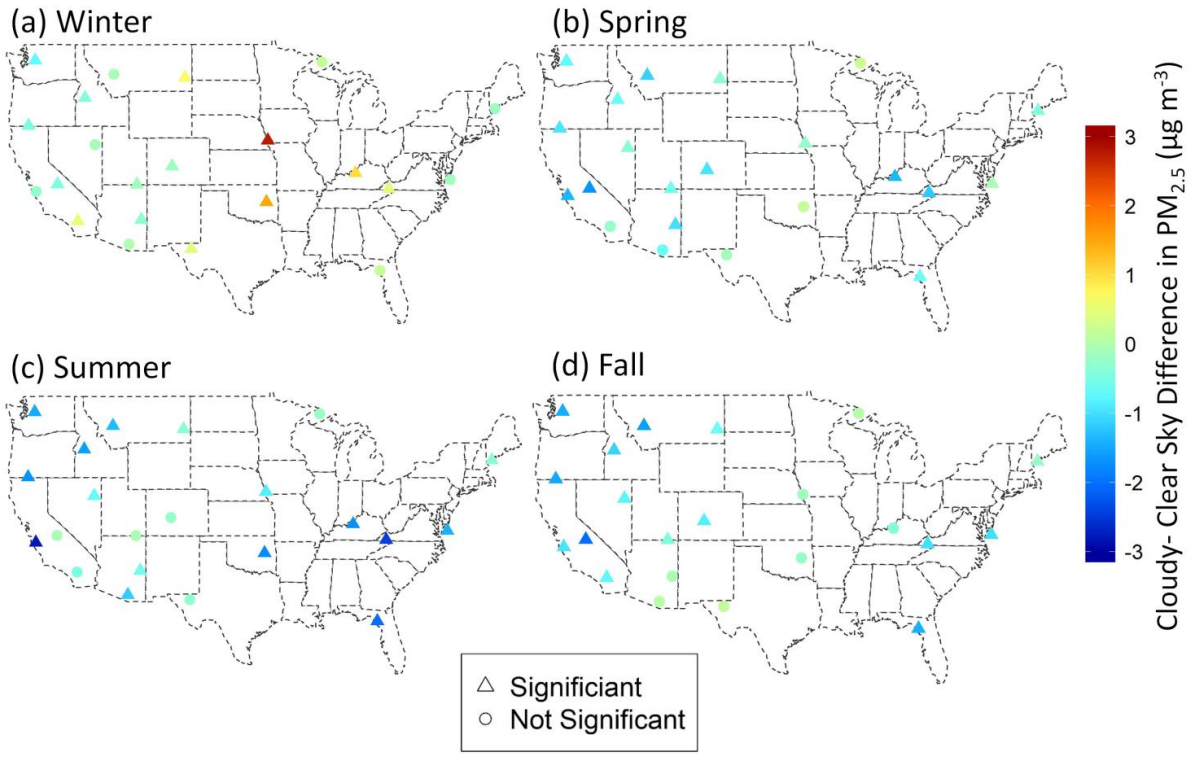


**Figure 3.4.** Maps of the difference in $PM_{2.5}$ mass concentration medians (Cloudy-Clear Sky) for all regions from 2010-2014 for (a) winter, (b) spring, (c) summer, and (d) fall. The color of the point corresponds to the magnitude of the difference. Triangles indicate that median differences are significant by the Mann-Whitney U Test.

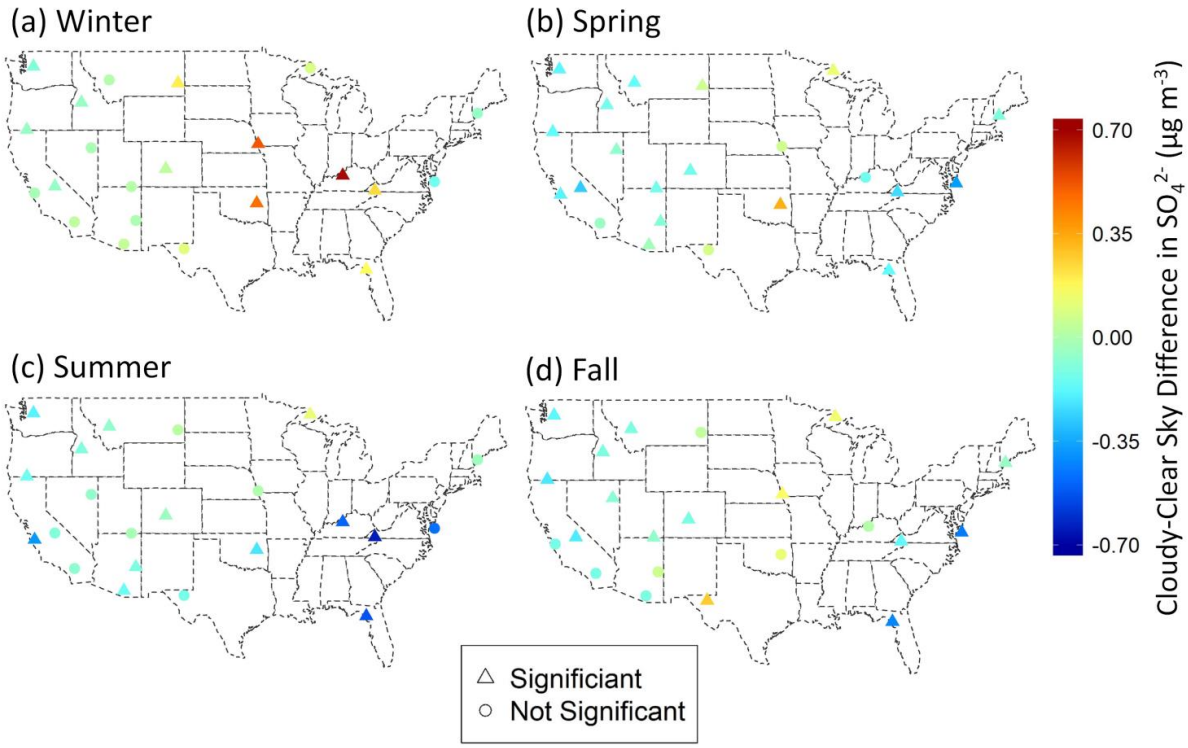


**Figure 3.5.** Maps of the difference in $SO_4^{2-}$ mass concentration medians (Cloudy-Clear Sky) for all regions from 2010-2014 for (a) winter, (b) spring, (c) summer, and (d) fall. The color of the point corresponds to the magnitude of the difference. Triangles indicate that median differences are significant by the Mann-Whitney U Test.

Outside of winter, significant $SO_4^{2-}$ mass concentrations are typically higher on Clear Sky days in the eastern US (Figure 3.5 and Table B5). Higher Clear Sky $SO_4^{2-}$ concentrations during summertime are associated with heat waves and stagnation events, which are characterized by a lack of ventilation in high pressure systems (Jacob and Winner, 2009; Wang and Angell, 1999) and higher electricity demand (Farkas et al., 2016) associated with emissions that form sulfate.

TOC mass concentrations are nearly always higher during Clear Sky times than Cloudy (Figure 3.7 and Table B7) in all chemical climatology regions across the CONUS, with the largest differences during summer and fall. Precursor VOC emissions (e.g., biogenic) and subsequent derived PM that contributes to OC differ by season and region (Donahue et al., 2009; Gentner et al., 2017; Youn et al., 2013). Increased sunlight under clear sky conditions leads to higher biogenic VOC emissions (Sakulyanontvittaya et al., 2008) and enhanced photolysis rates that facilitate hydroxyl radical production important to secondary organic aerosol formation (Tang et al., 2003). Organic aerosol hygroscopicity and water uptake is highly uncertain (Christiansen et al., 2019; Nguyen et al., 2015), and yet has profound impacts on top-of-atmosphere radiative forcing calculations (Rastak et al., 2017). We note that TOC is also influenced by primary sources of OC including wildland fires in the west and prescribed burning in the east which are not influenced by cloud presence (Spracklen et al., 2007; Tian et al., 2009; Zeng et al., 2008).

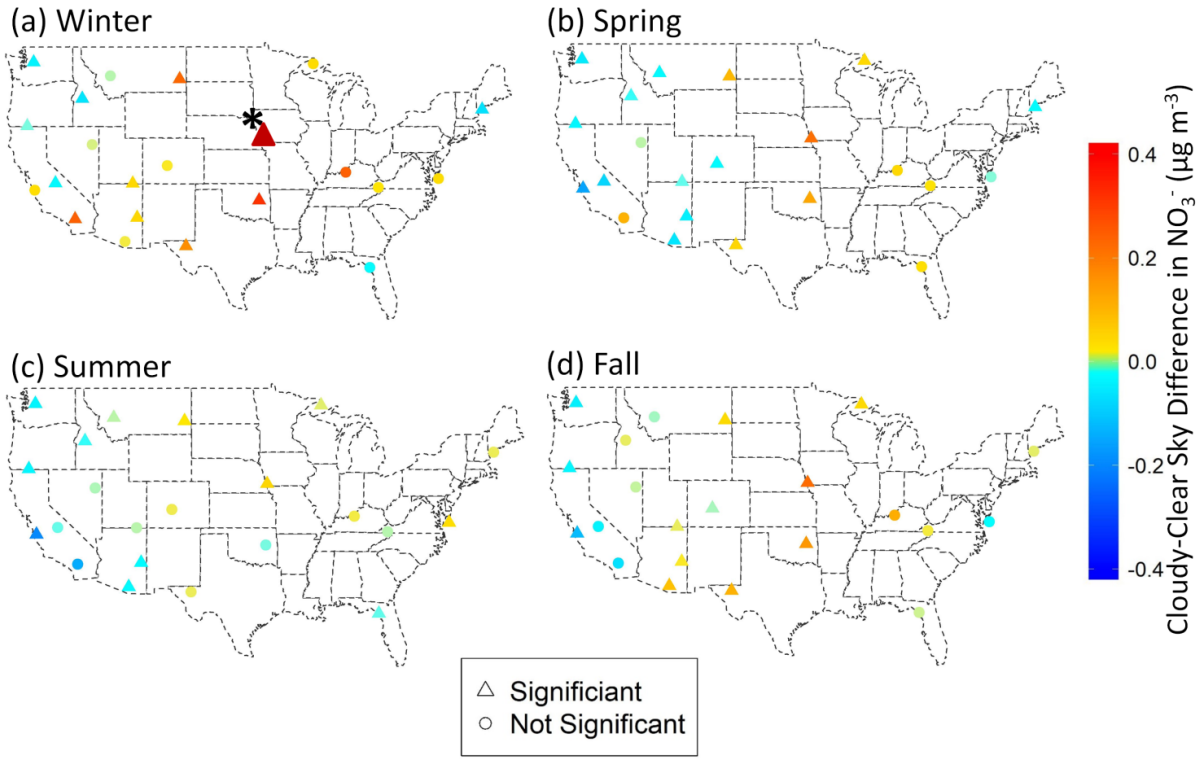


**Figure 3.6.** Maps of the difference in $NO_3^-$ mass concentration medians (Cloudy-Clear Sky) for all regions from 2010-2014 for (a) winter, (b) spring, (c) summer, and (d) fall. The color of the point corresponds to the magnitude of the difference. Triangles indicate that median differences are significant by the Mann-Whitney U Test. Note that the difference in medians for daily $NO_3^-$ concentrations in winter for the Central Great Plains (denoted with asterisk) is substantially larger than other regions (Cloudy median value is 1.07 µg $m^{-3}$ larger than Clear Sky).

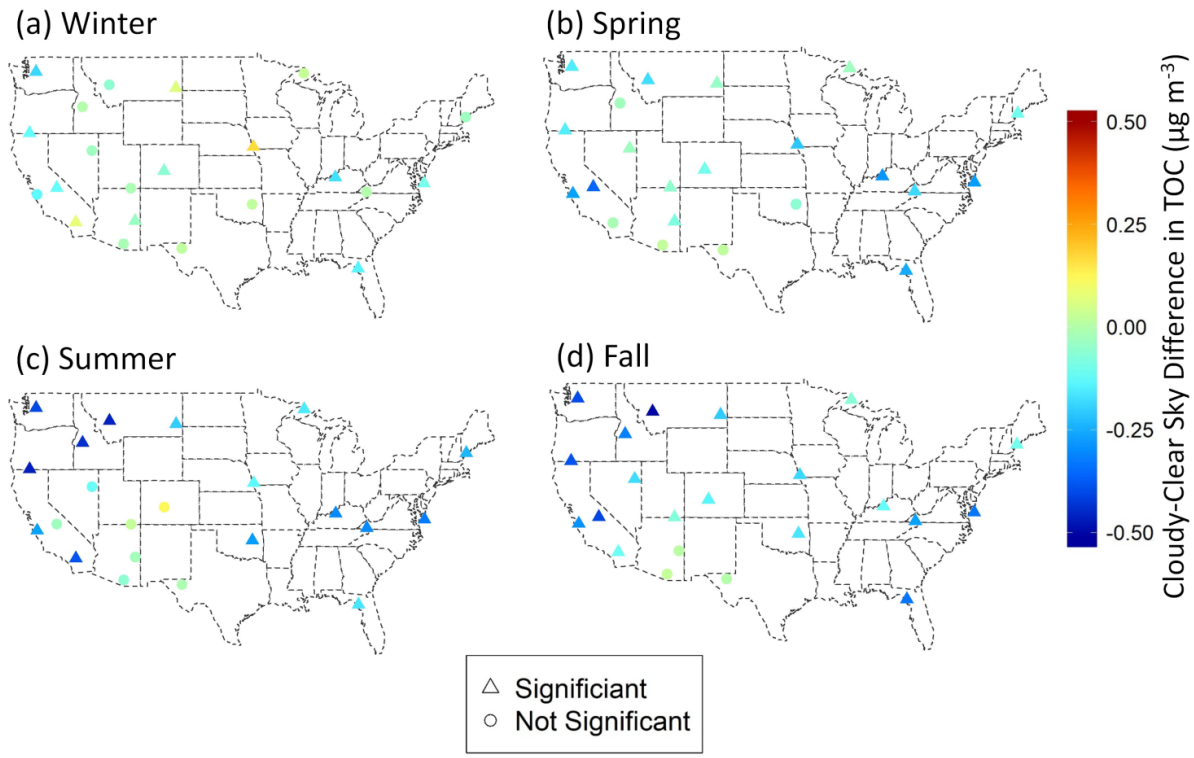


**Figure 3.7.** Maps of the difference in TOC mass concentration medians (Cloudy-Clear Sky) for all regions from 2010-2014 for (a) winter, (b) spring, (c) summer, and (d) fall. The color of the point corresponds to the magnitude of the difference. Triangles indicate that median differences are significant by the Mann-Whitney U Test.

### 3.4.2 $PM_{2.5}$ Mass Concentrations

Significant differences in $PM_{2.5}$ mass concentrations measured at IMPROVE monitoring locations are observed between Cloudy and Clear Sky conditions in the majority (>60%) of regions in any given season during 2010-2014 (Figure 3.4 and Table B4) and do not correlate with MODIS cloud fraction during any season in any region (Figure B8). In all regions, Clear Sky $PM_{2.5}$ concentrations are generally higher than Cloudy. Satellite AOT products used to derive $PM_{2.5}$ may overestimate the atmospheric burden across the CONUS, particularly during

summertime. Median All Sky $PM_{2.5}$ concentrations are also significantly different and typically lower than Clear Sky in multiple chemical climatology regions (Table B9). This suggests the clear sky bias in satellite data may impart a positive bias when assessing surface $PM_{2.5}$ trends in model applications for air quality, weather, and climate.

### 3.4.3 Case Study: The Mid South

ALW concentrations are significantly higher during Cloudy times than Clear Sky in the Mid South during all seasons (Table 3.1 and Figure 3.8). RH in the region is high year-round during Cloudy and Clear Sky periods alike, with the median greater than 60%. Gas-phase water vapor mixing ratios are sufficiently high that water availability is not limiting for ALW in the region for any season. Aerosol mass concentrations and chemical composition vary, however, and the effects on particle hygroscopicity can be seen in contrasting Cloudy and Clear Sky ALW concentrations among the seasons. For example, during Clear Sky conditions, the highest ALW mass concentrations occur during summer and spring, which correspond to the highest $SO_4^{2-}$ concentrations in the Mid South, and not when Clear Sky RH is highest (i.e., during winter). The largest absolute ALW concentrations and estimated growth factors occur during Cloudy times in the winter and spring, when $NO_3^-$ mass fraction and RH are highest. This is consistent with independent humidified nephelometer measurements by Jefferson et al., who found that aerosol growth rates are highest in the winter and spring at the SGP site within the Mid South chemical climatology region, and identify nitrate and RH as determining factors (Jefferson et al., 2017).

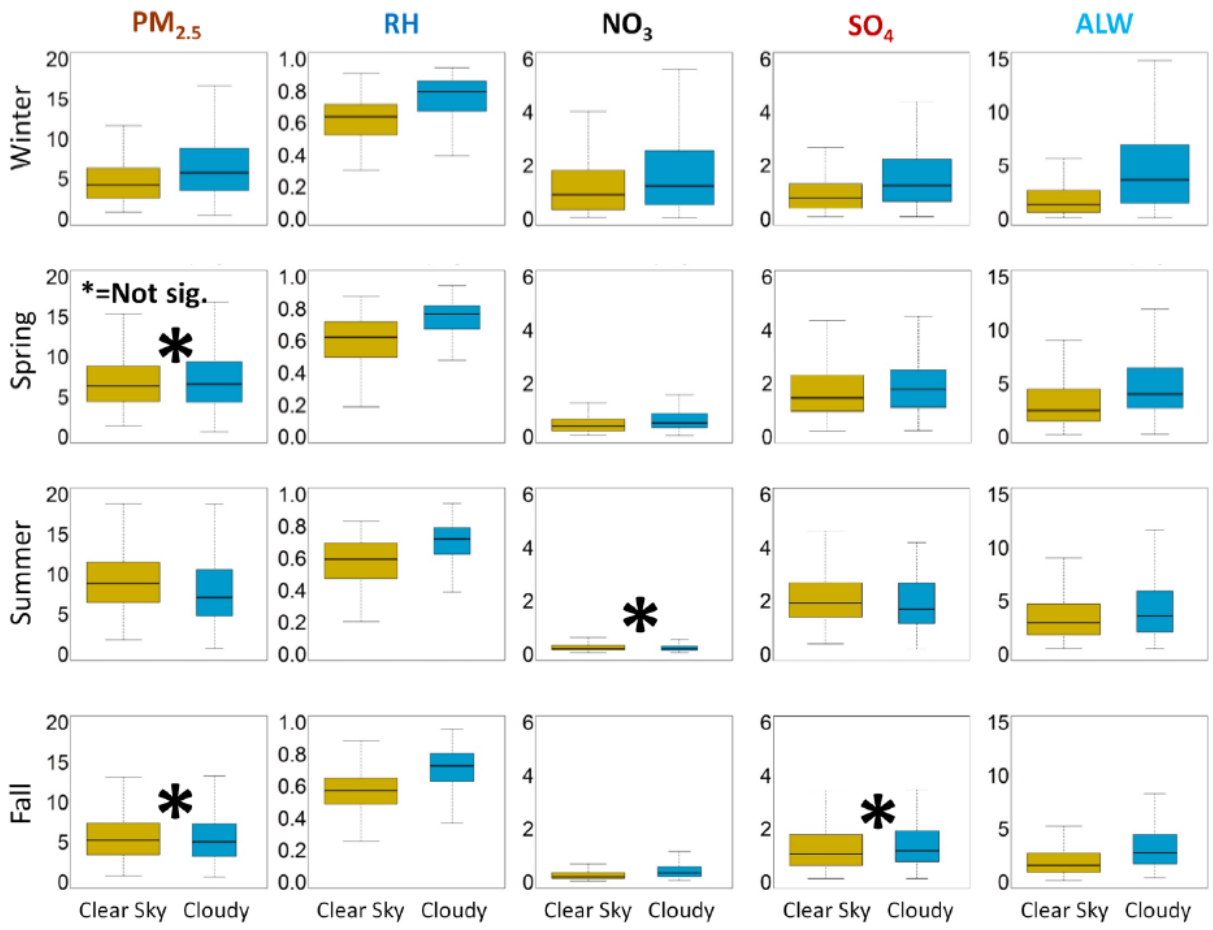


**Figure 3.8.** Box plots of cloudy and clear sky distributions of $PM_{2.5}$ and chemical constituent mass concentrations (µg $m^{-3}$) and RH in the Mid South for each season from 2010-2014. The width of the box plot is proportional to the number of observations. Note that potential outliers are not shown but are used in calculations. Asterisks denote Cloudy and Clear Sky differences that are *not* significant ($p<0.05$) by the Mann-Whitney U Test.

**Table 3.1.** Particle chemical constituent concentrations, meteorology, and growth factors during Cloudy (Cl) and Clear Sky (CS) times in the Mid South.

| | $SO_4^{2-}$ | | $NO_3^-$ | | ALW | | RH | | Growth Factors | |
|---|---|---|---|---|---|---|---|---|---|---|
| | CS | Cl | CS | Cl | CS | Cl | CS | Cl | CS | Cl |
| **Win** | 0.77 | 1.24 | 0.90 | 1.22 | 1.32 | 3.61 | 0.64 | 0.80 | 1.33 | 1.50 |
| **Spr** | 1.46 | 1.79 | 0.37 | 0.50 | 2.48 | 4.02 | 0.62 | 0.76 | 1.25 | 1.41 |
| **Sum** | 1.91 | 1.69 | 0.20 | 0.19 | 2.92 | 3.57 | 0.59 | 0.72 | 1.21 | 1.39 |
| **Fall** | 1.05 | 1.17 | 0.18 | 0.33 | 1.56 | 2.74 | 0.57 | 0.73 | 1.18 | 1.37 |

$NO_3^-$ concentrations are generally lower than $SO_4^{2-}$ in the Mid South, but $NO_3^-$ is more hygroscopic and provides influence over ALW patterns. Sulfate is traditionally considered dominant in determining absolute ALW mass concentrations in this region, and sulfate mass fraction is highest in summer (Carlton and Turpin, 2013; Gasparini et al., 2006). Similar to other regions of the CONUS, $SO_4^{2-}$ mass concentrations are greatest during summertime Clear Sky conditions due to transport (Parworth et al., 2015), increased rates of photochemistry (Stone et al., 2012), and increased electricity sector emissions during heat waves and stagnation events (Appel et al., 2011; Farkas et al., 2016), which generally occur on sunny days. Sulfate mass fraction is lowest in winter, when $NO_3^-$ concentrations are high due to cooler temperatures and transport of precursor species from nearby agricultural and surrounding urban areas (Parworth et al., 2015). Year-round $NO_3^-$ concentrations are higher during Cloudy conditions than Clear Sky, which are associated with lower temperatures. Under Cloudy conditions, the highest ALW concentrations and estimated growth factors occur during winter and spring, when $NO_3^-$ mass fraction and RH are highest. In another continental location, the Po Valley in Italy, $NO_3^-$ was found to control ALW concentrations with implications for secondary organic aerosol (Hodas et al., 2014). The Mid South is also a continental, agricultural area and aerosol growth may be subject to similar mechanisms.

## 3.5 Conclusions

Across the CONUS, statistically discernible differences among $PM_{2.5}$ and chemical constituent concentrations under Cloudy and Clear Sky conditions cannot be explained solely by physical mechanisms. The chemical properties of aerosol are important to explain differences in water uptake and particle composition under different meteorological conditions. While meteorological

phenomena such as pressure systems, winds, and air mixing affect $PM_{2.5}$ and chemical component concentrations, they are insufficient to explain chemical constituent differences between Cloudy and Clear Sky times. *In situ* chemical formation processes are necessary to fully explain temporal and spatial patterns. Spatially and seasonally, $PM_{2.5}$ and particle speciation information that lends insight into water uptake, particle properties, and particle growth is incomplete when information is gathered only during Clear Sky times. The work presented here indicates aerosol growth due to water uptake is greatest during satellite periods identified as Cloudy in many regions, when satellites are unable to remotely sense particle properties and impacts. This limits understanding of atmospheric particle burden and its climate-relevant physicochemical properties, which have implications for the prediction of weather (Kawecki and Steiner, 2018), air quality, and climate. This indicates that the clear sky bias affects accurate representation of ALW on cloudy days and suggests that without *in situ* chemical information, aerosol-cloud interactions and subsequent estimates of radiative forcings in models (Lin et al., 2016; Vogelmann et al., 2012) will remain a large uncertainty.

# CHAPTER FOUR

## THE CHANGING NATURE OF ORGANIC CARBON OVER THE UNITED STATES

Reproduced with permission from *Environmental Science and Technology*. Christiansen, A.E.; Carlton A.G.; Porter, W.C., The Changing Nature of Organic Carbon over the United States. Submitted for publication to *Environmental Science and Technology*. Unpublished work © 2020 American Chemical Society.

## 4.1 Abstract

Total organic carbon (TOC) mass concentrations are decreasing across the contiguous US (CONUS), most notably in the southeast US. We investigate decadal trends in organic carbon (OC) thermal fractions (OC1 (volatilizes at 140 °C), OC2 (280 °C), OC3 (480 °C), OC4 (580 °C)) and pyrolyzed carbon (PC) as measured and reported at 121 locations in the Interagency Monitoring of PROtected Visual Environments (IMPROVE) monitoring network from 2005-2015 for 23 chemical climatology regions across the CONUS. Reductions in PC and OC2 drive the observed and reported decadal decreases in TOC (TOC = OC1 + OC2 + OC3 + OC4 + PC) mass concentrations across the CONUS. OC2 decreases by 40% from 2005-2015, and PC decreases by 34%. The largest absolute mass decreases occur in the eastern US, and relative changes normalized to local concentrations are more uniform across the CONUS. In each region, OC is converted to organic mass (OM) using region-and-season-specific OM:OC ratios. Simulations with GEOS-Chem reproduce OM trends in all regions and suggest decreases across the CONUS, and especially in the eastern US, are due to aerosol liquid water (ALW) chemistry.

Individual model species, most notably secondary organic aerosol derived from isoprene oxidation products and formed in ALW, correlate significantly ($p<0.05$) with OM2 across the CONUS, even in arid western regions. Links among model species and OM fractions lend insight to changing chemical regimes with implications for particle phase state, viscosity, and oxidation state. These findings contribute to the growing body of literature that suggests federal air quality rules aimed at anthropogenic $SO_2$ and $NO_x$ emissions induce the co-benefit of further reducing fine particle mass through decreases in TOC, primarily through chemistry involving ALW. Results suggest that these benefits extend beyond the eastern US.

## 4.2 Introduction

Concentrations of organic carbon (OC), a major contributor to fine particulate matter ($PM_{2.5}$) mass (Zhang et al., 2007), have decreased over past decades across the contiguous US (CONUS), notably in the southeast US (Attwood et al., 2014; Blanchard et al., 2013; Malm et al., 2017; Nguyen et al., 2015; Ridley et al., 2018). Carbon-14 analysis at rural locations such as national parks revealed that most OC is non-fossil in these areas and presumably derived from biogenic emissions (Bench et al., 2007; Schichtel et al., 2008), which are projected to increase as the climate warms (Heald et al., 2008). In urban and near-urban locations, residential heating and cooking contributes some amount of non-fossil carbon-14, but this is not a significant contributor at remote locations (Heal, 2014; Schichtel et al., 2008). Smoke from wildfires, which are increasing in frequency, intensity, and acreage burned (Spracklen et al., 2009; Westerling, 2016), also contribute non-fossil carbon to total organic carbon (TOC). Decreases in OC are attributable to the effects of anthropogenic $NO_x$ and $SO_2$ regulations (Carlton et al., 2018a), the impetus of which was to reduce acid deposition in the eastern US and ozone mixing ratios. This reduces

surface mass concentrations of sulfate and nitrate (Ridley et al., 2018), hygroscopic PM constituents that facilitate aerosol liquid water (ALW) formation and secondary organic aerosol (SOA), in turn reducing contributions to OC in observations in the Southeast US (Nguyen et al., 2015) and in model simulations of the CONUS (Carlton et al., 2018a; Marais et al., 2017). The Community Multiscale Air Quality (CMAQ) and GEOS-Chem models better reproduce observed decadal trends most successfully when the SOA chemical mechanism includes water-mediated chemistry and uptake, in particular in the eastern US (Marais et al., 2016).

The Interagency Monitoring of PROtected Visual Environments (IMPROVE) network provides the longest continuous measurements of surface ambient concentrations of carbonaceous material in $PM_{2.5}$ across the US using thermal optical organic carbon/elemental carbon (OC/EC) analyzers (Khan et al., 2012; Meier and Schwab, 2011). Organic and elemental carbon mass concentrations are measured from the evolution of organic species from a filter at operationally-defined temperatures. Mass measurements of OC are made by heating filters in a helium environment to allow organic species to volatilize without oxidation on the filter. Organic species tend to pyrolyze above 300 ºC (Chow et al., 1993), and this pyrolysis is monitored and corrected via reflectance (Rau, 1986). The IMPROVE network defines four OC thermal fractions (OC1, OC2, OC3, and OC4) at temperatures ranging from 140-580 ºC (Chow et al., 2007), a protocol applied routinely since 2005, to minimize the amount of OC that undergoes pyrolysis during analysis (Chow et al., 2005, 2007; Rau, 1986). OC fraction measurements provide information about the volatility of the organic species within each fraction and not specific chemical identity. There are a number of uncertainties within these fractions including pyrolysis, interactions from other species (Baumgardner et al., 2012; Chow and Watson, 2002; Wang et al.,

2010), and analytical biases (Malm et al., 2020). However, previous studies have used OC fractions to provide chemical insight regarding speciation and sources (Aswini et al., 2019; Cao et al., 2005; Chow et al., 2004; Lim et al., 2012). Field campaigns in locations around the world, using a previous iteration of the IMPROVE thermal protocol, identify biomass burning and anthropogenic combustion processes as major sources of OC1 and OC2 (Aswini et al., 2019; Cao et al., 2005; Chow et al., 2004), and cooking emissions and dust as sources that contribute to OC3 and OC4 (Chow et al., 2004; Lim et al., 2012). A laboratory analysis of individual organic compounds found widely in the atmosphere (e.g., oxalic acid, levoglucosan, azelaic acid, and humic-like substances) found that as the molecular weight of an organic species increases, higher temperatures are needed for carbon evolution (Miyazaki et al., 2007). Efforts to identify specific organic functional groups (Dillner and Takahama, 2015; Kamruzzaman et al., 2018; Weakley et al., 2016) and other chemical properties, including viscosity (Rothfuss and Petters, 2017), from filters analyzed for TOC content are an active area of research.

Changing chemical regimes for ozone in response to decreases in anthropogenic $NO_x$ emissions in the atmosphere of the CONUS are noted in the literature (Simon et al., 2015). This changing photochemistry may also affect SOA formation pathways in ways that affect the overall nature of particulate organic carbon by altering speciation, degree of oxidation, and phase state. Volatile organic carbon (VOC) reacts with various oxidants and forms peroxy radicals ($RO_2$) in the presence of oxygen (Seinfeld and Pandis, 1998). Traditionally, the fate of an $RO_2$ species is assumed to be predominantly driven by its bimolecular reaction with NO, $HO_2$, or another $RO_2$. However, as $NO_x$ emissions decrease, autoxidation reactions are becoming more important, potentially leading to more highly oxidized organic species (Praske et al., 2018). Decadal

changes in OC fraction mass concentrations and relative fractional contribution to the total may indicate changes in SOA speciation, oxidation, and other properties. Hand et al. 2019 cautiously suggest that organic aerosol (OA) across the CONUS is increasingly aged and oxidized over time, although analytical bias in the separation of OC and EC confound interpretation (Malm et al., 2020).

Previous studies of temporal trends in OA and particulate OC focus on TOC measurements (Attwood et al., 2014; Nguyen et al., 2015; Ridley et al., 2018), and decadal trends in the individual thermal fractions have not received as much analysis in the literature. Here, we investigate geospatial and temporal trends in OC fractions to determine which contribute significantly to overall TOC decreases. We also track decadal changes in OA from 2005-2015 in the GEOS-Chem model to identify potential OC sources and formation mechanisms that may help to explain observed trends.

## 4.3 Materials and Methods

### 4.3.1 Surface Measurements and Estimates

IMPROVE network chemical speciation data were downloaded on 26 February 2020 for 121 sites across the CONUS with >80% of sampling days reported from 2005-2015 (IMPROVE Network, 2019) (Figure C1a). These years correspond to a change in the thermal protocol in 2005 (Chow et al., 2007) and a change in the instrument after 2015 (Chow et al., 2018). We use all reported values and uncertainties. Values below the method detection limit (MDL) are kept in the analysis when the value plus uncertainty is above the MDL. Uncertainties are reported as measures of standard deviation (Hyslop and White, 2008), and there is an equal chance that these

values fall above or below the MDL. Since these values may exceed the MDL, we keep them in our analysis. Rural sites are grouped into 23 chemical climatology regions defined by IMPROVE as having similar aerosol composition and topography (Figure C1b) (Malm et al., 2017), and each region in our analysis contains between 2 and 10 sites. We use surface mass concentration data of thermally-defined OC fractions OC1 (140 ºC), OC2 (280 ºC), OC3 (480 ºC), and OC4 (580 ºC), PC, and TOC (OC1 + OC2 + OC3 + OC4 + PC) across these chemical climatology regions. OC1 concentrations are assumed to be a lower bound due to volatilization of species during field latency, transport, and storage (Dillner et al., 2009). We report OC1 trends and concentrations since they are reported by the IMPROVE network, but we do not attempt to assign chemical meaning due to high levels of uncertainty. OC4 is the least volatile fraction.

The OC fractions are operationally defined, and there is debate about how method differences impact quantification of OC and EC (Baumgardner et al., 2012). IMPROVE uses one of several thermal/optical reflectance analysis protocols, and we limit our analysis to this method to avoid inter-comparison issues. Some analytical biases may still persist (Baumgardner et al., 2012; Chow and Watson, 2002; Dillner et al., 2009; Malm et al., 2011; Wang et al., 2010). Semi-volatile species, such as ammonium nitrate (Chow et al., 2015) and OC1, are lost from filter samples before and during analysis (Dillner et al., 2009; Malm et al., 2011). Metal salt particles, particularly ones containing copper and iron, can reduce the oxidation temperature of EC and enhance OC charring, affecting the OC/EC split and reported TOC concentrations (Wang et al., 2010). KCl and NaCl from biomass smoke and sea spray can also alter the temperature at which large organic compounds and EC evolve (Baumgardner et al., 2012). CONUS-averaged copper and iron concentrations do not appreciably change, and sea salt concentrations do not trend

positive or negative from 2005-2015 (Figure C2). Further, we use median values in our analysis to minimize the impact of episodic outliers, such as wildfires and biomass burning. Water-soluble organic carbon (WSOC) characteristic of rural aerosol is susceptible to pyrolysis during analysis (Khan et al., 2012). Total pyrolyzed carbon (PC) is measured in a separate category from the thermal fractions and cannot be assigned to a particular step in the temperature-ramp. Hence, reported mass concentrations for OC fractions are lower mass bounds because some of each fraction may be lost to charring and counted as PC (Khan et al., 2012). Recently, Malm et al. 2020 demonstrated that PC and EC co-evolve, causing lower-temperature oxidation of EC (Boparai et al., 2008; Subramanian et al., 2006), which biases TOC concentrations high because it includes some EC. It is difficult to quantitatively assess how PC impacts individual OC fraction trends. While there are uncertainties and precautions to take when using OC fraction data, the IMPROVE record is the oldest continuous TOC network in the CONUS, and the underutilized OC fraction data may facilitate insight regarding the controlling mechanisms responsible for the decrease in TOC and its changing nature.

The IMPROVE protocol measures particulate organic carbon, yet organic aerosol is composed of other elements such as hydrogen, oxygen, nitrogen, and sulfur that are not accounted for in these measurements. Often, an OM:OC ratio of 1.8 is applied as a factor to account for non-carbon organic mass, though ratios vary spatially, seasonally, and decadally, and depend on air mass origin (Aiken et al., 2008; El-Zanan et al., 2005; Hand et al., 2019; Philip et al., 2014; Simon et al., 2011). Several methods of OM:OC ratio determination are discussed in the literature. El-Zanan et al. 2005 experimentally determined OM:OC ratios at five IMPROVE sites representative of their chemical climatology regions using subsequent solvent extractions of

dichloromethane, acetone, and water. Other methods include multiple linear regression approaches based on reported IMPROVE measurements (Simon et al., 2011), a combination of aerosol mass spectrometers (AMS) and satellite $NO_2$ data (Philip et al., 2014), and functional group information derived from Fourier-Transform Infrared (FT-IR) spectra of IMPROVE samples (Ruthenburg et al., 2014). Across all analyses, OM:OC ratios ranged from 1.3 to 2.6. Ratios are highest in the summer and rural areas, and lowest in the winter and urban areas (Philip et al., 2014; Simon et al., 2011). Average OM:OC ratios across the CONUS may be increasing with time (Figure C3) (Hand et al., 2019), although analytical biases that apportion some light-absorbing carbon (LAC) to OC (Malm et al., 2020) cannot be ruled out.

We determine seasonal organic mass (OM) for all regions across the CONUS with >80% complete data from 2005-2015 using OM:OC ratios determined via mass balance using IMPROVE-defined reconstructed mass (Air Quality Research Center, 2019) and removing the 1.8 multiplier from OC (Eqn 4.1) as summarized in Malm et al. 2020 (El-Zanan et al., 2005; Lowenthal and Kumar, 2003; Malm et al., 2020).

$$OM{:}OC = \frac{PM_{2.5} - Amm.Sulf. - Amm.Nit. - EC - SOIL - 1.8*Cl}{OC} \quad (4.1)$$

Here, SOIL is equal to (2.2*Al + 2.49*Si + 1.63*Ca + 2.42*Fe + 1.94*Ti) (Air Quality Research Center, 2019). We convert IMPROVE-measured OC to OM estimates for a more direct comparison to GEOS-Chem simulations because the model provides OA mass concentrations. Each OC fraction and TOC is multiplied by the appropriate seasonal and regional OM:OC ratio, and they are referred to as OM fractions and TOM.

ALW mass concentrations are estimated using the thermodynamic equilibrium model ISORROPIA version 2.1, publicly available online (Fountoukis and Nenes, 2007). Temperature and relative humidity (RH) data were extracted from the North American Regional Reanalysis (NARR) model as in Nguyen et al. 2016b. 3-hour temperature and RH data are averaged to 24 hours to match the 24-hour sampling time of IMPROVE measurements. ALW concentrations are estimated at each available IMPROVE sampling day. We assume metastable conditions, in which the aerosol is composed of only an aqueous phase (Nguyen et al., 2014b; Rood et al., 1989), and use only $SO_4^{2-}$ and $NO_3^-$ mass concentrations since $NH_4^+$, which increases ALW, is not measured at IMPROVE sites. We do not include dust and organic species due to large water uptake uncertainties (Christiansen et al., 2019; Jathar et al., 2016; Metzger et al., 2018) and the spatial heterogeneity in dust, which would disproportionately affect uncertainties in ALW estimations across regions. Our approach affects absolute values of ALW, but it does not affect overall interpretation or broad trends, consistent with previous analyses which use the same method and include organic compounds (Nguyen et al., 2015) and dust (Christiansen et al., 2020) in sensitivity analyses of ALW estimates.

### 4.3.2 GEOS-Chem Modeling

Observations are paired in space and time via a nearest neighbor approach with model predictions from GEOS-Chem version 12.3.2 (http://acmg.seas.harvard.edu/geos) driven by the MERRA-2 reanalysis product (Gelaro et al., 2017) developed by the NASA Global Modeling and Assimilation Office (GMAO). Nested 0.5º x 0.625º simulations over North America are examined across 2005-2015 using output from global simulations run at 2º x 2.5º horizontal resolution to provide boundary conditions. Anthropogenic emissions for the United States are

taken from the National Emissions Inventory 2011 (NEI11) developed by the United States Environmental Protection Agency (EPA), as implemented in GEOS-Chem by Travis et al. 2016 and adjusted for trends over time using EPA's national annual scaling factors. Online biogenic emissions are provided by the Model of Emissions of Gases and Aerosols from Nature (MEGANv2.1) (Guenther et al., 2012) with updates for acetaldehyde emissions (Millet et al., 2010) and $CO_2$ dependence (Tai et al., 2013). Biogenic emissions vary over time based on ambient meteorological conditions, as do trends in leaf area index (LAI), which are captured using the MODIS-derived LAI data product from Yuan et al. 2011. Fire emissions are modeled using the fourth-generation global fire emissions database (GFED4) (Giglio et al., 2013; van der Werf et al., 2010). Inorganic aerosol thermodynamics are modeled using the ISORROPIA 2.2 module (Fountoukis and Nenes, 2007), while SOA formation is represented by the simplified Volatility Basis Set (VBS) approach of Pye et al. 2010 with the addition of the non-reversible aqueous-phase isoprene SOA scheme of Marais et al. 2016.

We determine the direction and significance of relative decadal trends in particulate OC, OC converted to OM, and predicted GEOS-Chem speciation bins (defined in Table C1) using Sen's slope and the Mann-Kendall test, non-parametric techniques that are resistant to outliers and account for seasonality, in R statistical software (Kendall, 1975; Mann, 1945; R Core Team, 2013; Sen, 1968; Theil, 1950). We define winter as December, January, and February (DJF), spring as March, April, and May (MAM), summer as June, July, and August (JJA), and fall as September, October, and November (SON).

## 4.4 Results and Discussion

Across the CONUS, absolute and relative OC1, OC2, and PC mass concentrations exhibit statistically significant ($p<0.05$) decreasing trends over time in all chemical climatology regions (Figures 4.1, C4), as does TOC with the exception of two regions in California. The median TOC concentration across the CONUS decreases from 0.78 μg $m^{-3}$ in 2005 to 0.64 μg $m^{-3}$ in 2015. OC2 and PC drive TOC mass concentration decreases. Species in OC2 may contain carboxylic acids, polyaromatic hydrocarbons (PAHs), and steranes (Meier and Schwab, 2011). PAHs and steranes are anthropogenic emissions markers for incomplete fossil fuel combustion and motor oil emissions (Abdel-Shafy and Mansour, 2016; Dat and Chang, 2017; Ruehl et al., 2011), and carboxylic acids originate from oxidation of biogenic and anthropogenic VOCs or direct emission from fossil fuel combustion and biomass burning (Ferrero et al., 2019). Changes in PC may be due to mis-apportioned EC (Malm et al., 2020), and some laboratory analyses connect PC to WSOC (Khan et al., 2012). OC2 and PC decreases are ubiquitous and significant ($p<0.05$), with the largest absolute and relative decreases occurring in the eastern US, where ALW mass concentrations and relative decreases in ALW are also greatest (Figures C4-C6) (Carlton and Turpin, 2013; Nguyen et al., 2016b). These decreases are generally larger than measurement uncertainties, especially in the southeast US (Figure C7). OC3 increases in three chemical climatology regions in the humid eastern US over the same time period, especially during summer and fall (Figure C8) after 2013.

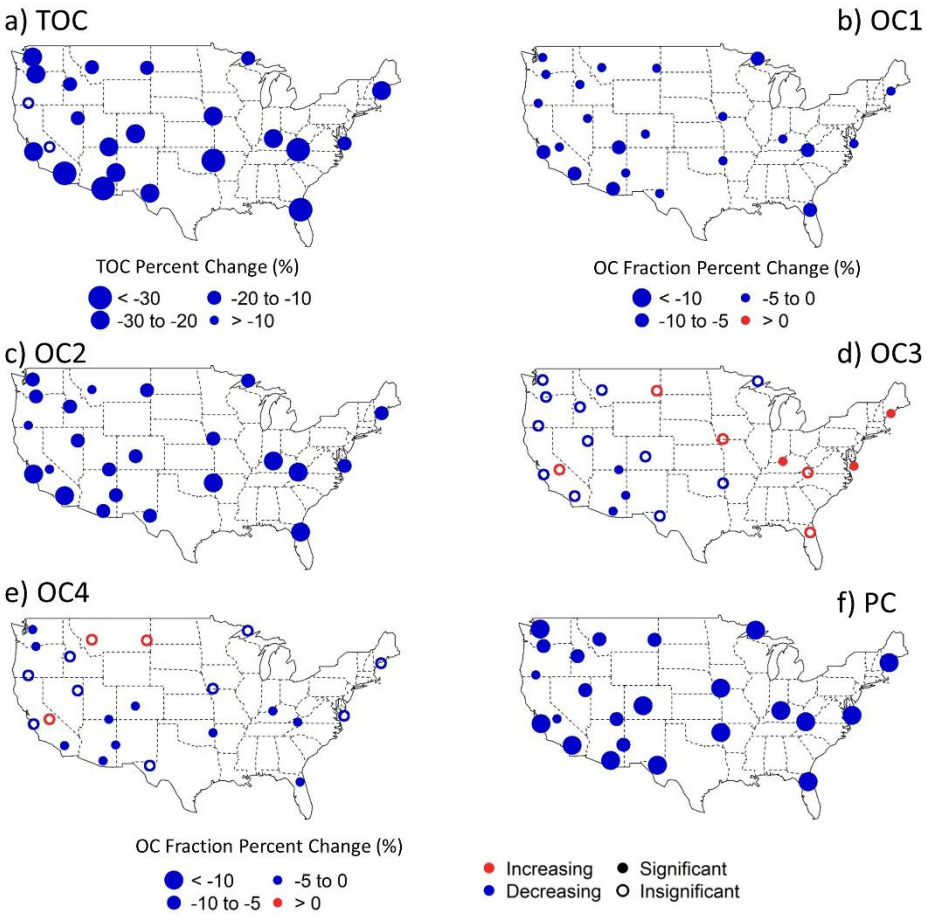


**Figure 4.1.** Maps of relative decadal trends (2005-2015) in a) TOC, b) OC1, c) OC2, d) OC3, e) OC4, and f) PC mass concentrations for each chemical climatology region. Size corresponds to the magnitude of the percent change. Red indicates an increasing trend, blue indicates a decrease, a colored circle indicates that the increase or decrease is significant ($p<0.05$) by the Mann-Kendall test, and an unfilled circle indicates the change is insignificant.

The magnitude of decadal changes among the OC fractions varies within and across regions, and OC fractional contributions to TOC differ from 2005-2015 (Figure 4.2). OC2 mass concentrations decrease significantly ($p<0.05$) by a total of 0.07 μg $m^{-3}$, from 23% of TOC to 17%. By contrast, OC3 mass concentrations across the CONUS increase by 0.03 μg $m^{-3}$, from 27% of TOC to 38%, and contribute the most by mass to CONUS-averaged TOC after 2010. Over the decade from 2005-2015, these increases are significant in three regions in the eastern US. OC4 mass concentrations decrease by less than 0.01 μg $m^{-3}$; however, the fractional

contribution of OC4 to TOC increases from 19% to 23%. Median publicly reported OC1 mass concentrations decrease by more than 50%. In 2005, across the CONUS, PC concentrations are higher than any OC fraction at 0.23 μg $m^{-3}$ and decrease to 0.15 μg $m^{-3}$ by 2015 (29% of TOC to 24%). The rate of decline for PC is significant, higher than that for any OC fraction, and is spatially consistent with the largest decreases in ALW (Figures C5, C6). Decadal declines in OC2 are statistically robust, larger than measurement uncertainties, and OC2 is less likely to pyrolyze than fractions evolving at higher temperatures (Chow et al., 1993).

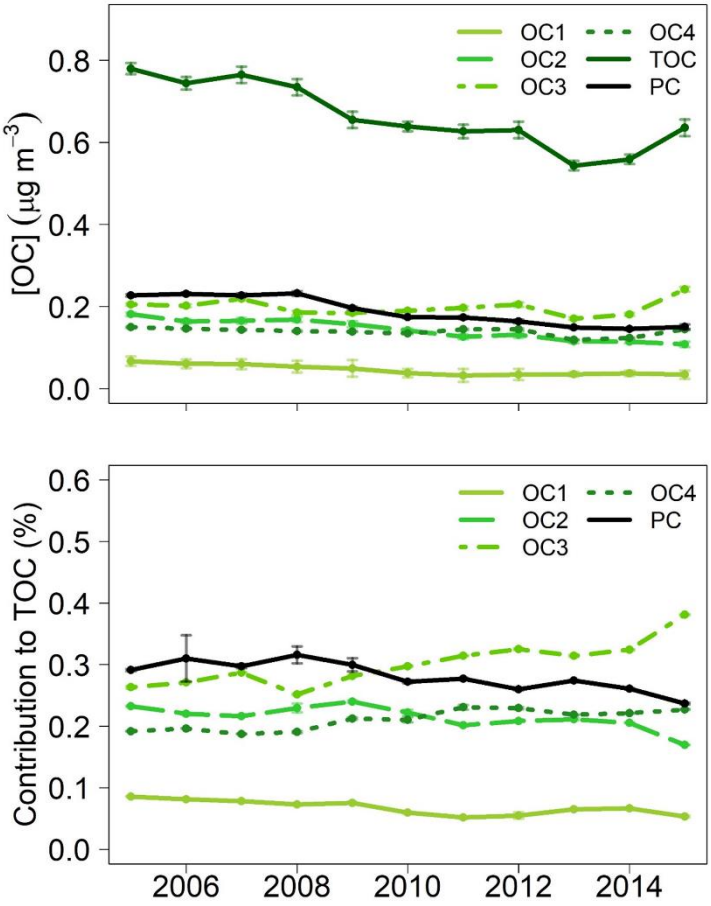


**Figure 4.2.** Decadal trends across the CONUS for a) TOC, OC fraction, and PC mass concentrations and b) fractional contribution of OC fractions and PC to TOC. Error bars represent the standard error of the medians.

GEOS-Chem reproduces spatial and temporal trends in IMPROVE-estimated total organic mass (TOM) using region-and-season-specific OM:OC ratios across the CONUS (Figure 4.3). Individual GEOS-Chem simulated organic aerosol speciation bin mass concentrations correlate significantly ($p<0.05$) with specific IMPROVE OM fractions in every region and season, offering plausible mechanistic insight to these changes. Significant correlations ($p<0.05$) between predicted OA and estimated OM fractions are found in each region and indicate that some chemical complexity tied to formation pathways is captured by OC fraction measurements in routine network data. Over all regions and seasons, we assess 13 model species (Table C1) and compare with OM fractions. We find 739 significant paired evaluations over 11 years in 23 regions. Correlations are positive and occur frequently among IMPROVE-measured OM2 and GEOS-Chem speciation bins representing water-mediated components; thus, we explore pathways and impacts of water-mediated chemistry.

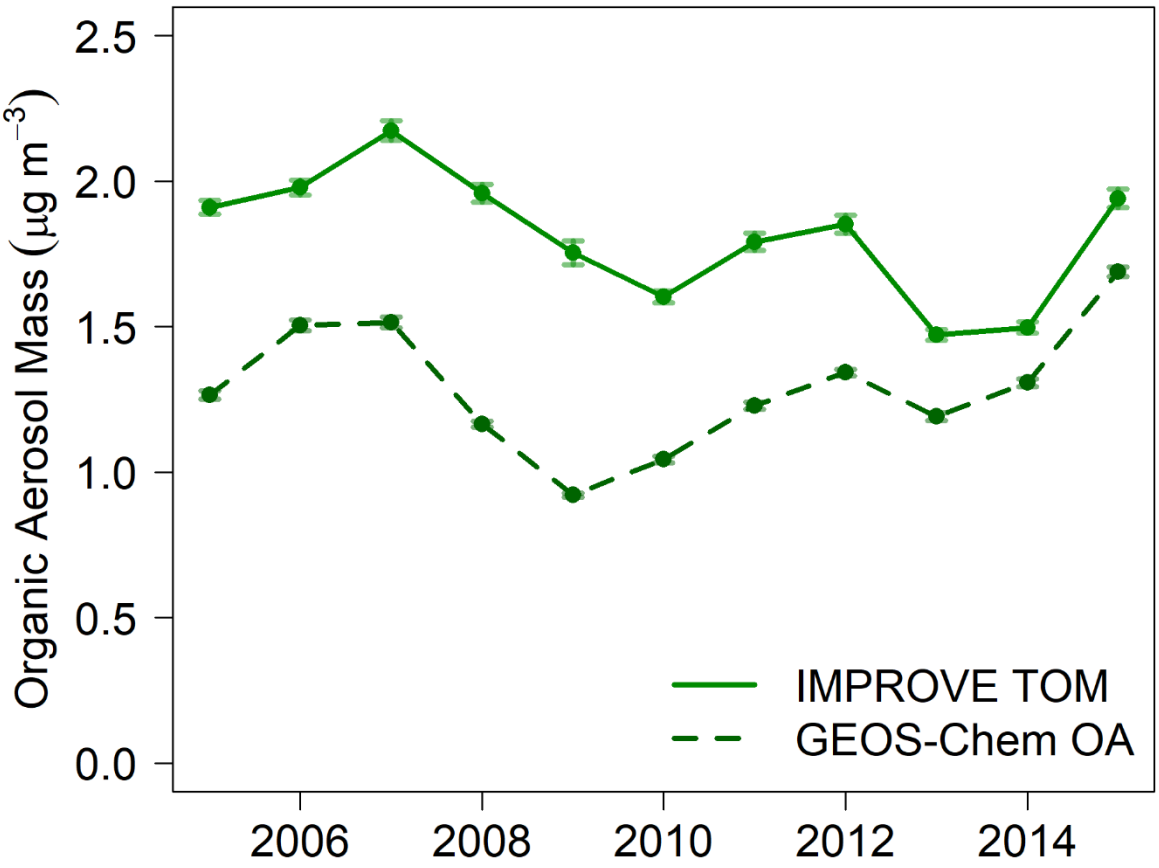


**Figure 4.3.** IMPROVE TOM and GEOS-Chem predictions of TOA across the CONUS from 2005-2015. Standard errors are represented via error bars.

Water-mediated chemistry predicted by GEOS-Chem is linked to observations in the OM fractions in multiple regions across the CONUS and provides plausible mechanistic explanations for observations. GEOS-Chem oxidation products of isoprene produced in the aqueous mechanism (ISOAAQ) correlate significantly ($p<0.05$) with OM2 in summer (Figure 4.4). This GEOS-Chem species includes carboxylic acids (Nguyen et al., 2010), which are formed from the aqueous-phase chemistry of isoprene oxidation products (Carlton et al., 2006; Tan et al., 2010)

and observed as part of OC2 in laboratory studies (Aswini et al., 2019; Cao et al., 2005; Chow et al., 2004). Statistical significance is also observed for ISOAAQ with OM1 and OM4 in some regions and seasons. This is consistent with laboratory studies that demonstrate evolution of individual compounds such as oxalic acid in one or more OC thermal fraction (Meier and Schwab, 2011).

Decreasing summertime measured OM2 trends correlate significantly ($p<0.05$) with decreases in measured ($R>0.9$) and predicted ($R>0.9$) $SO_4^{2-}$, ALW ($R>0.8$), and ISOAAQ, which includes species that require the presence of water to form (Figures C9, C10) (Nguyen et al., 2014a). The absolute and relative decreases are highest in the humid eastern US during summer, where decreases in ALW are largest (Figure C5). However, decreases in OM2, ALW and ISOAAQ occur in most regions across the CONUS. For example, in the Great Basin region, representative of arid areas of the US (Figure 4.4), predicted ALW mass and isoprene emissions are low (Wang et al., 2017b), yet relative decreases in OM2, ALW, and ISOAAQ are similar to observed trends in the eastern U.S. This is suggestive that water-mediated processes also play a determining role in TOC decreases outside humid locations of the eastern US.

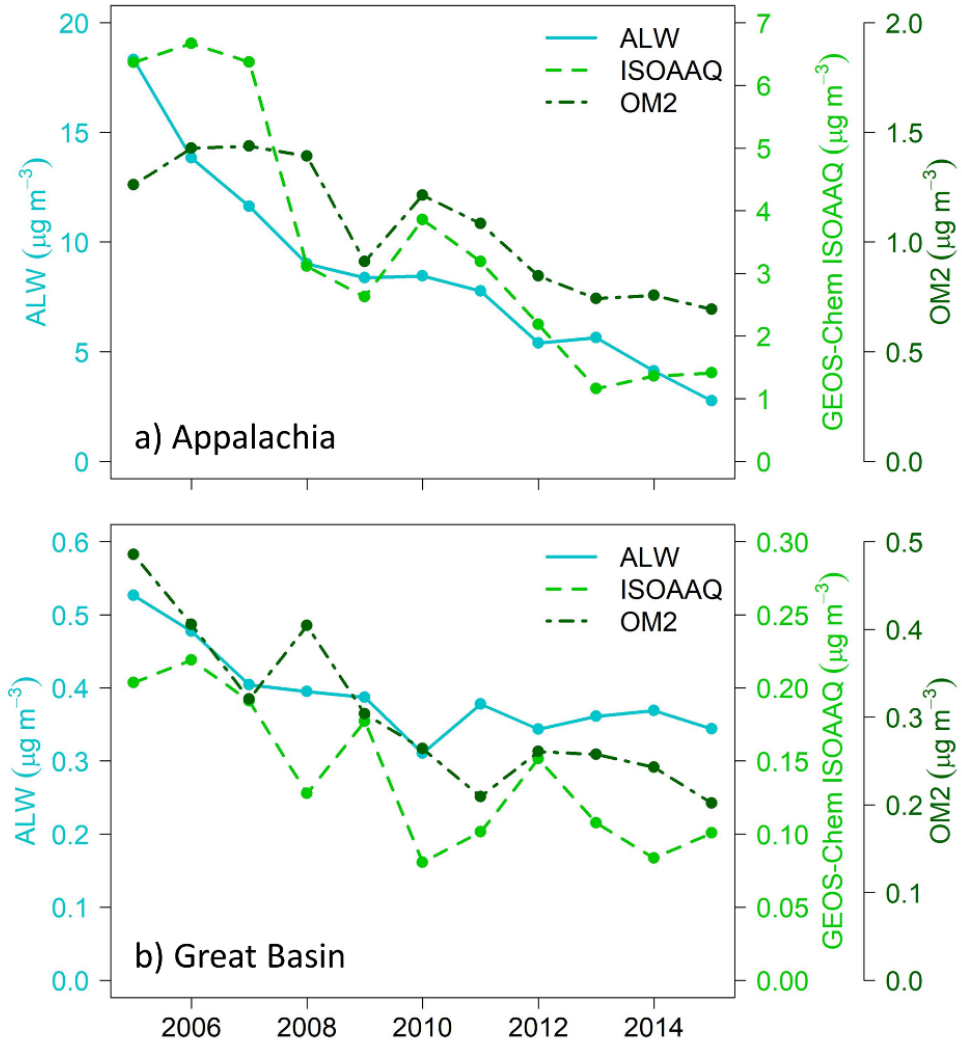


**Figure 4.4.** Decadal decreases in ALW, GEOS-Chem predicted ISOAAQ, and OM2 for a) Appalachia and b) Great Basin. Note the y-axes are different between panels.

GEOS-Chem also predicts increases in several speciation bins, including aerosol products of light aromatics (ASOA), terpene oxidation products (TSOA), aerosols from semi-volatile organic carbon (POA), and oxidation products of primary organic gas oxidation (OPOA) (Table C1 and Figure C11). Many of these changes, especially OPOA (Figure C12), are positively correlated with OM3, which also demonstrates increases. OPOA generally follows the same temporal pattern as OM3 in many regions, showing an increase in concentrations starting in the latter half

of our analysis (Figure C13). Increases in OPOA are linked to OM3 in spring, summer, and fall across the CONUS. While TOC is reported to be decreasing, increases among positively associated independent measurements and modeled species (i.e., OM3 and OPOA) warrant further study.

Changes in OC fractions and ALW suggest changing particle properties. ALW acts as a plasticizer, and decreases in ALW lead to more viscous particles in laboratory and model studies (O'Meara et al., 2016; Reid et al., 2018). It is also plausible that changes in the fractional contribution of the thermal OC fractions are indicative of altered OA viscosity (Champion et al., 2019; Yli-Juuti et al., 2017). PC decreases alongside ALW and has been linked in laboratory studies to WSOC (Khan et al., 2012), which may suggest decreasing WSOC concentrations. As noted previously, decreases in PC may be due to decreases in mis-apportioned light-absorbing carbon (LAC) (Malm et al., 2020). LAC is thought to be organic in nature (Malm et al., 2020) and could form from browning reactions in the atmosphere facilitated by ALW (Chang and Thompson, 2010; De Haan et al., 2009; Sareen et al., 2010). Organic speciation changes may also occur concurrent with decreasing $NO_x$ emissions and increasing importance of autoxidation reactions (Praske et al., 2018). These findings are consistent with a potential increase in OA viscosity and are supportive of the changing nature of organic chemical species and pathways in OA over the CONUS. This has implications for particle phase state, which affects processes including reactive uptake and particle growth (Li and Shiraiwa, 2019) through changing mass transfer and bulk diffusion (Berkemeier et al., 2016; Marshall et al., 2016), impacting ability to quantitatively model and accurately assess aerosol impacts on climate and air quality (Shiraiwa et al., 2017b). Increased particle viscosity leads to long particle-phase diffusion timescales,

which can prolong time needed for oxidation and degradation and increase long-range transport of pollutants.

Biogenic emissions of VOCs have not changed greatly in the CONUS over the decade analyzed here, and have even increased in some areas (Heald et al., 2008; Spracklen et al., 2009). Decreases, most notably in inorganic anthropogenic emissions of $SO_2$ and $NO_x$, contribute to decreasing OA concentrations through a variety of mechanisms (Lane et al., 2008; Marais et al., 2017; Nguyen et al., 2015). Models consistently suggest that the dominant impact is via ALW formation pathways (Carlton et al., 2018a; Carlton and Turpin, 2013; Marais et al., 2017). The largest decreases in OA predicted by GEOS-Chem are strongly linked to SOA formed via aqueous pathways. Observed decreases in individual OC fractions positively associated with GEOS-Chem organic aerosol are at least partially attributable to decreases in anthropogenic emissions, most notably inorganic compounds that affect aerosol hygroscopicity to facilitate ALW uptake and SOA formation. The consistencies among independent decadal surface measurements and modeling results in humid and arid regions alike suggests that some level of chemical information is captured in routine OC fraction measurements and reproduced by models. This may offer insights into changing chemical regimes and implications for phase state, viscosity, and oxidation state of OA in the CONUS. Proper assessment of the impacts of climate, energy, and regulatory policy requires that models make accurate predictions for the right reasons. The findings here are consistent with the hypothesis that ancillary benefits occur broadly across the CONUS from federal air quality rules aimed at ozone and acid rain through reductions in OA mass concentrations.

# CHAPTER FIVE

## SUMMARY AND FUTURE DIRECTIONS

## 5.1 Summary

### 5.1.1 Aerosol Optical Thickness: Organic Composition, Associated Particle Water, and Aloft Extinction

Surface measurements of particle mass are insufficient to fully explain trends of AOT summertime enhancement over the southeast US, as observed by MODIS and CALIOP. Satellite measurements differ up to a factor of 4 between summer and winter, while seasonal change in $PM_{2.5}$ shows negligible differences. ALW from inorganic particle components partially explains this discrepancy, but these associations differ by season. I hypothesized that ALW from organic components could help resolve this seasonal discrepancy and improve $PM_{2.5}$-AOT relationships. IMPROVE data was used at eight locations in two focus regions, Appalachia and the Colorado Plateau, with differing seasonal AOT patterns from 2007-2016. Organic hygroscopicity was estimated spanning the typical range for organic species in laboratory studies ($0.01 \leq \kappa \leq 0.20$) and organic ALW concentrations were calculated using κ-Kohler theory. AOT values are taken from MODIS, and vertical extinction from CALIPSO. I present findings that show decadal, seasonal, and spatial change in $PM_{2.5}$ that includes ALW is positively associated with AOT most closely in Appalachia during summer. I find that correlations are low in the Colorado Plateau, and that correlations between $PM_{2.5}$ and AOT are not significantly changed upon consideration of organic and inorganic contributions to ALW. Within the boundary layer, spatial trends, seasonal patterns, and vertical profiles of remotely sensed extinction qualitatively match patterns in integrated ALW. Extinction is enhanced above the boundary layer. Trends are unable to be reconciled

partly because of poorly described particle chemical composition and the inability of current approaches to assess aloft phenomena. To better assess water uptake and aerosol chemical properties, organic speciation must be better constrained, and this is an area for future study.

### 5.1.2 Differences in Fine Particle Chemical Composition on Clear and Cloudy Days

Satellite retrievals that are affected by cloudy conditions are often removed from final data products, which hinders knowledge of chemical composition during cloudy times. Cloud processing is an important source of aerosol mass and alters chemical composition. I investigated differences in $PM_{2.5}$ mass and chemical composition between cloudy and clear sky times. I hypothesized that there are quantitative differences in $PM_{2.5}$ chemical composition between cloudy and clear sky times in ways that impact particle hygroscopicity and water uptake. IMPROVE data were downloaded for sites across the CONUS with complete data from 2010-2014. Observations were paired in space and time with cloud flags from MODIS overpasses to attain two sets of observations, one during clear sky times and one during cloudy times. There are statistically discernible differences among $PM_{2.5}$ and chemical constituent concentrations under cloudy and clear sky conditions that cannot be explained solely by physical mechanisms. Chemical constituent concentrations are sufficiently changed between cloudy and clear sky periods to affect ALW. Differences in chemical constituent concentrations require *in situ* chemical formation processes to fully explain temporal and spatial patterns. This work indicates that aerosol growth due to water uptake is greatest during cloudy times, when satellites are unable to remotely sense particle properties and impacts. The clear sky bias affects accurate representation of ALW. Without *in situ* chemical information, aerosol-cloud interactions and estimates of radiative forcings in models will remain a large uncertainty.

### 5.1.3 The Changing Nature of Organic Carbon over the United States

TOC concentrations have been decreasing across the CONUS, and especially in the southeast US. I investigated if these trends are driven by specific OC fractions. IMPROVE data were downloaded for all sites across the CONUS with complete data from 2005-2015. I find that reductions in PC and OC2 drive observed and reported decadal decreases in TOC across the CONUS. Relative changes normalized to local concentrations are uniform across the CONUS, and the largest absolute changes occur in the eastern US. I also paired CONUS-wide observations of OC converted to OM with GEOS-Chem model simulations of OA to identify potential species classes or chemical regimes that may be changing over time. GEOS-Chem simulations reproduce OM trends across the CONUS and suggest that decreases are due to ALW chemistry. Individual model species simulated by GEOS-Chem, notably SOA derived from isoprene oxidation products and formed in ALW, correlate significantly with OM2 in regions across the CONUS, including arid regions. There are small increases in OM3 that are correlated with increases in GEOS-Chem model species, which is an interesting area for future study. Correlations between model species and OM fractions lend insight to changing chemical regimes with implications for particle phase state and viscosity. These findings agree with previous studies in the literature which suggest that decreasing ALW concentrations due to $SO_2$ and $NO_x$ emissions regulations also decrease TOC. These findings are consistent with literature that suggests federal air quality rules aimed at anthropogenic $SO_2$ and $NO_x$ emissions further reduce fine particle mass through decreases in TOC, primarily through chemistry involving ALW. Benefits are prevalent in the humid eastern US and also occur in arid regions.

### 5.1.4 Key Knowledge Gaps Identified

Chapter 3 discusses the differences in chemical composition that occur between cloudy and clear sky days, which affect particle hygroscopicity and water content. Currently, models are not sufficiently evaluated against aerosol data influenced by clouds or atmospheric water. Cloud processing and water-mediated reactions are essential to understanding the fate, transport, and radiative impacts of aerosol. One focus area for improvement is in the design of laboratory studies. Many experiments rely on low RH values of 10% or less, conditions that are atmospherically relevant only in extremely dry locations such as deserts. To encompass areas with higher ambient RH such as the southeast US, laboratory experiments must be designed that do not rely on extremely low RH conditions. Environmentally-relevant RH conditions, which are typically >60% for the southeast US, need to be employed, and the effects of varying RH conditions (as occur diurnally and seasonally) should continue to be investigated, despite the inherent difficulties such as complications from contaminants.

Further, the organic fraction of atmospheric aerosol is poorly characterized, which negatively impacts ability to model organic aerosol and its subsequent impacts. In particular, better description of organic composition and hygroscopicity is necessary, as illustrated in Chapter 2. Experiments to better characterize organic chemical composition and to increase understanding of its effects on particle hygroscopicity should be implemented to narrow this knowledge gap. Chapter 4 investigates how routine monitoring network site measurements offer potential insights into organic chemical composition, but much work is required to lower uncertainties regarding these measurements and to standardize and improve measurement techniques and analyses of organic carbon within and between long-term monitoring networks.

## 5.2 Future Directions

### 5.2.1 Effects of Changing Salt Molality on Organic Partitioning into Aerosols and Cloud Droplets

Inorganic salts (e.g., $SO_4^{2-}$, $NO_3^-$) promote the formation of ALW, which serves as a medium for the partitioning of water-soluble organic gases (Prisle et al., 2010) and is a dominant facilitator of SOA formation through aqueous processing (Carlton and Turpin, 2013; Hodas et al., 2014; McNeill, 2015). Beyond promoting ALW, inorganic salts can also react directly with organic compounds to form S- and N-containing species (Darer et al., 2011; Froyd et al., 2010; Lee et al., 2016), and they can alter the partitioning of organics to the condensed phase (Wang et al., 2014). Across the CONUS, summertime aerosol salt molality is estimated from ground-based observations to be >1 mol $kg^{-1}$. Sulfate molality in the eastern US has risen in recent years despite reductions in sulfate mass due to decreasing relative humidity, and nitrate molality is also increasing (Figure 5.1).

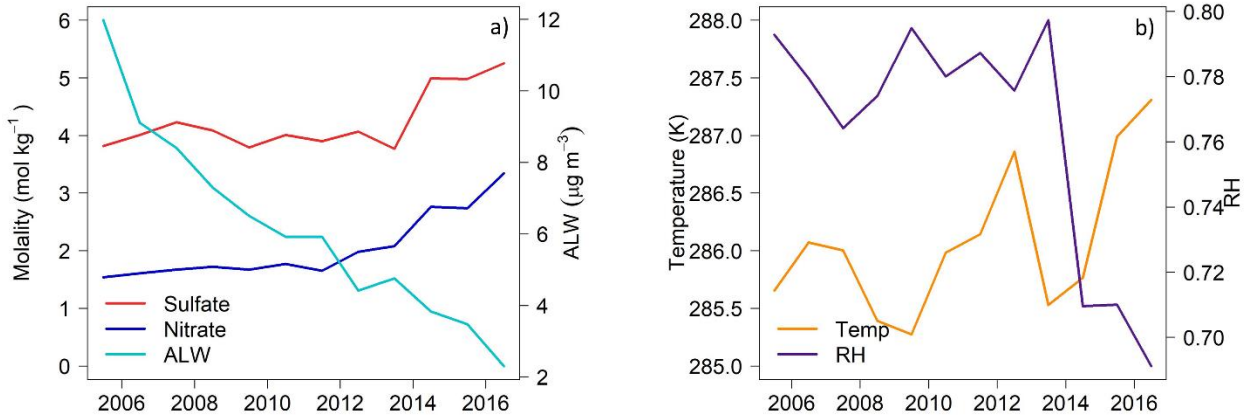


**Figure 5.1.** Annual average (a) $SO_4^{2-}$ molality, $NO_3^-$ molality, and ALW mass concentrations in the eastern US, and annual average (b) temperature and RH in the eastern US from 2005-2016.

The partitioning of chemical species to water is traditionally described using Henry's Law, which is valid only for ideal, dilute solutions. Particles are much too concentrated for standard Henry's Law constants ($K_H$) to apply. The presence of salts can alter the effective Henry's Law constant of an organic species by more than an order of magnitude, and this is dependent on salt, organic species, and concentration (Wang et al., 2014, 2017a). Inorganic salts impact the partitioning of organic species, such as α-dicarbonyls and naphthols, to water via salting-in and salting-out effects (Almeida et al., 1983; Waxman et al., 2015). Salting-in is defined as the phenomenon that occurs when the solubility of a substance in water increases with an increase in salt concentration. Conversely, salting-out occurs when the solubility of a substance in water decreases with increasing salt concentration. For example, the partitioning of glyoxal to the particle phase is enhanced in the presence of salts (salting-in) (Waxman et al., 2015), while the partitioning of methylglyoxal and butenedial are reduced by salts (salting-out) (Birdsall et al., 2019; Waxman et al., 2015). The relative effectiveness of salting effects is quantified via the Setschenow equation (Eqn 5.1).

$$log \frac{S_0}{S} = K_s C \quad (5.1)$$

Here, $S_0$ is the solubility of the solute in pure water, S is the solubility in salt solution, $K_s$ is the Setchenow coefficient, and C is the salt concentration. When salting-out occurs, $K_s$ is positive, and $K_s$ is negative when salting-in occurs. Salt effects are generally not included in model simulations. The implementation of Setschenow coefficients in CMAQ for glyoxal results in an increase in particle phase glyoxal by a factor of 3 (Sareen et al., 2017). Understanding the dramatic impact of salts on organic partitioning is essential to predicting the fate and transport of carbon. More experiments are required to apply Sestchenow coefficients to other organic gases and improve model representation of organic partitioning.

Water favors the partitioning of polar organic compounds, and the salting effect is most dramatic for polar organic species with high O:C ratios (Kampf et al., 2013; Waxman et al., 2015). The partitioning behavior of gases under high ionic strength conditions has only been studied for a small group of polar organic compounds (Birdsall et al., 2019; Kampf et al., 2013; Khan et al., 1995; Nguyen et al., 2014b; Waxman et al., 2015). Theoretical predictions of $K_H$ from computational approaches tend to worsen as molecules become more oxygenated and water-soluble (Raventos-Duran et al., 2010). Reducing uncertainty in $K_H$ values in highly concentrated solutions is essential to improving model predictions. Further, organic partitioning impacts particle phase state, which has important implications for aerosol hygroscopic growth, CCN activation, and effects on climate (Berkemeier et al., 2016). Many atmospherically relevant salt anions (e.g., $SO_4^{2-}$, $NO_3^-$, $Cl^-$) are observed to affect the partitioning of organic compounds into water, and although cations also impact partitioning, anions have a determining effect (Hyde et al., 2017).

In Chapter 4, I present evidence that suggests organic aerosol concentration and composition over the CONUS is changing in time and space (Figure 4.1). TOC concentrations have been decreasing, and this is driven by PC and OC2, fractions that are linked to organic components formed in ALW. As ALW concentrations decrease and salt molality increases, it is possible that salting effects may also play a role in the observed OC changes. If species that are expected to evolve in OC2 (e.g., carboxylic acids, steranes) salt-out, this could help to further explain changes in organic carbon over time. Further, I find evidence for potential increases in OC3 in the eastern US, which are also linked to various GEOS-Chem speciation bins. Interestingly, increases in OC3 occur after 2014, when sulfate and nitrate molality increase most greatly.

Species that evolve in OC3 may be more polar and viscous (Champion et al., 2019; Yli-Juuti et al., 2017), and if these species salt-in, this may help to explain decadal trends in OC3 as well as provide further evidence for changes in particle phase state. Understanding the salting behavior of atmospherically-relevant organic species could lend further insights into the decadal OC fraction trends observed in Chapter 4.

Organic partitioning in water can be investigated using mist chambers (Hennigan et al., 2018). Mist chambers operate by concentrating water-soluble gases from a high volume of air into mist droplets via turbulent mixing and have been employed previously in field studies (Sareen et al., 2016). Field and laboratory experiments should be performed to investigate salting effects on organic partitioning. Results from these experiments can be used in models to improve prediction of organic partitioning and SOA formation.

1) The tendency of individual atmospherically relevant species (e.g., glyoxal, methylglyoxal, methanol) to salt in or out should be tested via laboratory-based mist chamber experiments. The Carlton lab is currently constructing a parallel mist chamber sampling setup similar to the one in Hennigan et al. 2018. Here, one mist chamber is filled with nanopure water, and the other with dissolved salts of varying concentrations. These chambers can be run side-by-side to test the effects of common atmospheric inorganic salts (e.g., NaCl, KCl, ammonium sulfate, and ammonium nitrate) on the partitioning behavior of individual organic species. WSOC concentrations in the aqueous phase of both nanopure and salty water can be determined via a total organic carbon

analyzer. These mist chamber experiments can lead to the determination of Setschenow coefficients that can be implemented in models.

2) The Setschenow coefficients determined from these mist chamber experiments should then be implemented in atmospheric models such as CMAQ for individual compounds, with the goal of assessing the potential implications of salt-affected partitioning for the atmospheric carbon budget.

3) The tendency of organic species in ambient air to salt in or out should be tested via mist chambers deployed in the field. These experiments should be performed in multiple locations across the CONUS during different seasons to assess spatial and seasonal trends, as organic species and sources vary depending on location.

Results from these mist chamber and modeling experiments will lend insight into the way organic species are influenced by the presence of salts. The partitioning of organic species into water is also important from a health standpoint, as discussed in the next section (5.2.2).

### 5.2.2 Identifying the Role of Chemical Composition in Health Endpoints

A recent study (Babila et al., 2020) points out a discrepancy in the literature regarding the role of particulate sulfate in health endpoints. Sulfate is often positively correlated with increased health risk in epidemiology studies (Dockery et al., 1993, 1996; Raizenne et al., 1996), especially those performed in the humid eastern US. However, toxicology studies are unable to find mechanistic evidence for a direct association between sulfate and health endpoints (Reiss et al., 2007;

Schlesinger, 2007), and sulfate concentrations need to be increased up to 1000 μg $m^{-3}$, ~30 times above the NAAQS 24-hour standard, to observe effects on pulmonary function in humans (Schlesinger and Cassee, 2003).

Recent evidence suggests that sulfate itself is not the chemical species driving negative health endpoints, but that it rather acts as a surrogate for other species to impact the body. One possibility is that sulfate can provide the acidic environment necessary for various transition metals to dissolve in aerosol and subsequently enter the body, where they cause oxidative stress (Fang et al., 2017). Sulfate also promotes the uptake of ALW, which facilitates the partitioning of organic compounds to aerosols and the formation of SOA, especially in the eastern US (Carlton and Turpin, 2013). Organic compounds that partition into aerosol water may also partition into lung fluid when breathed in and negatively impact the body. For example, isoprene epoxydiol SOA, which can only form in the presence of ALW, causes oxidative stress in human bronchial epithelial cells, an effect that is not seen in control experiments using sulfate aerosol (Arashiro et al., 2018; Lin et al., 2017; Saffari et al., 2014; Verma et al., 2015). Associations between sulfate and health endpoints are often noted in the humid eastern US (Tsai et al., 2000) and not in the dry western US (Fairley, 1999; Mar et al., 2000), where ALW concentrations are low.

It is currently difficult to quantitatively assess the impact of ALW on health endpoints, as ALW concentrations are generally not measured, and the influence of water in both routine sampling and field studies is minimized, as discussed in Chapter 3. Babila et al. 2020 find that ALW concentrations from the routine monitoring network IMPROVE are biased low for most

locations. This may also impact the chemical composition that is recorded by the networks, as some semi-volatile species are also lost upon the equilibration of filters. This investigation warrants further research into the toxic effects of chemical constituents that are facilitated by the presence of ALW, such as WSOC. Partitioning of organic compounds into the particle phase that is affected by salt concentrations may alter the identity and concentration of organic species to which people are exposed, especially as salt concentrations increase over time. The testing of ambient samples to understand the effects of ambient organic species on health endpoints is essential.

Numerous previous experiments have been performed on the oxidative capacity of various atmospheric species, including WSOC (Verma et al., 2014), humic-like substances (Dou et al., 2015), and highly oxygenated organic aerosols (Verma et al., 2015). Assays typically used to assess oxidative potential include ascorbic acid (AA) and dithiothreitol (DTT), both of which are depleted by oxidation and mimic the interaction of pollutants and cellular antioxidants. These assays are not sensitive to sulfate, and the impacts of chemical constituents are likely due to secondary processing (Fang et al., 2017), such as partitioning and reaction in an aqueous medium. Experiments should be performed to evaluate the impact of inorganic salts on the partitioning of WSOC and subsequent potential health impacts such as ROS formation and oxidative potential.

1) Laboratory experiments to investigate the impact that salt concentrations have on the oxidative potential of individual species should be performed. Similar to the previous section (5.2.1), parallel mist chamber experiments (one mist chamber with nanopure

water, and the other with dissolved atmospherically relevant salts) should be run to investigate how the oxidative potential of individual water-soluble organic compounds changes in relation to partitioning. ROS generation potential of samples collected in the mist chambers can be assessed via DTT or AA assay.

2) Parallel mist chambers should be deployed in the field to conduct ambient sampling of WSOC for oxidative potential (as in Puthussery et al., 2018). As in the laboratory experiments, the ROS generation potential of extracts from both chambers can be measured via DTT or AA assay. These experiments should be performed in both humid and dry locations throughout the year to investigate the impacts of location and season on oxidative potential.

Results from these experiments will help to better constrain the role of ALW and salt molality in modulating health endpoints via the partitioning of water-soluble organic compounds.

# REFERENCES


Abdel-Shafy, H. I. and Mansour, M. S. M.: A review on polycyclic aromatic hydrocarbons: Source, environmental impact, effect on human health and remediation, Egypt. J. Pet., 25(1), 107–123, doi:10.1016/j.ejpe.2015.03.011, 2016.

Ackerman, A. S., Kirkpatrick, M. P., Stevens, D. E. and Toon, O. B.: The impact of humidity above stratiform clouds on indirect aerosol climate forcing, Nature, 432(7020), 1014–1017, doi:10.1038/nature03174, 2004.

Ahlm, L., Yli-Juuti, T., Schobesberger, S., Praplan, A. P., Kim, J., Tikkanen, O.-P., Lawler, M. J., Smith, J. N., Tröstl, J., Acosta Navarro, J. C., Baltensperger, U., Bianchi, F., Donahue, N. M., Duplissy, J., Franchin, A., Jokinen, T., Keskinen, H., Kirkby, J., Kürten, A., Laaksonen, A., Lehtipalo, K., Petäjä, T., Riccobono, F., Rissanen, M. P., Rondo, L., Schallhart, S., Simon, M., Winkler, P. M., Worsnop, D. R., Virtanen, A. and Riipinen, I.: Modeling the thermodynamics and kinetics of sulfuric acid-dimethylamine-water nanoparticle growth in the CLOUD chamber, Aerosol Sci. Technol., 50(10), 1017–1032, doi:10.1080/02786826.2016.1223268, 2016.

Aiken, A. C., DeCarlo, P. F., Kroll, J. H., Worsnop, D. R., Huffman, J. A., Docherty, K. S., Ulbrich, I. M., Mohr, C., Kimmel, J. R., Sueper, D., Sun, Y., Zhang, Q., Trimborn, A., Northway, M., Ziemann, P. J., Canagaratna, M. R., Onasch, T. B., Alfarra, M. R., Prevot, A. S. H., Dommen, J., Duplissy, J., Metzger, A., Baltensperger, U. and Jimenez, J. L.: O/C and OM/OC Ratios of Primary, Secondary, and Ambient Organic Aerosols with High-Resolution Time-of-Flight Aerosol Mass Spectrometry, Environ. Sci. Technol., 42(12), 4478–4485, doi:10.1021/es703009q, 2008.

Albrecht, B. A.: Aerosols, Cloud Microphysics, and Fractional Cloudiness, Science, 245(4923), 1227–1230, doi:10.1126/science.245.4923.1227, 1989.

Alexander, D. T. L., Crozier, P. A. and Anderson, J. R.: Brown Carbon Spheres in East Asian Outflow and Their Optical Properties, Science, 321(5890), 833–836, doi:10.1126/science.1155296, 2008.

Almeida, M. B., Alvarez, A. M., Miguel, E. M. D. and Hoyo, E. S. D.: Setchenow coefficients for naphthols by distribution method, Can. J. Chem., 61(2), 244–248, doi:10.1139/v83-043, 1983.

Alston, E. and Sokolik, I.: Assessment of Aerosol Radiative Forcing with 1-D Radiative Transfer Modeling in the U. S. South-East, Atmosphere, 9(7), 271, doi:10.3390/atmos9070271, 2018.

Altieri, K. E., Carlton, A. G., Lim, H.-J., Turpin, B. J. and Seitzinger, S. P.: Evidence for Oligomer Formation in Clouds: Reactions of Isoprene Oxidation Products, Environ. Sci. Technol., 40(16), 4956–4960, doi:10.1021/es052170n, 2006.

Altieri, K. E., Seitzinger, S. P., Carlton, A. G., Turpin, B. J., Klein, G. C. and Marshall, A. G.: Oligomers formed through in-cloud methylglyoxal reactions: Chemical composition, properties, and mechanisms investigated by ultra-high resolution FT-ICR mass spectrometry, Atmos. Environ., 42(7), 1476–1490, doi:10.1016/j.atmosenv.2007.11.015, 2008.

Andreae, M. O. and Gelencsér, A.: Black carbon or brown carbon? The nature of light-absorbing carbonaceous aerosols, Atmospheric Chem. Phys., 6(10), 3131–3148, doi:10.5194/acp-6-3131-2006, 2006.

Air Quality Research Center: Interagency Monitoring of Protected Visual Environments (IMPROVE) Semiannual Quality Assurance Report: January 1, 2018 through December 31, 2018, [online] Available from: http://vista.cira.colostate.edu/improve/wp-content/uploads/2019/11/IMPROVE_QAReport_11.15.2019.pdf, 2019.

Appel, K. W., Foley, K. M., Bash, J. O., Pinder, R. W., Dennis, R. L., Allen, D. J. and Pickering, K.: A multi-resolution assessment of the Community Multiscale Air Quality (CMAQ) model v4.7 wet deposition estimates for 2002–2006, Geosci. Model Dev., 4(2), 357–371, doi:10.5194/gmd-4-357-2011, 2011.

Arashiro, M., Lin, Y.-H., Zhang, Z., Sexton, K. G., Gold, A., Jaspers, I., Fry, R. C. and Surratt, J. D.: Effect of secondary organic aerosol from isoprene-derived hydroxyhydroperoxides on the expression of oxidative stress response genes in human bronchial epithelial cells, Environ. Sci. Process. Impacts, 20(2), 332–339, doi:10.1039/C7EM00439G, 2018.

Aswini, A. R., Hegde, P., Nair, P. R. and Aryasree, S.: Seasonal changes in carbonaceous aerosols over a tropical coastal location in response to meteorological processes, Sci. Total Environ., 656, 1261–1279, doi:10.1016/j.scitotenv.2018.11.366, 2019.

Atkinson, R. W., Mills, I. C., Walton, H. A. and Anderson, H. R.: Fine particle components and health—a systematic review and meta-analysis of epidemiological time series studies of daily mortality and hospital admissions, J. Expo. Sci. Environ. Epidemiol., 25(2), 208–214, doi:10.1038/jes.2014.63, 2015.

Attwood, A. R., Washenfelder, R. A., Brock, C. A., Hu, W., Baumann, K., Campuzano-Jost, P., Day, D. A., Edgerton, E. S., Murphy, D. M., Palm, B. B., McComiskey, A., Wagner, N. L., de Sá, S. S., Ortega, A., Martin, S. T., Jimenez, J. L. and Brown, S. S.: Trends in sulfate and organic aerosol mass in the Southeast U.S.: Impact on aerosol optical depth and radiative forcing: Aerosol mass and optical depth in SE US, Geophys. Res. Lett., 41(21), 7701–7709, doi:10.1002/2014GL061669, 2014.

Babila, J. E., Carlton, A. G., Hennigan, C. J. and Ghate, V. P.: On Aerosol Liquid Water and Sulfate Associations: The Potential for Fine Particulate Matter Biases, Atmosphere, 11(2), 194, doi:10.3390/atmos11020194, 2020.

Bar-Or, R. Z., Koren, I., Altaratz, O. and Fredj, E.: Radiative properties of humidified aerosols in cloudy environment, Atmospheric Res., 118, 280–294, doi:10.1016/j.atmosres.2012.07.014, 2012.

Barth, M. C.: Summary of the cloud chemistry modeling intercomparison: Photochemical box model simulation, J. Geophys. Res., 108(D7), doi:10.1029/2002JD002673, 2003.

Baumgardner, D., Popovicheva, O., Allan, J., Bernardoni, V., Cao, J., Cavalli, F., Cozic, J., Diapouli, E., Eleftheriadis, K., Genberg, P. J., Gonzalez, C., Gysel, M., John, A., Kirchstetter, T. W., Kuhlbusch, T. A. J., Laborde, M., Lack, D., Müller, T., Niessner, R., Petzold, A., Piazzalunga, A., Putaud, J. P., Schwarz, J., Sheridan, P., Subramanian, R., Swietlicki, E., Valli, G., Vecchi, R. and Viana, M.: Soot reference materials for instrument calibration and intercomparisons: a workshop summary with recommendations, Atmospheric Meas. Tech., 5(8), 1869–1887, doi:10.5194/amt-5-1869-2012, 2012.

Bell, M. L., Davis, D. L. and Fletcher, T.: A retrospective assessment of mortality from the London smog episode of 1952: the role of influenza and pollution., Environ. Health Perspect., 112(1), 6–8, doi:10.1289/ehp.6539, 2004.

Bench, G., Fallon, S., Schichtel, B., Malm, W. and McDade, C.: Relative contributions of fossil and contemporary carbon sources to $PM_{2.5}$ aerosols at nine Interagency Monitoring for Protection of Visual Environments (IMPROVE) network sites: Carbon Contribution to Aerosols, J. Geophys. Res. Atmospheres, 112(D10), doi:10.1029/2006JD007708, 2007.

Berkemeier, T., Steimer, S. S., Krieger, U. K., Peter, T., Pöschl, U., Ammann, M. and Shiraiwa, M.: Ozone uptake on glassy, semi-solid and liquid organic matter and the role of reactive oxygen intermediates in atmospheric aerosol chemistry, Phys. Chem. Chem. Phys., 18(18), 12662–12674, doi:10.1039/C6CP00634E, 2016.

Birdsall, A. W., Hensley, J. C., Kotowitz, P. S., Huisman, A. J. and Keutsch, F. N.: Single-particle experiments measuring humidity and inorganic salt effects on gas-particle partitioning of butenedial, Atmospheric Chem. Phys., 19(22), 14195–14209, doi:10.5194/acp-19-14195-2019, 2019.

Blanchard, C. L., Tanenbaum, S. and Hidy, G. M.: Source Attribution of Air Pollutant Concentrations and Trends in the Southeastern Aerosol Research and Characterization (SEARCH) Network, Environ. Sci. Technol., 47(23), 13536–13545, doi:10.1021/es402876s, 2013.

Blando, J. D. and Turpin, B. J.: Secondary organic aerosol formation in cloud and fog droplets: a literature evaluation of plausibility, Atmos. Environ., 34(10), 1623–1632, doi:10.1016/S1352-2310(99)00392-1, 2000.

Bond, T. C. and Bergstrom, R. W.: Light Absorption by Carbonaceous Particles: An Investigative Review, Aerosol Sci. Technol., 40(1), 27–67, doi:10.1080/02786820500421521, 2006.

Bond, T. C., Doherty, S. J., Fahey, D. W., Forster, P. M., Berntsen, T., DeAngelo, B. J., Flanner, M. G., Ghan, S., Kärcher, B., Koch, D., Kinne, S., Kondo, Y., Quinn, P. K., Sarofim, M. C., Schultz, M. G., Schulz, M., Venkataraman, C., Zhang, H., Zhang, S., Bellouin, N., Guttikunda, S. K., Hopke, P. K., Jacobson, M. Z., Kaiser, J. W., Klimont, Z., Lohmann, U., Schwarz, J. P., Shindell, D., Storelvmo, T., Warren, S. G. and Zender, C. S.: Bounding the role of black carbon in the climate system: A scientific assessment: Black Carbon in the Climate System, J. Geophys. Res. Atmospheres, 118(11), 5380–5552, doi:10.1002/jgrd.50171, 2013.

Bones, D. L., Henricksen, D. K., Mang, S. A., Gonsior, M., Bateman, A. P., Nguyen, T. B., Cooper, W. J. and Nizkorodov, S. A.: Appearance of strong absorbers and fluorophores in limonene-$O_3$ secondary organic aerosol due to $NH_4^+$-mediated chemical aging over long time scales, J. Geophys. Res., 115(D5), D05203, doi:10.1029/2009JD012864, 2010.

Boone, E. J., Laskin, A., Laskin, J., Wirth, C., Shepson, P. B., Stirm, B. H. and Pratt, K. A.: Aqueous Processing of Atmospheric Organic Particles in Cloud Water Collected via Aircraft Sampling, Environ. Sci. Technol., 49(14), 8523–8530, doi:10.1021/acs.est.5b01639, 2015.

Boparai, P., Lee, J. and Bond, T. C.: Revisiting Thermal-Optical Analyses of Carbonaceous Aerosol Using a Physical Model, Aerosol Sci. Technol., 42(11), 930–948, doi:10.1080/02786820802360690, 2008.

Boucher, O., Myhre, G. and Myhre, A.: Direct human influence of irrigation on atmospheric water vapour and climate, Clim. Dyn., 22(6–7), 597–603, doi:10.1007/s00382-004-0402-4, 2004.

Boucher, O., Randall, D., Artaxo, P., Bretherton, C., Feingold, G., Forster, P., Kerminen, V.-M., Kondo, Y., Liao, H., Lohmann, U., Rasch, P., Satheesh, S. K., Sherwood, S., Stevens, B. and Zhang, X. Y.: Clouds and Aerosols. In: Climate Change 2013: The Physical Science Basis, Contribution of Working Group I to the Fifth Assessment Report of the Intergovernmental Panel on Climate Change, edited by T. F. Stocker, D. Qin, G.-K. Plattner, M. Tignor, S. K. Allen, J. Boschung, A. Nauels, Y. Xia, V. Bex, and P. M. Midgley, 2013.

Bray, C. D., Battye, W., Aneja, V. P., Tong, D., Lee, P., Tang, Y. and Nowak, J. B.: Evaluating ammonia ($NH_3$) predictions in the NOAA National Air Quality Forecast Capability (NAQFC) using in-situ aircraft and satellite measurements from the CalNex2010 campaign, Atmos. Environ., 163, 65–76, doi:10.1016/j.atmosenv.2017.05.032, 2017.

Brock, C. A., Wagner, N. L., Anderson, B. E., Attwood, A. R., Beyersdorf, A., Campuzano-Jost, P., Carlton, A. G., Day, D. A., Diskin, G. S., Gordon, T. D., Jimenez, J. L., Lack, D. A., Liao, J., Markovic, M. Z., Middlebrook, A. M., Ng, N. L., Perring, A. E., Richardson, M. S., Schwarz, J. P., Washenfelder, R. A., Welti, A., Xu, L., Ziemba, L. D. and Murphy, D. M.: Aerosol optical properties in the southeastern United States in summer - Part 1: Hygroscopic growth, Atmospheric Chem. Phys., 16(8), 4987–5007, doi:10.5194/acp-16-4987-2016, 2016.

Burnett, R. T., Pope, C. A., III, Ezzati, M., Olives, C., Lim, S. S., Mehta, S., Shin, H. H., Singh, G., Hubbell, B., Brauer, M., Anderson, H. R., Smith, K. R., Balmes, J. R., Bruce, N. G., Kan, H., Laden, F., Prüss-Ustün, A., Turner, M. C., Gapstur, S. M., Diver, W. R. and Cohen, A.: An Integrated Risk Function for Estimating the Global Burden of Disease Attributable to Ambient Fine Particulate Matter Exposure, Environ. Health Perspect., doi:10.1289/ehp.1307049, 2014.

Cao, J. J., Wu, F., Chow, J. C., Lee, S. C., Li, Y., Chen, S. W., An, Z. S., Fung, K. K., Watson, J. G., Zhu, C. S. and Liu, S. X.: Characterization and source apportionment of atmospheric organic and elemental carbon during fall and winter of 2003 in Xi'an, China, Atmospheric Chem. Phys., 5(11), 3127–3137, doi:10.5194/acp-5-3127-2005, 2005.

Cappa, C. D., Che, D. L., Kessler, S. H., Kroll, J. H. and Wilson, K. R.: Variations in organic aerosol optical and hygroscopic properties upon heterogeneous OH oxidation, J. Geophys. Res., 116(D15), D15204, doi:10.1029/2011JD015918, 2011.

Carlton, A. G. and Turpin, B. J.: Particle partitioning potential of organic compounds is highest in the Eastern US and driven by anthropogenic water, Atmospheric Chem. Phys., 13(20), 10203–10214, doi:10.5194/acp-13-10203-2013, 2013.

Carlton, A. G., Turpin, B. J., Lim, H.-J., Altieri, K. E. and Seitzinger, S.: Link between isoprene and secondary organic aerosol (SOA): Pyruvic acid oxidation yields low volatility organic acids in clouds, Geophys. Res. Lett., 33(6), L06822, doi:10.1029/2005GL025374, 2006.

Carlton, A. G., Turpin, B. J., Altieri, K. E., Seitzinger, S., Reff, A., Lim, H.-J. and Ervens, B.: Atmospheric oxalic acid and SOA production from glyoxal: Results of aqueous photooxidation experiments, Atmos. Environ., 41(35), 7588–7602, doi:10.1016/j.atmosenv.2007.05.035, 2007.

Carlton, A. G., Turpin, B. J., Altieri, K. E., Seitzinger, S. P., Mathur, R., Roselle, S. J. and Weber, R. J.: CMAQ Model Performance Enhanced When In-Cloud Secondary Organic Aerosol is Included: Comparisons of Organic Carbon Predictions with Measurements, Environ. Sci. Technol., 42(23), 8798–8802, doi:10.1021/es801192n, 2008.

Carlton, A. G., Pye, H. O. T., Baker, K. R. and Hennigan, C. J.: Additional Benefits of Federal Air-Quality Rules: Model Estimates of Controllable Biogenic Secondary Organic Aerosol, Environ. Sci. Technol., 52(16), 9254–9265, doi:10.1021/acs.est.8b01869, 2018a.

Carlton, A. G., de Gouw, J., Jimenez, J. L., Ambrose, J. L., Attwood, A. R., Brown, S., Baker, K. R., Brock, C., Cohen, R. C., Edgerton, S., Farkas, C. M., Farmer, D., Goldstein, A. H., Gratz, L., Guenther, A., Hunt, S., Jaeglé, L., Jaffe, D. A., Mak, J., McClure, C., Nenes, A., Nguyen, T. K., Pierce, J. R., de Sa, S., Selin, N. E., Shah, V., Shaw, S., Shepson, P. B., Song, S., Stutz, J., Surratt, J. D., Turpin, B. J., Warneke, C., Washenfelder, R. A., Wennberg, P. O. and Zhou, X.: Synthesis of the Southeast Atmosphere Studies: Investigating Fundamental Atmospheric Chemistry Questions, Bull. Am. Meteorol. Soc., 99(3), 547–567, doi:10.1175/BAMS-D-16-0048.1, 2018b.

Champion, W. M., Rothfuss, N. E., Petters, M. D. and Grieshop, A. P.: Volatility and Viscosity Are Correlated in Terpene Secondary Organic Aerosol Formed in a Flow Reactor, Environ. Sci. Technol. Lett., 513–519, doi:10.1021/acs.estlett.9b00412, 2019.

Chang, J. L. and Thompson, J. E.: Characterization of colored products formed during irradiation of aqueous solutions containing $H_2O_2$ and phenolic compounds, Atmos. Environ., 44(4), 541–551, doi:10.1016/j.atmosenv.2009.10.042, 2010.

Chow, J., Watson, J. G., Chen, L.-W. A., Chang, M.-C. O. and Paredes-Miranda, G.: Comparison of the DRI/OGC and Model 2001 Thermal/Optical Carbon Analyzers, [online] Available from: http://vista.cira.colostate.edu/improve/Publications/GrayLit/013_CarbonAnalyzer/IMPROVECarbonAnalyzerAssessment.pdf (Accessed 14 November 2019), 2005.

Chow, J. C. and Watson, J. G.: $PM_{2.5}$ carbonate concentrations at regionally representative Interagency Monitoring of Protected Visual Environment sites: Carbonate Concentrations at IMPROVE Sites, J. Geophys. Res. Atmospheres, 107(D21), ICC 6-1-ICC 6-9, doi:10.1029/2001JD000574, 2002.

Chow, J. C., Watson, J. G., Pritchett, L. C., Pierson, W. R., Frazier, C. A. and Purcell, R. G.: The dri thermal/optical reflectance carbon analysis system: description, evaluation and applications in U.S. Air quality studies, Atmospheric Environ. Part Gen. Top., 27(8), 1185–1201, doi:10.1016/0960-1686(93)90245-T, 1993.

Chow, J. C., Watson, J. G., Kuhns, H., Etyemezian, V., Lowenthal, D. H., Crow, D., Kohl, S. D., Engelbrecht, J. P. and Green, M. C.: Source profiles for industrial, mobile, and area sources in the Big Bend Regional Aerosol Visibility and Observational study, Chemosphere, 54(2), 185–208, doi:10.1016/j.chemosphere.2003.07.004, 2004.

Chow, J. C., Watson, J. G., Chen, L.-W. A., Chang, M. C. O., Robinson, N. F., Trimble, D. and Kohl, S.: The IMPROVE_A Temperature Protocol for Thermal/Optical Carbon Analysis: Maintaining Consistency with a Long-Term Database, J. Air Waste Manag. Assoc., 57(9), 1014–1023, doi:10.3155/1047-3289.57.9.1014, 2007.

Chow, J. C., Lowenthal, D. H., Chen, L.-W. A., Wang, X. and Watson, J. G.: Mass reconstruction methods for $PM_{2.5}$: a review, Air Qual. Atmosphere Health, 8(3), 243–263, doi:10.1007/s11869-015-0338-3, 2015.

Chow, J. C., Watson, J. G., Green, M. C., Wang, X., Chen, L.-W. A., Trimble, D. L., Cropper, P. M., Kohl, S. D. and Gronstal, S. B.: Separation of brown carbon from black carbon for IMPROVE and Chemical Speciation Network $PM_{2.5}$ samples, J. Air Waste Manag. Assoc., 68(5), 494–510, doi:10.1080/10962247.2018.1426653, 2018.

Christiansen, A. E., Ghate, V. P. and Carlton, A. G.: Aerosol Optical Thickness: Organic Composition, Associated Particle Water, and Aloft Extinction, ACS Earth Space Chem., 3(3), 403–412, doi:10.1021/acsearthspacechem.8b00163, 2019.

Christiansen, A. E., Carlton, A. G. and Henderson, B. H.: Differences in Fine Particle Chemical Composition on Clear and Cloudy Days, Atmospheric Chem. Phys. Discuss., doi:10.5194/acp-2020-184, 2020.

Christopher, S. A. and Gupta, P.: Satellite Remote Sensing of Particulate Matter Air Quality: The Cloud-Cover Problem, J. Air Waste Manag. Assoc., 60(5), 596–602, doi:10.3155/1047-3289.60.5.596, 2010.

Clegg, S. L., Brimblecombe, P. and Wexler, A. S.: Thermodynamic Model of the System $H^+ - NH_4^+ - Na^+ - SO_4^{2-} - NO_3^- - Cl^- - H_2O$ at 298.15 K, J. Phys. Chem. A, 102(12), 2155–2171, doi:10.1021/jp973043j, 1998.

Cohen, A. J., Brauer, M., Burnett, R., Anderson, H. R., Frostad, J., Estep, K., Balakrishnan, K., Brunekreef, B., Dandona, L., Dandona, R., Feigin, V., Freedman, G., Hubbell, B., Jobling, A., Kan, H., Knibbs, L., Liu, Y., Martin, R., Morawska, L., Pope, C. A., Shin, H., Straif, K., Shaddick, G., Thomas, M., van Dingenen, R., van Donkelaar, A., Vos, T., Murray, C. J. L. and Forouzanfar, M. H.: Estimates and 25-year trends of the global burden of disease attributable to ambient air pollution: an analysis of data from the Global Burden of Diseases Study 2015, The Lancet, 389(10082), 1907–1918, doi:10.1016/S0140-6736(17)30505-6, 2017.

Crosbie, E., Youn, J.-S., Balch, B., Wonaschütz, A., Shingler, T., Wang, Z., Conant, W. C., Betterton, E. A. and Sorooshian, A.: On the competition among aerosol number, size and composition in predicting CCN variability: a multi-annual field study in an urbanized desert, Atmospheric Chem. Phys., 15(12), 6943–6958, doi:10.5194/acp-15-6943-2015, 2015.

Darer, A. I., Cole-Filipiak, N. C., O'Connor, A. E. and Elrod, M. J.: Formation and Stability of Atmospherically Relevant Isoprene-Derived Organosulfates and Organonitrates, Environ. Sci. Technol., 45(5), 1895–1902, doi:10.1021/es103797z, 2011.

Dat, N.-D. and Chang, M. B.: Review on characteristics of PAHs in atmosphere, anthropogenic sources and control technologies, Sci. Total Environ., 609, 682–693, doi:10.1016/j.scitotenv.2017.07.204, 2017.

De Haan, D. O., Corrigan, A. L., Smith, K. W., Stroik, D. R., Turley, J. J., Lee, F. E., Tolbert, M. A., Jimenez, J. L., Cordova, K. E. and Ferrell, G. R.: Secondary Organic Aerosol-Forming Reactions of Glyoxal with Amino Acids, Environ. Sci. Technol., 43(8), 2818–2824, doi:10.1021/es803534f, 2009.

Dillner, A. M. and Takahama, S.: Predicting ambient aerosol thermal-optical reflectance (TOR) measurements from infrared spectra: organic carbon, Atmospheric Meas. Tech., 8(3), 1097–1109, doi:10.5194/amt-8-1097-2015, 2015.

Dillner, A. M., Phuah, C. H. and Turner, J. R.: Effects of post-sampling conditions on ambient carbon aerosol filter measurements, Atmos. Environ., 43(37), 5937–5943, doi:10.1016/j.atmosenv.2009.08.009, 2009.

Docherty, K. S., Aiken, A. C., Huffman, J. A., Ulbrich, I. M., DeCarlo, P. F., Sueper, D., Worsnop, D. R., Snyder, D. C., Peltier, R. E., Weber, R. J., Grover, B. D., Eatough, D. J., Williams, B. J., Goldstein, A. H., Ziemann, P. J.

and Jimenez, J. L.: The 2005 Study of Organic Aerosols at Riverside (SOAR-1): instrumental intercomparisons and fine particle composition, Atmospheric Chem. Phys., 11(23), 12387–12420, doi:10.5194/acp-11-12387-2011, 2011.

Dockery, D. W., Pope, C. A., Xu, X., Spengler, J. D., Ware, J. H., Fay, M. E., Ferris, B. G. and Speizer, F. E.: An Association between Air Pollution and Mortality in Six U.S. Cities, N. Engl. J. Med., 329(24), 1753–1759, doi:10.1056/NEJM199312093292401, 1993.

Dockery, D. W., Cunningham, J., Damokosh, A. I., Neas, L. M., Spengler, J. D., Koutrakis, P., Ware, J. H., Raizenne, M. and Speizer, F. E.: Health effects of acid aerosols on North American children: respiratory symptoms., Environ. Health Perspect., 104(5), 500–505, doi:10.1289/ehp.96104500, 1996.

Donahue, N. M., Robinson, A. L. and Pandis, S. N.: Atmospheric organic particulate matter: From smoke to secondary organic aerosol, Atmos. Environ., 43(1), 94–106, doi:10.1016/j.atmosenv.2008.09.055, 2009.

van Donkelaar, A., Martin, R. V. and Park, R. J.: Estimating ground-level $PM_{2.5}$ using aerosol optical depth determined from satellite remote sensing, J. Geophys. Res., 111(D21), D21201, doi:10.1029/2005JD006996, 2006.

van Donkelaar, A., Martin, R. V., Brauer, M., Kahn, R., Levy, R., Verduzco, C. and Villeneuve, P. J.: Global Estimates of Ambient Fine Particulate Matter Concentrations from Satellite-Based Aerosol Optical Depth: Development and Application, Environ. Health Perspect., 118(6), 847–855, doi:10.1289/ehp.0901623, 2010.

van Donkelaar, A., Martin, R. V., Spurr, R. J. D. and Burnett, R. T.: High-Resolution Satellite-Derived $PM_{2.5}$ from Optimal Estimation and Geographically Weighted Regression over North America, Environ. Sci. Technol., 49(17), 10482–10491, doi:10.1021/acs.est.5b02076, 2015a.

van Donkelaar, A., Martin, R. V., Brauer, M. and Boys, B. L.: Use of Satellite Observations for Long-Term Exposure Assessment of Global Concentrations of Fine Particulate Matter, Environ. Health Perspect., 123(2), 135–143, doi:10.1289/ehp.1408646, 2015b.

Dou, J., Lin, P., Kuang, B.-Y. and Yu, J. Z.: Reactive Oxygen Species Production Mediated by Humic-like Substances in Atmospheric Aerosols: Enhancement Effects by Pyridine, Imidazole, and Their Derivatives, Environ. Sci. Technol., 49(11), 6457–6465, doi:10.1021/es5059378, 2015.

Duncan, B. N., Prados, A. I., Lamsal, L. N., Liu, Y., Streets, D. G., Gupta, P., Hilsenrath, E., Kahn, R. A., Nielsen, J. E., Beyersdorf, A. J., Burton, S. P., Fiore, A. M., Fishman, J., Henze, D. K., Hostetler, C. A., Krotkov, N. A., Lee, P., Lin, M., Pawson, S., Pfister, G., Pickering, K. E., Pierce, R. B., Yoshida, Y. and Ziemba, L. D.: Satellite data of atmospheric pollution for U.S. air quality applications: Examples of applications, summary of data end-user resources, answers to FAQs, and common mistakes to avoid, Atmos. Environ., 94, 647–662, doi:10.1016/j.atmosenv.2014.05.061, 2014.

Duong, H. T., Sorooshian, A., Craven, J. S., Hersey, S. P., Metcalf, A. R., Zhang, X., Weber, R. J., Jonsson, H., Flagan, R. C. and Seinfeld, J. H.: Water-soluble organic aerosol in the Los Angeles Basin and outflow regions: Airborne and ground measurements during the 2010 CalNex field campaign: WSOC in LA Basin and Outflows, J. Geophys. Res. Atmospheres, 116(D21), doi:10.1029/2011JD016674, 2011.

Ehn, M., Thornton, J. A., Kleist, E., Sipilä, M., Junninen, H., Pullinen, I., Springer, M., Rubach, F., Tillmann, R., Lee, B., Lopez-Hilfiker, F., Andres, S., Acir, I.-H., Rissanen, M., Jokinen, T., Schobesberger, S., Kangasluoma, J., Kontkanen, J., Nieminen, T., Kurtén, T., Nielsen, L. B., Jørgensen, S., Kjaergaard, H. G., Canagaratna, M., Maso, M. D., Berndt, T., Petäjä, T., Wahner, A., Kerminen, V.-M., Kulmala, M., Worsnop, D. R., Wildt, J. and Mentel, T. F.: A large source of low-volatility secondary organic aerosol, Nature, 506(7489), 476–479, doi:10.1038/nature13032, 2014.

El-Sayed, M. M. H., Amenumey, D. and Hennigan, C. J.: Drying-Induced Evaporation of Secondary Organic Aerosol during Summer, Environ. Sci. Technol., 50(7), 3626–3633, doi:10.1021/acs.est.5b06002, 2016.

El-Zanan, H. S., Lowenthal, D. H., Zielinska, B., Chow, J. C. and Kumar, N.: Determination of the organic aerosol mass to organic carbon ratio in IMPROVE samples, Chemosphere, 60(4), 485–496, doi:10.1016/j.chemosphere.2005.01.005, 2005.

Engelhart, G. J., Hildebrandt, L., Kostenidou, E., Mihalopoulos, N., Donahue, N. M. and Pandis, S. N.: Water content of aged aerosol, Atmospheric Chem. Phys., 11(3), 911–920, doi:10.5194/acp-11-911-2011, 2011.

Ervens, B.: Modeling the Processing of Aerosol and Trace Gases in Clouds and Fogs, Chem. Rev., 115(10), 4157–4198, doi:10.1021/cr5005887, 2015.

Ervens, B., Turpin, B. J. and Weber, R. J.: Secondary organic aerosol formation in cloud droplets and aqueous particles (aqSOA): a review of laboratory, field and model studies, Atmospheric Chem. Phys., 11(21), 11069–11102, doi:10.5194/acp-11-11069-2011, 2011.

Fairley, D.: Daily mortality and air pollution in Santa Clara County, California: 1989-1996., Environ. Health Perspect., 107(8), 637–641, doi:10.1289/ehp.99107637, 1999.

Fan, J., Wang, Y., Rosenfeld, D. and Liu, X.: Review of Aerosol–Cloud Interactions: Mechanisms, Significance, and Challenges, J. Atmospheric Sci., 73(11), 4221–4252, doi:10.1175/JAS-D-16-0037.1, 2016.

Fang, T., Guo, H., Zeng, L., Verma, V., Nenes, A. and Weber, R. J.: Highly Acidic Ambient Particles, Soluble Metals, and Oxidative Potential: A Link between Sulfate and Aerosol Toxicity, Environ. Sci. Technol., 51(5), 2611–2620, doi:10.1021/acs.est.6b06151, 2017.

Farkas, C. M., Moeller, M. D., Felder, F. A., Henderson, B. H. and Carlton, A. G.: High Electricity Demand in the Northeast U.S.: PJM Reliability Network and Peaking Unit Impacts on Air Quality, Environ. Sci. Technol., 50(15), 8375–8384, doi:10.1021/acs.est.6b01697, 2016.

Ferrero, L., Sangiorgi, G., Perrone, M., Rizzi, C., Cataldi, M., Markuszewski, P., Pakszys, P., Makuch, P., Petelski, T., Becagli, S., Traversi, R., Bolzacchini, E. and Zielinski, T.: Chemical Composition of Aerosol over the Arctic Ocean from Summer ARctic EXpedition (AREX) 2011–2012 Cruises: Ions, Amines, Elemental Carbon, Organic Matter, Polycyclic Aromatic Hydrocarbons, n-Alkanes, Metals, and Rare Earth Elements, Atmosphere, 10(2), 54, doi:10.3390/atmos10020054, 2019.

Finlayson-Pitts, B. J. and Pitts, J. N.: Chemistry of the upper and lower atmosphere: theory, experiments, and applications, Academic Press, San Diego., 2000.

Fletcher, R. D.: The Donora Smog Disaster - A Problem in Atmospheric Pollution, Weatherwise, 2(3), 56–60, doi:10.1080/00431672.1949.9930058, 1949.

Flores, J. M., Zhao, D. F., Segev, L., Schlag, P., Kiendler-Scharr, A., Fuchs, H., Watne, å. K., Bluvshtein, N., Mentel, Th. F., Hallquist, M. and Rudich, Y.: Evolution of the complex refractive index in the UV spectral region in ageing secondary organic aerosol, Atmospheric Chem. Phys., 14(11), 5793–5806, doi:10.5194/acp-14-5793-2014, 2014.

Ford, B. and Heald, C. L.: Aerosol loading in the Southeastern United States: reconciling surface and satellite observations, Atmospheric Chem. Phys., 13(18), 9269–9283, doi:10.5194/acp-13-9269-2013, 2013.

Fountoukis, C. and Nenes, A.: ISORROPIA II: a computationally efficient thermodynamic equilibrium model for $K^+$-$Ca^{2+}$-$Mg^{2+}$-$NH_4^+$-$Na^+$-$SO_4^{2-}$-$NO_3^-$-$Cl^-$-$H_2O$ aerosols, Atmospheric Chem. Phys., 7(17), 4639–4659, doi:10.5194/acp-7-4639-2007, 2007.

Froyd, K. D., Murphy, S. M., Murphy, D. M., de Gouw, J. A., Eddingsaas, N. C. and Wennberg, P. O.: Contribution of isoprene-derived organosulfates to free tropospheric aerosol mass, Proc. Natl. Acad. Sci., 107(50), 21360–21365, doi:10.1073/pnas.1012561107, 2010.

Garland, R. M., Ravishankara, A. R., Lovejoy, E. R., Tolbert, M. A. and Baynard, T.: Parameterization for the relative humidity dependence of light extinction: Organic-ammonium sulfate aerosol, J. Geophys. Res., 112(D19), D19303, doi:10.1029/2006JD008179, 2007.

Gasparini, R., Li, R., Collins, D. R., Ferrare, R. A. and Brackett, V. G.: Application of aerosol hygroscopicity measured at the Atmospheric Radiation Measurement Program's Southern Great Plains site to examine composition and evolution, J. Geophys. Res., 111(D5), D05S12, doi:10.1029/2004JD005448, 2006.

Gelaro, R., McCarty, W., Suárez, M. J., Todling, R., Molod, A., Takacs, L., Randles, C. A., Darmenov, A., Bosilovich, M. G., Reichle, R., Wargan, K., Coy, L., Cullather, R., Draper, C., Akella, S., Buchard, V., Conaty, A., da Silva, A. M., Gu, W., Kim, G.-K., Koster, R., Lucchesi, R., Merkova, D., Nielsen, J. E., Partyka, G., Pawson, S., Putman, W., Rienecker, M., Schubert, S. D., Sienkiewicz, M. and Zhao, B.: The Modern-Era Retrospective Analysis for Research and Applications, Version 2 (MERRA-2), J. Clim., 30(14), 5419–5454, doi:10.1175/JCLI-D-16-0758.1, 2017.

Gentner, D. R., Jathar, S. H., Gordon, T. D., Bahreini, R., Day, D. A., El Haddad, I., Hayes, P. L., Pieber, S. M., Platt, S. M., de Gouw, J., Goldstein, A. H., Harley, R. A., Jimenez, J. L., Prévôt, A. S. H. and Robinson, A. L.: Review of Urban Secondary Organic Aerosol Formation from Gasoline and Diesel Motor Vehicle Emissions, Environ. Sci. Technol., 51(3), 1074–1093, doi:10.1021/acs.est.6b04509, 2017.

Giglio, L., Randerson, J. T. and van der Werf, G. R.: Analysis of daily, monthly, and annual burned area using the fourth-generation global fire emissions database (GFED4): Analysis of Burned Area, J. Geophys. Res. Biogeosciences, 118(1), 317–328, doi:10.1002/jgrg.20042, 2013.

Gilardoni, S., Vignati, E., Marmer, E., Cavalli, F., Belis, C., Gianelle, V., Loureiro, A. and Artaxo, P.: Sources of carbonaceous aerosol in the Amazon basin, Atmospheric Chem. Phys., 11(6), 2747–2764, doi:10.5194/acp-11-2747-2011, 2011.

Goldstein, A. H., Koven, C. D., Heald, C. L. and Fung, I. Y.: Biogenic carbon and anthropogenic pollutants combine to form a cooling haze over the southeastern United States, Proc. Natl. Acad. Sci., 106(22), 8835–8840, doi:10.1073/pnas.0904128106, 2009.

Guenther, A. B., Jiang, X., Heald, C. L., Sakulyanontvittaya, T., Duhl, T., Emmons, L. K. and Wang, X.: The Model of Emissions of Gases and Aerosols from Nature version 2.1 (MEGAN2.1): an extended and updated framework for modeling biogenic emissions, Geosci. Model Dev., 5(6), 1471–1492, doi:10.5194/gmd-5-1471-2012, 2012.

Guo, H., Xu, L., Bougiatioti, A., Cerully, K. M., Capps, S. L., Hite, J. R., Carlton, A. G., Lee, S.-H., Bergin, M. H., Ng, N. L., Nenes, A. and Weber, R. J.: Fine-particle water and pH in the southeastern United States, Atmospheric Chem. Phys., 15(9), 5211–5228, doi:10.5194/acp-15-5211-2015, 2015.

Guo, Y., Tang, Q., Gong, D.-Y. and Zhang, Z.: Estimating ground-level $PM_{2.5}$ concentrations in Beijing using a satellite-based geographically and temporally weighted regression model, Remote Sens. Environ., 198, 140–149, doi:10.1016/j.rse.2017.06.001, 2017.

Gupta, P., Christopher, S. A., Wang, J., Gehrig, R., Lee, Y. and Kumar, N.: Satellite remote sensing of particulate matter and air quality assessment over global cities, Atmos. Environ., 40(30), 5880–5892, doi:10.1016/j.atmosenv.2006.03.016, 2006.

Hand, J. L., Copeland, S. A., Day, D. E., Dillner, A. M., Indresand, H., Malm, W. C., McDad, C. E., Moore, Jr., C. T., Pitchford, M. L., Schichtel, B. A. and Watson, J. G.: Spatial and Seasonal Patterns and Temporal Variability of Haze and its Constituents in the United States: Report V, [online] Available from: http://vista.cira.colostate.edu/improve/wp-content/uploads/2016/08/IMPROVE_V_FullReport.pdf (Accessed 18 March 2018), 2011.

Hand, J. L., Schichtel, B. A., Pitchford, M., Malm, W. C. and Frank, N. H.: Seasonal composition of remote and urban fine particulate matter in the United States, J. Geophys. Res. Atmospheres, 117(D5), D05209, doi:10.1029/2011JD017122, 2012.

Hand, J. L., Schichtel, B. A., Malm, W. C. and Frank, N. H.: Spatial and Temporal Trends in $PM_{2.5}$ Organic and Elemental Carbon across the United States, Adv. Meteorol., 2013, 1–13, doi:10.1155/2013/367674, 2013.

Hand, J. L., Prenni, A. J., Schichtel, B. A., Malm, W. C. and Chow, J. C.: Trends in remote $PM_{2.5}$ residual mass across the United States: Implications for aerosol mass reconstruction in the IMPROVE network, Atmos. Environ., 203, 141–152, doi:10.1016/j.atmosenv.2019.01.049, 2019.

Hauser, A.: NOAA AVHRR derived aerosol optical depth over land, J. Geophys. Res., 110(D8), doi:10.1029/2004JD005439, 2005.

Heal, M. R.: The application of carbon-14 analyses to the source apportionment of atmospheric carbonaceous particulate matter: a review, Anal. Bioanal. Chem., 406(1), 81–98, doi:10.1007/s00216-013-7404-1, 2014.

Heald, C. L., Henze, D. K., Horowitz, L. W., Feddema, J., Lamarque, J.-F., Guenther, A., Hess, P. G., Vitt, F., Seinfeld, J. H., Goldstein, A. H. and Fung, I.: Predicted change in global secondary organic aerosol concentrations in response to future climate, emissions, and land use change: Future Predicted Change in Global SOA, J. Geophys. Res. Atmospheres, 113(D5), D05211, doi:10.1029/2007JD009092, 2008.

Hems, R. F. and Abbatt, J. P. D.: Aqueous Phase Photo-oxidation of Brown Carbon Nitrophenols: Reaction Kinetics, Mechanism, and Evolution of Light Absorption, ACS Earth Space Chem., 2(3), 225–234, doi:10.1021/acsearthspacechem.7b00123, 2018.

Hennigan, C. J., El-Sayed, M. M. H. and Hodzic, A.: Detailed characterization of a mist chamber for the collection of water-soluble organic gases, Atmos. Environ., 188, 12–17, doi:10.1016/j.atmosenv.2018.06.019, 2018.

Hersey, S. P., Garland, R. M., Crosbie, E., Shingler, T., Sorooshian, A., Piketh, S. and Burger, R.: An overview of regional and local characteristics of aerosols in South Africa using satellite, ground, and modeling data, Atmospheric Chem. Phys., 15(8), 4259–4278, doi:10.5194/acp-15-4259-2015, 2015.

Hodas, N., Sullivan, A. P., Skog, K., Keutsch, F. N., Collett, J. L., Decesari, S., Facchini, M. C., Carlton, A. G., Laaksonen, A. and Turpin, B. J.: Aerosol Liquid Water Driven by Anthropogenic Nitrate: Implications for Lifetimes of Water-Soluble Organic Gases and Potential for Secondary Organic Aerosol Formation, Environ. Sci. Technol., 48(19), 11127–11136, doi:10.1021/es5025096, 2014.

Hodzic, A., Jimenez, J. L., Madronich, S., Canagaratna, M. R., DeCarlo, P. F., Kleinman, L. and Fast, J.: Modeling organic aerosols in a megacity: potential contribution of semi-volatile and intermediate volatility primary organic compounds to secondary organic aerosol formation, Atmospheric Chem. Phys., 10(12), 5491–5514, doi:10.5194/acp-10-5491-2010, 2010.

Holben, B. N., Eck, T. F., Slutsker, I., Tanré, D., Buis, J. P., Setzer, A., Vermote, E., Reagan, J. A., Kaufman, Y. J., Nakajima, T., Lavenu, F., Jankowiak, I. and Smirnov, A.: AERONET—A Federated Instrument Network and Data Archive for Aerosol Characterization, Remote Sens. Environ., 66(1), 1–16, doi:10.1016/S0034-4257(98)00031-5, 1998.

de Hoogh, K., Gulliver, J., Donkelaar, A. van, Martin, R. V., Marshall, J. D., Bechle, M. J., Cesaroni, G., Pradas, M. C., Dedele, A., Eeftens, M., Forsberg, B., Galassi, C., Heinrich, J., Hoffmann, B., Jacquemin, B., Katsouyanni, K., Korek, M., Künzli, N., Lindley, S. J., Lepeule, J., Meleux, F., de Nazelle, A., Nieuwenhuijsen, M., Nystad, W., Raaschou-Nielsen, O., Peters, A., Peuch, V.-H., Rouil, L., Udvardy, O., Slama, R., Stempfelet, M., Stephanou, E. G., Tsai, M. Y., Yli-Tuomi, T., Weinmayr, G., Brunekreef, B., Vienneau, D. and Hoek, G.: Development of West-European $PM_{2.5}$ and $NO_2$ land use regression models incorporating satellite-derived and chemical transport modelling data, Environ. Res., 151, 1–10, doi:10.1016/j.envres.2016.07.005, 2016.

Hsu, N. C., Tsay, S.-C., King, M. D. and Herman, J. R.: Aerosol Properties Over Bright-Reflecting Source Regions, IEEE Trans. Geosci. Remote Sens., 42(3), 557–569, doi:10.1109/TGRS.2004.824067, 2004.

Hsu, N. C., Tsay, S.-C., King, M. D. and Herman, J. R.: Deep Blue Retrievals of Asian Aerosol Properties During ACE-Asia, IEEE Trans. Geosci. Remote Sens., 44(11), 3180–3195, doi:10.1109/TGRS.2006.879540, 2006.

Hsu, N. C., Jeong, M.-J., Bettenhausen, C., Sayer, A. M., Hansell, R., Seftor, C. S., Huang, J. and Tsay, S.-C.: Enhanced Deep Blue aerosol retrieval algorithm: The second generation: Enhanced Deep Blue Aerosol Retrieval, J. Geophys. Res. Atmospheres, 118(16), 9296–9315, doi:10.1002/jgrd.50712, 2013.

Hyde, A. M., Zultanski, S. L., Waldman, J. H., Zhong, Y.-L., Shevlin, M. and Peng, F.: General Principles and Strategies for Salting-Out Informed by the Hofmeister Series, Org. Process Res. Dev., 21(9), 1355–1370, doi:10.1021/acs.oprd.7b00197, 2017.

Hyslop, N. and White, W.: An evaluation of interagency monitoring of protected visual environments (IMPROVE) collocated precision and uncertainty estimates, Atmos. Environ., 42(11), 2691–2705, doi:10.1016/j.atmosenv.2007.06.053, 2008.

IMPROVE Network: Federal Land Manager Environmental Database, [online] Available from: http://views.cira.colostate.edu/fed/DataWizard/Default.aspx (Accessed 26 May 2016), 2019.

Jacob, D. J. and Winner, D. A.: Effect of climate change on air quality, Atmos. Environ., 43(1), 51–63, doi:10.1016/j.atmosenv.2008.09.051, 2009.

Jaoui, M., Edney, E. O., Kleindienst, T. E., Lewandowski, M., Offenberg, J. H., Surratt, J. D. and Seinfeld, J. H.: Formation of secondary organic aerosol from irradiated $\alpha$-pinene/toluene/$NO_x$ mixtures and the effect of isoprene and sulfur dioxide, J. Geophys. Res., 113(D9), D09303, doi:10.1029/2007JD009426, 2008.

Jathar, S. H., Mahmud, A., Barsanti, K. C., Asher, W. E., Pankow, J. F. and Kleeman, M. J.: Water uptake by organic aerosol and its influence on gas/particle partitioning of secondary organic aerosol in the United States, Atmos. Environ., 129, 142–154, doi:10.1016/j.atmosenv.2016.01.001, 2016.

Jefferson, A., Hageman, D., Morrow, H., Mei, F. and Watson, T.: Seven years of aerosol scattering hygroscopic growth measurements from SGP: Factors influencing water uptake: Aerosol Scattering Hygroscopic Growth, J. Geophys. Res. Atmospheres, 122(17), 9451–9466, doi:10.1002/2017JD026804, 2017.

Jiang, H. and Feingold, G.: Effect of aerosol on warm convective clouds: Aerosol-cloud-surface flux feedbacks in a new coupled large eddy model, J. Geophys. Res., 111(D1), D01202, doi:10.1029/2005JD006138, 2006.

Jin, X., Fiore, A. M., Curci, G., Lyapustin, A., Civerolo, K., Ku, M., van Donkelaar, A. and Martin, R. V.: Assessing uncertainties of a geophysical approach to estimate surface fine particulate matter distributions from satellite-observed aerosol optical depth, Atmospheric Chem. Phys., 19(1), 295–313, doi:10.5194/acp-19-295-2019, 2019.

Jones, T. A. and Christopher, S. A.: Satellite and Radar Remote Sensing of Southern Plains Grass Fires: A Case Study, J. Appl. Meteorol. Climatol., 49(10), 2133–2146, doi:10.1175/2010JAMC2472.1, 2010.

Ju, J. and Roy, D. P.: The availability of cloud-free Landsat ETM+ data over the conterminous United States and globally, Remote Sens. Environ., 112(3), 1196–1211, doi:10.1016/j.rse.2007.08.011, 2008.

Kahn, R. A.: Multiangle Imaging Spectroradiometer (MISR) global aerosol optical depth validation based on 2 years of coincident Aerosol Robotic Network (AERONET) observations, J. Geophys. Res., 110(D10), doi:10.1029/2004JD004706, 2005.

Kaku, K. C., Reid, J. S., Hand, J. L., Edgerton, E. S., Holben, B. N., Zhang, J. and Holz, R. E.: Assessing the Challenges of Surface-Level Aerosol Mass Estimates From Remote Sensing During the SEAC$^4$RS and SEARCH

Campaigns: Baseline Surface Observations and Remote Sensing in the Southeastern United States, J. Geophys. Res. Atmospheres, 123(14), 7530–7562, doi:10.1029/2017JD028074, 2018.

Kalnay, E., Kanamitsu, M., Kistler, R., Collins, W., Deaven, D., Gandin, L., Iredell, M., Saha, S., White, G., Woollen, J., Zhu, Y., Leetmaa, A., Reynolds, R., Chelliah, M., Ebisuzaki, W., Higgins, W., Janowiak, J., Mo, K. C., Ropelewski, C., Wang, J., Jenne, R. and Joseph, D.: The NCEP/NCAR 40-Year Reanalysis Project, Bull. Am. Meteorol. Soc., 77(3), 437–471, doi:10.1175/1520-0477(1996)077<0437:TNYRP>2.0.CO;2, 1996.

Kampf, C. J., Waxman, E. M., Slowik, J. G., Dommen, J., Pfaffenberger, L., Praplan, A. P., Prévôt, A. S. H., Baltensperger, U., Hoffmann, T. and Volkamer, R.: Effective Henry's Law Partitioning and the Salting Constant of Glyoxal in Aerosols Containing Sulfate, Environ. Sci. Technol., 47(9), 4236–4244, doi:10.1021/es400083d, 2013.

Kamruzzaman, M., Takahama, S. and Dillner, A. M.: Quantification of amine functional groups and their influence on OM/OC in the IMPROVE network, Atmos. Environ., 172, 124–132, doi:10.1016/j.atmosenv.2017.10.053, 2018.

Kanakidou, M., Seinfeld, J. H., Pandis, S. N., Barnes, I., Dentener, F. J., Facchini, M. C., Van Dingenen, R., Ervens, B., Nenes, A., Nielsen, C. J., Swietlicki, E., Putaud, J. P., Balkanski, Y., Fuzzi, S., Horth, J., Moortgat, G. K., Winterhalter, R., Myhre, C. E. L., Tsigaridis, K., Vignati, E., Stephanou, E. G. and Wilson, J.: Organic aerosol and global climate modelling: a review, Atmospheric Chem. Phys., 5(4), 1053–1123, doi:10.5194/acp-5-1053-2005, 2005.

Kawamura, K. and Bikkina, S.: A review of dicarboxylic acids and related compounds in atmospheric aerosols: Molecular distributions, sources and transformation, Atmospheric Res., 170, 140–160, doi:10.1016/j.atmosres.2015.11.018, 2016.

Kawecki, S. and Steiner, A. L.: The Influence of Aerosol Hygroscopicity on Precipitation Intensity During a Mesoscale Convective Event, J. Geophys. Res. Atmospheres, 123(1), 424–442, doi:10.1002/2017JD026535, 2018.

Kawecki, S., Henebry, G. M. and Steiner, A. L.: Effects of Urban Plume Aerosols on a Mesoscale Convective System, J. Atmospheric Sci., 73(12), 4641–4660, doi:10.1175/JAS-D-16-0084.1, 2016.

Kendall, M. G.: Rank correlation methods, Charles Griffin, London., 1975.

Kessner, A. L., Wang, J., Levy, R. C. and Colarco, P. R.: Remote sensing of surface visibility from space: A look at the United States East Coast, Atmos. Environ., 81, 136–147, doi:10.1016/j.atmosenv.2013.08.050, 2013.

Khan, B., Hays, M. D., Geron, C. and Jetter, J.: Differences in the OC/EC Ratios that Characterize Ambient and Source Aerosols due to Thermal-Optical Analysis, Aerosol Sci. Technol., 46(2), 127–137, doi:10.1080/02786826.2011.609194, 2012.

Khan, I., Brimblecombe, P. and Clegg, S. L.: Solubilities of pyruvic acid and the lower (C1-C6) carboxylic acids. Experimental determination of equilibrium vapour pressures above pure aqueous and salt solutions, J. Atmospheric Chem., 22(3), 285–302, doi:10.1007/BF00696639, 1995.

Khan, M. S., Muhammad, S. S., Awan, M. S., Leitgeb, E., Grabner, M. and Kvicera, V.: Proceedings of the 2011 11th International Conference on Telecommunications (ConTEL 2011): Graz, Austria, 15 - 17 June 2011 ; [co-located with International Workshop of the EU COST Action IC 0802 - Propagation Tools and Data for Integrated Telecom, Navigation and Earth Observation Systems], edited by T. Plank, Technische Universität Graz, and Communications Society, IEEE, Piscataway, NJ. [online] Available from: http://ieeexplore.ieee.org/stamp/stamp.jsp?tp=&arnumber=5969930 (Accessed 21 January 2018), 2011.

Khlystov, A.: Water content of ambient aerosol during the Pittsburgh Air Quality Study, J. Geophys. Res., 110(D7), D07S10, doi:10.1029/2004JD004651, 2005.

Kim, H., Barkey, B. and Paulson, S. E.: Real Refractive Indices and Formation Yields of Secondary Organic Aerosol Generated from Photooxidation of Limonene and α-Pinene: The Effect of the HC/$NO_x$ Ratio, J. Phys. Chem. A, 116(24), 6059–6067, doi:10.1021/jp301302z, 2012.

Kim, P. S., Jacob, D. J., Fisher, J. A., Travis, K., Yu, K., Zhu, L., Yantosca, R. M., Sulprizio, M. P., Jimenez, J. L., Campuzano-Jost, P., Froyd, K. D., Liao, J., Hair, J. W., Fenn, M. A., Butler, C. F., Wagner, N. L., Gordon, T. D., Welti, A., Wennberg, P. O., Crounse, J. D., St. Clair, J. M., Teng, A. P., Millet, D. B., Schwarz, J. P., Markovic, M. Z. and Perring, A. E.: Sources, seasonality, and trends of southeast US aerosol: an integrated analysis of surface, aircraft, and satellite observations with the GEOS-Chem chemical transport model, Atmospheric Chem. Phys., 15(18), 10411–10433, doi:10.5194/acp-15-10411-2015, 2015.

King, M. D., Platnick, S., Menzel, W. P., Ackerman, S. A. and Hubanks, P. A.: Spatial and Temporal Distribution of Clouds Observed by MODIS Onboard the Terra and Aqua Satellites, IEEE Trans. Geosci. Remote Sens., 51(7), 3826–3852, doi:10.1109/TGRS.2012.2227333, 2013.

Kloog, I., Koutrakis, P., Coull, B. A., Lee, H. J. and Schwartz, J.: Assessing temporally and spatially resolved $PM_{2.5}$ exposures for epidemiological studies using satellite aerosol optical depth measurements, Atmos. Environ., 45(35), 6267–6275, doi:10.1016/j.atmosenv.2011.08.066, 2011.

Kovalskyy, V. and Roy, D.: A One Year Landsat 8 Conterminous United States Study of Cirrus and Non-Cirrus Clouds, Remote Sens., 7(1), 564–578, doi:10.3390/rs70100564, 2015.

Kreidenweis, S. M., Petters, M. D. and DeMott, P. J.: Single-parameter estimates of aerosol water content, Environ. Res. Lett., 3(3), 035002, doi:10.1088/1748-9326/3/3/035002, 2008.

Kumar, N., Chu, A. and Foster, A.: An empirical relationship between $PM_{2.5}$ and aerosol optical depth in Delhi Metropolitan, Atmos. Environ., 41(21), 4492–4503, doi:10.1016/j.atmosenv.2007.01.046, 2007.

Lambe, A. T., Cappa, C. D., Massoli, P., Onasch, T. B., Forestieri, S. D., Martin, A. T., Cummings, M. J., Croasdale, D. R., Brune, W. H., Worsnop, D. R. and Davidovits, P.: Relationship between Oxidation Level and Optical Properties of Secondary Organic Aerosol, Environ. Sci. Technol., 47(12), 6349–6357, doi:10.1021/es401043j, 2013.

Lamkaddam, H., Gratien, A., Pangui, E., Cazaunau, M., Picquet-Varrault, B. and Doussin, J.-F.: High-$NO_x$ Photooxidation of *n*-Dodecane: Temperature Dependence of SOA Formation, Environ. Sci. Technol., 51(1), 192–201, doi:10.1021/acs.est.6b03821, 2017.

Lane, T. E., Donahue, N. M. and Pandis, S. N.: Effect of $NO_x$ on Secondary Organic Aerosol Concentrations, Environ. Sci. Technol., 42(16), 6022–6027, doi:10.1021/es703225a, 2008.

Lang-Yona, N., Rudich, Y., Mentel, Th. F., Bohne, A., Buchholz, A., Kiendler-Scharr, A., Kleist, E., Spindler, C., Tillmann, R. and Wildt, J.: The chemical and microphysical properties of secondary organic aerosols from Holm Oak emissions, Atmospheric Chem. Phys., 10(15), 7253–7265, doi:10.5194/acp-10-7253-2010, 2010.

Laskin, J., Laskin, A., Roach, P. J., Slysz, G. W., Anderson, G. A., Nizkorodov, S. A., Bones, D. L. and Nguyen, L. Q.: High-Resolution Desorption Electrospray Ionization Mass Spectrometry for Chemical Characterization of Organic Aerosols, Anal. Chem., 82(5), 2048–2058, doi:10.1021/ac902801f, 2010.

Lavers, D. A., Ralph, F. M., Waliser, D. E., Gershunov, A. and Dettinger, M. D.: Climate change intensification of horizontal water vapor transport in CMIP5: Water Vapor Transport in CMIP5, Geophys. Res. Lett., 42(13), 5617–5625, doi:10.1002/2015GL064672, 2015.

Lee, B. H., Mohr, C., Lopez-Hilfiker, F. D., Lutz, A., Hallquist, M., Lee, L., Romer, P., Cohen, R. C., Iyer, S., Kurtén, T., Hu, W., Day, D. A., Campuzano-Jost, P., Jimenez, J. L., Xu, L., Ng, N. L., Guo, H., Weber, R. J., Wild, R. J., Brown, S. S., Koss, A., de Gouw, J., Olson, K., Goldstein, A. H., Seco, R., Kim, S., McAvey, K., Shepson, P.

B., Starn, T., Baumann, K., Edgerton, E. S., Liu, J., Shilling, J. E., Miller, D. O., Brune, W., Schobesberger, S., D'Ambro, E. L. and Thornton, J. A.: Highly functionalized organic nitrates in the southeast United States: Contribution to secondary organic aerosol and reactive nitrogen budgets, Proc. Natl. Acad. Sci., 113(6), 1516–1521, doi:10.1073/pnas.1508108113, 2016.

Lee, T. R. and De Wekker, S. F. J.: Estimating Daytime Planetary Boundary Layer Heights over a Valley from Rawinsonde Observations at a Nearby Airport: An Application to the Page Valley in Virginia, United States, J. Appl. Meteorol. Climatol., 55(3), 791–809, doi:10.1175/JAMC-D-15-0300.1, 2016.

Leibensperger, E. M., Mickley, L. J., Jacob, D. J., Chen, W.-T., Seinfeld, J. H., Nenes, A., Adams, P. J., Streets, D. G., Kumar, N. and Rind, D.: Climatic effects of 1950-2050 changes in US anthropogenic aerosols - Part 1: Aerosol trends and radiative forcing, Atmospheric Chem. Phys., 12(7), 3333–3348, doi:10.5194/acp-12-3333-2012, 2012.

Levy, R. C., Mattoo, S., Munchak, L. A., Remer, L. A., Sayer, A. M., Patadia, F. and Hsu, N. C.: The Collection 6 MODIS aerosol products over land and ocean, Atmospheric Meas. Tech., 6(11), 2989–3034, doi:10.5194/amt-6-2989-2013, 2013.

Li, C. and Martin, R. V.: Decadal Changes in Seasonal Variation of Atmospheric Haze over the Eastern United States: Connections with Anthropogenic Emissions and Implications for Aerosol Composition, Environ. Sci. Technol. Lett., 5(7), 413–418, doi:10.1021/acs.estlett.8b00295, 2018.

Li, J., Carlson, B. E. and Lacis, A. A.: How well do satellite AOD observations represent the spatial and temporal variability of $PM_{2.5}$ concentration for the United States?, Atmos. Environ., 102, 260–273, doi:10.1016/j.atmosenv.2014.12.010, 2015.

Li, L., Gong, J. and Zhou, J.: Spatial Interpolation of Fine Particulate Matter Concentrations Using the Shortest Wind-Field Path Distance, edited by Q. Sun, PLoS ONE, 9(5), e96111, doi:10.1371/journal.pone.0096111, 2014.

Li, S., Garay, M. J., Chen, L., Rees, E. and Liu, Y.: Comparison of GEOS-Chem aerosol optical depth with AERONET and MISR data over the contiguous United States, J. Geophys. Res. Atmospheres, 118(19), 11,228-11,241, doi:10.1002/jgrd.50867, 2013.

Li, Y.: Cloud Condensation Nuclei Activity and Hygroscopicity of Fresh and Aged Biomass Burning Particles, Pure Appl. Geophys., 176(1), 345–356, doi:10.1007/s00024-018-1903-0, 2019.

Li, Y. and Shiraiwa, M.: Timescales of secondary organic aerosols to reach equilibrium at various temperatures and relative humidities, Atmospheric Chem. Phys., 19(9), 5959–5971, doi:10.5194/acp-19-5959-2019, 2019.

Liao, H.: Interactions between tropospheric chemistry and aerosols in a unified general circulation model, J. Geophys. Res., 108(D1), 4001, doi:10.1029/2001JD001260, 2003.

Liao, H. and Seinfeld, J. H.: Global impacts of gas-phase chemistry-aerosol interactions on direct radiative forcing by anthropogenic aerosols and ozone, J. Geophys. Res., 110(D18), D18208, doi:10.1029/2005JD005907, 2005.

Lim, S., Lee, M., Lee, G., Kim, S., Yoon, S. and Kang, K.: Ionic and carbonaceous compositions of $PM_{10}$, $PM_{2.5}$ and $PM_{1.0}$ at Gosan ABC Superstation and their ratios as source signature, Atmospheric Chem. Phys., 12(4), 2007–2024, doi:10.5194/acp-12-2007-2012, 2012.

Lin, Y., Wang, Y., Pan, B., Hu, J., Liu, Y. and Zhang, R.: Distinct Impacts of Aerosols on an Evolving Continental Cloud Complex during the RACORO Field Campaign, J. Atmospheric Sci., 73(9), 3681–3700, doi:10.1175/JAS-D-15-0361.1, 2016.

Lin, Y.-H., Arashiro, M., Clapp, P. W., Cui, T., Sexton, K. G., Vizuete, W., Gold, A., Jaspers, I., Fry, R. C. and Surratt, J. D.: Gene Expression Profiling in Human Lung Cells Exposed to Isoprene-Derived Secondary Organic Aerosol, Environ. Sci. Technol., 51(14), 8166–8175, doi:10.1021/acs.est.7b01967, 2017.

Lippmann, M.: Toxicological and epidemiological studies of cardiovascular effects of ambient air fine particulate matter ($PM_{2.5}$) and its chemical components: Coherence and public health implications, Crit. Rev. Toxicol., 44(4), 299–347, doi:10.3109/10408444.2013.861796, 2014.

Liu, B., Ma, Y., Gong, W., Zhang, M., Wang, W. and Shi, Y.: Comparison of AOD from CALIPSO, MODIS, and Sun Photometer under Different Conditions over Central China, Sci. Rep., 8(1), doi:10.1038/s41598-018-28417-7, 2018.

Liu, J., Horowitz, L. W., Fan, S., Carlton, A. G. and Levy, H.: Global in-cloud production of secondary organic aerosols: Implementation of a detailed chemical mechanism in the GFDL atmospheric model AM3: Global In-Cloud Production of SOA, J. Geophys. Res. Atmospheres, 117(D15), doi:10.1029/2012JD017838, 2012.

Liu, Y., Park, R. J., Jacob, D. J., Li, Q., Kilaru, V. and Sarnat, J. A.: Mapping annual mean ground-level $PM_{2.5}$ concentrations using Multiangle Imaging Spectroradiometer aerosol optical thickness over the contiguous United States: Mapping Surface $PM_{2.5}$ Using MISR AOT, J. Geophys. Res. Atmospheres, 109(D22), D22206, doi:10.1029/2004JD005025, 2004.

Liu, Y., Schichtel, B. A. and Koutrakis, P.: Estimating Particle Sulfate Concentrations Using MISR Retrieved Aerosol Properties, IEEE J. Sel. Top. Appl. Earth Obs. Remote Sens., 2(3), 176–184, doi:10.1109/JSTARS.2009.2030153, 2009.

Liu, Y., Wang, Z., Wang, J., Ferrare, R. A., Newsom, R. K. and Welton, E. J.: The effect of aerosol vertical profiles on satellite-estimated surface particle sulfate concentrations, Remote Sens. Environ., 115(2), 508–513, doi:10.1016/j.rse.2010.09.019, 2011.

Logan, W.: Mortality in the London Fog Incident, 1952, The Lancet, 261(6755), 336–338, doi:10.1016/S0140-6736(53)91012-5, 1953.

Lowenthal, D. H. and Kumar, N.: $PM_{2.5}$ Mass and Light Extinction Reconstruction in IMPROVE, J. Air Waste Manag. Assoc., 53(9), 1109–1120, doi:10.1080/10473289.2003.10466264, 2003.

Ma, L. and Thompson, J. E.: Optical Properties of Dispersed Aerosols in the Near Ultraviolet (355 nm): Measurement Approach and Initial Data, Anal. Chem., 84(13), 5611–5617, doi:10.1021/ac3005814, 2012.

Malm, W. C., Sisler, J. F., Huffman, D., Eldred, R. A. and Cahill, T. A.: Spatial and seasonal trends in particle concentration and optical extinction in the United States, J. Geophys. Res., 99(D1), 1347, doi:10.1029/93JD02916, 1994.

Malm, W. C., Molenar, J. V., Eldred, R. A. and Sisler, J. F.: Examining the relationship among atmospheric aerosols and light scattering and extinction in the Grand Canyon area, J. Geophys. Res. Atmospheres, 101(D14), 19251–19265, doi:10.1029/96JD00552, 1996.

Malm, W. C., Schichtel, B. A. and Pitchford, M. L.: Uncertainties in $PM_{2.5}$ Gravimetric and Speciation Measurements and What We Can Learn from Them, J. Air Waste Manag. Assoc., 61(11), 1131–1149, doi:10.1080/10473289.2011.603998, 2011.

Malm, W. C., Schichtel, B. A., Hand, J. L. and Collett, J. L.: Concurrent Temporal and Spatial Trends in Sulfate and Organic Mass Concentrations Measured in the IMPROVE Monitoring Program: Trends in Sulfate and Organic Mass, J. Geophys. Res. Atmospheres, 122(19), 10,462-10,476, doi:10.1002/2017JD026865, 2017.

Malm, W. C., Schichtel, B. A., Hand, J. L. and Prenni, A. J.: Implications of Organic Mass to Carbon Ratios Increasing Over Time in the Rural United States, J. Geophys. Res. Atmospheres, 125(5), doi:10.1029/2019JD031480, 2020.

Mann, H. B.: Nonparametric Tests Against Trend, Econometrica, 13(3), 245–259, 1945.

Mao, J., Carlton, A., Cohen, R. C., Brune, W. H., Brown, S. S., Wolfe, G. M., Jimenez, J. L., Pye, H. O. T., Lee Ng, N., Xu, L., McNeill, V. F., Tsigaridis, K., McDonald, B. C., Warneke, C., Guenther, A., Alvarado, M. J., de Gouw, J., Mickley, L. J., Leibensperger, E. M., Mathur, R., Nolte, C. G., Portmann, R. W., Unger, N., Tosca, M. and Horowitz, L. W.: Southeast Atmosphere Studies: learning from model-observation syntheses, Atmospheric Chem. Phys., 18(4), 2615–2651, doi:10.5194/acp-18-2615-2018, 2018.

Mar, T. F., Norris, G. A., Koenig, J. Q. and Larson, T. V.: Associations between air pollution and mortality in Phoenix, 1995-1997., Environ. Health Perspect., 108(4), 347–353, doi:10.1289/ehp.00108347, 2000.

Marais, E. A., Jacob, D. J., Jimenez, J. L., Campuzano-Jost, P., Day, D. A., Hu, W., Krechmer, J., Zhu, L., Kim, P. S., Miller, C. C., Fisher, J. A., Travis, K., Yu, K., Hanisco, T. F., Wolfe, G. M., Arkinson, H. L., Pye, H. O. T., Froyd, K. D., Liao, J. and McNeill, V. F.: Aqueous-phase mechanism for secondary organic aerosol formation from isoprene: application to the southeast United States and co-benefit of $SO_2$ emission controls, Atmospheric Chem. Phys., 16(3), 1603–1618, doi:10.5194/acp-16-1603-2016, 2016.

Marais, E. A., Jacob, D. J., Turner, J. R. and Mickley, L. J.: Evidence of 1991–2013 decrease of biogenic secondary organic aerosol in response to $SO_2$ emission controls, Environ. Res. Lett., 12(5), 054018, doi:10.1088/1748-9326/aa69c8, 2017.

Marshall, F. H., Miles, R. E. H., Song, Y.-C., Ohm, P. B., Power, R. M., Reid, J. P. and Dutcher, C. S.: Diffusion and reactivity in ultraviscous aerosol and the correlation with particle viscosity, Chem. Sci., 7(2), 1298–1308, doi:10.1039/C5SC03223G, 2016.

Martin, R. V.: Satellite remote sensing of surface air quality, Atmos. Environ., 42(34), 7823–7843, doi:10.1016/j.atmosenv.2008.07.018, 2008.

McKeen, S., Grell, G., Peckham, S., Wilczak, J., Djalalova, I., Hsie, E.-Y., Frost, G., Peischl, J., Schwarz, J., Spackman, R., Holloway, J., de Gouw, J., Warneke, C., Gong, W., Bouchet, V., Gaudreault, S., Racine, J., McHenry, J., McQueen, J., Lee, P., Tang, Y., Carmichael, G. R. and Mathur, R.: An evaluation of real-time air quality forecasts and their urban emissions over eastern Texas during the summer of 2006 Second Texas Air Quality Study field study, J. Geophys. Res., 114, doi:10.1029/2008JD011697, 2009.

McKnight, P. E. and Najab, J.: Mann-Whitney U Test, in The Corsini Encyclopedia of Psychology, edited by I. B. Weiner and W. E. Craighead, John Wiley & Sons, Inc., Hoboken, NJ, USA., 2010.

McNeill, V. F.: Aqueous Organic Chemistry in the Atmosphere: Sources and Chemical Processing of Organic Aerosols, Environ. Sci. Technol., 49(3), 1237–1244, doi:10.1021/es5043707, 2015.

McNeill, V. F.: Atmospheric Aerosols: Clouds, Chemistry, and Climate, Annu. Rev. Chem. Biomol. Eng., 8(1), 427–444, doi:10.1146/annurev-chembioeng-060816-101538, 2017.

Meehl, G. A., Arblaster, J. M. and Chung, C. T. Y.: Disappearance of the southeast U.S. “warming hole” with the late 1990s transition of the Interdecadal Pacific Oscillation, Geophys. Res. Lett., 42(13), 5564–5570, doi:10.1002/2015GL064586, 2015.

Meier, S. M. and Schwab, J. J.: Beyond OC--A method to extract and interpret additional aerosol organic carbon fractions from thermal optical analysis of filter-based and continuous data, 2011.

Metzger, S., Abdelkader, M., Steil, B. and Klingmüller, K.: Aerosol water parameterization: long-term evaluation and importance, Atmospheric Chem. Phys. Discuss., 1–41, doi:10.5194/acp-2018-450, 2018.

Mielonen, T., Hienola, A., Kühn, T., Merikanto, J., Lipponen, A., Bergman, T., Korhonen, H., Kolmonen, P., Sogacheva, L., Ghent, D., Pitkänen, M., Arola, A., de Leeuw, G. and Kokkola, H.: Summertime Aerosol Radiative Effects and Their Dependence on Temperature over the Southeastern USA, Atmosphere, 9(5), 180, doi:10.3390/atmos9050180, 2018.

Millet, D. B., Guenther, A., Siegel, D. A., Nelson, N. B., Singh, H. B., de Gouw, J. A., Warneke, C., Williams, J., Eerdekens, G., Sinha, V., Karl, T., Flocke, F., Apel, E., Riemer, D. D., Palmer, P. I. and Barkley, M.: Global atmospheric budget of acetaldehyde: 3-D model analysis and constraints from in-situ and satellite observations, Atmospheric Chem. Phys., 10(7), 3405–3425, doi:10.5194/acp-10-3405-2010, 2010.

Mircea, M., Facchini, M. C., Decesari, S., Cavalli, F., Emblico, L., Fuzzi, S., Vestin, A., Rissler, J., Swietlicki, E., Frank, G., Andreae, M. O., Maenhaut, W., Rudich, Y. and Artaxo, P.: Importance of the organic aerosol fraction for modeling aerosol hygroscopic growth and activation: a case study in the Amazon Basin, Atmospheric Chem. Phys., 5(11), 3111–3126, doi:10.5194/acp-5-3111-2005, 2005.

Miyazaki, Y., Kondo, Y., Han, S., Koike, M., Kodama, D., Komazaki, Y., Tanimoto, H. and Matsueda, H.: Chemical characteristics of water-soluble organic carbon in the Asian outflow, J. Geophys. Res., 112(D22), D22S30, doi:10.1029/2007JD009116, 2007.

Mochida, M., Kuwata, M., Miyakawa, T., Takegawa, N., Kawamura, K. and Kondo, Y.: Relationship between hygroscopicity and cloud condensation nuclei activity for urban aerosols in Tokyo, J. Geophys. Res. Atmospheres, 111(D23), D23204, doi:10.1029/2005JD006980, 2006.

Moise, T., Flores, J. M. and Rudich, Y.: Optical Properties of Secondary Organic Aerosols and Their Changes by Chemical Processes, Chem. Rev., 115(10), 4400–4439, doi:10.1021/cr5005259, 2015.

Munger, J. W., Jacob, D. J. and Hoffmann, M. R.: The occurrence of bisulfite-aldehyde addition products in fog- and cloudwater, J. Atmospheric Chem., 1(4), 335–350, doi:10.1007/BF00053799, 1984.

Nakayama, T., Matsumi, Y., Sato, K., Imamura, T., Yamazaki, A. and Uchiyama, A.: Laboratory studies on optical properties of secondary organic aerosols generated during the photooxidation of toluene and the ozonolysis of $\alpha$-pinene, J. Geophys. Res. Atmospheres, 115(D24), D24204, doi:10.1029/2010JD014387, 2010.

National Aeronautics and Space Administration: Atmospheric Science Data Center, [online] Available from: https://eosweb.larc.nasa.gov/ (Accessed 16 February 2018a), 2018.

National Aeronautics and Space Administration: Global Change Master Directory, [online] Available from: https://gcmd.nasa.gov/, 2018b.

National Centers for Environmental Prediction North American Regional Reanalysis Model, [online] Available from: https://www.esrl.noaa.gov/psd/.

Nemery, B., Hoet, P. H. and Nemmar, A.: The Meuse Valley fog of 1930: an air pollution disaster, The Lancet, 357(9257), 704–708, doi:10.1016/S0140-6736(00)04135-0, 2001.

Ng, N. L., Kroll, J. H., Chan, A. W. H., Chhabra, P. S., Flagan, R. C. and Seinfeld, J. H.: Secondary organic aerosol formation from *m*-xylene, toluene, and benzene, Atmospheric Chem. Phys., 7(14), 3909–3922, doi:10.5194/acp-7-3909-2007, 2007.

Nguyen, T. B., Bateman, A. P., Bones, D. L., Nizkorodov, S. A., Laskin, J. and Laskin, A.: High-resolution mass spectrometry analysis of secondary organic aerosol generated by ozonolysis of isoprene, Atmos. Environ., 44(8), 1032–1042, doi:10.1016/j.atmosenv.2009.12.019, 2010.

Nguyen, T. B., Coggon, M. M., Bates, K. H., Zhang, X., Schwantes, R. H., Schilling, K. A., Loza, C. L., Flagan, R. C., Wennberg, P. O. and Seinfeld, J. H.: Organic aerosol formation from the reactive uptake of isoprene epoxydiols (IEPOX) onto non-acidified inorganic seeds, Atmospheric Chem. Phys., 14(7), 3497–3510, doi:10.5194/acp-14-3497-2014, 2014a.

Nguyen, T. K. V., Petters, M. D., Suda, S. R., Guo, H., Weber, R. J. and Carlton, A. G.: Trends in particle-phase liquid water during the Southern Oxidant and Aerosol Study, Atmospheric Chem. Phys., 14(20), 10911–10930, doi:10.5194/acp-14-10911-2014, 2014b.

Nguyen, T. K. V., Capps, S. L. and Carlton, A. G.: Decreasing Aerosol Water Is Consistent with OC Trends in the Southeast U.S., Environ. Sci. Technol., 49(13), 7843–7850, doi:10.1021/acs.est.5b00828, 2015.

Nguyen, T. K. V., Zhang, Q., Jimenez, J. L., Pike, M. and Carlton, A. G.: Liquid Water: Ubiquitous Contributor to Aerosol Mass, Environ. Sci. Technol. Lett., 3(7), 257–263, doi:10.1021/acs.estlett.6b00167, 2016a.

Nguyen, T. K. V., Ghate, V. P. and Carlton, A. G.: Reconciling satellite aerosol optical thickness and surface fine particle mass through aerosol liquid water: ALW and AOT, Geophys. Res. Lett., 43(22), 11,903-11,912, doi:10.1002/2016GL070994, 2016b.

Norris, J. R., Allen, R. J., Evan, A. T., Zelinka, M. D., O'Dell, C. W. and Klein, S. A.: Evidence for climate change in the satellite cloud record, Nature, 536(7614), 72–75, doi:10.1038/nature18273, 2016.

Novakov, T. and Penner, J. E.: Large contribution of organic aerosols to cloud-condensation-nuclei concentrations, Nature, 365(6449), 823–826, doi:10.1038/365823a0, 1993.

Odum, J. R., Hoffmann, T., Bowman, F., Collins, D., Flagan, R. C. and Seinfeld, J. H.: Gas/Particle Partitioning and Secondary Organic Aerosol Yields, Environ. Sci. Technol., 30(8), 2580–2585, 1996.

O'Meara, S., Topping, D. O. and McFiggans, G.: The rate of equilibration of viscous aerosol particles, Atmospheric Chem. Phys., 16(8), 5299–5313, doi:10.5194/acp-16-5299-2016, 2016.

Pankow, J. F.: An absorption model of the gas/aerosol partitioning involved in the formation of secondary organic aerosol, Atmos. Environ., 28(2), 189–193, doi:10.1016/1352-2310(94)90094-9, 1994.

Parworth, C., Fast, J., Mei, F., Shippert, T., Sivaraman, C., Tilp, A., Watson, T. and Zhang, Q.: Long-term measurements of submicrometer aerosol chemistry at the Southern Great Plains (SGP) using an Aerosol Chemical Speciation Monitor (ACSM), Atmos. Environ., 106, 43–55, doi:10.1016/j.atmosenv.2015.01.060, 2015.

Penner, J. E., Hegg, D. and Leaitch, R.: Peer Reviewed: Unraveling the role of aerosols in climate change, Environ. Sci. Technol., 35(15), 332A-340A, doi:10.1021/es0124414, 2001.

Petters, M. D. and Kreidenweis, S. M.: A single parameter representation of hygroscopic growth and cloud condensation nucleus activity, Atmospheric Chem. Phys., 7(8), 1961–1971, doi:10.5194/acp-7-1961-2007, 2007.

Philip, S., Martin, R. V., Pierce, J. R., Jimenez, J. L., Zhang, Q., Canagaratna, M. R., Spracklen, D. V., Nowlan, C. R., Lamsal, L. N., Cooper, M. J. and Krotkov, N. A.: Spatially and seasonally resolved estimate of the ratio of organic mass to organic carbon, Atmos. Environ., 87, 34–40, doi:10.1016/j.atmosenv.2013.11.065, 2014.

Pierce, J. R., Leaitch, W. R., Liggio, J., Westervelt, D. M., Wainwright, C. D., Abbatt, J. P. D., Ahlm, L., Al-Basheer, W., Cziczo, D. J., Hayden, K. L., Lee, A. K. Y., Li, S.-M., Russell, L. M., Sjostedt, S. J., Strawbridge, K. B., Travis, M., Vlasenko, A., Wentzell, J. J. B., Wiebe, H. A., Wong, J. P. S. and Macdonald, A. M.: Nucleation and condensational growth to CCN sizes during a sustained pristine biogenic SOA event in a forested mountain valley, Atmospheric Chem. Phys., 12(7), 3147–3163, doi:10.5194/acp-12-3147-2012, 2012.

Pitchford, M., Malm, W., Schichtel, B., Kumar, N., Lowenthal, D. and Hand, J.: Revised Algorithm for Estimating Light Extinction from IMPROVE Particle Speciation Data, J. Air Waste Manag. Assoc., 57(11), 1326–1336, doi:10.3155/1047-3289.57.11.1326, 2007.

Pitchford, M. L. and McMurry, P. H.: Relationship between measured water vapor growth and chemistry of atmospheric aerosol for Grand Canyon, Arizona, in winter 1990, Atmos. Environ., 28(5), 827–839, doi:10.1016/1352-2310(94)90242-9, 1994.

Platnick, S.: MODIS Atmosphere L3 Monthly Product, [online] Available from: http://dx.doi.org/10.5067/MODIS/MOD08_M3.061, 2015.

Pope, C. A. and Dockery, D. W.: Health Effects of Fine Particulate Air Pollution: Lines that Connect, J. Air Waste Manag. Assoc., 56(6), 709–742, doi:10.1080/10473289.2006.10464485, 2006.

Pope, C. A., Turner, M. C., Burnett, R. T., Jerrett, M., Gapstur, S. M., Diver, W. R., Krewski, D. and Brook, R. D.: Relationships Between Fine Particulate Air Pollution, Cardiometabolic Disorders, and Cardiovascular Mortality, Circ. Res., 116(1), 108–115, doi:10.1161/CIRCRESAHA.116.305060, 2015.

Pöschl, U.: Atmospheric Aerosols: Composition, Transformation, Climate and Health Effects, Angew. Chem. Int. Ed., 44(46), 7520–7540, doi:10.1002/anie.200501122, 2005.

Pöschl, U. and Shiraiwa, M.: Multiphase Chemistry at the Atmosphere–Biosphere Interface Influencing Climate and Public Health in the Anthropocene, Chem. Rev., 115(10), 4440–4475, doi:10.1021/cr500487s, 2015.

Praske, E., Otkjær, R. V., Crounse, J. D., Hethcox, J. C., Stoltz, B. M., Kjaergaard, H. G. and Wennberg, P. O.: Atmospheric autoxidation is increasingly important in urban and suburban North America, Proc. Natl. Acad. Sci., 115(1), 64–69, doi:10.1073/pnas.1715540115, 2018.

Pratt, K. A., Fiddler, M. N., Shepson, P. B., Carlton, A. G. and Surratt, J. D.: Organosulfates in cloud water above the Ozarks' isoprene source region, Atmos. Environ., 77, 231–238, doi:10.1016/j.atmosenv.2013.05.011, 2013.

Prenni, A. J., Petters, M. D., Kreidenweis, S. M., DeMott, P. J. and Ziemann, P. J.: Cloud droplet activation of secondary organic aerosol: Cloud Droplet Activation, J. Geophys. Res. Atmospheres, 112(D10), doi:10.1029/2006JD007963, 2007.

Prisle, N. L., Engelhart, G. J., Bilde, M. and Donahue, N. M.: Humidity influence on gas-particle phase partitioning of $\alpha$-pinene + $O_3$ secondary organic aerosol: RH SOA Partitioning, Geophys. Res. Lett., 37(1), L01802, doi:10.1029/2009GL041402, 2010.

Pruppacher, H. R. and Klett, J. D.: Microphysics of clouds and precipitation, Springer, Dordrecht ; New York., 2010.

Puthussery, J. V., Zhang, C. and Verma, V.: Development and field testing of an online instrument for measuring the real-time oxidative potential of ambient particulate matter based on dithiothreitol assay, Atmospheric Meas. Tech., 11(10), 5767–5780, doi:10.5194/amt-11-5767-2018, 2018.

Pye, H. O. T., Chan, A. W. H., Barkley, M. P. and Seinfeld, J. H.: Global modeling of organic aerosol: the importance of reactive nitrogen ($NO_x$ and $NO_3$), Atmospheric Chem. Phys., 10(22), 11261–11276, doi:10.5194/acp-10-11261-2010, 2010.

Pye, H. O. T., Pinder, R. W., Piletic, I. R., Xie, Y., Capps, S. L., Lin, Y.-H., Surratt, J. D., Zhang, Z., Gold, A., Luecken, D. J., Hutzell, W. T., Jaoui, M., Offenberg, J. H., Kleindienst, T. E., Lewandowski, M. and Edney, E. O.: Epoxide Pathways Improve Model Predictions of Isoprene Markers and Reveal Key Role of Acidity in Aerosol Formation, Environ. Sci. Technol., 47(19), 11056–11064, doi:10.1021/es402106h, 2013.

R Core Team: R: A language and environment for statistical computing., R Foundation for Statistical Computing, Vienna, Austria. [online] Available from: http://www.R-project.org/, 2013.

Raizenne, M., Neas, L. M., Damokosh, A. I., Dockery, D. W., Spengler, J. D., Koutrakis, P., Ware, J. H. and Speizer, F. E.: Health effects of acid aerosols on North American children: pulmonary function., Environ. Health Perspect., 104(5), 506–514, doi:10.1289/ehp.96104506, 1996.

Ramanathan, V. and Carmichael, G.: Global and regional climate changes due to black carbon, Nat. Geosci., 1(4), 221–227, doi:10.1038/ngeo156, 2008.

Rastak, N., Pajunoja, A., Acosta Navarro, J. C., Ma, J., Song, M., Partridge, D. G., Kirkevåg, A., Leong, Y., Hu, W. W., Taylor, N. F., Lambe, A., Cerully, K., Bougiatioti, A., Liu, P., Krejci, R., Petäjä, T., Percival, C., Davidovits, P., Worsnop, D. R., Ekman, A. M. L., Nenes, A., Martin, S., Jimenez, J. L., Collins, D. R., Topping, D. O., Bertram, A. K., Zuend, A., Virtanen, A. and Riipinen, I.: Microphysical explanation of the RH-dependent water affinity of biogenic organic aerosol and its importance for climate, Geophys. Res. Lett., 44(10), 5167–5177, doi:10.1002/2017GL073056, 2017.

Rau, J. A.: Residential wood combustion aerosol characterization as a function of size and source apportionment using chemical mass balance modeling, [online] Available from: https://digitalcollections.ohsu.edu/concern/etds/f7623c56g, 1986.

Raventos-Duran, T., Camredon, M., Valorso, R., Mouchel-Vallon, C. and Aumont, B.: Structure-activity relationships to estimate the effective Henry's law constants of organics of atmospheric interest, Atmospheric Chem. Phys., 10(16), 7643–7654, doi:10.5194/acp-10-7643-2010, 2010.

Redmond, H. and Thompson, J. E.: Evaluation of a quantitative structure–property relationship (QSPR) for predicting mid-visible refractive index of secondary organic aerosol (SOA), Phys. Chem. Chem. Phys., 13(15), 6872, doi:10.1039/c0cp02270e, 2011.

Reid, J. P., Bertram, A. K., Topping, D. O., Laskin, A., Martin, S. T., Petters, M. D., Pope, F. D. and Rovelli, G.: The viscosity of atmospherically relevant organic particles, Nat. Commun., 9(1), 956, doi:10.1038/s41467-018-03027-z, 2018.

Reiss, R., Anderson, E. L., Cross, C. E., Hidy, G., Hoel, D., McClellan, R. and Moolgavkar, S.: Evidence of Health Impacts of Sulfate-and Nitrate-Containing Particles in Ambient Air, Inhal. Toxicol., 19(5), 419–449, doi:10.1080/08958370601174941, 2007.

Remer, L. A., Kaufman, Y. J., Tanré, D., Mattoo, S., Chu, D. A., Martins, J. V., Li, R.-R., Ichoku, C., Levy, R. C., Kleidman, R. G., Eck, T. F., Vermote, E. and Holben, B. N.: The MODIS Aerosol Algorithm, Products, and Validation, J. Atmospheric Sci., 62(4), 947–973, doi:10.1175/JAS3385.1, 2005.

Remer, L. A., Mattoo, S., Levy, R. C. and Munchak, L. A.: MODIS 3 km aerosol product: algorithm and global perspective, Atmospheric Meas. Tech., 6(7), 1829–1844, doi:10.5194/amt-6-1829-2013, 2013.

Ridley, D. A., Heald, C. L., Ridley, K. J. and Kroll, J. H.: Causes and consequences of decreasing atmospheric organic aerosol in the United States, Proc. Natl. Acad. Sci., 115(2), 290–295, doi:10.1073/pnas.1700387115, 2018.

Rood, M. J., Shaw, M. A., Larson, T. V. and Covert, D. S.: Ubiquitous nature of ambient metastable aerosol, Nature, 337(6207), 537–539, doi:10.1038/337537a0, 1989.

Rothfuss, N. E. and Petters, M. D.: Influence of Functional Groups on the Viscosity of Organic Aerosol, Environ. Sci. Technol., 51(1), 271–279, doi:10.1021/acs.est.6b04478, 2017.

Ruehl, C. R., Ham, W. A. and Kleeman, M. J.: Temperature-induced volatility of molecular markers in ambient airborne particulate matter, Atmospheric Chem. Phys., 11(1), 67–76, doi:10.5194/acp-11-67-2011, 2011.

Ruthenburg, T. C., Perlin, P. C., Liu, V., McDade, C. E. and Dillner, A. M.: Determination of organic matter and organic matter to organic carbon ratios by infrared spectroscopy with application to selected sites in the IMPROVE network, Atmos. Environ., 86, 47–57, doi:10.1016/j.atmosenv.2013.12.034, 2014.

Ryerson, T. B., Andrews, A. E., Angevine, W. M., Bates, T. S., Brock, C. A., Cairns, B., Cohen, R. C., Cooper, O. R., de Gouw, J. A., Fehsenfeld, F. C., Ferrare, R. A., Fischer, M. L., Flagan, R. C., Goldstein, A. H., Hair, J. W., Hardesty, R. M., Hostetler, C. A., Jimenez, J. L., Langford, A. O., McCauley, E., McKeen, S. A., Molina, L. T., Nenes, A., Oltmans, S. J., Parrish, D. D., Pederson, J. R., Pierce, R. B., Prather, K., Quinn, P. K., Seinfeld, J. H., Senff, C. J., Sorooshian, A., Stutz, J., Surratt, J. D., Trainer, M., Volkamer, R., Williams, E. J. and Wofsy, S. C.: The 2010 California Research at the Nexus of Air Quality and Climate Change (CalNex) field study: CalNex 2010 Field Project Overview, J. Geophys. Res. Atmospheres, 118(11), 5830–5866, doi:10.1002/jgrd.50331, 2013.

Saffari, A., Daher, N., Shafer, M. M., Schauer, J. J. and Sioutas, C.: Global Perspective on the Oxidative Potential of Airborne Particulate Matter: A Synthesis of Research Findings, Environ. Sci. Technol., 48(13), 7576–7583, doi:10.1021/es500937x, 2014.

Sakulyanontvittaya, T., Duhl, T., Wiedinmyer, C., Helmig, D., Matsunaga, S., Potosnak, M., Milford, J. and Guenther, A.: Monoterpene and Sesquiterpene Emission Estimates for the United States, Environ. Sci. Technol., 42(5), 1623–1629, doi:10.1021/es702274e, 2008.

Samet, J. M., Zeger, S. L., Dominici, F. C., Coursac, I., Dockery, D. W., Schwartz, J. and Zanobetti, A.: The National Morbidity, Mortality, and Air Pollution Study. Part II: Morbilidy and Mortality from Air Pollution in the United States, Res. Rep. Health Eff. Inst., 94(Pt 2), 5–70, 2000.

Sareen, N., Schwier, A. N., Shapiro, E. L., Mitroo, D. and McNeill, V. F.: Secondary organic material formed by methylglyoxal in aqueous aerosol mimics, Atmospheric Chem. Phys., 10(3), 997–1016, doi:10.5194/acp-10-997-2010, 2010.

Sareen, N., Carlton, A. G., Surratt, J. D., Gold, A., Lee, B., Lopez-Hilfiker, F. D., Mohr, C., Thornton, J. A., Zhang, Z., Lim, Y. B. and Turpin, B. J.: Identifying precursors and aqueous organic aerosol formation pathways during the SOAS campaign, Atmospheric Chem. Phys., 16(22), 14409–14420, doi:10.5194/acp-16-14409-2016, 2016.

Sareen, N., Waxman, E. M., Turpin, B. J., Volkamer, R. and Carlton, A. G.: Potential of Aerosol Liquid Water to Facilitate Organic Aerosol Formation: Assessing Knowledge Gaps about Precursors and Partitioning, Environ. Sci. Technol., 51(6), 3327–3335, doi:10.1021/acs.est.6b04540, 2017.

Saxena, P., Hildemann, L. M., McMurry, P. H. and Seinfeld, J. H.: Organics alter hygroscopic behavior of atmospheric particles, J. Geophys. Res., 100(D9), 18755, doi:10.1029/95JD01835, 1995.

Schaap, M., Apituley, A., Timmermans, R. M. A., Koelemeijer, R. B. A. and de Leeuw, G.: Exploring the relation between aerosol optical depth and $PM_{2.5}$ at Cabauw, the Netherlands, Atmospheric Chem. Phys., 9(3), 909–925, doi:10.5194/acp-9-909-2009, 2009.

Schichtel, B. A., Malm, W. C., Bench, G., Fallon, S., McDade, C. E., Chow, J. C. and Watson, J. G.: Fossil and contemporary fine particulate carbon fractions at 12 rural and urban sites in the United States, J. Geophys. Res., 113(D2), doi:10.1029/2007JD008605, 2008.

Schichtel, B. A., Hand, J. L., Barna, M. G., Gebhart, K. A., Copeland, S., Vimont, J. and Malm, W. C.: Origin of Fine Particulate Carbon in the Rural United States, Environ. Sci. Technol., 51(17), 9846–9855, doi:10.1021/acs.est.7b00645, 2017.

Schlesinger, R. B.: The Health Impact of Common Inorganic Components of Fine Particulate Matter ($PM_{2.5}$) in Ambient Air: A Critical Review, Inhal. Toxicol., 19(10), 811–832, doi:10.1080/08958370701402382, 2007.

Schlesinger, R. B. and Cassee, F.: Atmospheric Secondary Inorganic Particulate Matter: The Toxicological Perspective as a Basis for Health Effects Risk Assessment, Inhal. Toxicol., 15(3), 197–235, doi:10.1080/08958370304503, 2003.

Schnaiter, M., Schmid, O., Petzold, A., Fritzsche, L., Klein, K. F., Andreae, M. O., Helas, G., Thielmann, A., Gimmler, M., Möhler, O., Linke, C. and Schurath, U.: Measurement of Wavelength-Resolved Light Absorption by Aerosols Utilizing a UV-VIS Extinction Cell, Aerosol Sci. Technol., 39(3), 249–260, doi:10.1080/027868290925958, 2005.

Seinfeld, J.: Black carbon and brown clouds: Atmospheric science, Nat. Geosci., 1(1), 15–16, doi:10.1038/ngeo.2007.62, 2008.

Seinfeld, J. H. and Pandis, S. N.: Atmospheric Chemistry and Physics: From Air Pollution to Climate Change, Wiley, New York., 1998.

Sen, P. K.: Estimates of the Regression Coefficient Based on Kendall's Tau, J. Am. Stat. Assoc., 63(324), 1379–1389, doi:10.1080/01621459.1968.10480934, 1968.

Shiraiwa, M., Ueda, K., Pozzer, A., Lammel, G., Kampf, C. J., Fushimi, A., Enami, S., Arangio, A. M., Fröhlich-Nowoisky, J., Fujitani, Y., Furuyama, A., Lakey, P. S. J., Lelieveld, J., Lucas, K., Morino, Y., Pöschl, U., Takahama, S., Takami, A., Tong, H., Weber, B., Yoshino, A. and Sato, K.: Aerosol Health Effects from Molecular to Global Scales, Environ. Sci. Technol., 51(23), 13545–13567, doi:10.1021/acs.est.7b04417, 2017a.

Shiraiwa, M., Li, Y., Tsimpidi, A. P., Karydis, V. A., Berkemeier, T., Pandis, S. N., Lelieveld, J., Koop, T. and Pöschl, U.: Global distribution of particle phase state in atmospheric secondary organic aerosols, Nat. Commun., 8(1), 15002, doi:10.1038/ncomms15002, 2017b.

Simon, H., Bhave, P. V., Swall, J. L., Frank, N. H. and Malm, W. C.: Determining the spatial and seasonal variability in OM/OC ratios across the US using multiple regression, Atmospheric Chem. Phys., 11(6), 2933–2949, doi:10.5194/acp-11-2933-2011, 2011.

Simon, H., Reff, A., Wells, B., Xing, J. and Frank, N.: Ozone Trends Across the United States over a Period of Decreasing $NO_x$ and VOC Emissions, Environ. Sci. Technol., 49(1), 186–195, doi:10.1021/es504514z, 2015.

Sisterson, D. L., Peppler, R. A., Cress, T. S., Lamb, P. J. and Turner, D. D.: The ARM Southern Great Plains (SGP) Site, Meteorol. Monogr., 57, 6.1-6.14, doi:10.1175/AMSMONOGRAPHS-D-16-0004.1, 2016.

Smith, R. L., Davis, J. M., Sacks, J., Speckman, P. and Styer, P.: Regression models for air pollution and daily mortality: analysis of data from Birmingham, Alabama, Environmetrics, 11, 719–743, 2000.

Song, W., Jia, H., Huang, J. and Zhang, Y.: A satellite-based geographically weighted regression model for regional $PM_{2.5}$ estimation over the Pearl River Delta region in China, Remote Sens. Environ., 154, 1–7, doi:10.1016/j.rse.2014.08.008, 2014.

Sorek-Hamer, M., Just, A. C. and Kloog, I.: Satellite remote sensing in epidemiological studies:, Curr. Opin. Pediatr., 28(2), 228–234, doi:10.1097/MOP.0000000000000326, 2016.

Sorooshian, A., Varutbangkul, V., Brechtel, F. J., Ervens, B., Feingold, G., Bahreini, R., Murphy, S. M., Holloway, J. S., Atlas, E. L., Buzorius, G., Jonsson, H., Flagan, R. C. and Seinfeld, J. H.: Oxalic acid in clear and cloudy atmospheres: Analysis of data from International Consortium for Atmospheric Research on Transport and Transformation 2004: Oxalic Acid Data Analysis from ICARTT, J. Geophys. Res. Atmospheres, 111(D23), doi:10.1029/2005JD006880, 2006.

Sorooshian, A., Hersey, S., Brechtel, F. J., Corless, A., Flagan, R. C. and Seinfeld, J. H.: Rapid, Size-Resolved Aerosol Hygroscopic Growth Measurements: Differential Aerosol Sizing and Hygroscopicity Spectrometer Probe (DASH-SP), Aerosol Sci. Technol., 42(6), 445–464, doi:10.1080/02786820802178506, 2008.

Spracklen, D. V., Logan, J. A., Mickley, L. J., Park, R. J., Yevich, R., Westerling, A. L. and Jaffe, D. A.: Wildfires drive interannual variability of organic carbon aerosol in the western U.S. in summer: Interannual Variability of OC Aerosol, Geophys. Res. Lett., 34(16), doi:10.1029/2007GL030037, 2007.

Spracklen, D. V., Mickley, L. J., Logan, J. A., Hudman, R. C., Yevich, R., Flannigan, M. D. and Westerling, A. L.: Impacts of climate change from 2000 to 2050 on wildfire activity and carbonaceous aerosol concentrations in the western United States, J. Geophys. Res., 114(D20), doi:10.1029/2008JD010966, 2009.

Spracklen, D. V., Jimenez, J. L., Carslaw, K. S., Worsnop, D. R., Evans, M. J., Mann, G. W., Zhang, Q., Canagaratna, M. R., Allan, J., Coe, H., McFiggans, G., Rap, A. and Forster, P.: Aerosol mass spectrometer constraint on the global secondary organic aerosol budget, Atmospheric Chem. Phys., 11(23), 12109–12136, doi:10.5194/acp-11-12109-2011, 2011.

Stone, D., Whalley, L. K. and Heard, D. E.: Tropospheric OH and $HO_2$ radicals: field measurements and model comparisons, Chem. Soc. Rev., 41(19), 6348, doi:10.1039/c2cs35140d, 2012.

Subramanian, R., Khlystov, A. Y. and Robinson, A. L.: Effect of Peak Inert-Mode Temperature on Elemental Carbon Measured Using Thermal-Optical Analysis, Aerosol Sci. Technol., 40(10), 763–780, doi:10.1080/02786820600714403, 2006.

Suda, S. R., Petters, M. D., Matsunaga, A., Sullivan, R. C., Ziemann, P. J. and Kreidenweis, S. M.: Hygroscopicity frequency distributions of secondary organic aerosols: Hygroscopicity Frequency Distributions, J. Geophys. Res. Atmospheres, 117(D4), doi:10.1029/2011JD016823, 2012.

Tackett, J. L., Winker, D. M., Getzewich, B. J., Vaughan, M. A., Young, S. A. and Kar, J.: CALIPSO lidar level 3 aerosol profile product: version 3 algorithm design, Atmospheric Meas. Tech., 11(7), 4129–4152, doi:10.5194/amt-11-4129-2018, 2018.

Tai, A. P. K., Mickley, L. J. and Jacob, D. J.: Correlations between fine particulate matter ($PM_{2.5}$) and meteorological variables in the United States: Implications for the sensitivity of $PM_{2.5}$ to climate change, Atmos. Environ., 44(32), 3976–3984, doi:10.1016/j.atmosenv.2010.06.060, 2010.

Tai, A. P. K., Mickley, L. J., Heald, C. L. and Wu, S.: Effect of $CO_2$ inhibition on biogenic isoprene emission: Implications for air quality under 2000 to 2050 changes in climate, vegetation, and land use: $CO_2$-Isoprene Interaction and Air Quality, Geophys. Res. Lett., 40(13), 3479–3483, doi:10.1002/grl.50650, 2013.

Tan, Y., Carlton, A. G., Seitzinger, S. P. and Turpin, B. J.: SOA from methylglyoxal in clouds and wet aerosols: Measurement and prediction of key products, Atmos. Environ., 44(39), 5218–5226, doi:10.1016/j.atmosenv.2010.08.045, 2010.

Tang, I. N.: Chemical and size effects of hygroscopic aerosols on light scattering coefficients, J. Geophys. Res. Atmospheres, 101(D14), 19245–19250, doi:10.1029/96JD03003, 1996.

Tang, Y., Carmichael, G. R., Uno, I., Woo, J.-H., Kurata, G., Lefer, B., Shetter, R. E., Huang, H., Anderson, B. E., Avery, M. A., Clarke, A. D. and Blake, D. R.: Impacts of aerosols and clouds on photolysis frequencies and photochemistry during TRACE-P: 2. Three-dimensional study using a regional chemical transport model: 3-D Photolysis and Photochemical Study, J. Geophys. Res. Atmospheres, 108(D21), doi:10.1029/2002JD003100, 2003.

Theil, H.: A rank-invariant method of linear and polynomial regression analysis I, II and III., Proc. R. Neth. Acad. Sci., 53, 386–392, 1950.

Tian, D., Hu, Y., Wang, Y., Boylan, J. W., Zheng, M. and Russell, A. G.: Assessment of Biomass Burning Emissions and Their Impacts on Urban and Regional $PM_{2.5}$ : A Georgia Case Study, Environ. Sci. Technol., 43(2), 299–305, doi:10.1021/es801827s, 2009.

Tian, J. and Chen, D.: A semi-empirical model for predicting hourly ground-level fine particulate matter ($PM_{2.5}$) concentration in southern Ontario from satellite remote sensing and ground-based meteorological measurements, Remote Sens. Environ., 114(2), 221–229, doi:10.1016/j.rse.2009.09.011, 2010.

Toon, O. B., Maring, H., Dibb, J., Ferrare, R., Jacob, D. J., Jensen, E. J., Luo, Z. J., Mace, G. G., Pan, L. L., Pfister, L., Rosenlof, K. H., Redemann, J., Reid, J. S., Singh, H. B., Thompson, A. M., Yokelson, R., Minnis, P., Chen, G., Jucks, K. W. and Pszenny, A.: Planning, implementation, and scientific goals of the Studies of Emissions and Atmospheric Composition, Clouds and Climate Coupling by Regional Surveys (SEAC$^4$RS) field mission: Planning SEAC4RS, J. Geophys. Res. Atmospheres, 121(9), 4967–5009, doi:10.1002/2015JD024297, 2016.

Tosca, M., Campbell, J., Garay, M., Lolli, S., Seidel, F., Marquis, J. and Kalashnikova, O.: Attributing Accelerated Summertime Warming in the Southeast United States to Recent Reductions in Aerosol Burden: Indications from Vertically-Resolved Observations, Remote Sens., 9(7), 674, doi:10.3390/rs9070674, 2017.

Travis, K. R., Jacob, D. J., Fisher, J. A., Kim, P. S., Marais, E. A., Zhu, L., Yu, K., Miller, C. C., Yantosca, R. M., Sulprizio, M. P., Thompson, A. M., Wennberg, P. O., Crounse, J. D., St. Clair, J. M., Cohen, R. C., Laughner, J. L., Dibb, J. E., Hall, S. R., Ullmann, K., Wolfe, G. M., Pollack, I. B., Peischl, J., Neuman, J. A. and Zhou, X.: Why do models overestimate surface ozone in the Southeast United States?, Atmospheric Chem. Phys., 16(21), 13561–13577, doi:10.5194/acp-16-13561-2016, 2016.

Trenberth, K. E., Fasullo, J. T. and Kiehl, J.: Earth's Global Energy Budget, Bull. Am. Meteorol. Soc., 90(3), 311–324, doi:10.1175/2008BAMS2634.1, 2009.

Tritscher, T., Dommen, J., DeCarlo, P. F., Gysel, M., Barmet, P. B., Praplan, A. P., Weingartner, E., Prévôt, A. S. H., Riipinen, I., Donahue, N. M. and Baltensperger, U.: Volatility and hygroscopicity of aging secondary organic aerosol in a smog chamber, Atmospheric Chem. Phys., 11(22), 11477–11496, doi:10.5194/acp-11-11477-2011, 2011.

Tröstl, J., Chuang, W. K., Gordon, H., Heinritzi, M., Yan, C., Molteni, U., Ahlm, L., Frege, C., Bianchi, F., Wagner, R., Simon, M., Lehtipalo, K., Williamson, C., Craven, J. S., Duplissy, J., Adamov, A., Almeida, J., Bernhammer, A.-K., Breitenlechner, M., Brilke, S., Dias, A., Ehrhart, S., Flagan, R. C., Franchin, A., Fuchs, C., Guida, R., Gysel, M., Hansel, A., Hoyle, C. R., Jokinen, T., Junninen, H., Kangasluoma, J., Keskinen, H., Kim, J., Krapf, M., Kürten, A., Laaksonen, A., Lawler, M., Leiminger, M., Mathot, S., Möhler, O., Nieminen, T., Onnela, A., Petäjä, T., Piel, F. M., Miettinen, P., Rissanen, M. P., Rondo, L., Sarnela, N., Schobesberger, S., Sengupta, K., Sipilä, M., Smith, J. N., Steiner, G., Tomè, A., Virtanen, A., Wagner, A. C., Weingartner, E., Wimmer, D., Winkler, P. M., Ye, P., Carslaw, K. S., Curtius, J., Dommen, J., Kirkby, J., Kulmala, M., Riipinen, I., Worsnop, D. R., Donahue, N. M. and Baltensperger, U.: The role of low-volatility organic compounds in initial particle growth in the atmosphere, Nature, 533(7604), 527–531, doi:10.1038/nature18271, 2016.

Tsai, F. C., Apte, M. G. and Daisey, J. M.: An Exploratory Analysis of the Relationship Between Mortality and the Chemical Composition of Airborne Particulate Matter, Inhal. Toxicol., 12(sup2), 121–135, doi:10.1080/08958378.2000.11463204, 2000.

Turner, M. C., Krewski, D., Pope, C. A., Chen, Y., Gapstur, S. M. and Thun, M. J.: Long-term Ambient Fine Particulate Matter Air Pollution and Lung Cancer in a Large Cohort of Never-Smokers, Am. J. Respir. Crit. Care Med., 184(12), 1374–1381, doi:10.1164/rccm.201106-1011OC, 2011.

Turpin, B. J. and Lim, H.-J.: Species Contributions to $PM_{2.5}$ Mass Concentrations: Revisiting Common Assumptions for Estimating Organic Mass, Aerosol Sci. Technol., 35(1), 602–610, doi:10.1080/02786820119445, 2001.

Twomey, S.: Influence of pollution on shortwave albedo of clouds, J. Atmospheric Sci., 34, 1149–1152, 1977.

Updyke, K. M., Nguyen, T. B. and Nizkorodov, S. A.: Formation of brown carbon via reactions of ammonia with secondary organic aerosols from biogenic and anthropogenic precursors, Atmos. Environ., 63, 22–31, doi:10.1016/j.atmosenv.2012.09.012, 2012.

US Environmental Protection Agency: Ambient Air Monitoring Strategy for State, Local, and Tribal Air Agencies, [online] Available from: https://www3.epa.gov/ttnamti1/files/ambient/monitorstrat/AAMS%20for%20SLTs%20%20-%20FINAL%20Dec%202008.pdf, 2008.

US EPA: Method Compendium: $PM_{2.5}$ Mass Weighing Laboratory Standard Operating Procedures for the Performance Evaluation Program, [online] Available from: https://www3.epa.gov/ttnamti1/files/ambient/pm25/qa/peplsop.pdf, 1998.

Verma, V., Fang, T., Guo, H., King, L., Bates, J. T., Peltier, R. E., Edgerton, E., Russell, A. G. and Weber, R. J.: Reactive oxygen species associated with water-soluble $PM_{2.5}$ in the southeastern United States: spatiotemporal trends and source apportionment, Atmospheric Chem. Phys., 14(23), 12915–12930, doi:10.5194/acp-14-12915-2014, 2014.

Verma, V., Fang, T., Xu, L., Peltier, R. E., Russell, A. G., Ng, N. L. and Weber, R. J.: Organic Aerosols Associated with the Generation of Reactive Oxygen Species (ROS) by Water-Soluble $PM_{2.5}$, Environ. Sci. Technol., 49(7), 4646–4656, doi:10.1021/es505577w, 2015.

Vogelmann, A. M., McFarquhar, G. M., Ogren, J. A., Turner, D. D., Comstock, J. M., Feingold, G., Long, C. N., Jonsson, H. H., Bucholtz, A., Collins, D. R., Diskin, G. S., Gerber, H., Lawson, R. P., Woods, R. K., Andrews, E., Yang, H.-J., Chiu, J. C., Hartsock, D., Hubbe, J. M., Lo, C., Marshak, A., Monroe, J. W., McFarlane, S. A., Schmid, B., Tomlinson, J. M. and Toto, T.: Racoro Extended-Term Aircraft Observations of Boundary Layer Clouds, Bull. Am. Meteorol. Soc., 93(6), 861–878, doi:10.1175/BAMS-D-11-00189.1, 2012.

Volkamer, R., Baidar, S., Campos, T. L., Coburn, S., DiGangi, J. P., Dix, B., Eloranta, E. W., Koenig, T. K., Morley, B., Ortega, I., Pierce, B. R., Reeves, M., Sinreich, R., Wang, S., Zondlo, M. A. and Romashkin, P. A.: Aircraft measurements of BrO, IO, glyoxal, $NO_2$, $H_2O$, $O_2$–$O_2$ and aerosol extinction profiles in the tropics: comparison with aircraft-/ship-based in situ and lidar measurements, Atmospheric Meas. Tech., 8(5), 2121–2148, doi:10.5194/amt-8-2121-2015, 2015.

Wagner, N. L., Brock, C. A., Angevine, W. M., Beyersdorf, A., Campuzano-Jost, P., Day, D., de Gouw, J. A., Diskin, G. S., Gordon, T. D., Graus, M. G., Holloway, J. S., Huey, G., Jimenez, J. L., Lack, D. A., Liao, J., Liu, X., Markovic, M. Z., Middlebrook, A. M., Mikoviny, T., Peischl, J., Perring, A. E., Richardson, M. S., Ryerson, T. B., Schwarz, J. P., Warneke, C., Welti, A., Wisthaler, A., Ziemba, L. D. and Murphy, D. M.: In situ vertical profiles of aerosol extinction, mass, and composition over the southeast United States during SENEX and SEAC$^4$RS: observations of a modest aerosol enhancement aloft, Atmospheric Chem. Phys., 15(12), 7085–7102, doi:10.5194/acp-15-7085-2015, 2015.

Wang, C., Lei, Y. D., Endo, S. and Wania, F.: Measuring and Modeling the Salting-out Effect in Ammonium Sulfate Solutions, Environ. Sci. Technol., 48(22), 13238–13245, doi:10.1021/es5035602, 2014.

Wang, C., Yuan, T., Wood, S. A., Goss, K.-U., Li, J., Ying, Q. and Wania, F.: Uncertain Henry's law constants compromise equilibrium partitioning calculations of atmospheric oxidation products, Atmospheric Chem. Phys., 17(12), 7529–7540, doi:10.5194/acp-17-7529-2017, 2017a.

Wang, J. and Christopher, S. A.: Intercomparison between satellite-derived aerosol optical thickness and $PM_{2.5}$ mass: Implications for air quality studies, Geophys. Res. Lett., 30(21), 2095, doi:10.1029/2003GL018174, 2003.

Wang, J., Xu, X., Henze, D. K., Zeng, J., Ji, Q., Tsay, S.-C. and Huang, J.: Top-down estimate of dust emissions through integration of MODIS and MISR aerosol retrievals with the GEOS-Chem adjoint model: Top-Down Estimate of Dust Emissions, Geophys. Res. Lett., 39(8), n/a-n/a, doi:10.1029/2012GL051136, 2012.

Wang, J. X. and Angell, J. K.: Air stagnation climatology for the United States, [online] Available from: https://www.arl.noaa.gov/documents/reports/atlas.pdf, 1999.

Wang, P., Schade, G., Estes, M. and Ying, Q.: Improved MEGAN predictions of biogenic isoprene in the contiguous United States, Atmos. Environ., 148, 337–351, doi:10.1016/j.atmosenv.2016.11.006, 2017b.

Wang, Y., Chung, A. and Paulson, S. E.: The effect of metal salts on quantification of elemental and organic carbon in diesel exhaust particles using thermal-optical evolved gas analysis, Atmospheric Chem. Phys., 10(23), 11447–11457, doi:10.5194/acp-10-11447-2010, 2010.

Waxman, E. M., Elm, J., Kurtén, T., Mikkelsen, K. V., Ziemann, P. J. and Volkamer, R.: Glyoxal and Methylglyoxal Setschenow Salting Constants in Sulfate, Nitrate, and Chloride Solutions: Measurements and Gibbs Energies, Environ. Sci. Technol., 49(19), 11500–11508, doi:10.1021/acs.est.5b02782, 2015.

Weakley, A. T., Takahama, S. and Dillner, A. M.: Ambient aerosol composition by infrared spectroscopy and partial least-squares in the chemical speciation network: Organic carbon with functional group identification, Aerosol Sci. Technol., 50(10), 1096–1114, doi:10.1080/02786826.2016.1217389, 2016.

van der Werf, G. R., Randerson, J. T., Giglio, L., Collatz, G. J., Mu, M., Kasibhatla, P. S., Morton, D. C., DeFries, R. S., Jin, Y. and van Leeuwen, T. T.: Global fire emissions and the contribution of deforestation, savanna, forest, agricultural, and peat fires (1997–2009), Atmospheric Chem. Phys., 10(23), 11707–11735, doi:10.5194/acp-10-11707-2010, 2010.

Westerling, A. L.: Increasing western US forest wildfire activity: sensitivity to changes in the timing of spring, Philos. Trans. R. Soc. B Biol. Sci., 371(1696), 20150178, doi:10.1098/rstb.2015.0178, 2016.

Xu, L. and Penner, J. E.: Global simulations of nitrate and ammonium aerosols and their radiative effects, Atmospheric Chem. Phys., 12(20), 9479–9504, doi:10.5194/acp-12-9479-2012, 2012.

Xue, H. and Feingold, G.: Large-Eddy Simulations of Trade Wind Cumuli: Investigation of Aerosol Indirect Effects, J. Atmospheric Sci., 63(6), 1605–1622, doi:10.1175/JAS3706.1, 2006.

Xue, H., Khalizov, A. F., Wang, L., Zheng, J. and Zhang, R.: Effects of dicarboxylic acid coating on the optical properties of soot, Phys. Chem. Chem. Phys., 11(36), 7869, doi:10.1039/b904129j, 2009.

Yli-Juuti, T., Pajunoja, A., Tikkanen, O., Buchholz, A., Faiola, C., Väisänen, O., Hao, L., Kari, E., Peräkylä, O., Garmash, O., Shiraiwa, M., Ehn, M., Lehtinen, K. and Virtanen, A.: Factors controlling the evaporation of secondary organic aerosol from α-pinene ozonolysis, Geophys. Res. Lett., 44(5), 2562–2570, doi:10.1002/2016GL072364, 2017.

Youn, J.-S., Wang, Z., Wonaschütz, A., Arellano, A., Betterton, E. A. and Sorooshian, A.: Evidence of aqueous secondary organic aerosol formation from biogenic emissions in the North American Sonoran Desert: Aqueous SOA Formation in Sonoran Desert, Geophys. Res. Lett., 40(13), 3468–3472, doi:10.1002/grl.50644, 2013.

Yu, S., Alapaty, K., Mathur, R., Pleim, J., Zhang, Y., Nolte, C., Eder, B., Foley, K. and Nagashima, T.: Attribution of the United States "warming hole": Aerosol indirect effect and precipitable water vapor, Sci. Rep., 4(1), 6929, doi:10.1038/srep06929, 2014.

Yuan, H., Dai, Y., Xiao, Z., Ji, D. and Shangguan, W.: Reprocessing the MODIS Leaf Area Index products for land surface and climate modelling, Remote Sens. Environ., 115(5), 1171–1187, doi:10.1016/j.rse.2011.01.001, 2011.

Zeng, T., Wang, Y., Yoshida, Y., Tian, D., Russell, A. G. and Barnard, W. R.: Impacts of Prescribed Fires on Air Quality over the Southeastern United States in Spring Based on Modeling and Ground/Satellite Measurements, Environ. Sci. Technol., 42(22), 8401–8406, doi:10.1021/es800363d, 2008.

Zhang, G., Rui, X. and Fan, Y.: Critical Review of Methods to Estimate $PM_{2.5}$ Concentrations within Specified Research Region, ISPRS Int. J. Geo-Inf., 7(9), 368, doi:10.3390/ijgi7090368, 2018a.

Zhang, H., Kondragunta, S., Laszlo, I., Liu, H., Remer, L. A., Huang, J., Superczynski, S. and Ciren, P.: An enhanced VIIRS aerosol optical thickness (AOT) retrieval algorithm over land using a global surface reflectance ratio database: Enhanced VIIRS AOT Retrieval Algorithm Land, J. Geophys. Res. Atmospheres, 121(18), 10,717-10,738, doi:10.1002/2016JD024859, 2016.

Zhang, H., Yee, L. D., Lee, B. H., Curtis, M. P., Worton, D. R., Isaacman-VanWertz, G., Offenberg, J. H., Lewandowski, M., Kleindienst, T. E., Beaver, M. R., Holder, A. L., Lonneman, W. A., Docherty, K. S., Jaoui, M., Pye, H. O. T., Hu, W., Day, D. A., Campuzano-Jost, P., Jimenez, J. L., Guo, H., Weber, R. J., de Gouw, J., Koss, A. R., Edgerton, E. S., Brune, W., Mohr, C., Lopez-Hilfiker, F. D., Lutz, A., Kreisberg, N. M., Spielman, S. R., Hering, S. V., Wilson, K. R., Thornton, J. A. and Goldstein, A. H.: Monoterpenes are the largest source of summertime organic aerosol in the southeastern United States, Proc. Natl. Acad. Sci., 115(9), 2038–2043, doi:10.1073/pnas.1717513115, 2018b.

Zhang, L., Jacob, D. J., Knipping, E. M., Kumar, N., Munger, J. W., Carouge, C. C., van Donkelaar, A., Wang, Y. X. and Chen, D.: Nitrogen deposition to the United States: distribution, sources, and processes, Atmospheric Chem. Phys., 12(10), 4539–4554, doi:10.5194/acp-12-4539-2012, 2012.

Zhang, Q., Jimenez, J. L., Canagaratna, M. R., Allan, J. D., Coe, H., Ulbrich, I., Alfarra, M. R., Takami, A., Middlebrook, A. M., Sun, Y. L., Dzepina, K., Dunlea, E., Docherty, K., DeCarlo, P. F., Salcedo, D., Onasch, T., Jayne, J. T., Miyoshi, T., Shimono, A., Hatakeyama, S., Takegawa, N., Kondo, Y., Schneider, J., Drewnick, F., Borrmann, S., Weimer, S., Demerjian, K., Williams, P., Bower, K., Bahreini, R., Cottrell, L., Griffin, R. J., Rautiainen, J., Sun, J. Y., Zhang, Y. M. and Worsnop, D. R.: Ubiquity and dominance of oxygenated species in organic aerosols in anthropogenically-influenced Northern Hemisphere midlatitudes: Ubiquity and Dominance of Oxygenated OA, Geophys. Res. Lett., 34(13), L13801, doi:10.1029/2007GL029979, 2007.

Zhang, Q., Jimenez, J. L., Canagaratna, M. R., Ulbrich, I. M., Ng, N. L., Worsnop, D. R. and Sun, Y.: Understanding atmospheric organic aerosols via factor analysis of aerosol mass spectrometry: a review, Anal. Bioanal. Chem., 401(10), 3045–3067, doi:10.1007/s00216-011-5355-y, 2011.

Zhang, X., Lin, Y.-H., Surratt, J. D. and Weber, R. J.: Sources, Composition and Absorption Ångström Exponent of Light-absorbing Organic Components in Aerosol Extracts from the Los Angeles Basin, Environ. Sci. Technol., 47(8), 3685–3693, doi:10.1021/es305047b, 2013.

Zhao, R., Lee, A. K. Y., Huang, L., Li, X., Yang, F. and Abbatt, J. P. D.: Photochemical processing of aqueous atmospheric brown carbon, Atmospheric Chem. Phys., 15(11), 6087–6100, doi:10.5194/acp-15-6087-2015, 2015.

Zhong, M. and Jang, M.: Light absorption coefficient measurement of SOA using a UV–Visible spectrometer connected with an integrating sphere, Atmos. Environ., 45(25), 4263–4271, doi:10.1016/j.atmosenv.2011.04.082, 2011.

Zhou, S., Collier, S., Jaffe, D. A. and Zhang, Q.: Free tropospheric aerosols at the Mt. Bachelor Observatory: more oxidized and higher sulfate content compared to boundary layer aerosols, Atmospheric Chem. Phys., 19(3), 1571–1585, doi:10.5194/acp-19-1571-2019, 2019.

Ziemba, L. D., Lee Thornhill, K., Ferrare, R., Barrick, J., Beyersdorf, A. J., Chen, G., Crumeyrolle, S. N., Hair, J., Hostetler, C., Hudgins, C., Obland, M., Rogers, R., Scarino, A. J., Winstead, E. L. and Anderson, B. E.: Airborne observations of aerosol extinction by in situ and remote-sensing techniques: Evaluation of particle hygroscopicity, Geophys. Res. Lett., 40(2), 417–422, doi:10.1029/2012GL054428, 2013.

# APPENDIX A

## SUPPORTING INFORMATION FOR CHAPTER 2

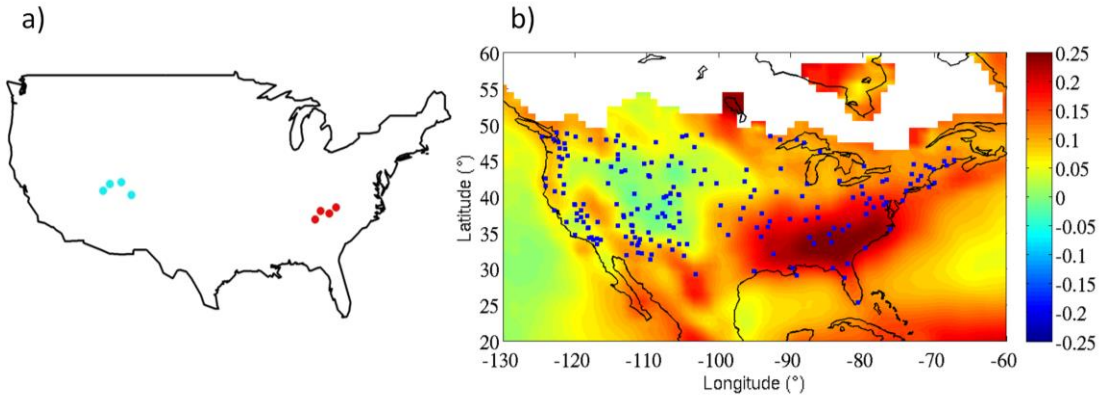


**Figure A1.** (a) Location of the four CO Plateau (blue) and four Appalachia (red) IMPROVE focus sites. (b) Average 2001-2014 seasonal differences (summer-winter) in MODIS AOT measurements with all IMPROVE network sites superimposed.

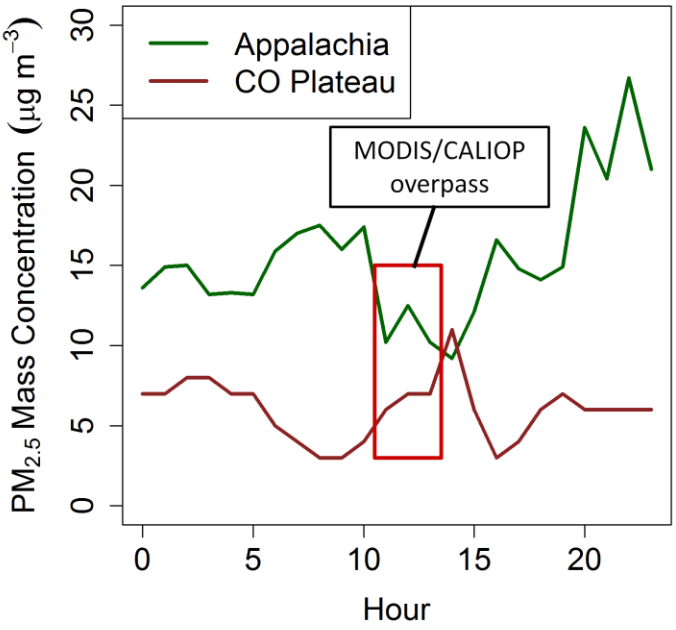


**Figure A2.** Diurnal variability in $PM_{2.5}$ measurements captured by EPA monitors during one representative day, 7/1/2010, at EPA monitoring locations within the Appalachia and CO Plateau regions (Bryson City, NC, and Red Wash, UT). The red box indicates times of MODIS and CALIPSO overpass.

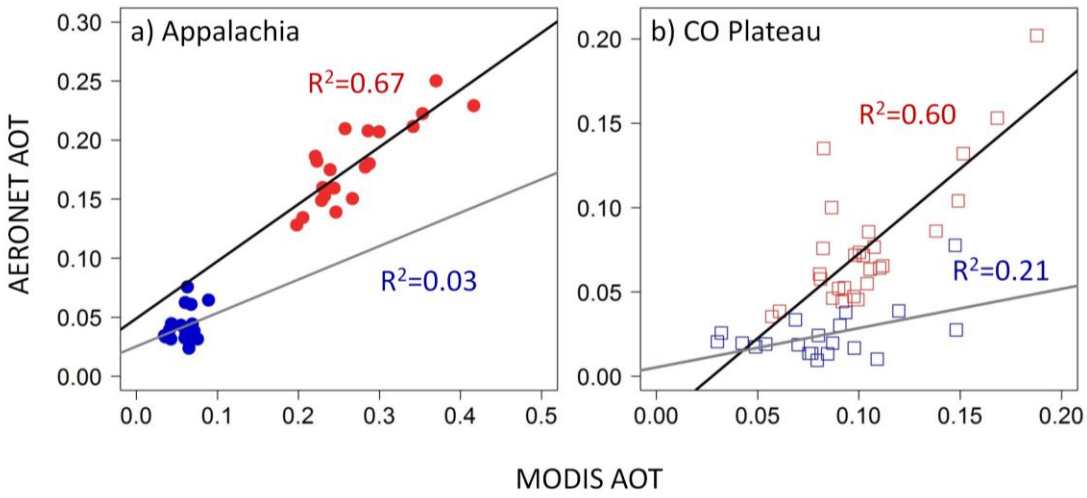


**Figure A3.** Monthly summer (red) and winter (blue) aggregate AERONET AOT at 500 nm versus monthly summer and winter aggregate MODIS AOT at 550 nm for (a) Appalachia and (b) the CO Plateau.

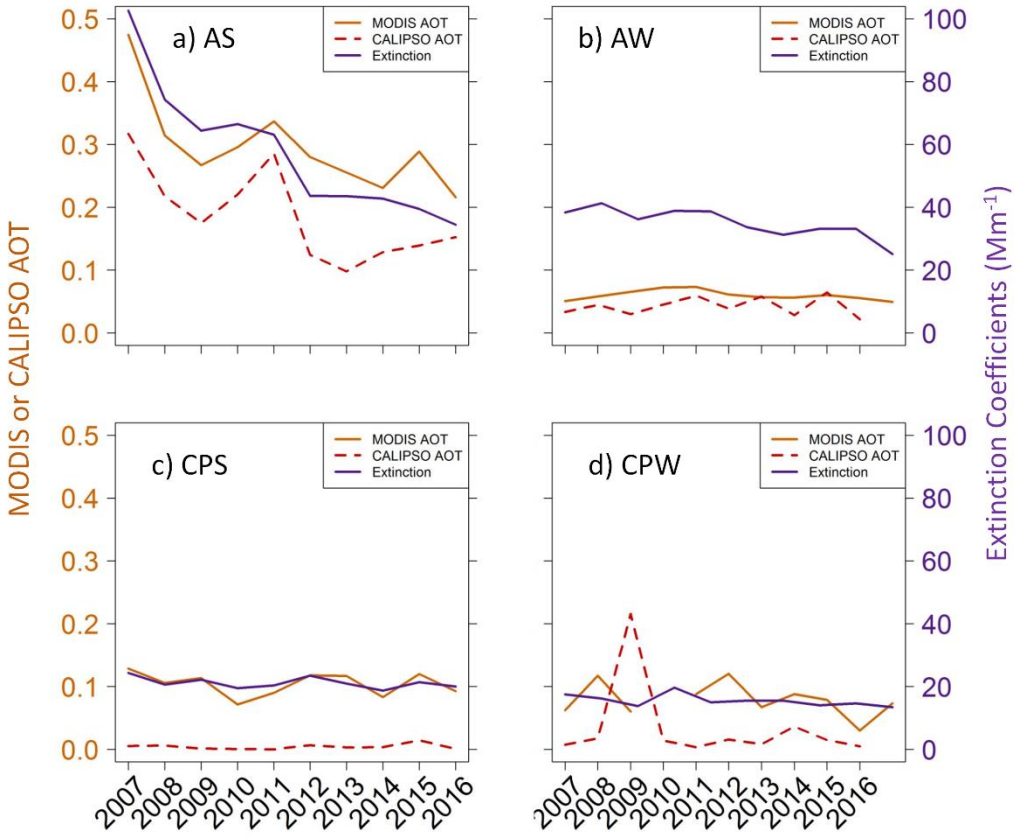


**Figure A4.** Extinction coefficients (purple) estimated using the IMPROVE algorithm plotted concurrently with MODIS (orange solid line) and CALIPSO (red dotted line) AOT in (a) Appalachia summer, (b) Appalachia winter, (c) CO Plateau summer, and (d) CO Plateau winter.

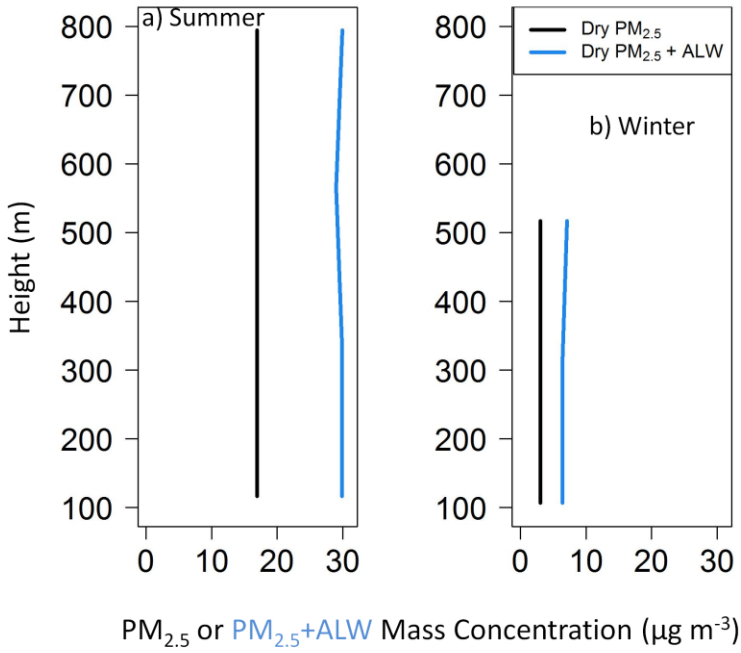


**Figure A5.** Representative (a) summer and (b) winter vertical profiles for dry $PM_{2.5}$ (black) and ALW (blue) mass concentrations for COHU1 (Appalachia) on 8/31/2012 and 12/8/2011, respectively. Dry $PM_{2.5}$ does not change with height in a well-mixed PBL, but ALW does, regardless of season.

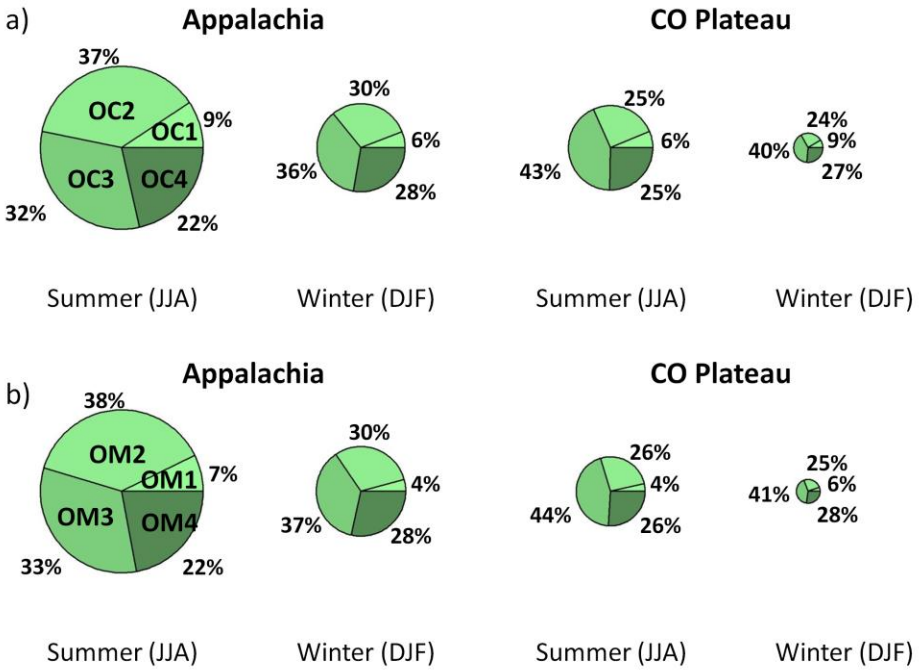


**Figure A6.** (a) Organic carbon and (b) organic mass fractionation contribution to total organic mass concentration by season and region from 2007-2016. The diameter of each pie chart is relative to the average Appalachia summer mass concentration in (a) and (b), respectively.

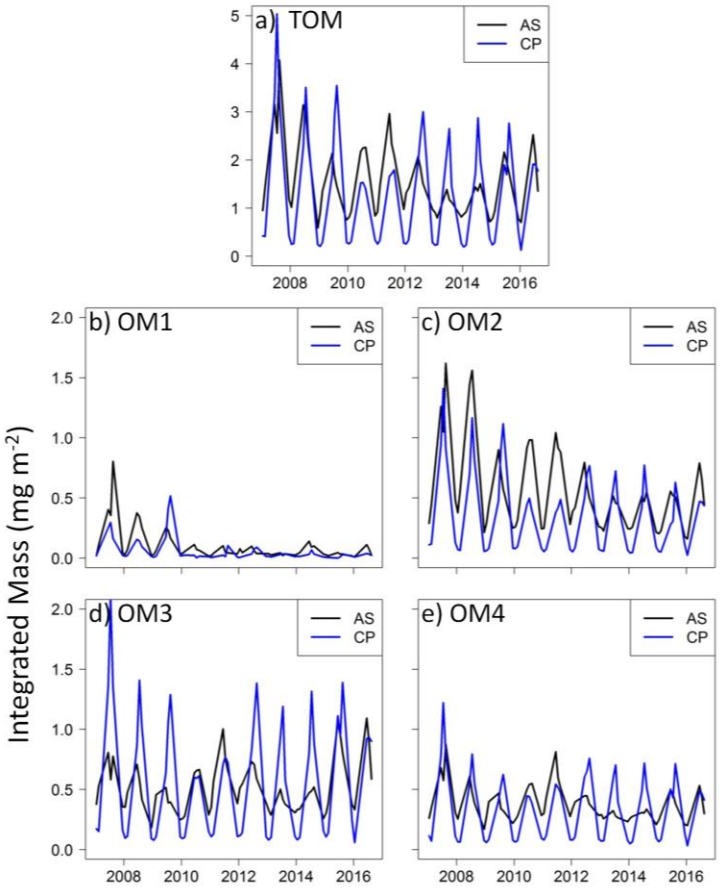


**Figure A7.** Seasonality in organic mass concentrations at the surface in Appalachia (black) and the CO Plateau (blue) for (a) TOM, (b) organic mass from OC1, (c) organic mass from OC2, (d) organic mass from OC3, and (e) organic mass from OC4.

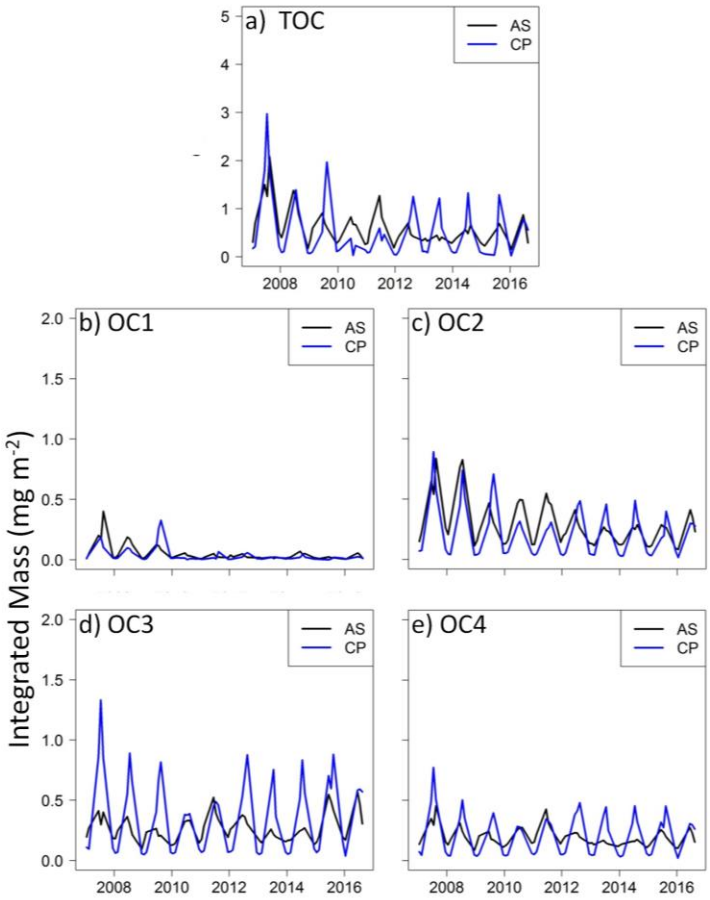


**Figure A8.** Seasonality in organic carbon concentrations at the surface in Appalachia (black) and the CO Plateau (blue) for (a) TOC, (b) OC1, (c) OC2, (d) OC3, and (e) OC4.

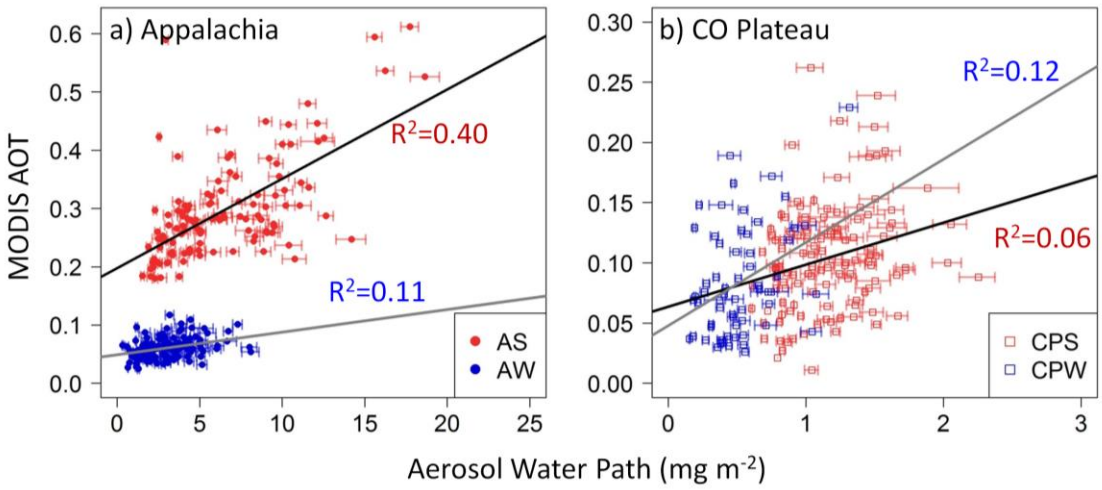


**Figure A9.** Monthly average aerosol water path (aerosol liquid water integrated through the planetary boundary layer) against MODIS AOT for all sites in (a) Appalachia (circles) and (b) CO Plateau (squares) summer (red) and winter (blue) for 2007-2016. The lines of best fit are shown for Appalachia summer (black) and winter (gray). Note that the axes are not equal between panels. Horizontal error bars indicate the uncertainty of organic contributions to ALW, with the left-hand side showing the low sensitivity ($\kappa_{org}$ = 0.01-0.04) and the right-hand side showing the high sensitivity ($\kappa_{org}$ = 0.17-0.20).

**Table A1.** The root mean square error between monthly average AERONET and MODIS AOT.

| | Appalachia Summer | Appalachia Winter | CO Plateau Summer | CO Plateau Winter |
|---|---|---|---|---|
| RSME | 0.10 | 0.02 | 0.04 | 0.06 |

**Table A2.** Correlation ($R^2$) and significance values for IMPROVE-estimated surface extinction and MODIS AOT from 2007 to 2016 by season and region. Bolded values indicate significant correlations.

| Region and Season | $R^2$ | p-value |
|---|---|---|
| **Appalachia Summer** | **0.76** | **<0.01** |
| **Appalachia Winter** | **0.11** | **<0.01** |
| **CO Plateau Summer** | **0.69** | **<0.01** |
| **CO Plateau Winter** | **0.10** | **0.01** |

**Table A3.** Correlations between monthly average aerosol water path, and $PM_{2.5}$ mass concentrations + aerosol water path and MODIS AOT for various $\kappa_{org}$ scenarios.

| Kappa assignment | Summer $R^2$ | Summer p-value | Winter $R^2$ | Winter p-value |
|---|---|---|---|---|
| | | ***Appalachia*** | | |
| Dry $PM_{2.5}$ | 0.48 | <0.01 | 0.16 | <0.01 |
| $PM_{2.5}$ + Inorganic ALW | 0.48 | <0.01 | 0.14 | <0.01 |
| $PM_{2.5}$ + Low $\kappa_{org}$ estimate | 0.48 | <0.01 | 0.14 | <0.01 |
| $PM_{2.5}$ + Med $\kappa_{org}$ estimate | 0.48 | <0.01 | 0.14 | <0.01 |
| $PM_{2.5}$ + High $\kappa_{org}$ estimate | 0.47 | <0.01 | 0.15 | <0.01 |
| $PM_{2.5}$ + All $\kappa_{org}$ =0.01 | 0.48 | <0.01 | 0.14 | <0.01 |
| $PM_{2.5}$ + All $\kappa_{org}$ =0.1 | 0.48 | <0.01 | 0.14 | <0.01 |
| $PM_{2.5}$ + All $\kappa_{org}$ =0.15 | 0.47 | <0.01 | 0.15 | <0.01 |
| $PM_{2.5}$ + All $\kappa_{org}$ =0.2 | 0.47 | <0.01 | 0.15 | <0.01 |
| | | ***CO Plateau*** | | |
| Dry $PM_{2.5}$ | 0.09 | <0.01 | 0.09 | <0.01 |
| $PM_{2.5}$ + Inorganic ALW | 0.10 | <0.01 | 0.11 | <0.01 |
| $PM_{2.5}$ + Low $\kappa_{org}$ estimate | 0.10 | <0.01 | 0.11 | <0.01 |
| $PM_{2.5}$ + Med $\kappa_{org}$ estimate | 0.11 | <0.01 | 0.11 | <0.01 |
| $PM_{2.5}$ + High $\kappa_{org}$ estimate | 0.11 | <0.01 | 0.12 | <0.01 |
| $PM_{2.5}$ + All $\kappa_{org}$ =0.01 | 0.10 | <0.01 | 0.11 | <0.01 |
| $PM_{2.5}$ + All $\kappa_{org}$ =0.1 | 0.10 | <0.01 | 0.11 | <0.01 |
| $PM_{2.5}$ + All $\kappa_{org}$ =0.15 | 0.11 | <0.01 | 0.11 | <0.01 |
| $PM_{2.5}$ + All $\kappa_{org}$ =0.2 | 0.11 | <0.01 | 0.12 | <0.01 |

**Table A4.** Linear trend analysis ($R^2$) and significance values for seasonal differences (summer-winter) in surface particle chemical component mass concentrations, MODIS AOT, and extinction over time from 2007 to 2016. Bolded values indicate significant correlations.

| Regional Seasonal Difference (Summer-Winter) | $R^2$ (Species Seasonal Difference vs. Time) | p-value |
|---|---|---|
| ***Appalachia*** | | |
| **Dry $PM_{2.5}$** | **0.53** | **0.01** |
| **Inorganic ALW** | **0.88** | **<0.01** |
| Organic ALW | -0.09 | 0.63 |
| **Sulfate** | **0.76** | **<0.01** |
| **Nitrate** | **0.43** | **0.02** |
| TOM | 0.04 | 0.28 |
| OM1 | 0.26 | 0.07 |
| **OM2** | **0.44** | **0.02** |
| OM3 | 0.27 | 0.07 |
| OM4 | 0.01 | 0.33 |
| **MODIS AOT** | **0.43** | **0.02** |
| **CALIPSO AOT** | **0.43** | **0.02** |
| **Extinction** | **0.75** | **<0.01** |
| ***CO Plateau*** | | |
| Dry $PM_{2.5}$ | -0.12 | 0.92 |
| Inorganic ALW | 0.02 | 0.31 |
| Organic ALW | 0.09 | 0.33 |
| Sulfate | -0.12 | 0.82 |
| Nitrate | 0.004 | 0.34 |
| TOM | -0.08 | 0.59 |
| OM1 | 0.11 | 0.18 |
| OM2 | 0.13 | 0.16 |
| OM3 | -0.11 | 0.79 |
| OM4 | -0.12 | 0.90 |
| MODIS AOT | -0.14 | 0.86 |
| CALIPSO AOT | -0.04 | 0.44 |
| Extinction | -0.12 | 0.83 |

# APPENDIX B

SUPPORTING INFORMATION FOR CHAPTER 3

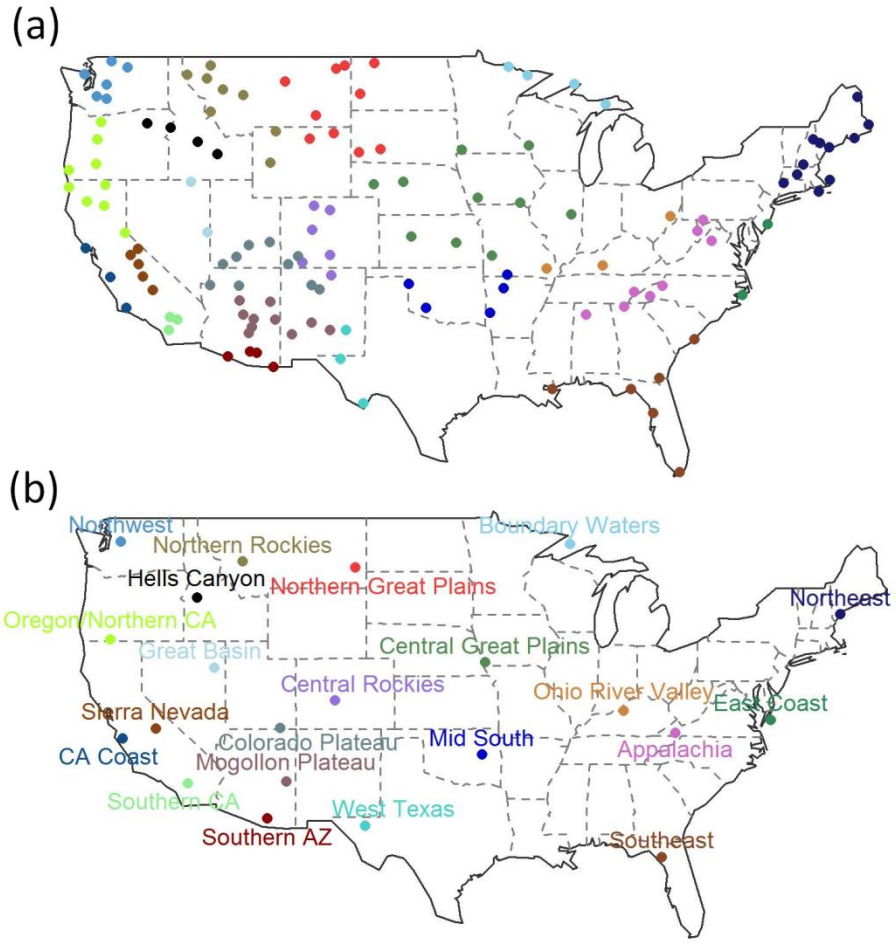


**Figure B1.** Locations of all a) IMPROVE network sites and b) chemical climatology regions. Each site is color-coded by region.

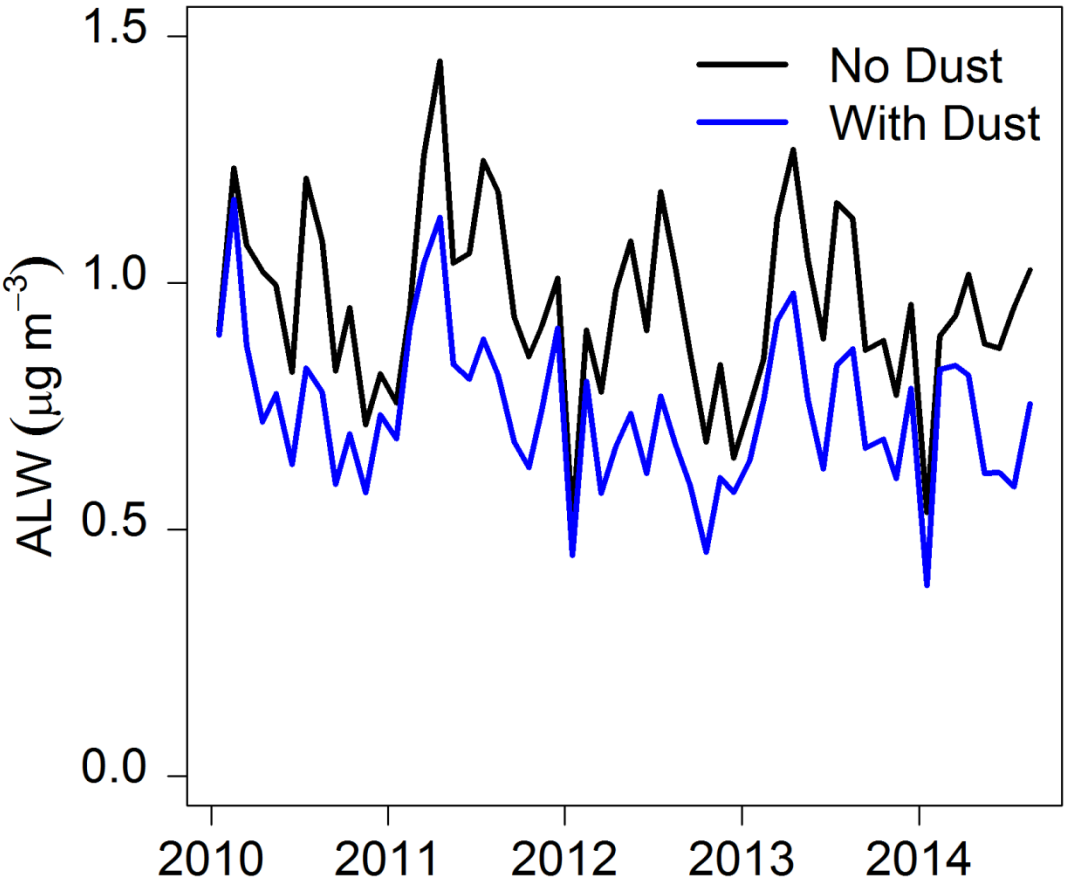


**Figure B2.** Median ALW mass concentrations calculated from ISORROPIA with dust ($Na^+$, $Ca^{2+}$, $K_+$, $Mg^{2+}$, $Cl^-$) included (blue line) and without dust (black line). In the dust sensitivity, cations form insoluble species with sulfate and precipitate. If ammonium were present, it would compete with dust for sulfate and form more soluble species and increase ALW. Here, the dust sensitivity likely represents a lower bound.

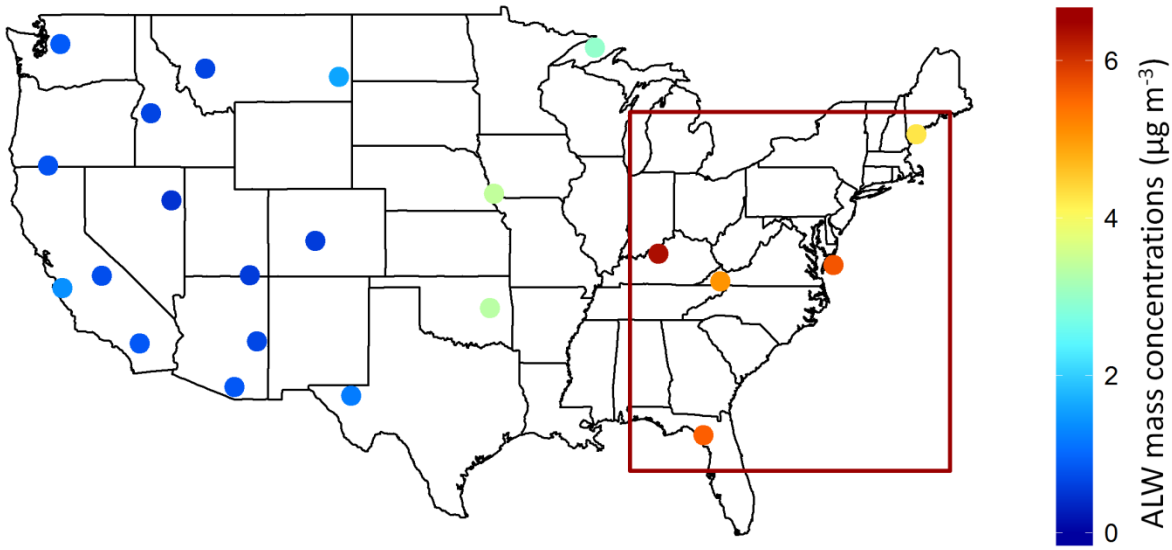


**Figure B3.** Average annual ALW mass concentrations across the CONUS. The largest concentrations are located east of the Mississippi River. The boxed area indicates the chemical climatology regions investigated in the eastern US ALW scenarios.

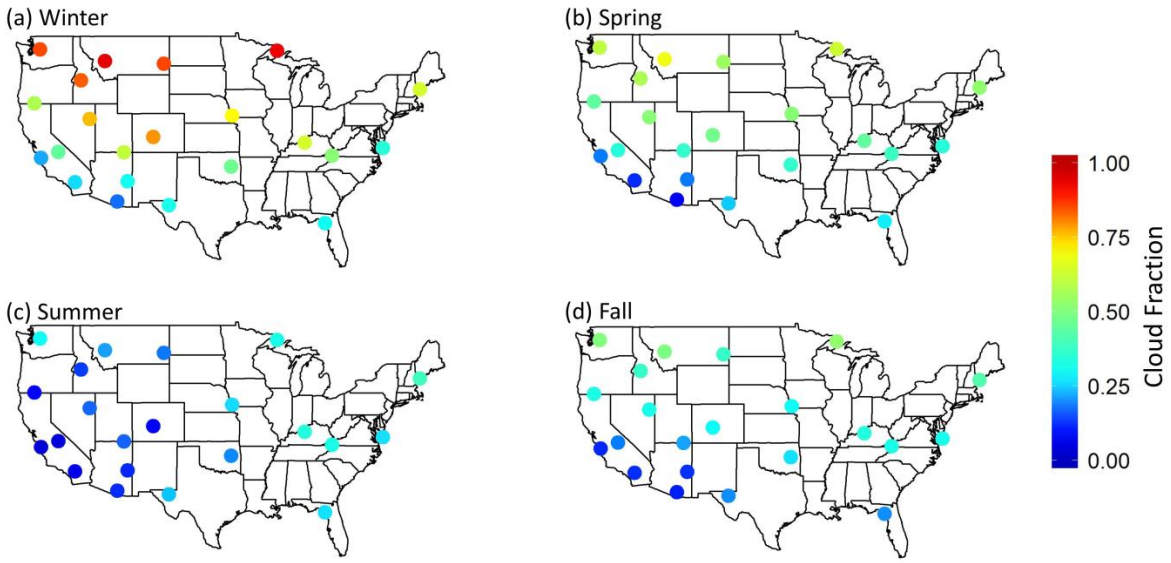


**Figure B4.** MODIS cloud fraction across the CONUS from 2010-2014 during a) winter, b) spring, c) summer, and d) fall. A hotter color indicates that a location is in cloud for a greater percentage of time.

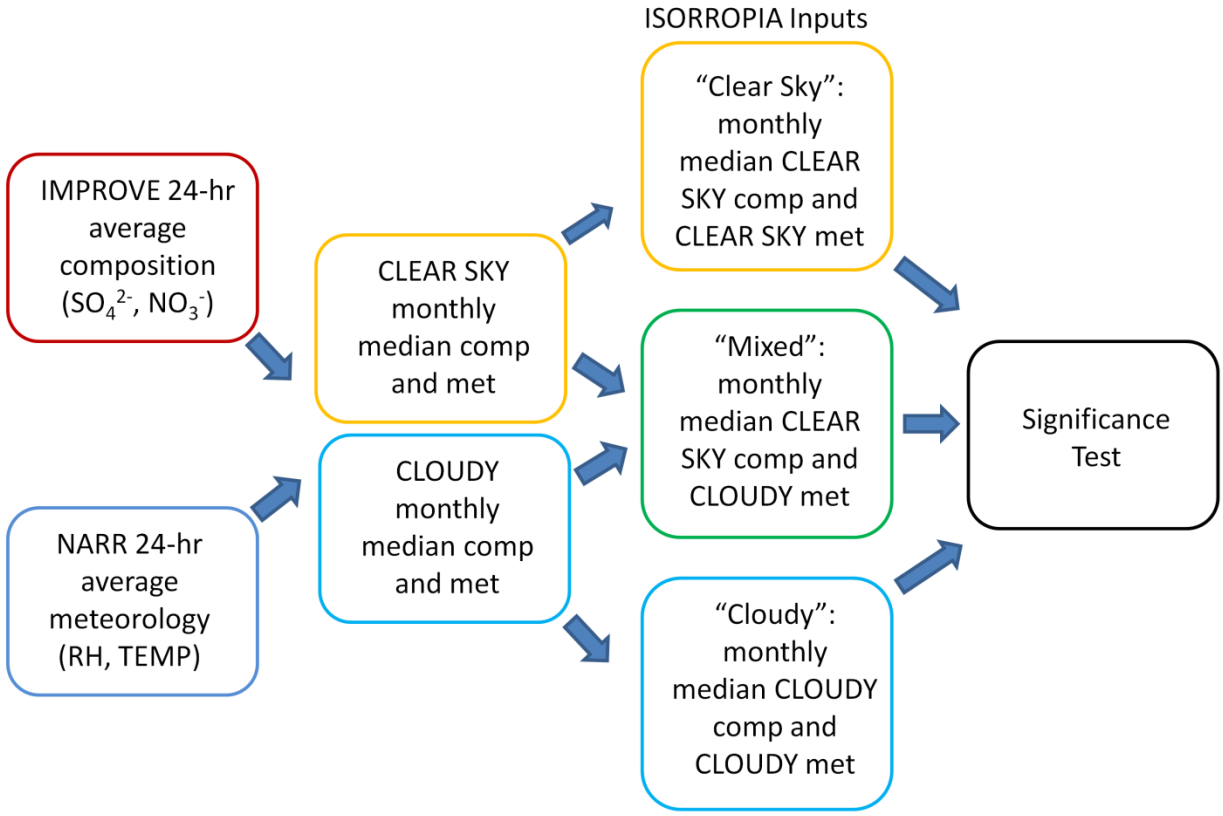


**Figure B5.** Flowchart describing how the three scenarios (Cloudy, Clear Sky, and Mixed) for the eastern US are performed and compared.

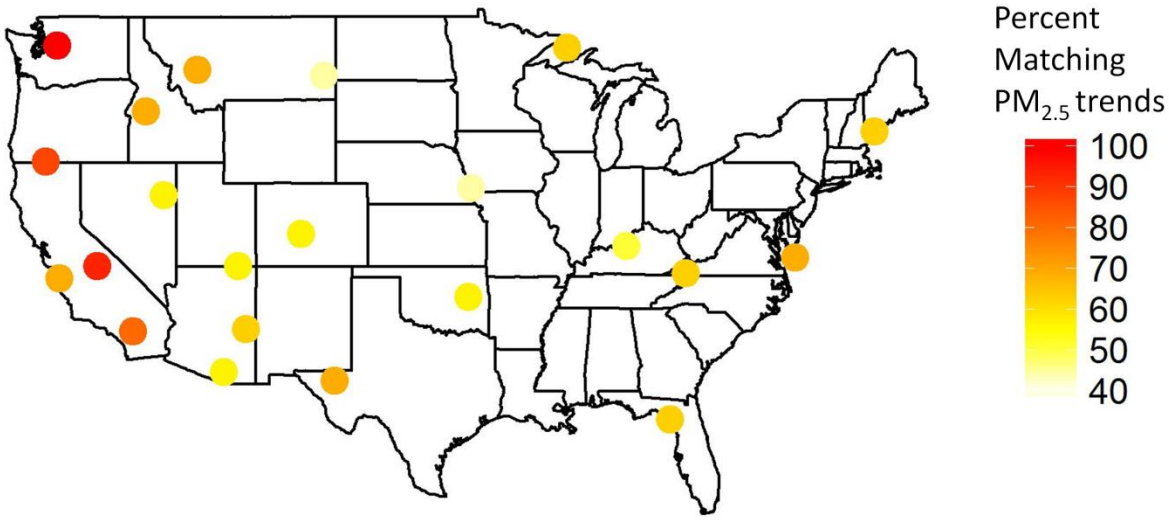


**Figure B6.** Percent of $PM_{2.5}$ chemical constituents ($SO_4^{2-}$, $NO_3^-$, TOC, ALW) in which cloudy-clear sky directional trends are the same as those of $PM_{2.5}$ in each region across the CONUS. For example, if median daily TOC is greater during Cloudy times, and median daily $PM_{2.5}$ is also greater during Cloudy times, this is counted as a match.

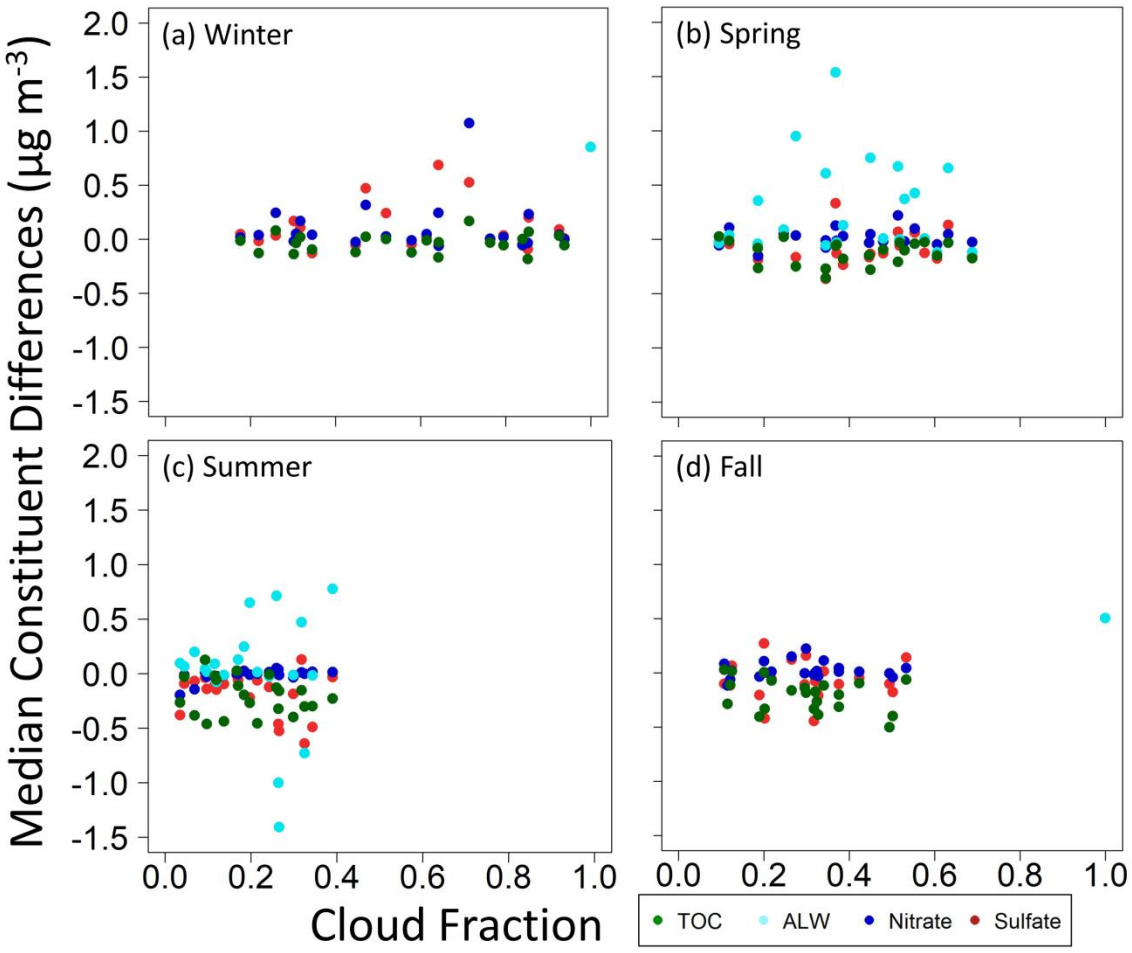


**Figure B7.** Plots of median Cloudy – Clear Sky differences by region (dots) in particle chemical constituents (colors) by MODIS median cloud fraction for a) winter, b) spring, c) summer, and d) fall. In each plot, $SO_4^{2-}$ is represented by red, $NO_3^-$ by dark blue, ALW by light blue, and TOC by green.

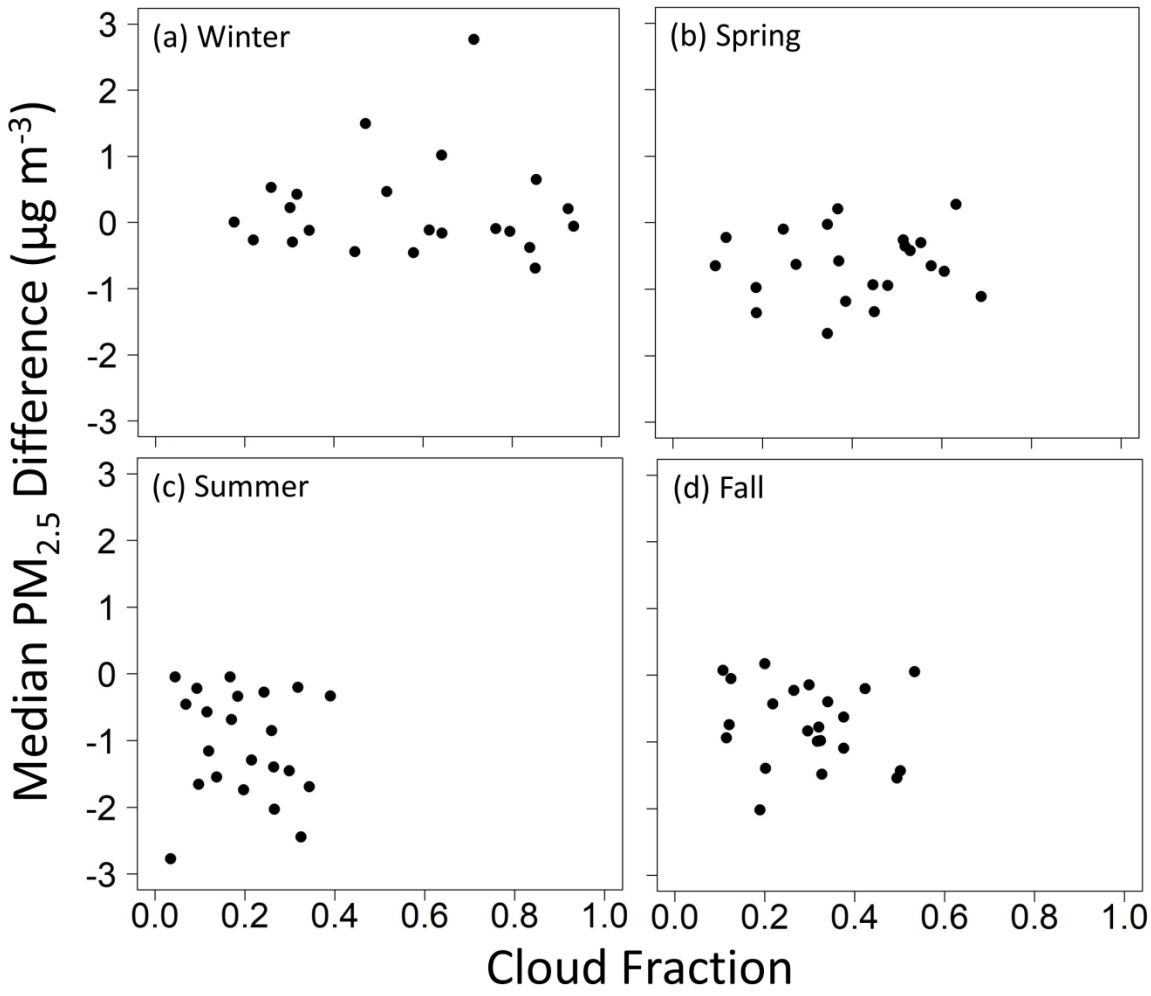


**Figure B8.** Plots of median Cloudy – Clear Sky differences by region (dots) in $PM_{2.5}$ by MODIS median cloud fraction for a) winter, b) spring, c) summer, and d) fall.

**Table B1.** Variable input conditions to ISORROPIA-II for each water uptake scenario.

| | **"Clear Sky"** | **"Cloudy"** | **"Mixed"** |
|---|---|---|---|
| **Meteorology MODIS classification – Clear Sky** | √ | | |
| **Meteorology MODIS classification – Cloudy** | | √ | √ |
| **$PM_{2.5}$ Chemical Composition MODIS classification – Clear Sky** | √ | | √ |
| **$PM_{2.5}$ Chemical Composition MODIS classification – Cloudy** | | √ | |

**Table B2.** Cloudy – Clear Sky and Cloudy – Mixed differences in each of the chemical climatology regions that comprise the eastern US. Negative values indicate that Cloudy concentrations are larger.

| Season | Cloudy – Clear $SO_4^{2-}$ | Cloudy – Clear $NO_3^-$ | Cloudy – Clear RH | Cloudy – Clear ALW | Cloudy – Mixed ALW |
|---|---|---|---|---|---|
| | **Ohio River Valley** | | | | |
| Winter | 0.57 | 0.26 | 0.08 | 4.08 | 2.39 |
| Spring | -0.15 | 0.00 | 0.04 | 0.83 | -0.44 |
| Summer | -0.28 | 0.01 | 0.05 | 0.75 | -0.67 |
| Fall | -0.01 | -0.01 | 0.10 | 1.17 | -0.02 |
| | **Appalachia** | | | | |
| Winter | 0.19 | 0.02 | 0.11 | 1.36 | 0.56 |
| Spring | -0.17 | -0.01 | 0.08 | 0.83 | -0.45 |
| Summer | -0.59 | 0.00 | 0.04 | -0.83 | -1.61 |
| Fall | -0.12 | 0.03 | 0.09 | 0.79 | -0.35 |
| | **Southeast** | | | | |
| Winter | 0.16 | -0.03 | 0.06 | 1.74 | 0.56 |
| Spring | -0.21 | -0.02 | 0.06 | 0.89 | -0.61 |
| Summer | -0.41 | -0.03 | 0.01 | -1.12 | -1.20 |
| Fall | -0.18 | -0.02 | 0.04 | -0.13 | -0.56 |
| | **East Coast** | | | | |
| Winter | -0.20 | 0.06 | 0.10 | 2.01 | -0.51 |
| Spring | -0.21 | -0.07 | 0.07 | 0.71 | -0.86 |
| Summer | 0.07 | 0.02 | 0.03 | 1.23 | 0.22 |
| Fall | -0.14 | 0.02 | 0.08 | 0.35 | -0.50 |
| | **Northeast** | | | | |
| Winter | -0.06 | -0.07 | 0.10 | 0.57 | -0.25 |
| Spring | -0.05 | -0.06 | 0.09 | 0.47 | -0.15 |
| Summer | 0.07 | 0.01 | 0.05 | 0.90 | 0.22 |
| Fall | -0.02 | 0.00 | 0.08 | 0.25 | -0.10 |

**Table B3.** Seasonal differences in ALW and RH medians (cloudy-clear sky) in all chemical climatology regions. Negative values indicate that clear sky temperatures are larger than cloudy. Bold and italicized values are significantly different by the Mann-Whitney U Test.

| Region | Spring | | Summer | | Fall | | Winter | |
|---|---|---|---|---|---|---|---|---|
| | ALW | RH | ALW | RH | ALW | RH | ALW | RH |
| Northwest | ***-0.12*** | ***0.12*** | -0.02 | ***0.13*** | ***-0.09*** | ***0.22*** | ***-0.12*** | ***0.08*** |
| OR/NorCal | ***-0.15*** | ***0.13*** | 0.01 | ***0.26*** | ***-0.05*** | ***0.30*** | 0.00 | ***0.19*** |
| CA Coast | ***0.35*** | ***0.21*** | 0.09 | ***0.39*** | ***0.66*** | ***0.28*** | ***0.24*** | ***0.21*** |
| Sierra NV | -0.06 | ***0.23*** | 0.06 | ***0.09*** | -0.03 | ***0.24*** | -0.01 | ***0.15*** |
| SoCal | 0.04 | ***0.03*** | 0.20 | ***0.16*** | -0.09 | ***0.10*** | ***0.16*** | ***0.23*** |
| HellsCyn | 0.01 | ***0.13*** | -0.01 | ***0.20*** | ***0.07*** | ***0.25*** | -0.02 | ***0.06*** |
| Great Basin | 0.00 | ***0.12*** | ***0.13*** | ***0.11*** | 0.02 | ***0.15*** | 0.01 | ***0.08*** |
| N Rockies | ***-0.12*** | ***0.13*** | 0.01 | ***0.14*** | ***0.06*** | ***0.21*** | -0.01 | 0.00 |
| CO Plateau | -0.03 | ***0.08*** | 0.02 | ***0.05*** | ***0.14*** | ***0.18*** | ***0.15*** | ***0.15*** |
| Mogollon Plateau | -0.04 | ***0.05*** | 0.09 | ***0.08*** | ***0.15*** | ***0.11*** | ***0.15*** | ***0.15*** |
| Southern AZ | -0.04 | 0.01 | -0.08 | ***0.11*** | 0.15 | ***0.07*** | 0.05 | 0.00 |
| N Great Plains | ***0.42*** | ***0.18*** | ***0.25*** | ***0.11*** | ***0.21*** | ***0.15*** | ***1.01*** | ***0.12*** |
| Central Rockies | 0.01 | ***0.15*** | 0.04 | ***0.08*** | 0.04 | ***0.17*** | ***0.14*** | ***0.14*** |
| West TX | 0.09 | 0.03 | -0.03 | 0.01 | ***0.38*** | ***0.09*** | ***0.22*** | 0.02 |
| Central Great Plains | ***0.67*** | ***0.10*** | ***0.71*** | ***0.11*** | ***0.59*** | ***0.12*** | ***2.48*** | ***0.14*** |
| Mid South | ***1.54*** | ***0.14*** | ***0.65*** | ***0.13*** | ***1.18*** | ***0.16*** | ***2.29*** | ***0.16*** |
| Boundary Waters | ***0.65*** | ***0.12*** | ***0.47*** | ***0.06*** | ***0.66*** | ***0.07*** | 0.13 | ***0.02*** |
| OH River Valley | ***0.75*** | ***0.07*** | -0.02 | ***0.05*** | ***1.50*** | ***0.11*** | ***4.58*** | ***0.10*** |
| Appalachia | 0.13 | ***0.09*** | ***-0.73*** | ***0.05*** | ***0.81*** | ***0.12*** | ***1.51*** | ***0.12*** |
| Southeast | ***0.95*** | ***0.06*** | ***-1.41*** | ***0.01*** | ***-0.70*** | ***0.04*** | ***1.63*** | ***0.06*** |
| E Coast | 0.61 | ***0.10*** | -1.00 | ***0.04*** | 0.40 | ***0.08*** | ***1.35*** | ***0.11*** |
| Northeast | ***0.37*** | ***0.10*** | ***0.78*** | ***0.06*** | ***0.43*** | ***0.09*** | ***0.75*** | ***0.10*** |

**Table B4.** Seasonal differences in reported $PM_{2.5}$ mass concentration medians (cloudy-clear sky) in all chemical climatology regions. Negative values indicate that clear sky concentrations are larger than cloudy. Bold and italicized values are significantly different by the Mann-Whitney U Test.

| Region | Spring | Summer | Fall | Winter |
|---|---|---|---|---|
| Northwest | ***-0.73*** | ***-1.46*** | ***-1.44*** | ***-0.69*** |
| OR/NorCal | ***-0.94*** | ***-1.66*** | ***-1.49*** | ***-0.46*** |
| CA Coast | ***-1.36*** | ***-2.77*** | ***-0.94*** | -0.27 |
| Sierra NV | ***-1.67*** | -0.05 | ***-2.02*** | ***-0.44*** |
| SoCal | -0.23 | -0.46 | ***-0.75*** | ***0.53*** |
| HellsCyn | ***-0.65*** | ***-1.55*** | ***-1.10*** | ***-0.38*** |
| Great Basin | ***-0.36*** | ***-0.69*** | ***-0.78*** | -0.10 |
| N Rockies | ***-1.12*** | ***-1.30*** | ***-1.55*** | -0.06 |
| CO Plateau | ***-0.58*** | -0.05 | ***-0.43*** | ***-0.12*** |
| Mogollon Plateau | ***-0.98*** | ***-0.57*** | -0.06 | ***-0.30*** |
| Southern AZ | -0.65 | ***-1.16*** | 0.07 | 0.00 |
| N Great Plains | ***-0.30*** | ***-0.34*** | ***-0.63*** | ***0.65*** |
| Central Rockies | ***-0.95*** | -0.22 | ***-0.84*** | ***-0.14*** |
| West TX | -0.10 | -0.28 | 0.17 | ***0.42*** |
| Central Great Plains | ***-0.26*** | ***-0.85*** | -0.15 | ***2.76*** |
| Mid South | 0.20 | ***-1.74*** | -0.23 | ***1.49*** |
| Boundary Waters | 0.27 | -0.20 | 0.05 | 0.20 |
| OH River Valley | ***-1.34*** | ***-1.70*** | -0.40 | ***1.02*** |
| Appalachia | ***-1.19*** | ***-2.45*** | ***-0.99*** | ***0.46*** |
| Southeast | ***-0.63*** | ***-2.03*** | ***-1.40*** | 0.22 |
| E Coast | ***-0.03*** | ***-1.40*** | ***-0.99*** | -0.12 |
| Northeast | ***-0.42*** | ***-0.33*** | ***-0.21*** | -0.16 |

**Table B5.** Seasonal differences in $SO_4^{2-}$ mass concentration medians (cloudy-clear sky) in all chemical climatology regions. Negative values indicate that clear sky $SO_4^{2-}$ concentrations are larger than cloudy. Bold and italicized values are significantly different by the Mann-Whitney U Test.

| Region | Spring | Summer | Fall | Winter |
|---|---|---|---|---|
| Northwest | ***-0.18*** | ***-0.19*** | ***-0.18*** | ***-0.09*** |
| OR/NorCal | ***-0.17*** | ***-0.14*** | ***-0.21*** | ***-0.05*** |
| CA Coast | ***-0.19*** | ***-0.38*** | -0.12 | -0.02 |
| Sierra NV | ***-0.27*** | -0.09 | ***-0.21*** | ***-0.05*** |
| SoCal | -0.04 | -0.07 | -0.12 | 0.03 |
| HellsCyn | ***-0.13*** | ***-0.10*** | ***-0.11*** | ***-0.05*** |
| Great Basin | ***-0.06*** | -0.06 | ***-0.08*** | -0.01 |
| N Rockies | ***-0.16*** | ***-0.06*** | ***-0.10*** | 0.01 |
| CO Plateau | ***-0.13*** | -0.01 | ***-0.06*** | 0.02 |
| Mogollon Plateau | ***-0.09*** | ***-0.11*** | 0.06 | -0.01 |
| Southern AZ | ***-0.03*** | ***-0.15*** | -0.10 | 0.04 |
| N Great Plains | ***0.06*** | 0.02 | 0.04 | ***0.20*** |
| Central Rockies | ***-0.13*** | ***-0.04*** | ***-0.11*** | ***0.03*** |
| West TX | 0.08 | -0.12 | ***0.27*** | 0.11 |
| Central Great Plains | 0.07 | 0.00 | ***0.16*** | ***0.52*** |
| Mid South | ***0.33*** | ***-0.22*** | 0.12 | ***0.47*** |
| Boundary Waters | ***0.13*** | ***0.13*** | ***0.14*** | 0.09 |
| OH River Valley | -0.14 | ***-0.49*** | 0.01 | ***0.68*** |
| Appalachia | ***-0.24*** | ***-0.64*** | ***-0.17*** | ***0.24*** |
| Southeast | ***-0.17*** | ***-0.53*** | ***-0.42*** | ***0.17*** |
| E Coast | ***-0.37*** | -0.46 | ***-0.44*** | -0.13 |
| Northeast | ***-0.10*** | -0.03 | ***-0.05*** | -0.05 |

**Table B6.** Seasonal differences in $NO_3^-$ mass concentration medians (cloudy-clear sky) in all chemical climatology regions. Negative values indicate that clear sky $NO_3^-$ concentrations are larger than cloudy. Bold and italicized values are significantly different by the Mann-Whitney U Test.

| Region | Spring | Summer | Fall | Winter |
|---|---|---|---|---|
| Northwest | ***-0.05*** | ***-0.03*** | ***-0.04*** | ***-0.04*** |
| OR/NorCal | ***-0.03*** | ***-0.03*** | ***-0.03*** | ***-0.01*** |
| CA Coast | ***-0.15*** | ***-0.20*** | ***-0.12*** | 0.04 |
| Sierra NV | ***-0.08*** | -0.02 | -0.04 | ***-0.03*** |
| SoCal | 0.11 | -0.14 | -0.06 | ***0.24*** |
| HellsCyn | ***-0.02*** | ***-0.02*** | 0.01 | ***-0.06*** |
| Great Basin | 0.00 | -0.01 | 0.00 | 0.00 |
| N Rockies | ***-0.03*** | ***0.00*** | -0.01 | 0.00 |
| CO Plateau | ***-0.02*** | 0.00 | ***0.01*** | ***0.04*** |
| Mogollon Plateau | ***-0.04*** | ***-0.02*** | ***0.02*** | ***0.05*** |
| Southern AZ | ***-0.06*** | ***-0.02*** | ***0.08*** | 0.01 |
| N Great Plains | ***0.10*** | ***0.02*** | ***0.04*** | ***0.23*** |
| Central Rockies | ***-0.02*** | 0.01 | ***-0.01*** | 0.02 |
| West TX | ***0.05*** | 0.01 | ***0.11*** | ***0.17*** |
| Central Great Plains | ***0.22*** | ***0.05*** | ***0.22*** | ***1.07*** |
| Mid South | ***0.13*** | -0.01 | ***0.15*** | ***0.32*** |
| Boundary Waters | ***0.05*** | ***0.01*** | ***0.04*** | 0.04 |
| OH River Valley | 0.05 | 0.01 | 0.11 | 0.24 |
| Appalachia | 0.03 | 0.00 | 0.01 | 0.02 |
| Southeast | 0.03 | ***-0.02*** | 0.00 | -0.02 |
| E Coast | -0.01 | ***0.04*** | -0.02 | 0.04 |
| Northeast | ***-0.02*** | 0.01 | 0.01 | ***-0.06*** |

**Table B7.** Seasonal differences in TOC mass concentration medians (cloudy-clear sky) in all chemical climatology regions. Negative values indicate that clear sky TOC concentrations are larger than cloudy. Bold and italicized values are significantly different by the Mann-Whitney U Test.

| Region | Spring | Summer | Fall | Winter |
|---|---|---|---|---|
| Northwest | ***-0.15*** | ***-0.40*** | ***-0.40*** | ***-0.18*** |
| OR/NorCal | ***-0.15*** | ***-0.46*** | ***-0.39*** | ***-0.12*** |
| CA Coast | ***-0.27*** | ***-0.27*** | ***-0.29*** | -0.13 |
| Sierra NV | ***-0.36*** | -0.03 | ***-0.41*** | ***-0.12*** |
| SoCal | -0.01 | ***-0.38*** | ***-0.11*** | ***0.08*** |
| HellsCyn | -0.03 | ***-0.44*** | ***-0.32*** | 0.00 |
| Great Basin | ***-0.03*** | -0.11 | ***-0.17*** | -0.03 |
| N Rockies | ***-0.18*** | ***-0.46*** | ***-0.50*** | -0.06 |
| CO Plateau | ***-0.05*** | 0.03 | ***-0.07*** | -0.01 |
| Mogollon Plateau | ***-0.08*** | -0.02 | 0.01 | ***-0.04*** |
| Southern AZ | 0.02 | -0.06 | 0.03 | -0.01 |
| N Great Plains | ***-0.04*** | ***-0.20*** | ***-0.20*** | ***0.07*** |
| Central Rockies | ***-0.10*** | 0.13 | ***-0.14*** | ***-0.06*** |
| West TX | 0.02 | -0.01 | 0.00 | 0.02 |
| Central Great Plains | ***-0.21*** | ***-0.13*** | ***-0.18*** | ***0.17*** |
| Mid South | -0.06 | ***-0.27*** | ***-0.16*** | 0.02 |
| Boundary Waters | ***-0.03*** | ***-0.16*** | ***-0.06*** | 0.03 |
| OH River Valley | ***-0.28*** | ***-0.30*** | ***-0.12*** | ***-0.17*** |
| Appalachia | ***-0.18*** | ***-0.30*** | ***-0.26*** | 0.00 |
| Southeast | ***-0.25*** | ***-0.16*** | ***-0.33*** | ***-0.14*** |
| E Coast | ***-0.27*** | ***-0.32*** | ***-0.33*** | ***-0.10*** |
| Northeast | ***-0.10*** | ***-0.23*** | ***-0.10*** | -0.03 |

**Table B8.** Seasonal differences in temperature medians (cloudy-clear sky) in all chemical climatology regions. Negative values indicate that clear sky temperatures are larger than cloudy. Bold and italicized values are significantly different by the Mann-Whitney U Test.

| Region | Spring | Summer | Fall | Winter |
|---|---|---|---|---|
| Northwest | ***-1.65*** | ***-3.69*** | ***-4.60*** | -0.41 |
| OR/NorCal | ***-1.89*** | ***-3.67*** | ***-6.26*** | ***-1.02*** |
| CA Coast | ***-1.42*** | ***-4.41*** | ***-3.40*** | 0.54 |
| Sierra NV | ***-5.91*** | 0.44 | ***-7.64*** | ***-1.65*** |
| SoCal | -2.40 | 2.60 | -2.85 | -0.37 |
| HellsCyn | ***-3.10*** | ***-4.87*** | ***-7.93*** | ***-1.47*** |
| Great Basin | ***-2.50*** | -0.13 | ***-4.99*** | ***-0.65*** |
| N Rockies | ***-4.07*** | ***-4.60*** | ***-7.10*** | ***-2.40*** |
| CO Plateau | ***-4.31*** | ***1.26*** | ***-5.62*** | ***-4.36*** |
| Mogollon Plateau | ***-3.78*** | 0.56 | ***-3.34*** | ***-2.03*** |
| Southern AZ | -0.46 | 0.43 | ***-4.54*** | -0.21 |
| N Great Plains | ***-4.92*** | ***-2.78*** | ***-7.49*** | ***-4.58*** |
| Central Rockies | ***-6.33*** | ***-1.01*** | ***-7.29*** | ***-4.11*** |
| West TX | -0.84 | -0.33 | -0.01 | 0.22 |
| Central Great Plains | ***-3.42*** | ***-1.82*** | ***-1.94*** | ***-4.10*** |
| Mid South | -0.37 | ***-2.13*** | -0.44 | -0.21 |
| Boundary Waters | ***-5.10*** | -0.86 | ***-4.34*** | ***-5.71*** |
| OH River Valley | -0.94 | ***-1.29*** | 0.45 | -1.33 |
| Appalachia | ***-2.11*** | ***-0.93*** | 0.88 | -0.79 |
| Southeast | ***-1.43*** | ***-0.80*** | 0.84 | ***0.69*** |
| E Coast | -0.72 | ***-0.85*** | 2.06 | ***1.97*** |
| Northeast | ***-3.28*** | ***-0.80*** | ***-1.38*** | ***-1.68*** |

**Table B9.** Seasonal all sky (clear and cloudy data) and clear sky differences in $PM_{2.5}$ mass concentration medians (all sky-clear sky) in all chemical climatology regions. Negative values indicate that clear sky $PM_{2.5}$ concentrations are larger than all sky. Bold and italicized values are significantly different by the Mann-Whitney U Test.

| Region | Spring | Summer | Fall | Winter |
|---|---|---|---|---|
| Northwest | ***-0.47*** | ***-0.40*** | ***-0.68*** | ***-0.65*** |
| OR/NorCal | ***-0.46*** | ***-0.14*** | ***-0.52*** | ***-0.27*** |
| CA Coast | -0.21 | -0.07 | -0.14 | -0.05 |
| Sierra NV | ***-0.67*** | -0.01 | ***-0.36*** | ***-0.21*** |
| SoCal | -0.08 | -0.04 | -0.03 | 0.11 |
| HellsCyn | ***-0.42*** | -0.18 | ***-0.45*** | -0.31 |
| Great Basin | -0.12 | -0.13 | ***-0.22*** | -0.07 |
| N Rockies | ***-0.82*** | ***-0.29*** | ***-0.91*** | -0.05 |
| CO Plateau | ***-0.22*** | -0.01 | ***-0.08*** | -0.06 |
| Mogollon Plateau | ***-0.16*** | -0.06 | -0.01 | -0.09 |
| Southern AZ | -0.01 | -0.15 | 0.02 | 0.00 |
| N Great Plains | ***-0.15*** | -0.06 | ***-0.27*** | ***0.42*** |
| Central Rockies | ***-0.36*** | -0.03 | ***-0.24*** | -0.11 |
| West TX | -0.02 | -0.13 | 0.02 | 0.13 |
| Central Great Plains | -0.14 | -0.23 | -0.05 | ***1.69*** |
| Mid South | 0.12 | -0.40 | -0.05 | ***0.58*** |
| Boundary Waters | 0.11 | -0.05 | 0.02 | 0.19 |
| OH River Valley | -0.78 | ***-0.72*** | -0.17 | 0.67 |
| Appalachia | ***-0.42*** | ***-0.78*** | ***-0.30*** | 0.22 |
| Southeast | -0.19 | ***-0.74*** | ***-0.34*** | 0.07 |
| E Coast | -0.01 | -0.36 | -0.18 | -0.05 |
| Northeast | ***-0.21*** | ***-0.12*** | -0.11 | -0.08 |

# APPENDIX C

SUPPORTING INFORMATION FOR CHAPTER 4

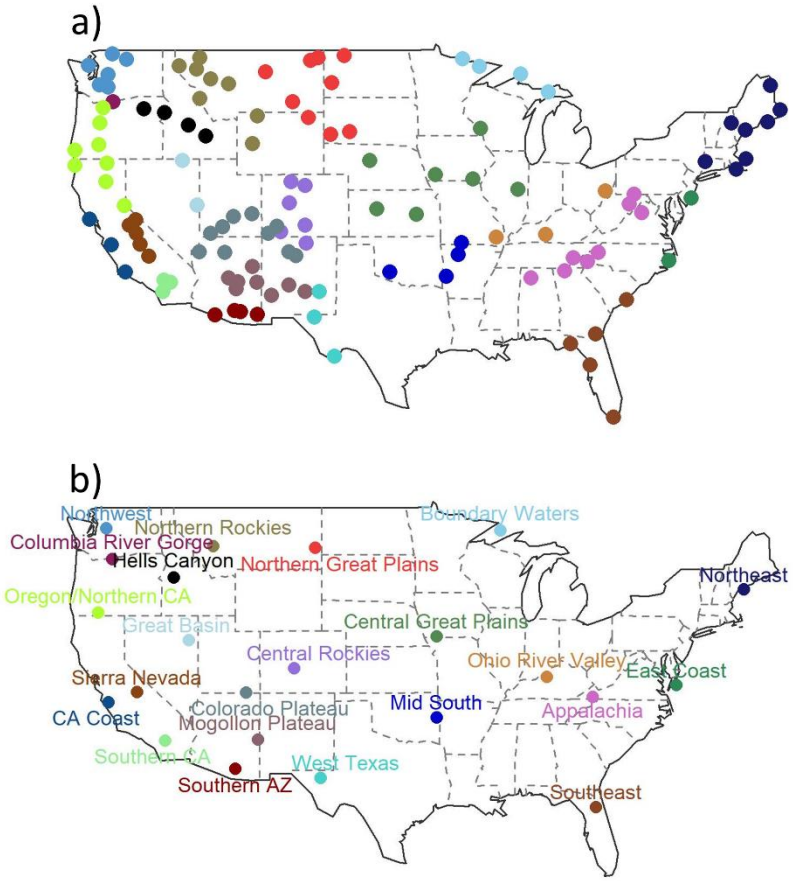


**Figure C1.** Locations of (a) sites and (b) chemical climatology regions.

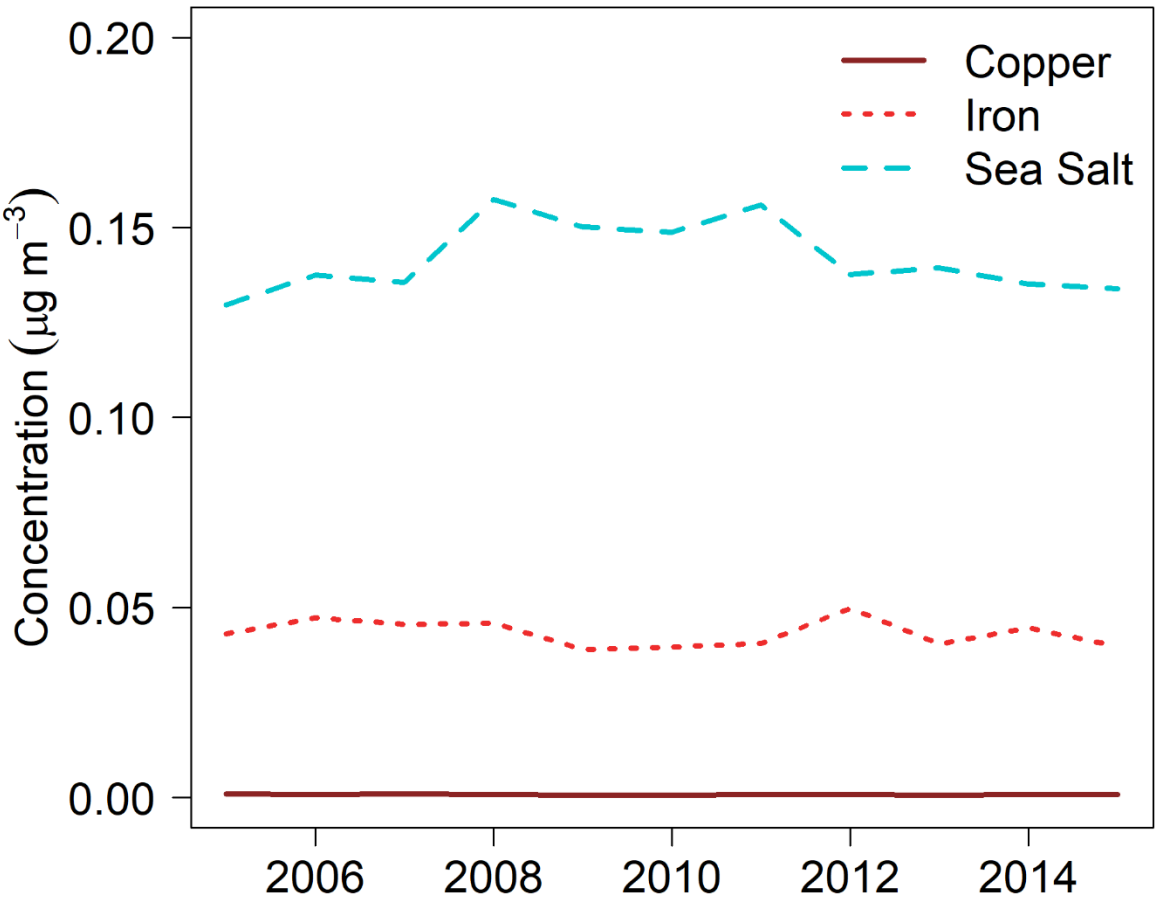


**Figure C2.** Decadal trends in species (copper, iron, and sea salt) mass concentrations that may interfere with OC fraction evolution.

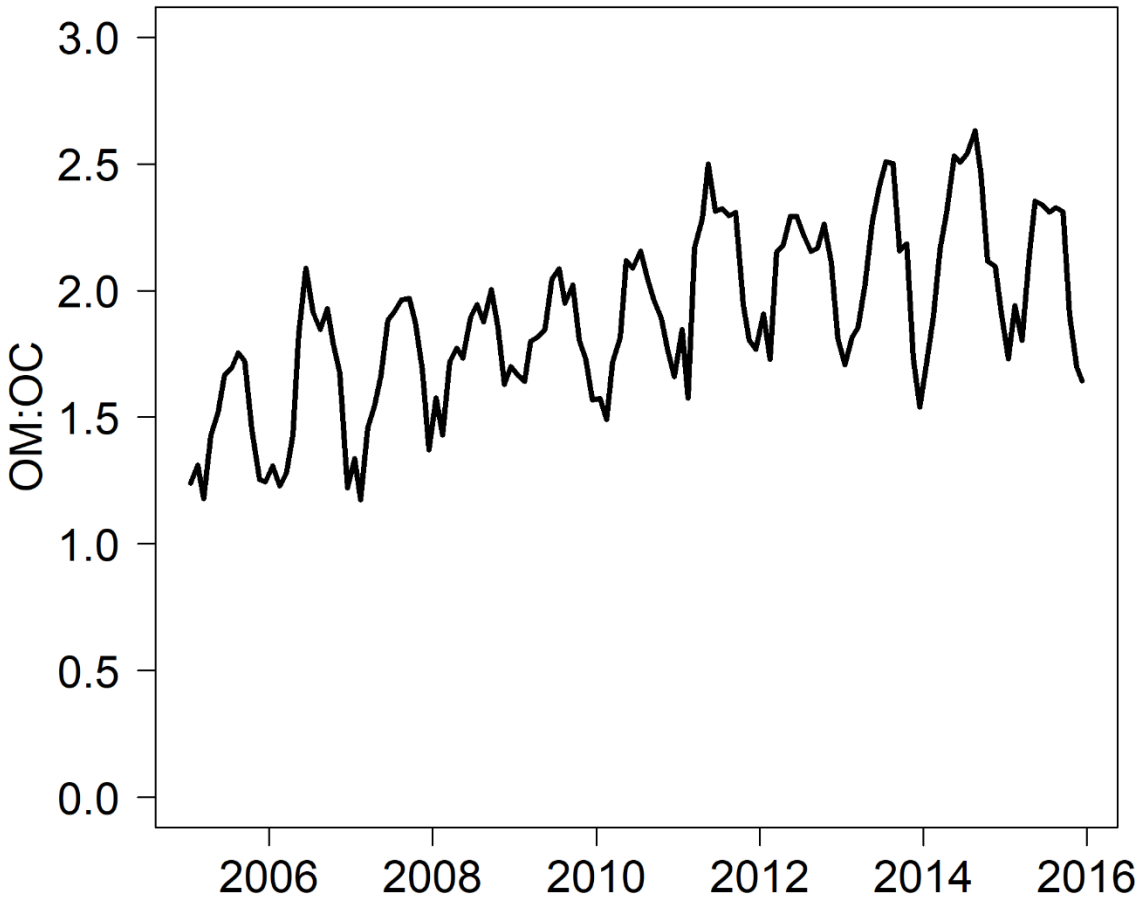


**Figure C3.** CONUS-averaged OM:OC ratios for all seasons and regions from 2005-2015.

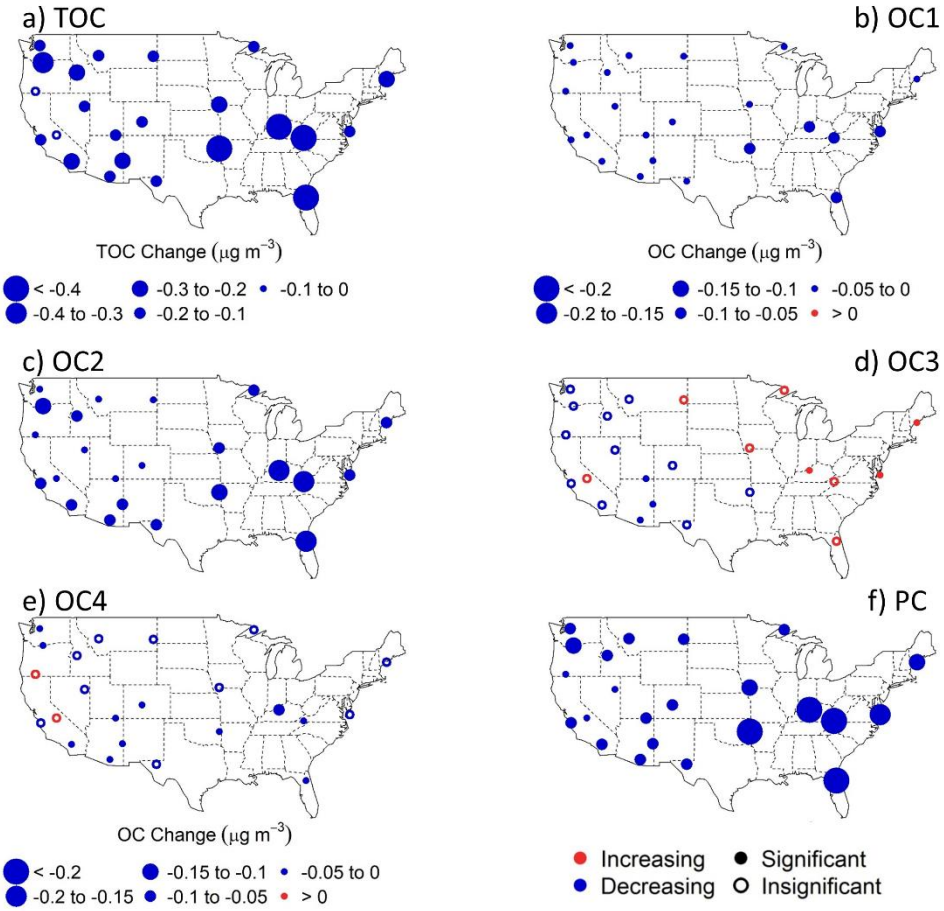


**Figure C4.** Absolute decadal changes (2005-2015) a) TOC, b) OC1, c) OC2, d) OC3, e) OC4, and f) PC mass concentrations for each chemical climatology region. Size corresponds to the magnitude of change. Red indicates an increasing trend, blue indicates a decrease, a colored circle indicates that the increase or decrease is significant ($p<0.05$) by the Mann-Kendall test, and an unfilled circle indicates that the change is insignificant.

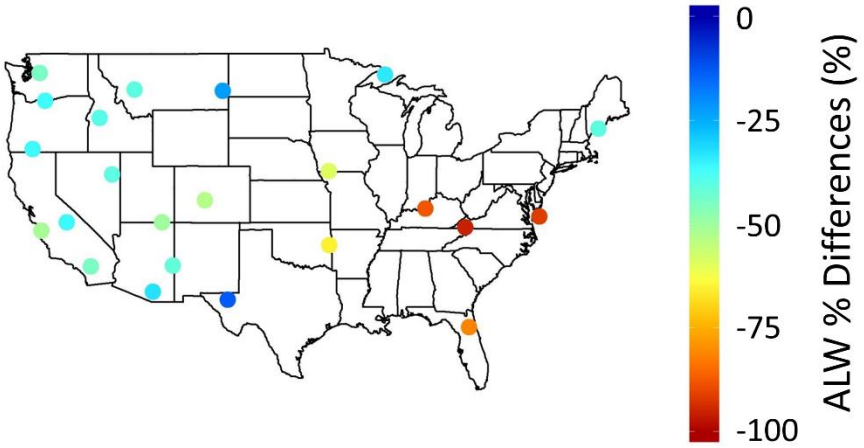


**Figure C5.** Decadal (2005-2015) percent differences in ALW mass concentrations at each chemical climatology region across the CONUS.

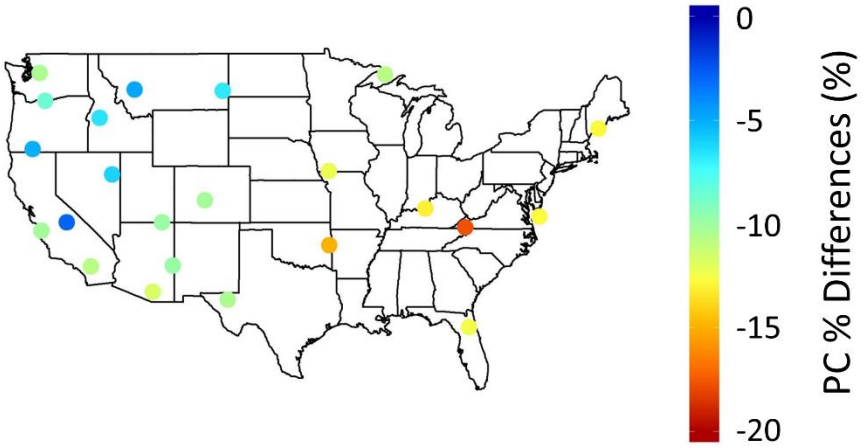


**Figure C6.** Decadal (2005-2015) percent changes in PC during a) winter, b) spring, c) summer, and d) fall for each chemical climatology region. The color represents the magnitude of the change, and a filled circle represents a significant change.

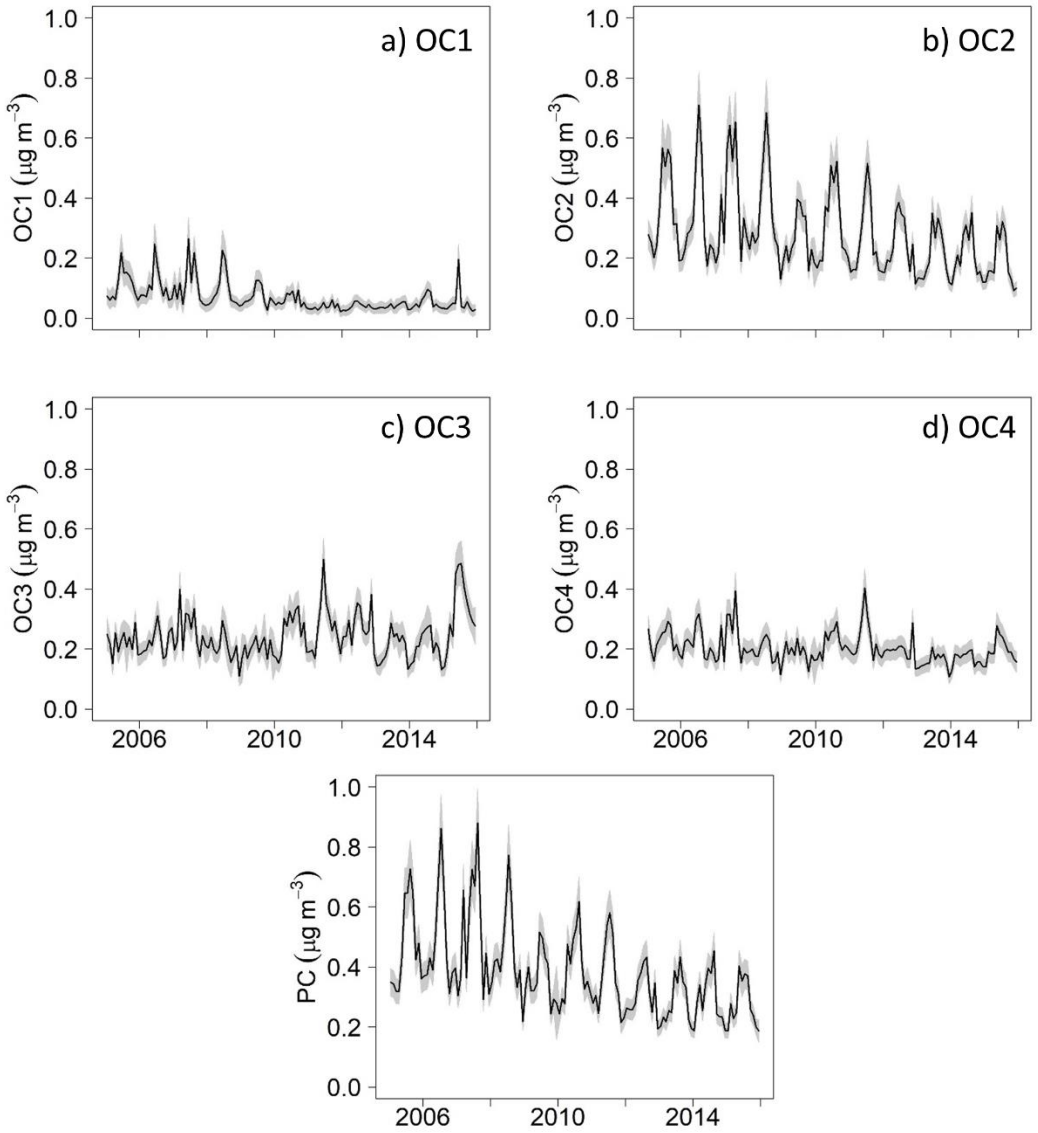


**Figure C7.** Decadal trends in OC fraction a) OC1, b) OC2, c) OC3, d) OC4, and e) PC mass concentrations from 2005-2015 in Appalachia, a representative region. The black line is the median OC concentration, and the gray background represents the uncertainty.

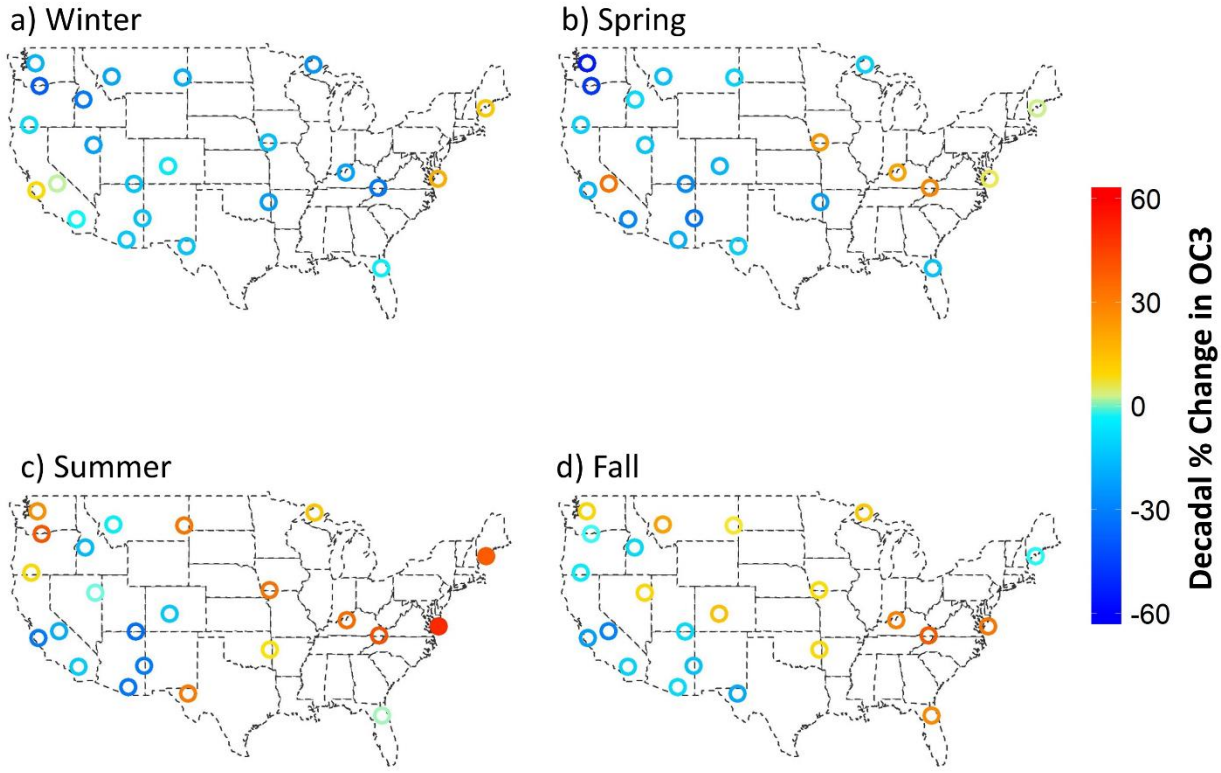


**Figure C8.** Decadal (2005-2015) percent changes in OC3 during a) winter, b) spring, c) summer, and d) fall for each chemical climatology region. The color represents the magnitude of the change, and a filled circle represents a significant change.

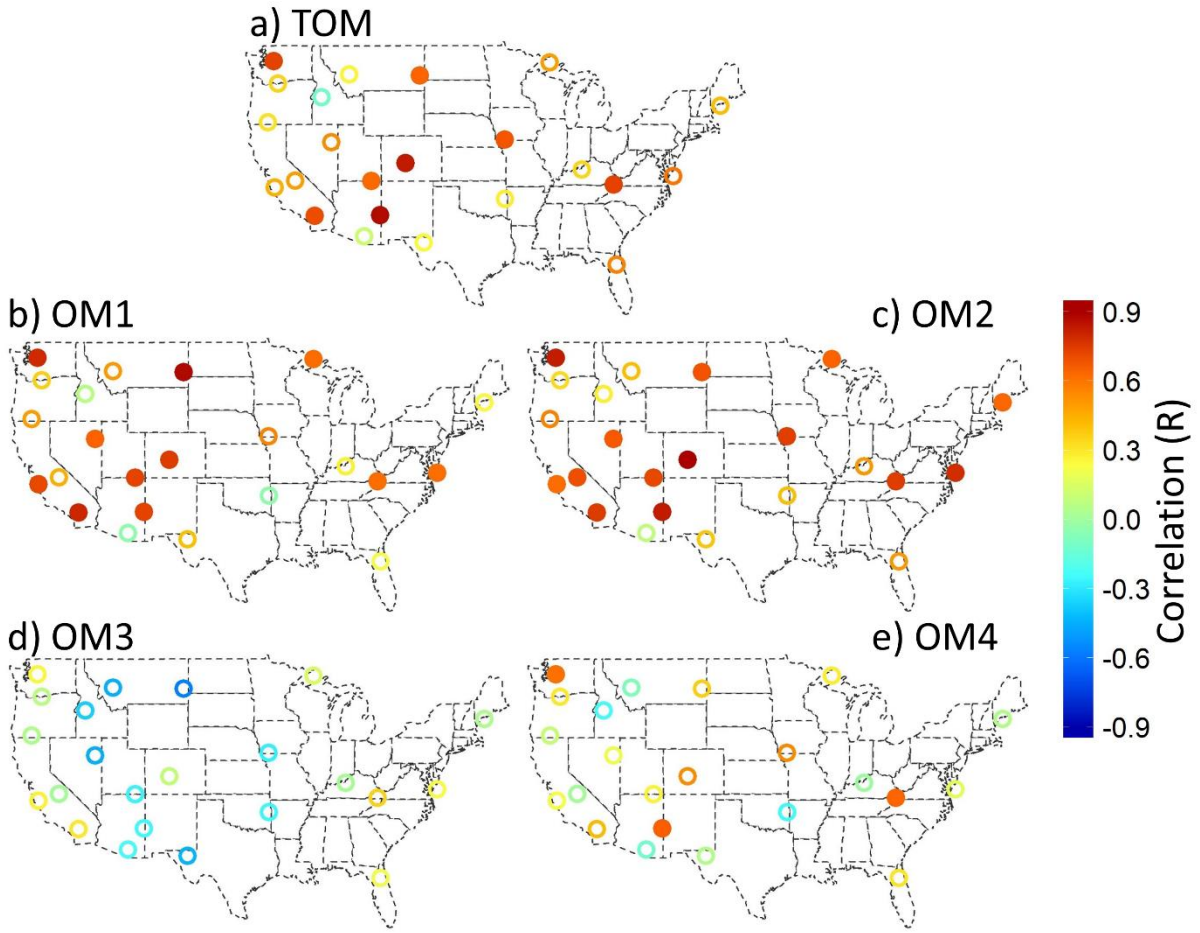


**Figure C9.** Decadal (2005-2015) correlations (R) between summertime GEOS-Chem predicted ISOAAQ and IMPROVE-measured a) TOM, b) OM1, c) OM2, d) OM3, and e) OM4 for each chemical climatology region. The color represents the magnitude of the correlation, and a filled circle represents a significant change.

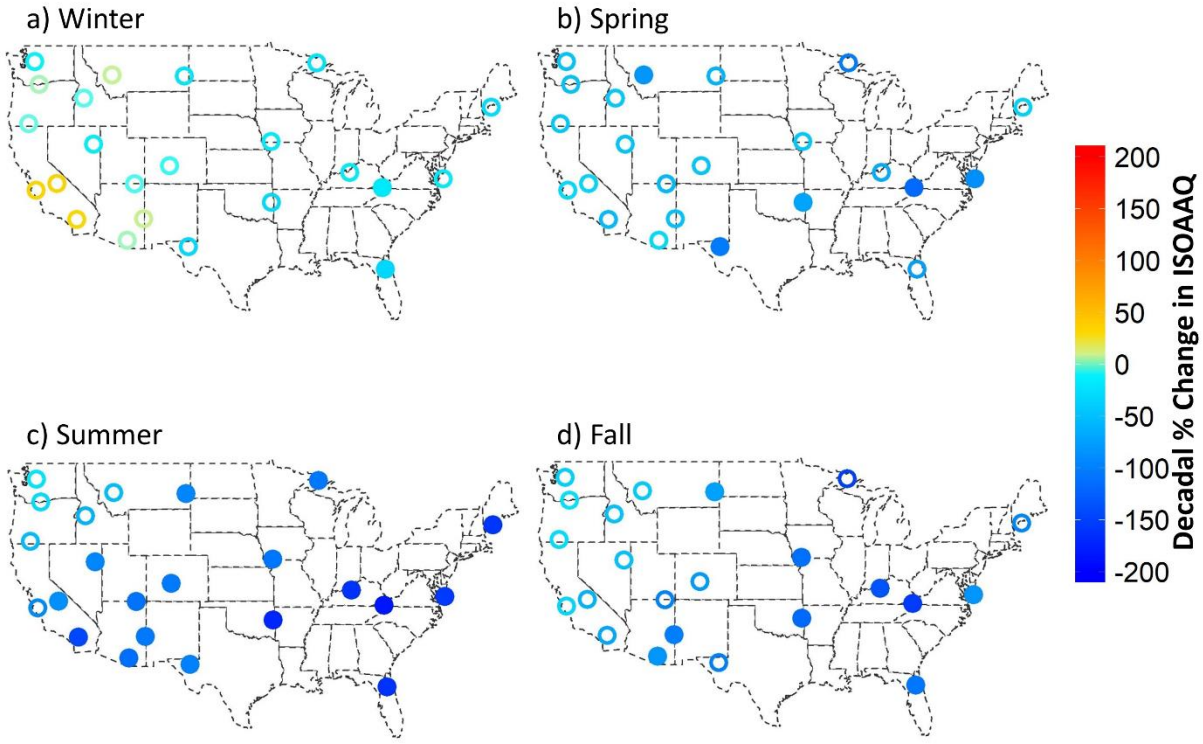


**Figure C10.** Decadal (2005-2015) percent changes in GEOS-Chem ISOAAQ during a) winter, b) spring, c) summer, and d) fall for each chemical climatology region. The color represents the magnitude of the change, and a filled circle represents a significant change.

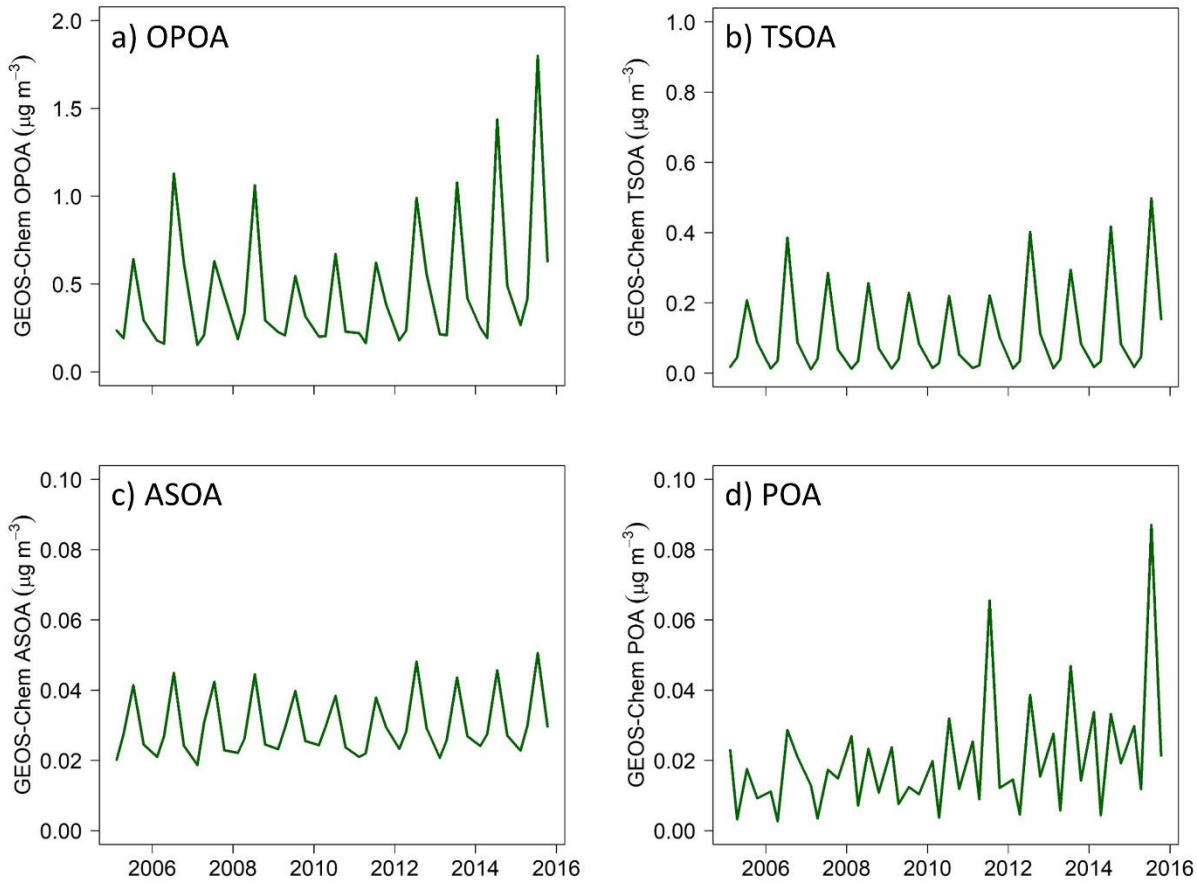


**Figure C11.** Decadal trends for species predicted to increase in GEOS-Chem, including a) OPOA, b) TSOA, c) ASOA, and d) POA. Note that the y-axes are not the same between panels for better visualization of trends over time.

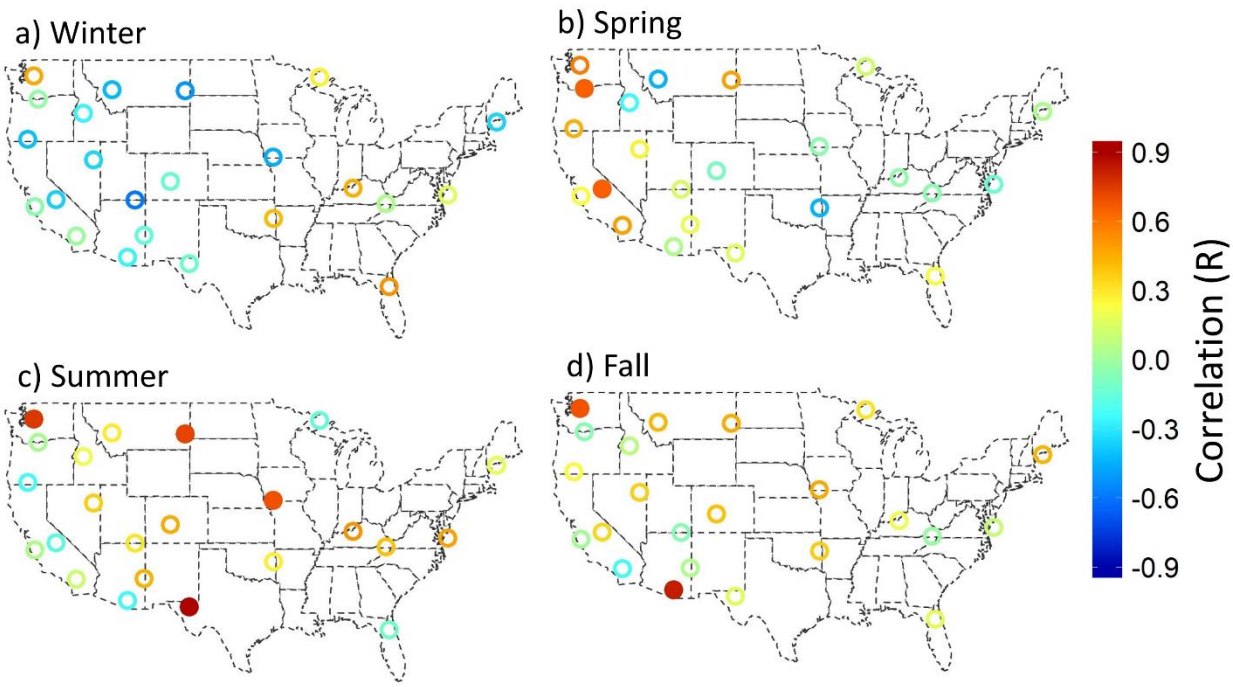


**Figure C12.** Correlations between OM3 and OPOA in a) winter, b) spring, c) summer, and d) fall in each chemical climatology region across the CONUS. The color represents the strength of the correlation, and a filled circle represents a significant correlation.

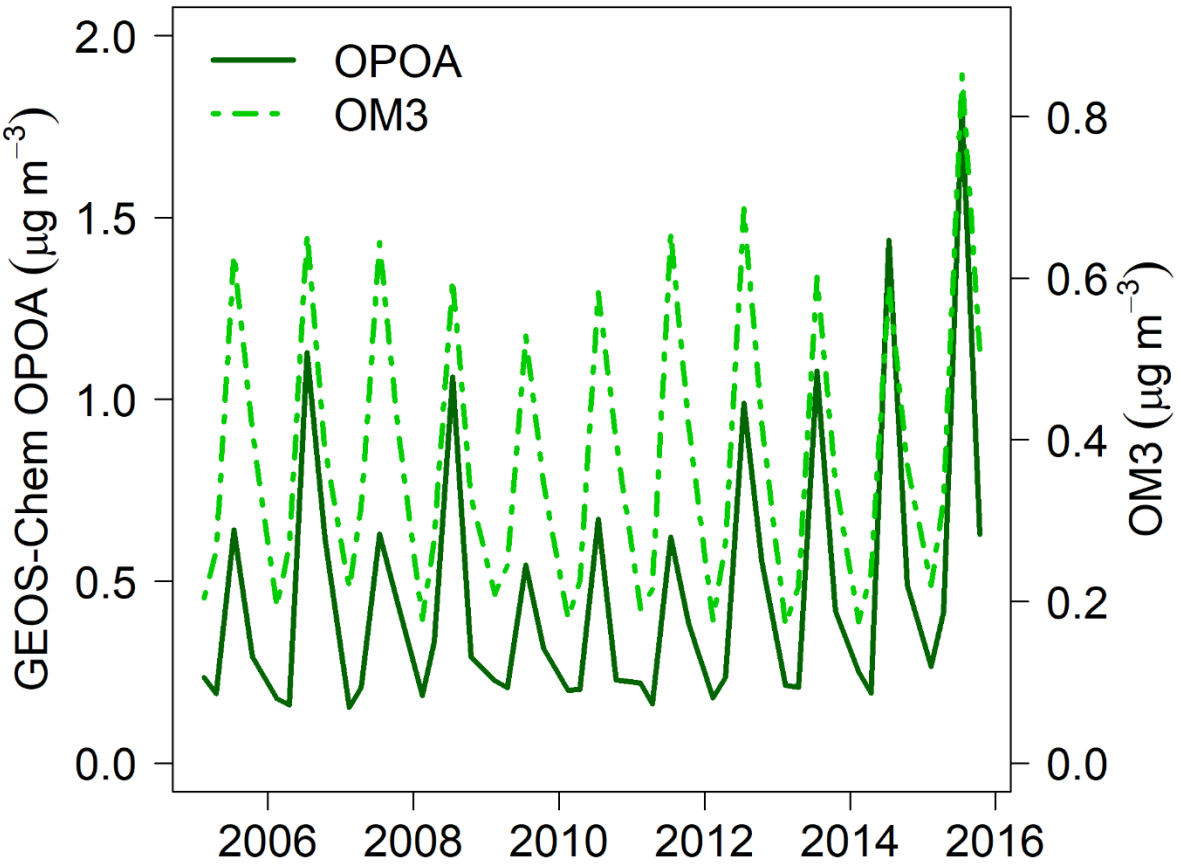


**Figure C13.** Decadal trends in GEOS-Chem predicted OPOA and IMPROVE-measured OM3 across the CONUS from 2005-2015.

**Table C1.** Definitions of all GEOS-Chem speciation bins considered in this analysis.

| GEOS-Chem Speciation Bin | Definition |
|---|---|
| **ASOA** | Aerosol products of light aromatics + IVOC oxidation |
| **TSOA** | Aerosol products of terpene oxidation |
| **ISOA** | Aerosol products of isoprene oxidation |
| **ISOAAQ** | Aerosol from aqueous isoprene mechanism |
| **OPOA** | Aerosol products of primary organic gas oxidation |
| **POA** | Aerosols from SVOCs |
| **OA** | Sum of organic aerosol |
| **BC** | Black carbon |
| **INDIOL** | Aerosol-phase organonitrate hydrolysis product |
| **SAL** | Sea salt aerosol |
| **NIT** | Nitrate |
| **SO4** | Sulfate |
| **NH4** | Ammonium |

# APPENDIX D

## R CODE FOR CHAPTER 2

```
#R code for 2019 ACS Earth and Space Chemistry paper
#Christiansen et al. 2019

#Main paper figures
#All these figures were manipulated into publication-ready images in powerpoint

########################
#Figure 1: stacked barcharts#
########################
#MODIS AOT data
Modis <- read.csv("C:/Users/stor/Documents/ALW and OC paper/2005-2016
analysis/newdata_alllevels/modis_aod_month.csv")
modis$SE_AOD_low <- modis$SE_AOD-modis$SE_AOD_SD
modis$SE_AOD_hi <- modis$SE_AOD+modis$SE_AOD_SD
modis$MW_AOD_low <- modis$MW_AOD-modis$MW_AOD_SD
modis$MW_AOD_hi <- modis$MW_AOD+modis$MW_AOD_SD
modis$Year <- ifelse(modis$Month=="12",modis$Year <- as.numeric(modis$year)+1,
modis$Year <- modis$year)
aotsummer <- subset(modis, Month=="6"|Month=="7"|Month=="8")
aotwinter <- subset(modis, Month=="12"|Month=="1"|Month=="2")
aotsummermeans <- aggregate(aotsummer, by=list(aotsummer$Year), FUN="mean", na.rm=T)
aotwintermeans <- aggregate(aotwinter, by=list(aotwinter$Year), FUN="mean", na.rm=T)

#Integrated speciation data (integrated from surface to top of PBL)
Kapint <- read.csv("C:/Users/stor/Documents/ALW and OC paper/2005-2016
analysis/newdata_alllevels/data 2001-2016/focus_2001-2016_intunder95-1.csv")
kapint$Date <- as.Date(as.character(kapint$Date), format="%m/%d/%Y")
kapint$Year <- ifelse(kapint$Month=="12",kapint$Year<- as.numeric(kapint$year)+1,
kapint$Year <- kapint$year)
library(zoo)
yq <- as.yearqtr(as.yearmon(kapint$Date,"%Y-%m-%d")+1/12)
kapint$season <- factor(format(yq,"%q"), levels=1:4,
labels=c("winter","spring","summer","fall"))

kapint$totwater <- (kapint$alw_org_fixed+kapint$alw_inorg)/1000
kapint$totwater_L <- (kapint$alw_low_fixed+kapint$alw_inorg)/1000
kapint$totwater_H <- (kapint$alw_high_fixed+kapint$alw_inorg)/1000

kapint$PMwater <-( kapint$MF.Val/1000)+kapint$totwater
```

```
kapint$PMwater_L <- (kapint$MF.Val/1000)+kapint$totwater_L
kapint$PMwater_H <- (kapint$MF.Val/1000)+kapint$totwater_H

kapint$totwater_0.01 <- (kapint$alw_0.01+kapint$alw_inorg)/1000
kapint$totwater_0.1 <- (kapint$alw_0.1+kapint$alw_inorg)/1000
kapint$totwater_0.15 <- (kapint$alw_0.15+kapint$alw_inorg)/1000
kapint$totwater_0.2 <- (kapint$alw_0.2+kapint$alw_inorg)/1000
kapint$PMwater_0.01 <- (kapint$MF.Val/1000)+kapint$totwater_0.01
kapint$PMwater_0.1 <- (kapint$MF.Val/1000)+kapint$totwater_0.1
kapint$PMwater_0.15 <- (kapint$MF.Val/1000)+kapint$totwater_0.15
kapint$PMwater_0.2 <- (kapint$MF.Val/1000)+kapint$totwater_0.2

kapint$PMinorg <- (kapint$MF.Val+kapint$alw_inorg)/1000

kapint$alw_inorg <- kapint$alw_inorg/1000
kapint$alw_org_fixed <- kapint$alw_org_fixed/1000
kapint$NO3 <- kapint$NO3/1000
kapint$SO4 <- kapint$SO4/1000
kapint$OMtot <- kapint$OMtot/1000
kapint$PM25 <- kapint$MF.Val/1000
kapint$OM1 <- kapint$OM1/1000
kapint$OM2 <- kapint$OM2/1000
kapint$OM3 <- kapint$OM3/1000
kapint$OM4 <- kapint$OM4/1000

#Break speciation data into west (CO Plateau) and southeast (Appalachia)
west <- subset(kapint,
SiteCode=="BRCA1"|SiteCode=="CANY1"|SiteCode=="CAPI1"|SiteCode=="MEVE1")
se <- subset(kapint,
SiteCode=="COHU1"|SiteCode=="GRSM1"|SiteCode=="SHRO1"|SiteCode=="LIGO1")

#set to 2007-2016
se2 <- subset(se, Year>=2007&Year<=2016)
sesummer <- subset(se2, season=="summer")
sesummer<-sesummer[sesummer$totwater<quantile(sesummer$totwater,0.95,na.rm=T),]
sewinter <- subset(se2,season=="winter")
sewinter<-sewinter[sewinter$totwater<quantile(sewinter$totwater,0.95,na.rm=T),]
west2 <- subset(west,Year>=2007&Year<=2016)
wsummer <- subset(west2,season=="summer")
wsummer<-wsummer[wsummer$totwater<quantile(wsummer$totwater,0.95,na.rm=T),]
wwinter <- subset(west2,season=="winter")
wwinter<-wwinter[wwinter$totwater<quantile(wwinter$totwater,0.95,na.rm=T),]

#aggregate by year
sesummermeans<-aggregate(sesummer,by=list(sesummer$Year), FUN="mean",na.rm=T)
sewintermeans<-aggregate(sewinter,by=list(sewinter$Year), FUN="mean",na.rm=T)
```

```
wsummermeans<-aggregate(wsummer,by=list(wsummer$Year), FUN="mean",na.rm=T)
wwintermeans<-aggregate(wwinter,by=list(wwinter$Year), FUN="mean",na.rm=T)

#PBL data
pbldata<-read.csv("C:/Users/stor/Documents/ALW and OC paper/2005-2016
analysis/pbl_data/pbl-season-1.csv")
pbldata$Group.2<-as.Date(as.character(pbldata$Group.2), format="%m/%d/%Y")
pbldata$Date<-pbldata$Group.2
sepbl<-
subset(pbldata,SiteCode=="COHU1"|SiteCode=="GRSM1"|SiteCode=="LIGO1"|SiteCode=="S
HRO1")
wpbl<-
subset(pbldata,SiteCode=="BRCA1"|SiteCode=="CAPI1"|SiteCode=="CANY1"|SiteCode=="M
EVE1")

#set years
sepbl2<-subset(sepbl,year>=2007&year<=2016)
wpbl2<-subset(wpbl,year>=2007&year<=2016)
sepblsummer<-subset(sepbl2,season=="summer")
sepblwinter<-subset(sepbl2,season=="winter")
wpblsummer<-subset(wpbl2,season=="summer")
wpblwinter<-subset(wpbl2,season=="winter")

#aggregate by year
sespblmeans<-aggregate(sepblsummer, by=list(sepblsummer$year), FUN="mean",na.rm=T)
sewpblmeans<-aggregate(sepblwinter,by=list(sepblwinter$year), FUN="mean",na.rm=T)
wspblmeans<-aggregate(wpblsummer,by=list(wpblsummer$year), FUN="mean",na.rm=T)
wwpblmeans<-aggregate(wpblwinter,by=list(wpblwinter$year), FUN="mean",na.rm=T)

#appalachia summer
sesummerdfrm<-
data.frame(Year=sesummermeans$Group.1,alw_orgtot=sesummermeans$alw_org_fixed,alw_in
org=sesummermeans$alw_inorg,NO3=sesummermeans$NO3,SO4=sesummermeans$SO4,OMto
t=sesummermeans$OMtot)
names(sesummerdfrm)<-c("Year", "Org Water", "Inorg Water", "Nitrate", "Sulfate","TOM")
test<-as.matrix(sesummerdfrm)
sesummerdfrm3<-subset(test,select=c(`Org Water`,`Inorg Water`, Nitrate, Sulfate, TOM))
sesummerdfrm3.t<-t(sesummerdfrm3)

jpeg("C:/Users/stor/Documents/ALW and OC paper/2005-2016 analysis/newdata_alllevels/data
2001-
2016/fixed_paper_plots/modis_plots/stacked_AS2.jpg",height=4,width=8,units="in",res=300)
par(mar=c(5,3,2,8.5))
bp<-barplot(sesummerdfrm3.t, col=c("turquoise4", "cadetblue1", "mediumblue", "firebrick",
"green4"), las=1, cex.axis=2, xaxt="n", ylim=c(0,20))
```

```
legend(x=1,y=16,pch=c(16,16,16,16,16,16),col=c("green4", "firebrick",
"mediumblue","cadetblue1","turquoise4","white"),legend=c("TOM", "Sulfate", "Nitrate",
"Inorganic Water", "Organic Water",""),
cex=1.7,x.intersp=1.3,text.width=2,bty="n",ncol=3,yjust=0,xpd=T)
labs<-seq(2007,2016,by=1)
text(cex=2,x=bp-0.3,y=-3.5,labels=paste(labs),xpd=T,srt=35)
text("Appalachia Summer",x=9,y=15,cex=2)
par(new=T)
plot(aotsummermeans$Year,aotsummermeans$SE_AOD,type="l",col="orange2",lty=3,lwd=8,yl
im=c(0,0.5),ylab=NA,xlab=NA,axes=F)
axis(side=4,at=seq(0,0.5,by=0.1),cex.axis=2,las=1,col.axis="orange3")
par(new=T)
plot(sespblmeans$year,sespblmeans$PBL,type="l",col="orangered1",lty=1,lwd=6,ylim=c(800,2
400),ylab=NA,xlab=NA,axes=F)
axis(side=4,at=seq(800,2400,by=400),cex.axis=2,las=1, col.axis="orangered2",line=3.8)
dev.off()

#appalachia winter
sewinterdfrm<-data.frame(Year=sewintermeans$Group.1,
alw_orgtot=sewintermeans$alw_org_fixed, alw_inorg=sewintermeans$alw_inorg,
NO3=sewintermeans$NO3, SO4=sewintermeans$SO4, OMtot=sewintermeans$OMtot)
names(sewinterdfrm)<-c("Year", "Org Water", "Inorg Water", "Nitrate", "Sulfate", "TOM")
test<-as.matrix(sewinterdfrm)
sewinterdfrm3<-subset(test, select=c(`Org Water`,`Inorg Water`, Nitrate, Sulfate, TOM))
sewinterdfrm3.t<-t(sewinterdfrm3)

jpeg("C:/Users/stor/Documents/ALW and OC paper/2005-2016 analysis/newdata_alllevels/data
2001-2016/fixed_paper_plots/modis_plots/stacked_AW2.jpg", height=4, width=8, units="in",
res=300)
par(mar=c(5,3,2,8.5))
bp<-barplot(sewinterdfrm3.t, col=c("turquoise4", "cadetblue1", "mediumblue", "firebrick",
"green4"), las=1, cex.axis=2, xaxt="n", ylim=c(0,20))
labs<-seq(2007,2016,by=1)
text(cex=2,x=bp-0.3,y=-3.5,labels=paste(labs),xpd=T,srt=35)
text("Appalachia Winter",x=9.25,y=15,cex=2)
par(new=T)
plot(aotwintermeans$Year,aotwintermeans$SE_AOD,type="l",col="orange2",lty=3,lwd=8,ylim
=c(0,0.5),ylab=NA,xlab=NA,axes=F)
axis(side=4,at=seq(0,0.5,by=0.1),cex.axis=2,las=1,col.axis="orange3")
par(new=T)
plot(sewpblmeans$year,sewpblmeans$PBL,type="l",col="orangered1",lty=1,lwd=6,ylim=c(800,
2400),ylab=NA,xlab=NA,axes=F)
axis(side=4,at=seq(800,2400,by=400),cex.axis=2,las=1,col.axis="orangered2",line=3.8)
dev.off()

#co plateau summer
```

```
wsummerdfrm<-data.frame(Year=wsummermeans$Group.1,
alw_orgtot=wsummermeans$alw_org_fixed, alw_inorg=wsummermeans$alw_inorg,
NO3=wsummermeans$NO3, SO4=wsummermeans$SO4, OMtot=wsummermeans$OMtot)
names(wsummerdfrm)<-c("Year","Org Water","Inorg Water", "Nitrate", "Sulfate","TOM")
test<-as.matrix(wsummerdfrm)
wsummerdfrm3<-subset(test,select=c(`Org Water`,`Inorg Water`, Nitrate, Sulfate, TOM))
wsummerdfrm3.t<-t(wsummerdfrm3)

jpeg("C:/Users/stor/Documents/ALW and OC paper/2005-2016 analysis/newdata_alllevels/data
2001-
2016/fixed_paper_plots/modis_plots/stacked_CPS2.jpg",height=4,width=8,units="in",res=300)
par(mar=c(5,3,2,8.5))
bp<-
barplot(wsummerdfrm3.t,col=c("turquoise4","cadetblue1","mediumblue","firebrick","green4"),la
s=1,cex.axis=2,xaxt="n",ylim=c(0,20))
labs<-seq(2007,2016,by=1)
text(cex=2,x=bp-0.3,y=-3.5,labels=paste(labs),xpd=T,srt=35)
text("CO Plateau Summer",x=8.75,y=14,cex=2)
par(new=T)
plot(aotsummermeans$Year,aotsummermeans$MW_AOD,type="l",col="orange2",lty=3,lwd=8,
ylim=c(0,0.5),ylab=NA,xlab=NA,axes=F)
axis(side=4,at=seq(0,0.5,by=0.1),cex.axis=2,las=1,col.axis="orange3")
par(new=T)
plot(wspblmeans$year,wspblmeans$PBL,type="l",col="orangered1",lty=1,lwd=6,ylim=c(800,24
00),ylab=NA,xlab=NA,axes=F)
axis(side=4,at=seq(800,2400,by=400),cex.axis=2,las=1,col.axis="orangered2",line=3.8)
dev.off()

#co plateau winter
wwinterdfrm<-
data.frame(Year=wwintermeans$Group.1,alw_orgtot=wwintermeans$alw_org_fixed,alw_inorg=
wwintermeans$alw_inorg,NO3=wwintermeans$NO3,SO4=wwintermeans$SO4,OMtot=wwinter
means$OMtot)
names(wwinterdfrm)<-c("Year","Org Water","Inorg Water","Nitrate","Sulfate","TOM")
test<-as.matrix(wwinterdfrm)
wwinterdfrm3<-subset(test,select=c(`Org Water`,`Inorg Water`, Nitrate, Sulfate, TOM))
wwinterdfrm3.t<-t(wwinterdfrm3)

jpeg("C:/Users/stor/Documents/ALW and OC paper/2005-2016 analysis/newdata_alllevels/data
2001-
2016/fixed_paper_plots/modis_plots/stacked_CPW2.jpg",height=4,width=8,units="in",res=300)
par(mar=c(5,3,2,8.5))
bp<-
barplot(wwinterdfrm3.t,col=c("turquoise4","cadetblue1","mediumblue","firebrick","green4"),las
=1,cex.axis=2,xaxt="n",ylim=c(0,20))
labs<-seq(2007,2016,by=1)
```

```
text(cex=2,x=bp-0.3,y=-3.5,labels=paste(labs),xpd=T,srt=35)
text("CO Plateau Winter",x=9,y=15,cex=2)
par(new=T)
plot(wwpblmeans$year,wwpblmeans$PBL,type="l",col="orangered1",lty=1,lwd=6,ylim=c(800,
2400),ylab=NA,xlab=NA,axes=F)
axis(side=4,at=seq(800,2400,by=400),cex.axis=2,las=1,col.axis="orangered2",line=3.8)
par(new=T)
plot(aotwintermeans$Year,aotwintermeans$MW_AOD,type="l",col="orange2",lty=3,lwd=8,yli
m=c(0,0.5),ylab=NA,xlab=NA,axes=F)
axis(side=4,at=seq(0,0.5,by=0.1),cex.axis=2,las=1,col.axis="orange3")
dev.off()

################################################
#Figure 2: Scatter plots of MODIS AOT vs PM2.5 + ALW#
################################################
kapint2<-subset(kapint,Year>=2007&Year<=2016)
kapint3<-subset(kapint,season=="summer"|season=="winter")
brca<-subset(kapint3,SiteCode=="BRCA1")
cany<-subset(kapint3,SiteCode=="CANY1")
capi<-subset(kapint3,SiteCode=="CAPI1")
meve<-subset(kapint3,SiteCode=="MEVE1")
cohu<-subset(kapint3,SiteCode=="COHU1")
grsm<-subset(kapint3,SiteCode=="GRSM1")
ligo<-subset(kapint3,SiteCode=="LIGO1")
shro<-subset(kapint3,SiteCode=="SHRO1")

brcameans<-aggregate(brca,by=list(brca$Month,brca$Year),FUN="mean",na.rm=T)
canymeans<-aggregate(cany,by=list(cany$Month,cany$Year),FUN="mean",na.rm=T)
capimeans<-aggregate(capi,by=list(capi$Month,capi$Year),FUN="mean",na.rm=T)
mevemeans<-aggregate(meve,by=list(meve$Month,meve$Year),FUN="mean",na.rm=T)
cohumeans<-aggregate(cohu,by=list(cohu$Month,cohu$Year),FUN="mean",na.rm=T)
grsmmeans<-aggregate(grsm,by=list(grsm$Month,grsm$Year),FUN="mean",na.rm=T)
ligomeans<-aggregate(ligo,by=list(ligo$Month,ligo$Year),FUN="mean",na.rm=T)
shromeans<-aggregate(shro,by=list(shro$Month,shro$Year),FUN="mean",na.rm=T)

modis<-read.csv("C:/Users/Amy/Desktop/Research/ALW and OC/ALW and OC paper/2005-
2016 analysis/data 2001-2016/modis_aod_month.csv")
modis$SE_AOD_low<-modis$SE_AOD-modis$SE_AOD_SD
modis$SE_AOD_hi<-modis$SE_AOD+modis$SE_AOD_SD
modis$MW_AOD_low<-modis$MW_AOD-modis$MW_AOD_SD
modis$MW_AOD_hi<-modis$MW_AOD+modis$MW_AOD_SD
modis$Year<-ifelse(modis$Month=="12",modis$Year<-
as.numeric(modis$year)+1,modis$Year<-modis$year)

modis2<-
subset(modis,Month=="12"|Month=="1"|Month=="2"|Month=="6"|Month=="7"|Month=="8")
```

```
modis2$Year<-ifelse(modis2$Month=="12",modis2$Year<-
as.numeric(modis2$year)+1,modis2$Year<-modis2$year)
modis2$Group.2<-modis2$Year
modis2$Group.1<-modis2$Month

brcaintmeans<-merge(brcameans,modis2,by=c("Group.1","Group.2"))
brcaintmeanssummer<-
subset(brcaintmeans,brcaintmeans$Group.1==6|brcaintmeans$Group.1==7|brcaintmeans$Group.
1==8)
brcaintmeanssummer$AOT<-brcaintmeanssummer$BRCA1
brcaintmeanswinter<-
subset(brcaintmeans,brcaintmeans$Group.1==12|brcaintmeans$Group.1==1|brcaintmeans$Grou
p.1==2)
brcaintmeanswinter$AOT<-brcaintmeanswinter$BRCA1

canyintmeans<-merge(canymeans,modis2,by=c("Group.1","Group.2"))
canyintmeanssummer<-
subset(canyintmeans,canyintmeans$Group.1==6|canyintmeans$Group.1==7|canyintmeans$Grou
p.1==8)
canyintmeanssummer$AOT<-canyintmeanssummer$CANY1
canyintmeanswinter<-
subset(canyintmeans,canyintmeans$Group.1==12|canyintmeans$Group.1==1|canyintmeans$Gro
up.1==2)
canyintmeanswinter$AOT<-canyintmeanswinter$CANY1

capiintmeans<-merge(capimeans,modis2,by=c("Group.1","Group.2"))
capiintmeanssummer<-
subset(capiintmeans,capiintmeans$Group.1==6|capiintmeans$Group.1==7|capiintmeans$Group.
1==8)
capiintmeanssummer$AOT<-capiintmeanssummer$CAPI1
capiintmeanswinter<-
subset(capiintmeans,capiintmeans$Group.1==12|capiintmeans$Group.1==1|capiintmeans$Grou
p.1==2)
capiintmeanswinter$AOT<-capiintmeanswinter$CAPI1

meveintmeans<-merge(mevemeans,modis2,by=c("Group.1","Group.2"))
meveintmeanssummer<-
subset(meveintmeans,meveintmeans$Group.1==6|meveintmeans$Group.1==7|meveintmeans$G
roup.1==8)
meveintmeanssummer$AOT<-meveintmeanssummer$MEVE1
meveintmeanswinter<-
subset(meveintmeans,meveintmeans$Group.1==12|meveintmeans$Group.1==1|meveintmeans$
Group.1==2)
meveintmeanswinter$AOT<-meveintmeanswinter$MEVE1

cohuintmeans<-merge(cohumeans,modis2,by=c("Group.1","Group.2"))
```

```
cohuintmeanssummer<-
subset(cohuintmeans,cohuintmeans$Group.1==6|cohuintmeans$Group.1==7|cohuintmeans$Gro
up.1==8)
cohuintmeanssummer$AOT<-cohuintmeanssummer$COHU1
cohuintmeanswinter<-
subset(cohuintmeans,cohuintmeans$Group.1==12|cohuintmeans$Group.1==1|cohuintmeans$Gr
oup.1==2)
cohuintmeanswinter$AOT<-cohuintmeanswinter$COHU1

grsmintmeans<-merge(grsmmeans,modis2,by=c("Group.1","Group.2"))
grsmintmeanssummer<-
subset(grsmintmeans,grsmintmeans$Group.1==6|grsmintmeans$Group.1==7|grsmintmeans$Gro
up.1==8)
grsmintmeanssummer$AOT<-grsmintmeanssummer$GRSM1
grsmintmeanswinter<-
subset(grsmintmeans,grsmintmeans$Group.1==12|grsmintmeans$Group.1==1|grsmintmeans$Gr
oup.1==2)
grsmintmeanswinter$AOT<-grsmintmeanswinter$GRSM1

ligointmeans<-merge(ligomeans,modis2,by=c("Group.1","Group.2"))
ligointmeanssummer<-
subset(ligointmeans,ligointmeans$Group.1==6|ligointmeans$Group.1==7|ligointmeans$Group.1
==8)
ligointmeanssummer$AOT<-ligointmeanssummer$LIGO1
ligointmeanswinter<-
subset(ligointmeans,ligointmeans$Group.1==12|ligointmeans$Group.1==1|ligointmeans$Group.
1==2)
ligointmeanswinter$AOT<-ligointmeanswinter$LIGO1

shrointmeans<-merge(shromeans,modis2,by=c("Group.1","Group.2"))
shrointmeanssummer<-
subset(shrointmeans,shrointmeans$Group.1==6|shrointmeans$Group.1==7|shrointmeans$Group.
1==8)
shrointmeanssummer$AOT<-shrointmeanssummer$SHRO1
shrointmeanswinter<-
subset(shrointmeans,shrointmeans$Group.1==12|shrointmeans$Group.1==1|shrointmeans$Grou
p.1==2)
shrointmeanswinter$AOT<-shrointmeanswinter$SHRO1

newdf<-
rbind(brcaintmeanssummer,canyintmeanssummer,capiintmeanssummer,meveintmeanssummer)
newdf1<-
rbind(brcaintmeanswinter,canyintmeanswinter,capiintmeanswinter,meveintmeanswinter)

#co plateau scatterplots
```

```
jpeg("C:/Users/stor/Documents/ALW and OC paper/2005-2016 analysis/newdata_alllevels/data
2001-2016/reviewer_plots/cop_sites_pmwater.jpg",width=6,height=6,units="in",res=300)
plot(newdf$PMwater,newdf$AOT,pch=22,cex=1,col="firebrick2",xlim=c(0,20),xaxt="n",ylim=
c(0,0.3),yaxt="n",las=1,xlab="",ylab="",main="",cex.main=1.5,cex.axis=1.2,cex.lab=1.3)
axis(side=1,at=seq(0,20,by=5),las=1,cex.axis=1.5)
axis(side=2,at=seq(0,0.3,by=0.05),las=1,cex.axis=1.5)
arrows(newdf$PMwater_L,newdf$AOT,newdf$PMwater_H,newdf$AOT,
length=0.05,angle=90,code=3,col=adjustcolor("firebrick2",alpha.f=0.5),lwd=2)
points(newdf1$PMwater,newdf1$AOT,pch=22,cex=1,col="mediumblue",xlab="",xaxt="n",ylab
="",main="")
arrows(newdf1$PMwater_L,newdf1$AOT,newdf1$PMwater_H,newdf1$AOT,
length=0.05,angle=90,code=3,col=adjustcolor("mediumblue",alpha.f=0.5),lwd=2)
legend("bottomright",legend=c("CPS","CPW"),col=c("firebrick2","mediumblue"),pch=c(22,22),
cex=1.5)
linfit<-lm(newdf$AOT~newdf$PMwater)
summary(linfit)
abline(linfit,lwd=3)
linfit2<-lm(newdf1$AOT~newdf1$PMwater)
summary(linfit2)
abline(linfit2,lwd=3,col="gray50")
dev.off()

#appalachia scatterplots
newdf2<-
rbind(cohuintmeanssummer,grsmintmeanssummer,ligointmeanssummer,shrointmeanssummer)
newdf3<-
rbind(cohuintmeanswinter,grsmintmeanswinter,ligointmeanswinter,shrointmeanswinter)

jpeg("C:/Users/stor/Documents/ALW and OC paper/2005-2016 analysis/newdata_alllevels/data
2001-2016/reviewer_plots/app_sites_pmwater.jpg",width=6,height=6,units="in",res=300)
plot(newdf2$PMwater,newdf2$AOT,pch=16,cex=1,col="firebrick2",xlim=c(0,50),xaxt="n",yli
m=c(0,0.62),yaxt="n",las=1,xlab="",ylab="",main="",cex.main=1.5,cex.axis=1.2,cex.lab=1.3)
axis(side=1,at=seq(0,50,by=10),las=1,cex.axis=1.5)
axis(side=2,at=seq(0,0.62,by=0.1),las=1,cex.axis=1.5)
arrows(newdf2$PMwater_L,newdf2$AOT,newdf2$PMwater_H,newdf2$AOT,
length=0.05,angle=90,code=3,col=adjustcolor("firebrick2",alpha.f=0.5),lwd=2)
points(newdf3$PMwater,newdf3$AOT,pch=16,cex=1,col="mediumblue",xlab="",xaxt="n",ylab
="",main="")
arrows(newdf3$PMwater_L,newdf3$AOT,newdf3$PMwater_H,newdf3$AOT,
length=0.05,angle=90,code=3,col=adjustcolor("mediumblue",alpha.f=0.5),lwd=2)
legend("bottomright",legend=c("AS","AW"),col=c("firebrick2","mediumblue"),pch=c(16,16),ce
x=1.5)
linfit<-lm(newdf2$AOT~newdf2$PMwater)
summary(linfit)
abline(linfit,lwd=3)
linfit2<-lm(newdf3$AOT~newdf3$PMwater)
```

```
summary(linfit2)
abline(linfit2,lwd=3,col="gray50")
dev.off()

##################################
#Figure 3: extinction and ALW profiles#
##################################
allext<-read.csv("C:/Users/stor/Documents/MATLAB/all_ext_all_alts.csv")
allext$alt.m<-allext$alt.km*1000

summer<-data.frame(alt=allext$alt.m,SiteCode=allext$SiteCode,
Jun2006=allext$X6.1.2006,Jul2006=allext$X7.1.2006,Aug2006=allext$X8.1.2006,
Jun2007=allext$X6.1.2007,Jul2007=allext$X7.1.2007,Aug2007=allext$X8.1.2007,
Jun2008=allext$X6.1.2008,Jul2008=allext$X7.1.2008,Aug2008=allext$X8.1.2008,
Jun2009=allext$X6.1.2009,Jul2009=allext$X7.1.2009,Aug2009=allext$X8.1.2009,
Jun2010=allext$X6.1.2010,Jul2010=allext$X7.1.2010,Aug2010=allext$X8.1.2010,
Jun2011=allext$X6.1.2011,Jul2011=allext$X7.1.2011,Aug2011=allext$X8.1.2011,
Jun2012=allext$X6.1.2012,Jul2012=allext$X7.1.2012,Aug2012=allext$X8.1.2012,
Jun2013=allext$X6.1.2013,Jul2013=allext$X7.1.2013,Aug2013=allext$X8.1.2013,
Jun2014=allext$X6.1.2014,Jul2014=allext$X7.1.2014,Aug2014=allext$X8.1.2014,
Jun2015=allext$X6.1.2015,Jul2015=allext$X7.1.2015,Aug2015=allext$X8.1.2015,
Jun2016=allext$X6.1.2016,Jul2016=allext$X7.1.2016,Aug2016=allext$X8.1.2016)

winter<-data.frame(alt=allext$alt.m,SiteCode=allext$SiteCode,
Dec2006=allext$X12.1.2006,Jan2007=allext$X1.1.2007,Feb2007=allext$X2.1.2007,
Dec2007=allext$X12.1.2007,Jan2008=allext$X1.1.2008,Feb2008=allext$X2.1.2008,
Dec2008=allext$X12.1.2008,Jan2009=allext$X1.1.2009,Feb2009=allext$X2.1.2009,
Dec2009=allext$X12.1.2009,Jan2010=allext$X1.1.2010,Feb2010=allext$X2.1.2010,
Dec2010=allext$X12.1.2010,Jan2011=allext$X1.1.2011,Feb2011=allext$X2.1.2011,
Dec2011=allext$X12.1.2011,Jan2012=allext$X1.1.2012,Feb2012=allext$X2.1.2012,
Dec2012=allext$X12.1.2012,Jan2013=allext$X1.1.2013,Feb2013=allext$X2.1.2013,
Dec2013=allext$X12.1.2013,Jan2014=allext$X1.1.2014,Feb2014=allext$X2.1.2014,
Dec2014=allext$X12.1.2014,Jan2015=allext$X1.1.2015,Feb2015=allext$X2.1.2015,
Dec2015=allext$X12.1.2015,Jan2016=allext$X1.1.2016)

sesummer<-
subset(summer,SiteCode=="COHU1"|SiteCode=="GRSM1"|SiteCode=="LIGO1"|SiteCode=="
SHRO1")
sewinter<-
subset(winter,SiteCode=="COHU1"|SiteCode=="GRSM1"|SiteCode=="LIGO1"|SiteCode=="S
HRO1")
wsummer<-
subset(summer,SiteCode=="BRCA1"|SiteCode=="CANY1"|SiteCode=="CAPI1"|SiteCode=="
MEVE1")
```

```
wwinter<-
subset(winter,SiteCode=="BRCA1"|SiteCode=="CANY1"|SiteCode=="CAPI1"|SiteCode=="M
EVE1")

#need to get an average value at each altitude
sesummeragg<-aggregate(sesummer,by=list(sesummer$alt),FUN="mean",na.rm=T)
sewinteragg<-aggregate(sewinter,by=list(sewinter$alt),FUN="mean",na.rm=T)
wsummeragg<-aggregate(wsummer,by=list(wsummer$alt),FUN="mean",na.rm=T)
wwinteragg<-aggregate(wwinter,by=list(wwinter$alt),FUN="mean",na.rm=T)

#want to get seasonal averages for each year
sesummeragg2<-subset(sesummeragg,sesummeragg$alt>0)
sewinteragg2<-subset(sewinteragg,sewinteragg$alt>0)
wsummeragg2<-subset(wsummeragg,wsummeragg$alt>0)
wwinteragg2<-subset(wwinteragg,wwinteragg$alt>0)

#write loop that goes "for each altitude, average all the months"
#alternatively,
sesummervals<-data.frame(alt=sesummeragg[,2],extavgs=rowMeans(sesummeragg[,-1:-
3],na.rm=T))
sewintervals<-data.frame(alt=sewinteragg[,2],extavgs=rowMeans(sewinteragg[,-1:-3],na.rm=T))
wsummervals<-data.frame(alt=wsummeragg[,2],extavgs=rowMeans(wsummeragg[,-1:-
3],na.rm=T))
wwintervals<-data.frame(alt=wwinteragg[,2],extavgs=rowMeans(wwinteragg[,-1:-3],na.rm=T))

#water data at all pressure levels
allpress<-read.csv("C:/Users/stor/Documents/ALW and OC paper/2005-2016
analysis/newdata_alllevels/data 2001-2016/combined_2001-2016_allpressures.csv")
allpress$Date<-as.Date(as.character(allpress$Date),format="%m/%d/%Y")
allpress$year<-substring(allpress$Date,1,4)
allpress$Month<-substring(allpress$Date,6,7)
allpress$year<-as.numeric(allpress$year)
allpress$Month<-as.numeric(allpress$Month)
library(zoo)
yq<-as.yearqtr(as.yearmon(allpress$Date,"%Y-%m-%d")+1/12)
allpress$season<-
factor(format(yq,"%q"),levels=1:4,labels=c("winter","spring","summer","fall"))
allpress$Year<-ifelse(allpress$Month=="12",allpress$year+1,allpress$year) #to match DJF
assignments
allpress$LayerOrgWater<-as.numeric(as.character(allpress$LayerOrgWater))
allpress$Masswo<-as.numeric(as.character(allpress$Masswo))
allpress$totwater<-allpress$water+allpress$Masswo
allpress$PM25water<-allpress$water+allpress$Masswo+allpress$MF.Val
allpress2<-subset(allpress,totwater>0)
allpress2<-subset(allpress2,RH<0.95)
```

```
#merge with pbldata
pbldata<-read.csv("C:/Users/stor/Documents/ALW and OC paper/2005-2016
analysis/pbl_data/pbl-season-1.csv")
pbldata$Group.2<-as.Date(as.character(pbldata$Group.2),format="%m/%d/%Y")
pbldata$Date<-pbldata$Group.2
allpress3<-merge(pbldata,allpress2,by=c("Date","SiteCode"))

#now need to only keep data that is below the PBL
allpress3$BelowPBL<-ifelse(allpress3$Height>allpress3$PBL,NA,allpress3$Height)
completeFun<-function(allpress3,BelowPBL){
  completeVec<-complete.cases(allpress3[,BelowPBL])
  return(allpress3[completeVec,])
}

allpress4<-completeFun(allpress3,"BelowPBL")
west<-
subset(allpress4,allpress4$SiteCode=="BRCA1"|allpress4$SiteCode=="CANY1"|allpress4$Site
Code=="CAPI1"|allpress4$SiteCode=="MEVE1")
se<-
subset(allpress4,allpress4$SiteCode=="COHU1"|allpress4$SiteCode=="GRSM1"|allpress4$Site
Code=="LIGO1"|allpress4$SiteCode=="SHRO1")
se2<-subset(se,Year>=2007&Year<=2016)
sesummer<-subset(se2,season.x=="summer")
sesummer<-sesummer[sesummer$totwater<quantile(sesummer$totwater,0.95,na.rm=T),]
sewinter<-subset(se2,season.x=="winter")
sewinter<-sewinter[sewinter$totwater<quantile(sewinter$totwater,0.95,na.rm=T),]
west2<-subset(west,Year>=2007&Year<=2016)
wsummer<-subset(west2,season.x=="summer")
wsummer<-wsummer[wsummer$totwater<quantile(wsummer$totwater,0.95,na.rm=T),]
wwinter<-subset(west,season.x=="winter")
wwinter<-wwinter[wwinter$totwater<quantile(wwinter$totwater,0.95,na.rm=T),]

#co plateau extinction and water vertical profiles
wsummer2<-subset(wsummer,wsummer$Height<2164)#mean PBL height for co plateau
summer, all years
wsummer2means<-aggregate(wsummer2,by=list(wsummer2$pressure),FUN="mean",na.rm=T)
wwinter2<-subset(wwinter,wwinter$Height<1000)#mean PBL height for co plateau winter, all
years
wwinter2means<-aggregate(wwinter2,by=list(wwinter2$pressure),FUN="mean",na.rm=T)
wsummervals2<-subset(wsummervals,wsummervals$alt>0)
wsummervals2[is.na(wsummervals2)]<-0
wwintervals2<-subset(wwintervals,wwintervals$alt>0)
wwintervals2[is.na(wwintervals2)]<-0
```

```
jpeg("C:/Users/stor/Documents/ALW and OC paper/2005-2016 analysis/newdata_alllevels/data 2001-
2016/fixed_paper_plots/COP_profile_withEXT_avgs.jpg",height=6,width=6,units="in",res=300)
par(mar=c(5.1,5,4.1,2.1))
plot(wsummer2means$totwater,wsummer2means$Height,type="l",lty=2,lwd=4,col="firebrick2",
xlim=c(0,10),ylim=c(0,2200),xlab=NA,ylab=NA,yaxt="n",xaxt="n")
axis(side=1,at=seq(0,10,by=2),labels=F)
labs<-seq(0,10,by=2)
text(seq(0,10,by=2),par("usr")[3]-0.1,labels=labs,srt=0,xpd=T,cex=2,adj=c(0.5,1.8))
axis(side=2,at=seq(0,2200,by=400),cex.axis=2,las=1)
points(wwinter2means$totwater,wwinter2means$Height,type="l",lty=2,lwd=4,col="mediumblue
",xlab=NA,ylab=NA,yaxt="n",xaxt="n")
par(new=T)
plot(wsummervals2$extavgs,wsummervals2$alt,type="l",ylim=c(0,2200),xlim=c(0,0.1),lty=1,lw
d=4,col="sienna",xlab=NA,ylab=NA,yaxt="n",xaxt="n")
axis(side=1,at=seq(0,0.1,by=0.02),labels=F,col.ticks="sienna",lwd.ticks=3,line=3,col="sienna",l
wd=2)
labs2<-seq(0,0.1,0.02)
text(seq(0,0.1,by=0.02),par("usr")[3]-
0.1,labels=labs2,srt=0,xpd=T,cex=2,adj=c(0.5,4),col="sienna")
points(wwintervals2$extavgs,wwintervals2$alt,type="l",ylim=c(0,2200),lty=3,lwd=4,col="sienn
a")
legend("bottomright",legend=c("Summer ALW","Winter ALW","Summer Extinction","Winter
Extinction"),lty=c(2,2,1,3),col=c("firebrick2","mediumblue","sienna","sienna"),cex=1.2,lwd=c(4
,4,4,4))
dev.off()

#appalachia extinction and water vertical profiles
sesummer2<-subset(sesummer,sesummer$Height<939)#mean PBL height for app summer
sesummer2means<-aggregate(sesummer2,by=list(sesummer2$pressure),FUN="mean",na.rm=T)
sewinter2<-subset(sewinter,sewinter$Height<842)#mean PBL height for app winter
sewinter2means<-aggregate(sewinter2,by=list(sewinter2$pressure),FUN="mean",na.rm=T)
sesummervals2<-subset(sesummervals,sesummervals$alt>0)
sesummervals2[is.na(sesummervals2)]<-0
sewintervals2<-subset(sewintervals,sewintervals$alt>0)
sewintervals2[is.na(sewintervals2)]<-0

jpeg("C:/Users/stor/Documents/ALW and OC paper/2005-2016 analysis/newdata_alllevels/data 2001-
2016/fixed_paper_plots/App_profile_withEXT_avgs.jpg",height=6,width=6,units="in",res=300)
par(mar=c(5.1,5,4.1,2.1))
plot(sesummer2means$totwater,sesummer2means$Height,type="l",lty=2,lwd=4,col="firebrick2"
,xlim=c(0,10),ylim=c(0,2200),xlab=NA,ylab=NA,yaxt="n",xaxt="n")
axis(side=1,at=seq(0,10,by=2),labels=F)
labs<-seq(0,10,by=2)
text(seq(0,10,by=2),par("usr")[3]-0.1,labels=labs,srt=0,xpd=T,cex=2,adj=c(0.5,1.8))
```

```
axis(side=2,at=seq(0,2200,by=400),cex.axis=2,las=1)
points(sewinter2means$totwater,sewinter2means$Height,type="l",lty=2,lwd=4,col="mediumblu
e",xlab=NA,ylab=NA,yaxt="n",xaxt="n")
par(new=T)
plot(sesummervals2$extavgs,sesummervals2$alt,type="l",ylim=c(0,2200),xlim=c(0,0.1),lty=1,l
wd=4,col="sienna",xlab=NA,ylab=NA,yaxt="n",xaxt="n")
axis(side=1,at=seq(0,0.1,by=0.02),labels=F,col.ticks="sienna",lwd.ticks=3,line=3,col="sienna",l
wd=2)
labs2<-seq(0,0.1,0.02)
text(seq(0,0.1,by=0.02),par("usr")[3]-
0.1,labels=labs2,srt=0,xpd=T,cex=2,adj=c(0.5,4),col="sienna")
points(sewintervals2$extavgs,sewintervals2$alt,type="l",ylim=c(0,2200),lty=3,lwd=4,col="sienn
a")
dev.off()

####################################
#Figure 4: Integrated OM stacked barcharts#
####################################

alldata<-read.csv("C:/Users/stor/Documents/ALW and OC paper/2005-2016
analysis/newdata_alllevels/data 2001-2016/focus_2001-2016_intunder95-1.csv")
alldata$Date<-as.Date(as.character(alldata$Date),format="%m/%d/%Y")
alldata$Month<-substring(alldata$Date,6,7)
alldata$Month<-as.numeric(alldata$Month)
alldata$Year<-ifelse(alldata$Month=="12",alldata$year+1,alldata$year) #to match DJF
assignments

alldata$totwater<-alldata$alw_orgtot+alldata$alw_inorg
alldata2<-subset(alldata,totwater>0)
alldata3<-subset(alldata2,Year>=2007&Year<=2016)

#put all units into mg/m^2
alldata3$OM1<-alldata3$OM1/1000
alldata3$OM2<-alldata3$OM2/1000
alldata3$OM3<-alldata3$OM3/1000
alldata3$OM4<-alldata3$OM4/1000

se<-
subset(alldata3,SiteCode=="COHU1"|SiteCode=="GRSM1"|SiteCode=="LIGO1"|SiteCode=="S
HRO1")
west<-
subset(alldata3,SiteCode=="BRCA1"|SiteCode=="CAPI1"|SiteCode=="CANY1"|SiteCode=="
MEVE1")

sesummer<-subset(se,se$season=="summer")
sewinter<-subset(se,se$season=="winter")
```

```
wsummer<-subset(west,west$season=="summer")
wwinter<-subset(west,west$season=="winter")

sesummer<-sesummer[sesummer$totwater<quantile(sesummer$totwater,0.95),]
sewinter<-sewinter[sewinter$totwater<quantile(sewinter$totwater,0.95),]
wsummer<-wsummer[wsummer$totwater<quantile(wsummer$totwater,0.95),]
wwinter<-wwinter[wwinter$totwater<quantile(wwinter$totwater,0.95),]

sesummermeans<-aggregate(sesummer,by=list(sesummer$Year),FUN="mean",na.rm=T)
sewintermeans<-aggregate(sewinter,by=list(sewinter$Year),FUN="mean",na.rm=T)
wsummermeans<-aggregate(wsummer,by=list(wsummer$Year),FUN="mean",na.rm=T)
wwintermeans<-aggregate(wwinter,by=list(wwinter$Year),FUN="mean",na.rm=T)

#appalachia summer
sesummerdfrm<-
data.frame(Year=sesummermeans$Group.1,OM1=sesummermeans$OM1,OM2=sesummermean
s$OM2,OM3=sesummermeans$OM3,OM4=sesummermeans$OM4)
names(sesummerdfrm)<-c("Year","OM1","OM2","OM3","OM4")
test<-as.matrix(sesummerdfrm)
sesummerdfrm3<-subset(test,select=c(OM1, OM2, OM3, OM4))
sesummerdfrm3.t<-t(sesummerdfrm3)

jpeg("C:/Users/stor/Documents/ALW and OC paper/2005-2016 analysis/newdata_alllevels/data
2001-
2016/fixed_paper_plots/orgfracs_stack_SES_big.jpg",height=4,width=8,units="in",res=300)
par(mar=c(5,3,2,8.5))
bp<-
barplot(sesummerdfrm3.t,col=c("palegreen1","palegreen2","palegreen3","palegreen4"),las=1,cex
.axis=2,xaxt="n",ylim=c(0,5))
legend(x=-
0,y=4.5,pch=c(16,16,16,16,16),col=c("palegreen4","palegreen3","palegreen2","palegreen1"),leg
end=c("OM4","OM3","OM2","OM1"),cex=2,x.intersp=0.5,text.width=1.3,bty="n",ncol=4,yjust
=0,xpd=T)
labs<-seq(2007,2016,by=1)
text(cex=2,x=bp-0.3,y=-0.75,labels=paste(labs),xpd=T,srt=35)
text("Appalachia Summer",x=8.5,y=4,cex=2)
dev.off()

#appalachia winter
sewinterdfrm<-
data.frame(Year=sewintermeans$Group.1,OM1=sewintermeans$OM1,OM2=sewintermeans$O
M2,OM3=sewintermeans$OM3,OM4=sewintermeans$OM4)
names(sewinterdfrm)<-c("Year","OM1","OM2","OM3","OM4")
test<-as.matrix(sewinterdfrm)
sewinterdfrm3<-subset(test,select=c(OM1, OM2, OM3, OM4))
sewinterdfrm3.t<-t(sewinterdfrm3)
```

```
jpeg("C:/Users/stor/Documents/ALW and OC paper/2005-2016 analysis/newdata_alllevels/data
2001-
2016/fixed_paper_plots/orgfracs_stack_SEW_big.jpg",height=4,width=8,units="in",res=300)
par(mar=c(5,3,2,8.5))
bp<-
barplot(sewinterdfrm3.t,col=c("palegreen1","palegreen2","palegreen3","palegreen4"),las=1,cex.a
xis=2,xaxt="n",ylim=c(0,5))
labs<-seq(2007,2016,by=1)
text(cex=2,x=bp-0.3,y=-0.75,labels=paste(labs),xpd=T,srt=35)
text("Appalachia Winter",x=8.5,y=4,cex=2)

dev.off()

#co plateau summer
wsummerdfrm<-
data.frame(Year=wsummermeans$Group.1,OM1=wsummermeans$OM1,OM2=wsummermeans
$OM2,OM3=wsummermeans$OM3,OM4=wsummermeans$OM4)
names(wsummerdfrm)<-c("Year","OM1","OM2","OM3","OM4")
test<-as.matrix(wsummerdfrm)
wsummerdfrm3<-subset(test,select=c(OM1, OM2, OM3, OM4))
wsummerdfrm3.t<-t(wsummerdfrm3)

jpeg("C:/Users/stor/Documents/ALW and OC paper/2005-2016 analysis/newdata_alllevels/data
2001-
2016/fixed_paper_plots/orgfracs_stack_WS_big.jpg",height=4,width=8,units="in",res=300)
par(mar=c(5,3,2,8.5))
bp<-
barplot(wsummerdfrm3.t,col=c("palegreen1","palegreen2","palegreen3","palegreen4"),las=1,cex
.axis=2,xaxt="n",ylim=c(0,5))
labs<-seq(2007,2016,by=1)
text(cex=2,x=bp-0.3,y=-0.75,labels=paste(labs),xpd=T,srt=35)
text("CO Plateau Summer",x=8,y=4,cex=2)
dev.off()

#co plateau winter
wwinterdfrm<-
data.frame(Year=wwintermeans$Group.1,OM1=wwintermeans$OM1,OM2=wwintermeans$OM
2,OM3=wwintermeans$OM3,OM4=wwintermeans$OM4)
names(wwinterdfrm)<-c("Year","OM1","OM2","OM3","OM4")
test<-as.matrix(wwinterdfrm)
wwinterdfrm3<-subset(test,select=c(OM1, OM2, OM3, OM4))
wwinterdfrm3.t<-t(wwinterdfrm3)
```

```
jpeg("C:/Users/stor/Documents/ALW and OC paper/2005-2016 analysis/newdata_alllevels/data 2001-
2016/fixed_paper_plots/orgfracs_stack_WW_big.jpg",height=4,width=8,units="in",res=300)
par(mar=c(5,3,2,8.5))
bp<-
barplot(wwinterdfrm3.t,col=c("palegreen1","palegreen2","palegreen3","palegreen4"),las=1,cex.a
xis=2,xaxt="n",ylim=c(0,5))
labs<-seq(2007,2016,by=1)
text(cex=2,x=bp-0.3,y=-0.75,labels=paste(labs),xpd=T,srt=35)
text("CO Plateau Winter",x=8,y=4,cex=2)
dev.off()
```

```
#Supporting Information code
#Christiansen et al. 2019

############################
#Figure S1. Focus site locations#
############################
library(maps)

jpeg("C:/Users/stor/Documents/ALW and OC
paper/plots/sitemap.jpg",width=6,height=4,units="in",res=300)

par(oma=c(0,0,0,0))
map('state',lty=1,lwd=2,interior=F,col="black")
#map("state", boundary = FALSE, lty = 2, add = TRUE,col="black")
points(x=c(-111.2926,-112.1736,-109.821,-
108.4907),y=c(38.3022,37.6184,38.4587,37.1984),col="turquoise1",pch=16)
points(x=c(-84.6265,-83.9416,-82.7744,-
81.9331),y=c(34.7852,35.6334,35.3937,35.9723),col="red",pch=16)

dev.off()

################################
#Figure S2. PM2.5 Diurnal Variability#
################################
epa<-read.csv("C:/Users/stor/Documents/ALW and OC paper/EPA_24hr_PM25.csv")

#appalachia
bryson<-subset(epa,epa$Site=="BrysonCity")
unique(bryson$Day)
head(bryson$Day)
tail(bryson$Day)

#co plateau
deadman<-subset(epa,epa$Site=="Deadman")
unique(deadman$Day)
head(deadman$Day)
tail(deadman$Day)

#overlapping years are 2009, 2010, 2011
#so choose summer 2010
#maybe july

bryson$Day<-as.Date(as.character(bryson$Day),format="%m/%d/%Y")
deadman$Day<-as.Date(as.character(deadman$Day),format="%m/%d/%Y")

bryson$Month<-substring(bryson$Day,6,7)
```

```
deadman$Month<-substring(deadman$Day,6,7)

bryson$year<-substring(bryson$Day,1,4)
deadman$year<-substring(deadman$Day,1,4)

bryson2<-subset(bryson,Month=="07"&year=="2010")
deadman2<-subset(deadman,Month=="07"&year=="2010")

#we'll do 7/1/2010 to keep it simple
bry<-subset(bryson2,Day=="2010-07-01")
dea<-subset(deadman2,Day=="2010-07-01")

bry$Hour<-substring(bry$Date,12,13)
bry$Hour<-as.numeric(bry$Hour)
dea$Hour<-substring(dea$Date,12,13)
dea$Hour<-as.numeric(dea$Hour)

tiff("C:/Users/stor/Documents/ALW and OC paper/2005-2016
analysis/newdata_alllevels/daily_variability_plots/Hourly_PM25.tiff",height=6,width=6,units="i
n",res=300)
par(mar=c(5.1,5,4.1,3))
plot(bry$Hour,bry$PM25,type="l",ylim=c(0,30),col="darkgreen",lwd=3,cex.axis=1.5,
    ylab=expression("PM"[2.5]~"Mass Concentration"~~(mu*g~m^{-
3})),xlab="Hour",cex.lab=1.5)
lines(dea$Hour,dea$PM25,type="l",col="brown4",lwd=3,xlab="",ylab="")
rect(10.5,3,13.5,15,col=NA,border="red3",lwd=3)
legend("topleft",legend=c("Appalachia","CO
Plateau"),lty=c(1,1),lwd=c(3,3),col=c("darkgreen","brown4"),cex=1.5)
dev.off()

##################################
#Figure S3. AERONET vs MODIS AOT#
##################################

#comparing AERONET AOD at 500 nm to MODIS AOD at 550 nm
#will need to use aggregated data since sites don't line up exactly
#first, load in modis data
modis<-read.csv("C:/Users/stor/Documents/ALW and OC paper/2005-2016
analysis/newdata_alllevels/modis_aod_month.csv")
modis$Year<-ifelse(modis$Month=="12",modis$Year<-
as.numeric(modis$year)+1,modis$Year<-modis$year)
modissummer<-subset(modis,Month=="6"|Month=="7"|Month=="8")
modiswinter<-subset(modis,Month=="12"|Month=="1"|Month=="2")

#now load in AERONET data
```

```
aero<-read.csv("C:/Users/stor/Documents/ALW and OC paper/2005-2016
analysis/AERONET_AOD.csv")
aero$Year<-ifelse(aero$Month=="12",aero$Year<-as.numeric(aero$year)+1,aero$Year<-
aero$year)
aerosummer<-subset(aero,Month=="6"|Month=="7"|Month=="8")
aerowinter<-subset(aero,Month=="12"|Month=="1"|Month=="2")

#combine datasets
summercombo<-merge(modissummer,aerosummer,by=c("Month","Year"))
wintercombo<-merge(modiswinter,aerowinter,by=c("Month","Year"))

jpeg("C:/Users/stor/Documents/ALW and OC paper/2005-2016 analysis/newdata_alllevels/data
2001-
2016/reviewer_plots/appalachia_aeronet_modis.jpg",height=6,width=6,units="in",res=300)
plot(summercombo$SE_AOD.x,summercombo$SE_AOD.y,xlim=c(0,0.5),ylim=c(0,0.3),cex.axi
s=1.5,ylab="",xlab="",
    las=1,pch=16,col="firebrick2",cex=2)
points(wintercombo$SE_AOD.x,wintercombo$SE_AOD.y,ylab="",xlab="",xaxt="n",yaxt="n",p
ch=16,col="mediumblue",cex=2)
abline(lm(summercombo$SE_AOD.y~summercombo$SE_AOD.x),lwd=3)
abline(lm(wintercombo$SE_AOD.y~wintercombo$SE_AOD.x),lwd=3,col="gray50")
dev.off()

jpeg("C:/Users/stor/Documents/ALW and OC paper/2005-2016 analysis/newdata_alllevels/data
2001-2016/reviewer_plots/cop_aeronet_modis.jpg",height=6,width=6,units="in",res=300)
plot(summercombo$MW_AOD.x,summercombo$MW_AOD.y,xlim=c(0,0.2),ylim=c(0,0.21),ce
x.axis=1.5,ylab="",xlab="",
    las=1,pch=22,col="firebrick2",cex=2)
points(wintercombo$MW_AOD.x,wintercombo$MW_AOD.y,ylab="",xlab="",xaxt="n",yaxt="
n",pch=22,col="mediumblue",cex=2)
abline(lm(summercombo$MW_AOD.y~summercombo$MW_AOD.x),lwd=3)
abline(lm(wintercombo$MW_AOD.y~wintercombo$MW_AOD.x),lwd=3,col="gray50")
dev.off()


#########################################################
#Figure S4. Extinction coefficients and MODIS/CALIPSO AOT#
#########################################################
aot<-read.csv("C:/Users/stor/Documents/ALW and OC paper/2005-2016
analysis/focus_aot_means07-16-1.csv")
aotsummer<-subset(aot,season=="summer")
aotwinter<-subset(aot,season=="winter")
aotsummermeans<-aggregate(aotsummer,by=list(aotsummer$Year),FUN="mean",na.rm=T)
aotwintermeans<-aggregate(aotwinter,by=list(aotwinter$Year),FUN="mean",na.rm=T)
```

```
modis<-read.csv("C:/Users/stor/Documents/ALW and OC paper/2005-2016
analysis/newdata_alllevels/modis_aod_month.csv")
modis$Year<-ifelse(modis$Month=="12",modis$Year<-
as.numeric(modis$year)+1,modis$Year<-modis$year)
modissummer<-subset(modis,Month=="6"|Month=="7"|Month=="8")
modiswinter<-subset(modis,Month=="12"|Month=="1"|Month=="2")
modissummermeans<-
aggregate(modissummer,by=list(modissummer$Year),FUN="mean",na.rm=T)
modiswintermeans<-aggregate(modiswinter,by=list(modiswinter$Year),FUN="mean",na.rm=T)

ext<-read.csv("C:/Users/stor/Documents/ALW and OC paper/2005-2016
analysis/new_extinction/combo_extinction.csv")
ext$Date<-as.Date(as.character(ext$Date),format="%m/%d/%Y")
ext$Month<-substring(ext$Date,6,7)
ext$Month<-as.numeric(ext$Month)
ext$year<-substring(ext$Date,1,4)
ext$year<-as.numeric(ext$year)
library(zoo)
yq<-as.yearqtr(as.yearmon(ext$Date,"%Y-%m-%d")+1/12)
ext$season<-factor(format(yq,"%q"),levels=1:4,labels=c("winter","spring","summer","fall"))
ext$Year<-ifelse(ext$Month=="12",ext$year+1,ext$year) #to match DJF assignments
ext<-subset(ext,ext$pressure=="1000")
ext<-subset(ext,ext$RH<0.95)
west<-
subset(ext,SiteCode=="BRCA1"|SiteCode=="CANY1"|SiteCode=="CAPI1"|SiteCode=="MEV
E1")
se<-
subset(ext,SiteCode=="COHU1"|SiteCode=="GRSM1"|SiteCode=="LIGO1"|SiteCode=="SHR
O1")
se2<-subset(se,Year>=2007&Year<=2016)
sesummer<-subset(se2,season=="summer")
sewinter<-subset(se2,season=="winter")
west2<-subset(west,Year>=2007&Year<=2016)
wsummer<-subset(west2,season=="summer")
wwinter<-subset(west2,season=="winter")
#average everything by Year
sesummermeans<-aggregate(sesummer,by=list(sesummer$Year),FUN="mean",na.rm=T)
sewintermeans<-aggregate(sewinter,by=list(sewinter$Year),FUN="mean",na.rm=T)
wsummermeans<-aggregate(wsummer,by=list(wsummer$Year),FUN="mean",na.rm=T)
wwintermeans<-aggregate(wwinter,by=list(wwinter$Year),FUN="mean",na.rm=T)

#plots
jpeg("C:/Users/stor/Documents/ALW and OC paper/2005-2016
analysis/new_extinction/AS_bext_modisAOT_calipsoAOT.jpg",width=6,height=6,units="in",res
=300)
par(mar=c(5.1,4.3,4.1,4))
```

```
plot(modissummermeans$Year,modissummermeans$SE_AOD,ylim=c(0,0.5),type="l",col="dark
orange3",lwd=3,xaxt="n",xlab="",ylab="",las=1,cex.axis=2,col.axis="darkorange3")
axis(side=1,at=seq(2007,2016,by=1),labels=F)
labs<-seq(2007,2016,by=1)
text(seq(2007,2016,by=1),par("usr")[3]-0.05,labels=labs,srt=45,xpd=T,cex=2,adj=c(0.7,0.5))
lines(aotsummermeans$Year,aotsummermeans$SE_AOD,type="l",lty=2,col="red3",lwd=3,xaxt
="n",xlab="",ylab="")
par(new=T)
plot(sesummermeans$Year,sesummermeans$bext,type="l",col="purple4",lwd=3,ylim=c(0,100),
xaxt="n",yaxt="n",xlab="",ylab="")
axis(side=4,las=1,cex.axis=2,col.axis="purple4")

legend("topright",legend=c("MODIS AOT","CALIPSO
AOT","Extinction"),col=c("darkorange3","red3","purple4"),lty=c(1,2,1),lwd=3)

dev.off()

###
jpeg("C:/Users/stor/Documents/ALW and OC paper/2005-2016
analysis/new_extinction/AW_bext_modisAOT_calipsoAOT.jpg",width=6,height=6,units="in",re
s=300)
par(mar=c(5.1,4.3,4.1,4))

plot(modiswintermeans$Year,modiswintermeans$SE_AOD,ylim=c(0,0.5),type="l",col="darkora
nge3",lwd=3,xaxt="n",xlab="",ylab="",las=1,cex.axis=2,col.axis="darkorange3")
axis(side=1,at=seq(2007,2016,by=1),labels=F)
labs<-seq(2007,2016,by=1)
text(seq(2007,2016,by=1),par("usr")[3]-0.05,labels=labs,srt=45,xpd=T,cex=2,adj=c(0.7,0.5))
lines(aotwintermeans$Year,aotwintermeans$SE_AOD,type="l",lty=2,col="red3",lwd=3,xaxt="n
",xlab="",ylab="")
par(new=T)
plot(sewintermeans$Year,sewintermeans$bext,type="l",col="purple4",lwd=3,ylim=c(0,100),xax
t="n",yaxt="n",xlab="",ylab="")
axis(side=4,las=1,cex.axis=2,col.axis="purple4")

legend("topright",legend=c("MODIS AOT","CALIPSO
AOT","Extinction"),col=c("darkorange3","red3","purple4"),lty=c(1,2,1),lwd=3)

dev.off()

###
jpeg("C:/Users/stor/Documents/ALW and OC paper/2005-2016
analysis/new_extinction/CPS_bext_modisAOT_calipsoAOT.jpg",width=6,height=6,units="in",r
es=300)
par(mar=c(5.1,4.3,4.1,4))
```

```
plot(modissummermeans$Year,modissummermeans$MW_AOD,ylim=c(0,0.5),type="l",col="da
rkorange3",lwd=3,xaxt="n",xlab="",ylab="",las=1,cex.axis=2,col.axis="darkorange3")
axis(side=1,at=seq(2007,2016,by=1),labels=F)
labs<-seq(2007,2016,by=1)
text(seq(2007,2016,by=1),par("usr")[3]-0.05,labels=labs,srt=45,xpd=T,cex=2,adj=c(0.7,0.5))
lines(aotsummermeans$Year,aotsummermeans$MW_AOD,type="l",lty=2,col="red3",lwd=3,xa
xt="n",xlab="",ylab="")
par(new=T)
plot(wsummermeans$Year,wsummermeans$bext,type="l",col="purple4",lwd=3,ylim=c(0,100),x
axt="n",yaxt="n",xlab="",ylab="")
axis(side=4,las=1,cex.axis=2,col.axis="purple4")

legend("topright",legend=c("MODIS AOT","CALIPSO
AOT","Extinction"),col=c("darkorange3","red3","purple4"),lty=c(1,2,1),lwd=3)

dev.off()

###
jpeg("C:/Users/stor/Documents/ALW and OC paper/2005-2016
analysis/new_extinction/CPW_bext_modisAOT_calipsoAOT.jpg",width=6,height=6,units="in",r
es=300)
par(mar=c(5.1,4.3,4.1,4))

plot(modiswintermeans$Year,modiswintermeans$MW_AOD,ylim=c(0,0.5),type="l",col="darko
range3",lwd=3,xaxt="n",xlab="",ylab="",las=1,cex.axis=2,col.axis="darkorange3")
axis(side=1,at=seq(2007,2016,by=1),labels=F)
labs<-seq(2007,2016,by=1)
text(seq(2007,2016,by=1),par("usr")[3]-0.05,labels=labs,srt=45,xpd=T,cex=2,adj=c(0.7,0.5))
lines(aotwintermeans$Year,aotwintermeans$MW_AOD,type="l",lty=2,col="red3",lwd=3,xaxt="
n",xlab="",ylab="")
par(new=T)
plot(wwintermeans$Year,wwintermeans$bext,type="l",col="purple4",lwd=3,ylim=c(0,100),xaxt
="n",yaxt="n",xlab="",ylab="")
axis(side=4,las=1,cex.axis=2,col.axis="purple4")

legend("topright",legend=c("MODIS AOT","CALIPSO
AOT","Extinction"),col=c("darkorange3","red3","purple4"),lty=c(1,2,1),lwd=3)

dev.off()

########################
#Figure S5. Vertical profiles#
########################
```

```
allpress<-read.csv("C:/Users/stor/Documents/ALW and OC paper/2005-2016
analysis/newdata_alllevels/data 2001-2016/combined_2001-2016_allpressures.csv")
allpress$Date<-as.Date(as.character(allpress$Date),format="%m/%d/%Y")
allpress$year<-substring(allpress$Date,1,4)
allpress$Month<-substring(allpress$Date,6,7)
allpress$year<-as.numeric(allpress$year)
allpress$Month<-as.numeric(allpress$Month)
library(zoo)
yq<-as.yearqtr(as.yearmon(allpress$Date,"%Y-%m-%d")+1/12)
allpress$season<-
factor(format(yq,"%q"),levels=1:4,labels=c("winter","spring","summer","fall"))
allpress$Year<-ifelse(allpress$Month=="12",allpress$year+1,allpress$year) #to match DJF
assignments
allpress$LayerOrgWater<-as.numeric(as.character(allpress$LayerOrgWater))
allpress$Masswo<-as.numeric(as.character(allpress$Masswo))
allpress$totwater<-allpress$water+allpress$Masswo
allpress$PM25water<-allpress$water+allpress$Masswo+allpress$MF.Val
allpress2<-subset(allpress,totwater>0)
allpress2<-subset(allpress2,RH<0.95)

#merge with pbldata
pbldata<-read.csv("C:/Users/stor/Documents/ALW and OC paper/2005-2016
analysis/pbl_data/pbl-season-1.csv")
pbldata$Group.2<-as.Date(as.character(pbldata$Group.2),format="%m/%d/%Y")
pbldata$Date<-pbldata$Group.2
allpress3<-merge(pbldata,allpress2,by=c("Date","SiteCode"))
#now need to only keep data that is below the PBL
allpress3$BelowPBL<-ifelse(allpress3$Height>allpress3$PBL,NA,allpress3$Height)
completeFun<-function(allpress3,BelowPBL){
  completeVec<-complete.cases(allpress3[,BelowPBL])
  return(allpress3[completeVec,])
}
allpress4<-completeFun(allpress3,"BelowPBL")
west<-
subset(allpress4,allpress4$SiteCode=="BRCA1"|allpress4$SiteCode=="CANY1"|allpress4$Site
Code=="CAPI1"|allpress4$SiteCode=="MEVE1")
se<-
subset(allpress4,allpress4$SiteCode=="COHU1"|allpress4$SiteCode=="GRSM1"|allpress4$Site
Code=="LIGO1"|allpress4$SiteCode=="SHRO1")
se2<-subset(se,Year>=2007&Year<=2016)
sesummer<-subset(se2,season.x=="summer")
sesummer<-sesummer[sesummer$totwater<quantile(sesummer$totwater,0.95,na.rm=T),]
sewinter<-subset(se2,season.x=="winter")
sewinter<-sewinter[sewinter$totwater<quantile(sewinter$totwater,0.95,na.rm=T),]
west2<-subset(west,Year>=2007&Year<=2016)
wsummer<-subset(west2,season.x=="summer")
```

```
wsummer<-wsummer[wsummer$totwater<quantile(wsummer$totwater,0.95,na.rm=T),]
wwinter<-subset(west,season.x=="winter")
wwinter<-wwinter[wwinter$totwater<quantile(wwinter$totwater,0.95,na.rm=T),]

sesummer2<-subset(sesummer,sesummer$Height<939)
sewinter2<-subset(sewinter,sewinter$Height<842)

day<-subset(sesummer2,Date=="2011-08-31")
day$PM25water<-day$MF.Val+day$water+day$Masswo
cohuday<-subset(day,SiteCode=="COHU1")

day2<-subset(sewinter2,Date=="2011-12-08")
day2$PM25water<-day2$MF.Val+day2$water+day2$Masswo
cohuday2<-subset(day2,SiteCode=="COHU1")

jpeg("C:/Users/stor/Documents/ALW and OC paper/2005-2016 analysis/newdata_alllevels/data
2001-
2016/fixed_paper_plots/Appalachia_profiles_sameaxis.jpg",height=6,width=6,units="in",res=30
0)
par(mfrow=c(1,2))
plot(cohuday$MF.Val,cohuday$Height,type="l",xlim=c(0,31),ylim=c(100,800),las=1,lwd=3,col
="black",
    xlab="",ylab="",cex.axis=1.5,xaxt="n")
lines(cohuday$PM25water,cohuday$Height,lwd=3,col="dodgerblue2")
axis(side=1,at=seq(0,31,by=10),las=1,cex.axis=1.5)
plot(cohuday2$MF.Val,cohuday2$Height,type="l",xlim=c(0,31),ylim=c(100,800),las=1,lwd=3,c
ol="black",
    ylab="",xlab="",cex.axis=1.5,xaxt="n")
lines(cohuday2$PM25water,cohuday2$Height,lwd=3,col="dodgerblue2")
axis(side=1,at=seq(0,31,by=10),las=1,cex.axis=1.5)
legend("topright",legend=c(expression("Dry PM"[2.5]),expression("Dry PM"[2.5]~"+
ALW")),col=c("black","dodgerblue2"),lty=c(1,1),lwd=c(3,3),cex=0.9)
dev.off()

########################
#Figure S6. OM Pie charts#
########################

allpress<-read.csv("C:/Users/stor/Documents/ALW and OC paper/2005-2016
analysis/newdata_alllevels/data 2001-2016/combined_2001-2016_allpressures.csv")

allpress$Date<-as.Date(as.character(allpress$Date),format="%m/%d/%Y")
allpress$year<-substring(allpress$Date,1,4)
allpress$Month<-substring(allpress$Date,6,7)

allpress$year<-as.numeric(allpress$year)
```

```
allpress$Month<-as.numeric(allpress$Month)

library(zoo)
yq<-as.yearqtr(as.yearmon(allpress$Date,"%Y-%m-%d")+1/12)
allpress$season<-
factor(format(yq,"%q"),levels=1:4,labels=c("winter","spring","summer","fall"))
allpress$Year<-ifelse(allpress$Month=="12",allpress$year+1,allpress$year) #to match DJF
assignments

allpress$LayerOrgWater<-as.numeric(as.character(allpress$LayerOrgWater))
allpress$totwater<-(allpress$LayerOrgWater+allpress$LayerInorgWater)/1000

allpress2<-subset(allpress,totwater>0)
allpress2<-subset(allpress2,RH<0.95)

#merge with pbldata
pbldata<-read.csv("C:/Users/stor/Documents/ALW and OC paper/2005-2016
analysis/pbl_data/pbl-season-1.csv")
pbldata$Group.2<-as.Date(as.character(pbldata$Group.2),format="%m/%d/%Y")
pbldata$Date<-pbldata$Group.2
allpress3<-merge(pbldata,allpress2,by=c("Date","SiteCode"))
#now need to only keep data that is below the PBL
allpress3$BelowPBL<-ifelse(allpress3$Height>allpress3$PBL,NA,allpress3$Height)

completeFun<-function(allpress3,BelowPBL){
  completeVec<-complete.cases(allpress3[,BelowPBL])
  return(allpress3[completeVec,])
}

allpress4<-completeFun(allpress3,"BelowPBL")

west<-
subset(allpress4,allpress4$SiteCode=="BRCA1"|allpress4$SiteCode=="CANY1"|allpress4$Site
Code=="CAPI1"|allpress4$SiteCode=="MEVE1")
se<-
subset(allpress4,allpress4$SiteCode=="COHU1"|allpress4$SiteCode=="GRSM1"|allpress4$Site
Code=="LIGO1"|allpress4$SiteCode=="SHRO1")

se2<-subset(se,Year>=2007&Year<=2016)
se2<-subset(se2,pressure=="1000")
sesummer<-subset(se2,season.x=="summer")
sesummer<-sesummer[sesummer$totwater<quantile(sesummer$totwater,0.95,na.rm=T),]
sewinter<-subset(se2,season.x=="winter")
sewinter<-sewinter[sewinter$totwater<quantile(sewinter$totwater,0.95,na.rm=T),]
west2<-subset(west,Year>=2007&Year<=2016)
west2<-subset(west2,pressure=="1000")
```

```
wsummer<-subset(west2,season.x=="summer")
wsummer<-wsummer[wsummer$totwater<quantile(wsummer$totwater,0.95,na.rm=T),]
wwinter<-subset(west,season.x=="winter")
wwinter<-wwinter[wwinter$totwater<quantile(wwinter$totwater,0.95,na.rm=T),]

jpeg("C:/Users/stor/Documents/ALW and OC paper/2005-2016 analysis/newdata_alllevels/data
2001-2016/pie charts/surf_organic matter w.jpg",height=6,width=6,units="in",res=300)

slices<-c(mean(wsummer$OM1,na.rm=T),mean(wsummer$OM2,na.rm=T),
        mean(wsummer$OM3,na.rm=T),mean(wsummer$OM4,na.rm=T))
slices2<-c(mean(wwinter$OM1,na.rm=T),mean(wwinter$OM2,na.rm=T),
         mean(wwinter$OM3,na.rm=T),mean(wwinter$OM4,na.rm=T))
pct <- round(slices/sum(slices)*100)
pct2<-round(slices2/sum(slices2)*100)
lbls<-c("OM1","OM2","OM3","OM4")
cols<-c("palegreen","palegreen2","palegreen3","palegreen4")
lbls2<-c("OM1","OM2","OM3","OM4")
lbls<-paste(lbls,pct) #add percent to chart
lbls2<-paste(lbls2,pct2)
lbls <- paste(lbls,"%",sep="") # add % to labels
lbls2 <- paste(lbls2,"%",sep="") # add % to labels
par(mfrow=c(1,2)) #1 row, 2 columns
pie(slices, labels=NA, col=cols, xlab="",radius=(sum(slices)/2.194027)*0.8)#relative to mean
SES mass
#mtext(side=3, text="SE Summer vs Winter", line=1, adj=-4)
pie(slices2, labels=NA, col=cols, xlab="",radius=(sum(slices2)/2.194027)*0.8)#relative to mean
SES mass

dev.off()

#######################
#Figure S7. OM seasonality#
#######################

allpress<-read.csv("C:/Users/stor/Documents/ALW and OC paper/2005-2016
analysis/newdata_alllevels/data 2001-2016/combined_2001-2016_allpressures.csv")
allpress$Date<-as.Date(as.character(allpress$Date),format="%m/%d/%Y")
allpress$year<-substring(allpress$Date,1,4)
allpress$Month<-substring(allpress$Date,6,7)
allpress$year<-as.numeric(allpress$year)
allpress$Month<-as.numeric(allpress$Month)
library(zoo)
yq<-as.yearqtr(as.yearmon(allpress$Date,"%Y-%m-%d")+1/12)
allpress$season<-
factor(format(yq,"%q"),levels=1:4,labels=c("winter","spring","summer","fall"))
```

```
allpress$Year<-ifelse(allpress$Month=="12",allpress$year+1,allpress$year) #to match DJF
assignments
allpress$Masswo<-as.numeric(as.character(allpress$Masswo))
allpress$totwater<-allpress$water+allpress$Masswo
allpress<-subset(allpress,allpress$totwater>0)
allpress2<-subset(allpress,allpress$pressure=="1000")

west<-
subset(allpress2,allpress2$SiteCode=="BRCA1"|allpress2$SiteCode=="CANY1"|allpress2$Site
Code=="CAPI1"|allpress2$SiteCode=="MEVE1")
se<-
subset(allpress2,allpress2$SiteCode=="COHU1"|allpress2$SiteCode=="GRSM1"|allpress2$Site
Code=="LIGO1"|allpress2$SiteCode=="SHRO1")
se2<-subset(se,Year>=2007&Year<=2016)
west2<-subset(west,Year>=2007&Year<=2016)
west3<-aggregate(west2,by=list(west2$year,west2$Month),FUN="mean",na.rm=T)
se3<-aggregate(se2,by=list(se2$year,se2$Month),FUN="mean",na.rm=T)

se4<-subset(se3,se3$RH<0.95)
west4<-subset(west3,west3$RH<0.95)
se4<-se4[se4$totwater<quantile(se4$totwater,0.95),]
west4<-west4[west4$totwater<quantile(west4$totwater,0.95),]

se4<-subset(se4,OMtot<9)#removing one heck of an outlier

###unrelated
sesummer<-subset(se4,se4$Month=="6"|se4$Month=="7"|se4$Month=="8")
sewinter<-subset(se4,se4$Month=="12"|se4$Month=="1"|se4$Month=="2")
wsummer<-subset(west4,west4$Month=="6"|west4$Month=="7"|west4$Month=="8")
wwinter<-subset(west4,west4$Month=="12"|west4$Month=="1"|west4$Month=="2")
wilcox.test(sesummer$OMtot,sewinter$OMtot,alternative="two.sided")
wilcox.test(wsummer$OMtot,wwinter$OMtot,alternative="two.sided")
wilcox.test(sesummer$OM1,sewinter$OM1,alternative="two.sided")
wilcox.test(wsummer$OM1,wwinter$OM1,alternative="two.sided")
wilcox.test(sesummer$OM2,sewinter$OM2,alternative="two.sided")
wilcox.test(wsummer$OM2,wwinter$OM2,alternative="two.sided")
wilcox.test(sesummer$OM3,sewinter$OM3,alternative="two.sided")
wilcox.test(wsummer$OM3,wwinter$OM3,alternative="two.sided")
wilcox.test(sesummer$OM4,sewinter$OM4,alternative="two.sided")
wilcox.test(wsummer$OM4,wwinter$OM4,alternative="two.sided")
t.test(sesummer$OMtot,sewinter$OMtot,alternative="two.sided")
t.test(wsummer$OMtot,wwinter$OMtot,alternative="two.sided")
t.test(sesummer$OM1,sewinter$OM1,alternative="two.sided")
t.test(wsummer$OM1,wwinter$OM1,alternative="two.sided")
t.test(sesummer$OM2,sewinter$OM2,alternative="two.sided")
t.test(wsummer$OM2,wwinter$OM2,alternative="two.sided")
```

```
t.test(sesummer$OM3,sewinter$OM3,alternative="two.sided")
t.test(wsummer$OM3,wwinter$OM3,alternative="two.sided")
t.test(sesummer$OM4,sewinter$OM4,alternative="two.sided")
t.test(wsummer$OM4,wwinter$OM4,alternative="two.sided")
###

#plots
jpeg("C:/Users/stor/Documents/ALW and OC paper/2005-2016 analysis/newdata_alllevels/data
2001-2016/om seasonality/OMtot.jpg",height=6,width=6,units="in",res=300)
i<-order(se4$Date)
lo.pred<-predict(loess(se4$OMtot~as.numeric(se4$Date),span=0.1),na.action=na.exclude)
plot(se4$Date[i],lo.pred[i],type="l",ylim=c(0,3.5),lwd=3,las=1,ylab="OMtot",xlab="Date",cex.a
xis=1.5,cex.lab=1.5)
i<-order(west4$Date)
lo.pred<-predict(loess(west4$OMtot~as.numeric(west4$Date),span=0.1),na.action=na.exclude)
lines(west4$Date[i],lo.pred[i],type="l",col="blue",lwd=3)
legend("topright",legend=c("SE","W"),col=c("black","blue"),lty=c(1,1),lwd=c(3,3),cex=1.5)
dev.off()

jpeg("C:/Users/stor/Documents/ALW and OC paper/2005-2016 analysis/newdata_alllevels/data
2001-2016/om seasonality/OM1.jpg",height=6,width=6,units="in",res=300)
i<-order(se4$Date)
lo.pred<-predict(loess(se4$OM1~as.numeric(se4$Date),span=0.1),na.action=na.exclude)
plot(se4$Date[i],lo.pred[i],type="l",ylim=c(0,1.5),lwd=3,las=1,ylab="OM1",xlab="Date",cex.axi
s=1.5,cex.lab=1.5)
i<-order(west4$Date)
lo.pred<-predict(loess(west4$OM1~as.numeric(west4$Date),span=0.1),na.action=na.exclude)
lines(west4$Date[i],lo.pred[i],type="l",col="blue",lwd=3)
legend("topright",legend=c("SE","W"),col=c("black","blue"),lty=c(1,1),lwd=c(3,3),cex=1.5)
dev.off()

jpeg("C:/Users/stor/Documents/ALW and OC paper/2005-2016 analysis/newdata_alllevels/data
2001-2016/om seasonality/OM2.jpg",height=6,width=6,units="in",res=300)
i<-order(se4$Date)
lo.pred<-predict(loess(se4$OM2~as.numeric(se4$Date),span=0.1),na.action=na.exclude)
plot(se4$Date[i],lo.pred[i],type="l",ylim=c(0,1.5),lwd=3,las=1,ylab="OM2",xlab="Date",cex.axi
s=1.5,cex.lab=1.5)
i<-order(west4$Date)
lo.pred<-predict(loess(west4$OM2~as.numeric(west4$Date),span=0.1),na.action=na.exclude)
lines(west4$Date[i],lo.pred[i],type="l",col="blue",lwd=3)
legend("topright",legend=c("SE","W"),col=c("black","blue"),lty=c(1,1),lwd=c(3,3),cex=1.5)
dev.off()

jpeg("C:/Users/stor/Documents/ALW and OC paper/2005-2016 analysis/newdata_alllevels/data
2001-2016/om seasonality/OM3.jpg",height=6,width=6,units="in",res=300)
i<-order(se4$Date)
```

```
lo.pred<-predict(loess(se4$OM3~as.numeric(se4$Date),span=0.1),na.action=na.exclude)
plot(se4$Date[i],lo.pred[i],type="l",ylim=c(0,1.5),lwd=3,las=1,ylab="OM3",xlab="Date",cex.axi
s=1.5,cex.lab=1.5)
i<-order(west4$Date)
lo.pred<-predict(loess(west4$OM3~as.numeric(west4$Date),span=0.1),na.action=na.exclude)
lines(west4$Date[i],lo.pred[i],type="l",col="blue",lwd=3)
legend("topright",legend=c("SE","W"),col=c("black","blue"),lty=c(1,1),lwd=c(3,3),cex=1.5)
dev.off()

jpeg("C:/Users/stor/Documents/ALW and OC paper/2005-2016 analysis/newdata_alllevels/data
2001-2016/om seasonality/OM4.jpg",height=6,width=6,units="in",res=300)
i<-order(se4$Date)
lo.pred<-predict(loess(se4$OM4~as.numeric(se4$Date),span=0.1),na.action=na.exclude)
plot(se4$Date[i],lo.pred[i],type="l",ylim=c(0,1.5),lwd=3,las=1,ylab="OM4",xlab="Date",cex.axi
s=1.5,cex.lab=1.5)
i<-order(west4$Date)
lo.pred<-predict(loess(west4$OM4~as.numeric(west4$Date),span=0.1),na.action=na.exclude)
lines(west4$Date[i],lo.pred[i],type="l",col="blue",lwd=3)
legend("topright",legend=c("SE","W"),col=c("black","blue"),lty=c(1,1),lwd=c(3,3),cex=1.5)
dev.off()

########################
#Figure S8. OC seasonality#
########################

#plots for OC instead
jpeg("C:/Users/stor/Documents/ALW and OC paper/2005-2016 analysis/newdata_alllevels/data
2001-2016/om seasonality/OCtot.jpg",height=6,width=6,units="in",res=300)
i<-order(se4$Date)
lo.pred<-predict(loess(se4$OCtot~as.numeric(se4$Date),span=0.1),na.action=na.exclude)
plot(se4$Date[i],lo.pred[i],type="l",ylim=c(0,3.5),lwd=3,las=1,ylab="OCtot",xlab="Date",cex.a
xis=1.5,cex.lab=1.5)
i<-order(west4$Date)
lo.pred<-predict(loess(west4$OCtot~as.numeric(west4$Date),span=0.1),na.action=na.exclude)
lines(west4$Date[i],lo.pred[i],type="l",col="blue",lwd=3)
legend("topright",legend=c("SE","W"),col=c("black","blue"),lty=c(1,1),lwd=c(3,3),cex=1.5)
dev.off()

jpeg("C:/Users/stor/Documents/ALW and OC paper/2005-2016 analysis/newdata_alllevels/data
2001-2016/om seasonality/OC1.jpg",height=6,width=6,units="in",res=300)
i<-order(se4$Date)
lo.pred<-predict(loess(se4$OC1f.Value~as.numeric(se4$Date),span=0.1),na.action=na.exclude)
plot(se4$Date[i],lo.pred[i],type="l",ylim=c(0,1.5),lwd=3,las=1,ylab="OC1",xlab="Date",cex.axi
s=1.5,cex.lab=1.5)
i<-order(west4$Date)
```

```
lo.pred<-
predict(loess(west4$OC1f.Value~as.numeric(west4$Date),span=0.1),na.action=na.exclude)
lines(west4$Date[i],lo.pred[i],type="l",col="blue",lwd=3)
legend("topright",legend=c("SE","W"),col=c("black","blue"),lty=c(1,1),lwd=c(3,3),cex=1.5)
dev.off()

jpeg("C:/Users/stor/Documents/ALW and OC paper/2005-2016 analysis/newdata_alllevels/data
2001-2016/om seasonality/OC2.jpg",height=6,width=6,units="in",res=300)
i<-order(se4$Date)
lo.pred<-predict(loess(se4$OC2f.Value~as.numeric(se4$Date),span=0.1),na.action=na.exclude)
plot(se4$Date[i],lo.pred[i],type="l",ylim=c(0,1.5),lwd=3,las=1,ylab="OC2",xlab="Date",cex.axi
s=1.5,cex.lab=1.5)
i<-order(west4$Date)
lo.pred<-
predict(loess(west4$OC2f.Value~as.numeric(west4$Date),span=0.1),na.action=na.exclude)
lines(west4$Date[i],lo.pred[i],type="l",col="blue",lwd=3)
legend("topright",legend=c("SE","W"),col=c("black","blue"),lty=c(1,1),lwd=c(3,3),cex=1.5)
dev.off()

jpeg("C:/Users/stor/Documents/ALW and OC paper/2005-2016 analysis/newdata_alllevels/data
2001-2016/om seasonality/OC3.jpg",height=6,width=6,units="in",res=300)
i<-order(se4$Date)
lo.pred<-predict(loess(se4$OC3f.Value~as.numeric(se4$Date),span=0.1),na.action=na.exclude)
plot(se4$Date[i],lo.pred[i],type="l",ylim=c(0,1.5),lwd=3,las=1,ylab="OC3",xlab="Date",cex.axi
s=1.5,cex.lab=1.5)
i<-order(west4$Date)
lo.pred<-
predict(loess(west4$OC3f.Value~as.numeric(west4$Date),span=0.1),na.action=na.exclude)
lines(west4$Date[i],lo.pred[i],type="l",col="blue",lwd=3)
legend("topright",legend=c("SE","W"),col=c("black","blue"),lty=c(1,1),lwd=c(3,3),cex=1.5)
dev.off()

jpeg("C:/Users/stor/Documents/ALW and OC paper/2005-2016 analysis/newdata_alllevels/data
2001-2016/om seasonality/OC4.jpg",height=6,width=6,units="in",res=300)
i<-order(se4$Date)
lo.pred<-predict(loess(se4$OC4f.Value~as.numeric(se4$Date),span=0.1),na.action=na.exclude)
plot(se4$Date[i],lo.pred[i],type="l",ylim=c(0,1.5),lwd=3,las=1,ylab="OC4",xlab="Date",cex.axi
s=1.5,cex.lab=1.5)
i<-order(west4$Date)
lo.pred<-
predict(loess(west4$OC4f.Value~as.numeric(west4$Date),span=0.1),na.action=na.exclude)
lines(west4$Date[i],lo.pred[i],type="l",col="blue",lwd=3)
legend("topright",legend=c("SE","W"),col=c("black","blue"),lty=c(1,1),lwd=c(3,3),cex=1.5)
dev.off()
```

```
##################################
#Figure S9. Aerosol water path vs AOT#
##################################

modis<-read.csv("C:/Users/stor/Documents/ALW and OC paper/2005-2016
analysis/newdata_alllevels/modis_aod_month.csv")
modis$SE_AOD_low<-modis$SE_AOD-modis$SE_AOD_SD
modis$SE_AOD_hi<-modis$SE_AOD+modis$SE_AOD_SD
modis$MW_AOD_low<-modis$MW_AOD-modis$MW_AOD_SD
modis$MW_AOD_hi<-modis$MW_AOD+modis$MW_AOD_SD
modis$Year<-ifelse(modis$Month=="12",modis$Year<-
as.numeric(modis$year)+1,modis$Year<-modis$year)
aotsummer<-subset(modis,Month=="6"|Month=="7"|Month=="8")
aotwinter<-subset(modis,Month=="12"|Month=="1"|Month=="2")
aotsummermeans<-aggregate(aotsummer,by=list(aotsummer$Year),FUN="mean",na.rm=T)
aotwintermeans<-aggregate(aotwinter,by=list(aotwinter$Year),FUN="mean",na.rm=T)



kapint<-read.csv("C:/Users/stor/Documents/ALW and OC paper/2005-2016
analysis/newdata_alllevels/data 2001-2016/focus_2001-2016_intunder95-1.csv")
kapint<-read.csv("C:/Users/Amy/Desktop/Research/ALW and OC/ALW and OC paper/2005-
2016 analysis/data 2001-2016/focus_2001-2016_intunder95-1.csv")
kapint$Date<-as.Date(as.character(kapint$Date),format="%m/%d/%Y")
kapint$Year<-ifelse(kapint$Month=="12",kapint$Year<-
as.numeric(kapint$year)+1,kapint$Year<-kapint$year)
library(zoo)
yq<-as.yearqtr(as.yearmon(kapint$Date,"%Y-%m-%d")+1/12)
kapint$season<-factor(format(yq,"%q"),levels=1:4,labels=c("winter","spring","summer","fall"))

kapint$totwater<-(kapint$alw_org_fixed+kapint$alw_inorg)/1000
kapint$totwater_L<-(kapint$alw_low_fixed+kapint$alw_inorg)/1000
kapint$totwater_H<-(kapint$alw_high_fixed+kapint$alw_inorg)/1000

kapint$PMwater<-(kapint$MF.Val/1000)+kapint$totwater
kapint$PMwater_L<-(kapint$MF.Val/1000)+kapint$totwater_L
kapint$PMwater_H<-(kapint$MF.Val/1000)+kapint$totwater_H

kapint$totwater_0.01<-(kapint$alw_0.01+kapint$alw_inorg)/1000
kapint$totwater_0.1<-(kapint$alw_0.1+kapint$alw_inorg)/1000
kapint$totwater_0.15<-(kapint$alw_0.15+kapint$alw_inorg)/1000
kapint$totwater_0.2<-(kapint$alw_0.2+kapint$alw_inorg)/1000
kapint$PMwater_0.01<-(kapint$MF.Val/1000)+kapint$totwater_0.01
kapint$PMwater_0.1<-(kapint$MF.Val/1000)+kapint$totwater_0.1
kapint$PMwater_0.15<-(kapint$MF.Val/1000)+kapint$totwater_0.15
kapint$PMwater_0.2<-(kapint$MF.Val/1000)+kapint$totwater_0.2
```

```
kapint$PMinorg<-(kapint$MF.Val+kapint$alw_inorg)/1000

kapint$alw_inorg<-kapint$alw_inorg/1000
kapint$alw_org_fixed<-kapint$alw_org_fixed/1000
kapint$NO3<-kapint$NO3/1000
kapint$SO4<-kapint$SO4/1000
kapint$OMtot<-kapint$OMtot/1000
kapint$PM25<-kapint$MF.Val/1000
kapint$OM1<-kapint$OM1/1000
kapint$OM2<-kapint$OM2/1000
kapint$OM3<-kapint$OM3/1000
kapint$OM4<-kapint$OM4/1000

kapint2<-subset(kapint,Year>=2007&Year<=2016)
kapint3<-subset(kapint,season=="summer"|season=="winter")
brca<-subset(kapint3,SiteCode=="BRCA1")
cany<-subset(kapint3,SiteCode=="CANY1")
capi<-subset(kapint3,SiteCode=="CAPI1")
meve<-subset(kapint3,SiteCode=="MEVE1")
cohu<-subset(kapint3,SiteCode=="COHU1")
grsm<-subset(kapint3,SiteCode=="GRSM1")
ligo<-subset(kapint3,SiteCode=="LIGO1")
shro<-subset(kapint3,SiteCode=="SHRO1")

#summer and winter by site
brcasummer<-subset(brca,season=="summer")
brcasummer<-
brcasummer[brcasummer$totwater<quantile(brcasummer$totwater,0.95,na.rm=T),]
brcawinter<-subset(brca,season=="winter")
brcawinter<-brcawinter[brcawinter$totwater<quantile(brcawinter$totwater,0.95,na.rm=T),]

canysummer<-subset(cany,season=="summer")
canysummer<-
canysummer[canysummer$totwater<quantile(canysummer$totwater,0.95,na.rm=T),]
canywinter<-subset(cany,season=="winter")
canywinter<-canywinter[canywinter$totwater<quantile(canywinter$totwater,0.95,na.rm=T),]

capisummer<-subset(capi,season=="summer")
capisummer<-
capisummer[capisummer$totwater<quantile(capisummer$totwater,0.95,na.rm=T),]
capiwinter<-subset(capi,season=="winter")
capiwinter<-capiwinter[capiwinter$totwater<quantile(capiwinter$totwater,0.95,na.rm=T),]

mevesummer<-subset(meve,season=="summer")
```

```
mevesummer<-
mevesummer[mevesummer$totwater<quantile(mevesummer$totwater,0.95,na.rm=T),]
mevewinter<-subset(meve,season=="winter")
mevewinter<-mevewinter[mevewinter$totwater<quantile(mevewinter$totwater,0.95,na.rm=T),]

cohusummer<-subset(cohu,season=="summer")
cohusummer<-
cohusummer[cohusummer$totwater<quantile(cohusummer$totwater,0.95,na.rm=T),]
cohuwinter<-subset(cohu,season=="winter")
cohuwinter<-cohuwinter[cohuwinter$totwater<quantile(cohuwinter$totwater,0.95,na.rm=T),]

grsmsummer<-subset(grsm,season=="summer")
grsmsummer<-
grsmsummer[grsmsummer$totwater<quantile(grsmsummer$totwater,0.95,na.rm=T),]
grsmwinter<-subset(grsm,season=="winter")
grsmwinter<-grsmwinter[grsmwinter$totwater<quantile(grsmwinter$totwater,0.95,na.rm=T),]

ligosummer<-subset(ligo,season=="summer")
ligosummer<-ligosummer[ligosummer$totwater<quantile(ligosummer$totwater,0.95,na.rm=T),]
ligowinter<-subset(ligo,season=="winter")
ligowinter<-ligowinter[ligowinter$totwater<quantile(ligowinter$totwater,0.95,na.rm=T),]

shrosummer<-subset(shro,season=="summer")
shrosummer<-
shrosummer[shrosummer$totwater<quantile(shrosummer$totwater,0.95,na.rm=T),]
shrowinter<-subset(shro,season=="winter")
shrowinter<-shrowinter[shrowinter$totwater<quantile(shrowinter$totwater,0.95,na.rm=T),]

#aggregate by year for each site
brcasummermeans<-aggregate(brcasummer,by=list(brcasummer$Year),FUN="mean",na.rm=T)
brcawintermeans<-aggregate(brcawinter,by=list(brcawinter$Year),FUN="mean",na.rm=T)
canysummermeans<-
aggregate(canysummer,by=list(canysummer$Year),FUN="mean",na.rm=T)
canywintermeans<-aggregate(canywinter,by=list(canywinter$Year),FUN="mean",na.rm=T)
capisummermeans<-aggregate(capisummer,by=list(capisummer$Year),FUN="mean",na.rm=T)
capiwintermeans<-aggregate(capiwinter,by=list(capiwinter$Year),FUN="mean",na.rm=T)
mevesummermeans<-
aggregate(mevesummer,by=list(mevesummer$Year),FUN="mean",na.rm=T)
mevewintermeans<-aggregate(mevewinter,by=list(mevewinter$Year),FUN="mean",na.rm=T)
cohusummermeans<-
aggregate(cohusummer,by=list(cohusummer$Year),FUN="mean",na.rm=T)
cohuwintermeans<-aggregate(cohuwinter,by=list(cohuwinter$Year),FUN="mean",na.rm=T)
grsmsummermeans<-
aggregate(grsmsummer,by=list(grsmsummer$Year),FUN="mean",na.rm=T)
grsmwintermeans<-aggregate(grsmwinter,by=list(grsmwinter$Year),FUN="mean",na.rm=T)
ligosummermeans<-aggregate(ligosummer,by=list(ligosummer$Year),FUN="mean",na.rm=T)
```

```
ligowintermeans<-aggregate(ligowinter,by=list(ligowinter$Year),FUN="mean",na.rm=T)
shrosummermeans<-aggregate(shrosummer,by=list(shrosummer$Year),FUN="mean",na.rm=T)
shrowintermeans<-aggregate(shrowinter,by=list(shrowinter$Year),FUN="mean",na.rm=T)

brcameans<-aggregate(brca,by=list(brca$Month,brca$Year),FUN="mean",na.rm=T)
canymeans<-aggregate(cany,by=list(cany$Month,cany$Year),FUN="mean",na.rm=T)
capimeans<-aggregate(capi,by=list(capi$Month,capi$Year),FUN="mean",na.rm=T)
mevemeans<-aggregate(meve,by=list(meve$Month,meve$Year),FUN="mean",na.rm=T)
cohumeans<-aggregate(cohu,by=list(cohu$Month,cohu$Year),FUN="mean",na.rm=T)
grsmmeans<-aggregate(grsm,by=list(grsm$Month,grsm$Year),FUN="mean",na.rm=T)
ligomeans<-aggregate(ligo,by=list(ligo$Month,ligo$Year),FUN="mean",na.rm=T)
shromeans<-aggregate(shro,by=list(shro$Month,shro$Year),FUN="mean",na.rm=T)
modis2<-
subset(modis,Month=="12"|Month=="1"|Month=="2"|Month=="6"|Month=="7"|Month=="8")
modis2$Year<-ifelse(modis2$Month=="12",modis2$Year<-
as.numeric(modis2$year)+1,modis2$Year<-modis2$year)
modis2$Group.2<-modis2$Year
modis2$Group.1<-modis2$Month
brcaintmeans<-merge(brcameans,modis2,by=c("Group.1","Group.2"))
brcaintmeanssummer<-
subset(brcaintmeans,brcaintmeans$Group.1==6|brcaintmeans$Group.1==7|brcaintmeans$Group.
1==8)
brcaintmeanssummer$AOT<-brcaintmeanssummer$BRCA1
brcaintmeanswinter<-
subset(brcaintmeans,brcaintmeans$Group.1==12|brcaintmeans$Group.1==1|brcaintmeans$Grou
p.1==2)
brcaintmeanswinter$AOT<-brcaintmeanswinter$BRCA1

canyintmeans<-merge(canymeans,modis2,by=c("Group.1","Group.2"))
canyintmeanssummer<-
subset(canyintmeans,canyintmeans$Group.1==6|canyintmeans$Group.1==7|canyintmeans$Grou
p.1==8)
canyintmeanssummer$AOT<-canyintmeanssummer$CANY1
canyintmeanswinter<-
subset(canyintmeans,canyintmeans$Group.1==12|canyintmeans$Group.1==1|canyintmeans$Gro
up.1==2)
canyintmeanswinter$AOT<-canyintmeanswinter$CANY1

capiintmeans<-merge(capimeans,modis2,by=c("Group.1","Group.2"))
capiintmeanssummer<-
subset(capiintmeans,capiintmeans$Group.1==6|capiintmeans$Group.1==7|capiintmeans$Group.
1==8)
capiintmeanssummer$AOT<-capiintmeanssummer$CAPI1
capiintmeanswinter<-
subset(capiintmeans,capiintmeans$Group.1==12|capiintmeans$Group.1==1|capiintmeans$Grou
p.1==2)
```

```
capiintmeanswinter$AOT<-capiintmeanswinter$CAPI1

meveintmeans<-merge(mevemeans,modis2,by=c("Group.1","Group.2"))
meveintmeanssummer<-
subset(meveintmeans,meveintmeans$Group.1==6|meveintmeans$Group.1==7|meveintmeans$G
roup.1==8)
meveintmeanssummer$AOT<-meveintmeanssummer$MEVE1
meveintmeanswinter<-
subset(meveintmeans,meveintmeans$Group.1==12|meveintmeans$Group.1==1|meveintmeans$
Group.1==2)
meveintmeanswinter$AOT<-meveintmeanswinter$MEVE1

cohuintmeans<-merge(cohumeans,modis2,by=c("Group.1","Group.2"))
cohuintmeanssummer<-
subset(cohuintmeans,cohuintmeans$Group.1==6|cohuintmeans$Group.1==7|cohuintmeans$Gro
up.1==8)
cohuintmeanssummer$AOT<-cohuintmeanssummer$COHU1
cohuintmeanswinter<-
subset(cohuintmeans,cohuintmeans$Group.1==12|cohuintmeans$Group.1==1|cohuintmeans$Gr
oup.1==2)
cohuintmeanswinter$AOT<-cohuintmeanswinter$COHU1

grsmintmeans<-merge(grsmmeans,modis2,by=c("Group.1","Group.2"))
grsmintmeanssummer<-
subset(grsmintmeans,grsmintmeans$Group.1==6|grsmintmeans$Group.1==7|grsmintmeans$Gro
up.1==8)
grsmintmeanssummer$AOT<-grsmintmeanssummer$GRSM1
grsmintmeanswinter<-
subset(grsmintmeans,grsmintmeans$Group.1==12|grsmintmeans$Group.1==1|grsmintmeans$Gr
oup.1==2)
grsmintmeanswinter$AOT<-grsmintmeanswinter$GRSM1

ligointmeans<-merge(ligomeans,modis2,by=c("Group.1","Group.2"))
ligointmeanssummer<-
subset(ligointmeans,ligointmeans$Group.1==6|ligointmeans$Group.1==7|ligointmeans$Group.1
==8)
ligointmeanssummer$AOT<-ligointmeanssummer$LIGO1
ligointmeanswinter<-
subset(ligointmeans,ligointmeans$Group.1==12|ligointmeans$Group.1==1|ligointmeans$Group.
1==2)
ligointmeanswinter$AOT<-ligointmeanswinter$LIGO1

shrointmeans<-merge(shromeans,modis2,by=c("Group.1","Group.2"))
shrointmeanssummer<-
subset(shrointmeans,shrointmeans$Group.1==6|shrointmeans$Group.1==7|shrointmeans$Group.
1==8)
```

```
shrointmeanssummer$AOT<-shrointmeanssummer$SHRO1
shrointmeanswinter<-
subset(shrointmeans,shrointmeans$Group.1==12|shrointmeans$Group.1==1|shrointmeans$Grou
p.1==2)
shrointmeanswinter$AOT<-shrointmeanswinter$SHRO1


newdf2<-
rbind(cohuintmeanssummer,grsmintmeanssummer,ligointmeanssummer,shrointmeanssummer)

jpeg("C:/Users/stor/Documents/ALW and OC paper/2005-2016 analysis/newdata_alllevels/data
2001-2016/reviewer_plots/app_sites_totwater.jpg",width=6,height=6,units="in",res=300)

plot(newdf2$totwater,newdf2$AOT,pch=16,cex=1,col="firebrick2",xlim=c(0,25),xaxt="n",ylim
=c(0,0.62),yaxt="n",las=1,xlab="",ylab="",main="",cex.main=1.5,cex.axis=1.2,cex.lab=1.3)
axis(side=1,at=seq(0,25,by=5),las=1,cex.axis=1.5)
axis(side=2,at=seq(0,0.62,by=0.1),las=1,cex.axis=1.5)
arrows(newdf2$totwater_L,newdf2$AOT,newdf2$totwater_H,newdf2$AOT,
     length=0.05,angle=90,code=3,col=adjustcolor("firebrick2",alpha.f=0.5),lwd=2)
#title(ylab=expression("Column AOT"),line=3.1,cex.lab=1.3)
#mtext("a) TOM ALW",side=3,line=-2,cex=1.5,adj=0.01)
points(newdf3$totwater,newdf3$AOT,pch=16,cex=1,col="mediumblue",xlab="",xaxt="n",ylab=
"",main="")
arrows(newdf3$totwater_L,newdf3$AOT,newdf3$totwater_H,newdf3$AOT,
     length=0.05,angle=90,code=3,col=adjustcolor("mediumblue",alpha.f=0.5),lwd=2)

legend("bottomright",legend=c("AS","AW"),col=c("firebrick2","mediumblue"),pch=c(16,16),ce
x=1.5)

linfit<-lm(newdf2$AOT~newdf2$totwater)
summary(linfit)
abline(linfit,lwd=3)

linfit2<-lm(newdf3$AOT~newdf3$totwater)
summary(linfit2)
abline(linfit2,lwd=3,col="gray50")

dev.off()


newdf<-
rbind(brcaintmeanssummer,canyintmeanssummer,capiintmeanssummer,meveintmeanssummer)

jpeg("C:/Users/stor/Documents/ALW and OC paper/2005-2016 analysis/newdata_alllevels/data
2001-2016/reviewer_plots/cop_sites_totwater.jpg",width=6,height=6,units="in",res=300)
```

```
plot(newdf$totwater,newdf$AOT,pch=22,cex=1,col="firebrick2",xlim=c(0,3),xaxt="n",ylim=c(
0,0.3),yaxt="n",las=1,xlab="",ylab="",main="",cex.main=1.5,cex.axis=1.2,cex.lab=1.3)
axis(side=1,at=seq(0,3,by=1),las=1,cex.axis=1.5)
axis(side=2,at=seq(0,0.3,by=0.05),las=1,cex.axis=1.5)
arrows(newdf$totwater_L,newdf$AOT,newdf$totwater_H,newdf$AOT,
     length=0.05,angle=90,code=3,col=adjustcolor("firebrick2",alpha.f=0.5),lwd=2)
#title(ylab=expression("Column AOT"),line=3.1,cex.lab=1.3)
#mtext("a) TOM ALW",side=3,line=-2,cex=1.5,adj=0.01)
points(newdf1$totwater,newdf1$AOT,pch=22,cex=1,col="mediumblue",xlab="",xaxt="n",ylab=
"",main="")
arrows(newdf1$totwater_L,newdf1$AOT,newdf1$totwater_H,newdf1$AOT,
     length=0.05,angle=90,code=3,col=adjustcolor("mediumblue",alpha.f=0.5),lwd=2)

legend("bottomright",legend=c("CPS","CPW"),col=c("firebrick2","mediumblue"),pch=c(22,22),
cex=1.5)

linfit<-lm(newdf$AOT~newdf$totwater)
summary(linfit)
abline(linfit,lwd=3)

linfit2<-lm(newdf1$AOT~newdf1$totwater)
summary(linfit2)
abline(linfit2,lwd=3,col="gray50")

dev.off()
```

# APPENDIX E

## R CODE FOR CHAPTER 3

```
#Cloudy vs Clear Sky PM2.5 chemical constituent differences
#Code for all figures and tables

#Main Paper

##############################
#Figure 1. Eastern US comparisons#
##############################

cmetschem<-read.csv("C:/Users/stor/Documents/Satellites/eastern_combo_isotest.csv")

#break into seasons
dfrmwinter<-subset(cmetschem,Month=="12"|Month=="1"|Month=="2")
dfrmspring<-subset(cmetschem,Month=="3"|Month=="4"|Month=="5")
dfrmsummer<-subset(cmetschem,Month=="6"|Month=="7"|Month=="8")
dfrmfall<-subset(cmetschem,Month=="9"|Month=="10"|Month=="11")

#winter boxplot
jpeg("C:/Users/stor/Documents/Satellites/new_water_test/EasternTEST_Winter.jpg",height=6,w
idth=6,units="in",res=300)
boxplot(dfrmwinter$water_sun,dfrmwinter$water_cloud,dfrmwinter$water_test,las=1,cex.axis=
2,ylim=c(0,8),

na.action=na.exclude,medcol="black",col=c("gold3","deepskyblue3","green4"),outline=F,yaxt="
n",xaxt="n",varwidth=T)
axis(side=2,at=seq(0,8,by=2),line=-0.8,cex.axis=2,tick=F,las=1)
title("Eastern US Winter",line=1,cex.main=2)
axis(side=1,at=seq(1,3,by=1),labels=c("Clear
Sky","Cloudy","Mixed"),line=0,cex.axis=1.5,tick=F)
dev.off()

#spring boxplot
jpeg("C:/Users/stor/Documents/Satellites/new_water_test/EasternTEST_Spring.jpg",height=6,wi
dth=6,units="in",res=300)
boxplot(dfrmspring$water_sun,dfrmspring$water_cloud,dfrmspring$water_test,las=1,cex.axis=2
,ylim=c(0,8),

na.action=na.exclude,medcol="black",col=c("gold3","deepskyblue3","green4"),outline=F,yaxt="
n",xaxt="n",varwidth=T)
```

```
axis(side=2,at=seq(0,8,by=2),line=-0.8,cex.axis=2,tick=F,las=1)
title("Eastern US Spring",line=1,cex.main=2)
axis(side=1,at=seq(1,3,by=1),labels=c("Clear
Sky","Cloudy","Mixed"),line=0,cex.axis=1.5,tick=F)
dev.off()

#summer boxplot
jpeg("C:/Users/stor/Documents/Satellites/new_water_test/EasternTEST_Summer.jpg",height=6,
width=6,units="in",res=300)
boxplot(dfrmsummer$water_sun,dfrmsummer$water_cloud,dfrmsummer$water_test,las=1,cex.a
xis=2,ylim=c(0,8),

na.action=na.exclude,medcol="black",col=c("gold3","deepskyblue3","green4"),outline=F,yaxt="
n",xaxt="n",varwidth=T)
axis(side=2,at=seq(0,8,by=2),line=-0.8,cex.axis=2,tick=F,las=1)
title("Eastern US Summer",line=1,cex.main=2)
axis(side=1,at=seq(1,3,by=1),labels=c("Clear
Sky","Cloudy","Mixed"),line=0,cex.axis=1.5,tick=F)
dev.off()

#fall boxplot
jpeg("C:/Users/stor/Documents/Satellites/new_water_test/EasternTEST_Fall.jpg",height=6,widt
h=6,units="in",res=300)
boxplot(dfrmfall$water_sun,dfrmfall$water_cloud,dfrmfall$water_test,las=1,cex.axis=2,ylim=c(
0,8),

na.action=na.exclude,medcol="black",col=c("gold3","deepskyblue3","green4"),outline=F,yaxt="
n",xaxt="n",varwidth=T)
axis(side=2,at=seq(0,8,by=2),line=-0.8,cex.axis=2,tick=F,las=1)
title("Eastern US Fall",line=1,cex.main=2)
axis(side=1,at=seq(1,3,by=1),labels=c("Clear
Sky","Cloudy","Mixed"),line=0,cex.axis=1.5,tick=F)
dev.off()

#significance tests
#cloudy vs sunny
wilcox.test(dfrmwinter$water_sun,dfrmwinter$water_cloud,alternative="two.sided")
wilcox.test(dfrmspring$water_sun,dfrmspring$water_cloud,alternative="two.sided")
wilcox.test(dfrmsummer$water_sun,dfrmsummer$water_cloud,alternative="two.sided")
wilcox.test(dfrmfall$water_sun,dfrmfall$water_cloud,alternative="two.sided")

#cloudy vs mixed
wilcox.test(dfrmwinter$water_test,dfrmwinter$water_cloud,alternative="two.sided")
wilcox.test(dfrmspring$water_test,dfrmspring$water_cloud,alternative="two.sided")
wilcox.test(dfrmsummer$water_test,dfrmsummer$water_cloud,alternative="two.sided")
wilcox.test(dfrmfall$water_test,dfrmfall$water_cloud,alternative="two.sided")
```

```
############################
#Figure 2. Eastern US box plots#
############################
cmetschem<-read.csv("C:/Users/stor/Documents/Satellites/eastern_combo_isotest.csv")

#seasons
dfrmwinter<-subset(cmetschem,Month=="12"|Month=="1"|Month=="2")
dfrmspring<-subset(cmetschem,Month=="3"|Month=="4"|Month=="5")
dfrmsummer<-subset(cmetschem,Month=="6"|Month=="7"|Month=="8")
dfrmfall<-subset(cmetschem,Month=="9"|Month=="10"|Month=="11")

#####
#NO3#
#####

#spring
jpeg("C:/Users/stor/Documents/Satellites/easternUS_boxplots/spring_NO3_meds.jpg",height=6,
width=6,units="in",res=300)
boxplot(dfrmspring$NO3_SUN,dfrmspring$NO3_CLOUD,las=1,cex.axis=2.5,ylim=c(0,0.6),

na.action=na.exclude,medcol="black",col=c("gold3","deepskyblue3"),outline=F,xaxt="n",varwi
dth=T)
title(main=expression(bold("EUS Spring NO"[3])),cex.main=2,line=2)
axis(side=1,at=seq(1,2,by=1),labels=c("Clear Sky","Cloudy"),line=0.5,cex.axis=2.5,tick=F)
dev.off()

#summer
jpeg("C:/Users/stor/Documents/Satellites/easternUS_boxplots/summer_NO3_meds.jpg",height=
6,width=6,units="in",res=300)
boxplot(dfrmsummer$NO3_SUN,dfrmsummer$NO3_CLOUD,las=1,cex.axis=2.5,ylim=c(0,0.6)
,

na.action=na.exclude,medcol="black",col=c("gold3","deepskyblue3"),outline=F,xaxt="n",varwi
dth=T)
title(main=expression(bold("EUS Summer NO"[3])),cex.main=2,line=2)
axis(side=1,at=seq(1,2,by=1),labels=c("Clear Sky","Cloudy"),line=0.5,cex.axis=2.5,tick=F)
dev.off()

#fall
jpeg("C:/Users/stor/Documents/Satellites/easternUS_boxplots/fall_NO3_meds.jpg",height=6,wi
dth=6,units="in",res=300)
boxplot(dfrmfall$NO3_SUN,dfrmfall$NO3_CLOUD,las=1,cex.axis=2.5,ylim=c(0,0.6),

na.action=na.exclude,medcol="black",col=c("gold3","deepskyblue3"),outline=F,xaxt="n",varwi
dth=T)
```

```
title(main=expression(bold("EUS Fall NO"[3])),cex.main=2,line=2)
axis(side=1,at=seq(1,2,by=1),labels=c("Clear Sky","Cloudy"),line=0.5,cex.axis=2.5,tick=F)
dev.off()

#winter
jpeg("C:/Users/stor/Documents/Satellites/easternUS_boxplots/winter_NO3_meds.jpg",height=6,
width=6,units="in",res=300)
boxplot(dfrmwinter$NO3_SUN,dfrmwinter$NO3_CLOUD,las=1,cex.axis=2.5,ylim=c(0,0.6),

na.action=na.exclude,medcol="black",col=c("gold3","deepskyblue3"),outline=F,xaxt="n",varwi
dth=T)
title(main=expression(bold("EUS Winter NO"[3])),cex.main=2,line=2)
axis(side=1,at=seq(1,2,by=1),labels=c("Clear Sky","Cloudy"),line=0.5,cex.axis=2.5,tick=F)
dev.off()

#####
#SO4#
#####

#spring
jpeg("C:/Users/stor/Documents/Satellites/easternUS_boxplots/spring_SO4_meds.jpg",height=6,
width=6,units="in",res=300)
boxplot(dfrmspring$SO4_SUN,dfrmspring$SO4_CLOUD,las=1,cex.axis=2.5,ylim=c(0,2.8),

na.action=na.exclude,medcol="black",col=c("gold3","deepskyblue3"),outline=F,xaxt="n",varwi
dth=T)
title(main=expression(bold("EUS Spring SO"[4])),cex.main=2,line=2)
axis(side=1,at=seq(1,2,by=1),labels=c("Clear Sky","Cloudy"),line=0.5,cex.axis=2.5,tick=F)
dev.off()

#summer
jpeg("C:/Users/stor/Documents/Satellites/easternUS_boxplots/summer_SO4_meds.jpg",height=6
,width=6,units="in",res=300)
boxplot(dfrmsummer$SO4_SUN,dfrmsummer$SO4_CLOUD,las=1,cex.axis=2.5,ylim=c(0,2.8),

na.action=na.exclude,medcol="black",col=c("gold3","deepskyblue3"),outline=F,xaxt="n",varwi
dth=T)
title(main=expression(bold("EUS Summer SO"[4])),cex.main=2,line=2)
axis(side=1,at=seq(1,2,by=1),labels=c("Clear Sky","Cloudy"),line=0.5,cex.axis=2.5,tick=F)
dev.off()

#fall
jpeg("C:/Users/stor/Documents/Satellites/easternUS_boxplots/fall_SO4_meds.jpg",height=6,wid
th=6,units="in",res=300)
boxplot(dfrmfall$SO4_SUN,dfrmfall$SO4_CLOUD,las=1,cex.axis=2.5,ylim=c(0,2.8),
```

```
na.action=na.exclude,medcol="black",col=c("gold3","deepskyblue3"),outline=F,xaxt="n",varwi
dth=T)
title(main=expression(bold("EUS Fall SO"[4])),cex.main=2,line=2)
axis(side=1,at=seq(1,2,by=1),labels=c("Clear Sky","Cloudy"),line=0.5,cex.axis=2.5,tick=F)
dev.off()

#winter
jpeg("C:/Users/stor/Documents/Satellites/easternUS_boxplots/winter_SO4_meds.jpg",height=6,
width=6,units="in",res=300)
boxplot(dfrmwinter$SO4_SUN,dfrmwinter$SO4_CLOUD,las=1,cex.axis=2.5,ylim=c(0,2.8),

na.action=na.exclude,medcol="black",col=c("gold3","deepskyblue3"),outline=F,xaxt="n",varwi
dth=T)
title(main=expression(bold("EUS Winter SO"[4])),cex.main=2,line=2)
axis(side=1,at=seq(1,2,by=1),labels=c("Clear Sky","Cloudy"),line=0.5,cex.axis=2.5,tick=F)
dev.off()

#######
#PM2.5#
#######

#spring
jpeg("C:/Users/stor/Documents/Satellites/easternUS_boxplots/spring_PM25_meds.jpg",height=6
,width=6,units="in",res=300)
boxplot(dfrmspring$MF.Value.x,dfrmspring$MF.Value.y,las=1,cex.axis=2.5,ylim=c(0,10.2),

na.action=na.exclude,medcol="black",col=c("gold3","deepskyblue3"),outline=F,xaxt="n",varwi
dth=T)
title(main=expression(bold("EUS Spring PM"[2.5])),cex.main=2,line=2)
axis(side=1,at=seq(1,2,by=1),labels=c("Clear Sky","Cloudy"),line=0.5,cex.axis=2.5,tick=F)
dev.off()

#summer
jpeg("C:/Users/stor/Documents/Satellites/easternUS_boxplots/summer_PM25_meds.jpg",height
=6,width=6,units="in",res=300)
boxplot(dfrmsummer$MF.Value.x,dfrmsummer$MF.Value.y,las=1,cex.axis=2.5,ylim=c(0,10.2),

na.action=na.exclude,medcol="black",col=c("gold3","deepskyblue3"),outline=F,xaxt="n",varwi
dth=T)
title(main=expression(bold("EUS Summer PM"[2.5])),cex.main=2,line=2)
axis(side=1,at=seq(1,2,by=1),labels=c("Clear Sky","Cloudy"),line=0.5,cex.axis=2.5,tick=F)
dev.off()

#fall
```

```
jpeg("C:/Users/stor/Documents/Satellites/easternUS_boxplots/fall_PM25_meds.jpg",height=6,w
idth=6,units="in",res=300)
boxplot(dfrmfall$MF.Value.x,dfrmfall$MF.Value.y,las=1,cex.axis=2.5,ylim=c(0,10.2),

na.action=na.exclude,medcol="black",col=c("gold3","deepskyblue3"),outline=F,xaxt="n",varwi
dth=T)
title(main=expression(bold("EUS Fall PM"[2.5])),cex.main=2,line=2)
axis(side=1,at=seq(1,2,by=1),labels=c("Clear Sky","Cloudy"),line=0.5,cex.axis=2.5,tick=F)
dev.off()

#winter
jpeg("C:/Users/stor/Documents/Satellites/easternUS_boxplots/winter_PM25_meds.jpg",height=6
,width=6,units="in",res=300)
boxplot(dfrmwinter$MF.Value.x,dfrmwinter$MF.Value.y,las=1,cex.axis=2.5,ylim=c(0,10.2),

na.action=na.exclude,medcol="black",col=c("gold3","deepskyblue3"),outline=F,xaxt="n",varwi
dth=T)
title(main=expression(bold("EUS Winter PM"[2.5])),cex.main=2,line=2)
axis(side=1,at=seq(1,2,by=1),labels=c("Clear Sky","Cloudy"),line=0.5,cex.axis=2.5,tick=F)
dev.off()

####
#RH#
####

#spring
jpeg("C:/Users/stor/Documents/Satellites/easternUS_boxplots/spring_RH_meds.jpg",height=6,w
idth=6,units="in",res=300)
boxplot(dfrmspring$RH_SUN,dfrmspring$RH_CLOUD,las=1,cex.axis=2.5,ylim=c(0,1),

na.action=na.exclude,medcol="black",col=c("gold3","deepskyblue3"),outline=F,xaxt="n",varwi
dth=T)
title(main=expression(bold("CONUS Spring RH")),cex.main=2,line=2)
axis(side=1,at=seq(1,2,by=1),labels=c("Clear Sky","Cloudy"),line=0.5,cex.axis=2.5,tick=F)
dev.off()

#summer
jpeg("C:/Users/stor/Documents/Satellites/easternUS_boxplots/summer_RH_meds.jpg",height=6,
width=6,units="in",res=300)
boxplot(dfrmsummer$RH_SUN,dfrmsummer$RH_CLOUD,las=1,cex.axis=2.5,ylim=c(0,1),

na.action=na.exclude,medcol="black",col=c("gold3","deepskyblue3"),outline=F,xaxt="n",varwi
dth=T)
title(main=expression(bold("EUS Summer RH")),cex.main=2,line=2)
axis(side=1,at=seq(1,2,by=1),labels=c("Clear Sky","Cloudy"),line=0.5,cex.axis=2.5,tick=F)
dev.off()
```

```
#fall
jpeg("C:/Users/stor/Documents/Satellites/easternUS_boxplots/fall_RH_meds.jpg",height=6,widt
h=6,units="in",res=300)
boxplot(dfrmfall$RH_SUN,dfrmfall$RH_CLOUD,las=1,cex.axis=2.5,ylim=c(0,1),

na.action=na.exclude,medcol="black",col=c("gold3","deepskyblue3"),outline=F,xaxt="n",varwi
dth=T)
title(main=expression(bold("EUS Fall RH")),cex.main=2,line=2)
axis(side=1,at=seq(1,2,by=1),labels=c("Clear Sky","Cloudy"),line=0.5,cex.axis=2.5,tick=F)
dev.off()

#winter
jpeg("C:/Users/stor/Documents/Satellites/easternUS_boxplots/winter_RH_meds.jpg",height=6,w
idth=6,units="in",res=300)
boxplot(dfrmwinter$RH_SUN,dfrmwinter$RH_CLOUD,las=1,cex.axis=2.5,ylim=c(0,1),

na.action=na.exclude,medcol="black",col=c("gold3","deepskyblue3"),outline=F,xaxt="n",varwi
dth=T)
title(main=expression(bold("EUS Winter RH")),cex.main=2,line=2)
axis(side=1,at=seq(1,2,by=1),labels=c("Clear Sky","Cloudy"),line=0.5,cex.axis=2.5,tick=F)
dev.off()

############################
#Figure 3. Differences in ALW#
############################
regionswin<-
read.csv("C:/Users/stor/Documents/Satellites/regions_allwinters_sca_fixedsites.csv")
regionsspring<-
read.csv("C:/Users/stor/Documents/Satellites/regions_allsprings_sca_fixedsites.csv")
regionssum<-
read.csv("C:/Users/stor/Documents/Satellites/regions_allsummers_sca_fixedsites.csv")
regionsfall<-read.csv("C:/Users/stor/Documents/Satellites/regions_allfalls_sca_fixedsites.csv")

regionswin$ALW_diff<-regionswin$med_ALW_CLOUD-regionswin$med_ALW_SUN
regionsspring$ALW_diff<-regionsspring$med_ALW_CLOUD-regionsspring$med_ALW_SUN
regionssum$ALW_diff<-regionssum$med_ALW_CLOUD-regionssum$med_ALW_SUN
regionsfall$ALW_diff<-regionsfall$med_ALW_CLOUD-regionsfall$med_ALW_SUN

regionswin$alwsig<-ifelse(regionswin$ALW_scp<0.05,"Y","N")
regionsspring$alwsig<-ifelse(regionsspring$ALW_scp<0.05,"Y","N")
regionssum$alwsig<-ifelse(regionssum$ALW_scp<0.05,"Y","N")
regionsfall$alwsig<-ifelse(regionsfall$ALW_scp<0.05,"Y","N")

#winter ALW differences
```

```
jpeg("C:/Users/stor/Documents/Satellites/colorbar_maps/ALW_winter.jpg",height=6,width=8,units="in",res=300)
states<-map_data("state")
g<-
ggplot(data=states,aes(x=long,y=lat))+geom_polygon(aes(group=group),fill="white",colour="#333333",linetype="dashed")+coord_fixed(1.3)+guides(fill=F)
g
g+geom_point(data=regionswin,aes(x=regionswin$avglon,y=regionswin$avglat,

colour=ALW_diff,shape=alwsig),size=4)+guides(shape=F)+scale_shape_manual(values=c(19,17))+
  scale_colour_gradientn(colours=matlab.like(22),limits=c(-2.5,2.5),breaks=c(-2.5,-2.0,-1.5,-1.0,-0.5,0,0.5,1.0,1.5,2.0,2.5))+
  labs(x="",y="",title="")+

theme(panel.background=element_blank(),axis.ticks=element_blank(),axis.text=element_blank(),
      legend.title=element_blank(),legend.text=element_text(size=16),
      plot.title=element_text(hjust=0.5,size=16),legend.key.height=unit(0.7,"in"))
dev.off()

#spring ALW differences
jpeg("C:/Users/stor/Documents/Satellites/colorbar_maps/ALW_spring.jpg",height=6,width=8,units="in",res=300)
states<-map_data("state")
g<-
ggplot(data=states,aes(x=long,y=lat))+geom_polygon(aes(group=group),fill="white",colour="#333333",linetype="dashed")+coord_fixed(1.3)+guides(fill=F)
g
g+geom_point(data=regionsspring,aes(x=regionsspring$avglon,y=regionsspring$avglat,

colour=ALW_diff,shape=alwsig),size=4)+guides(shape=F)+scale_shape_manual(values=c(19,17))+
  scale_colour_gradientn(colours=matlab.like(22),limits=c(-2.5,2.5),breaks=c(-2.5,-2.0,-1.5,-1.0,-0.5,0,0.5,1.0,1.5,2.0,2.5))+
  labs(x="",y="",title="")+

theme(panel.background=element_blank(),axis.ticks=element_blank(),axis.text=element_blank(),
      legend.title=element_blank(),legend.text=element_text(size=16),
      plot.title=element_text(hjust=0.5,size=16),legend.key.height=unit(0.7,"in"))
dev.off()

#summer ALW differences
jpeg("C:/Users/stor/Documents/Satellites/colorbar_maps/ALW_summer.jpg",height=6,width=8,units="in",res=300)
```

```
states<-map_data("state")
g<-
ggplot(data=states,aes(x=long,y=lat))+geom_polygon(aes(group=group),fill="white",colour="#3
33333",linetype="dashed")+coord_fixed(1.3)+guides(fill=F)
g
g+geom_point(data=regionssum,aes(x=regionssum$avglon,y=regionssum$avglat,

colour=ALW_diff,shape=alwsig),size=4)+guides(shape=F)+scale_shape_manual(values=c(19,1
7))+
  scale_colour_gradientn(colours=matlab.like(22),limits=c(-2.5,2.5),breaks=c(-2.5,-2.0,-1.5,-1.0,-
0.5,0,0.5,1.0,1.5,2.0,2.5))+
  labs(x="",y="",title="")+

theme(panel.background=element_blank(),axis.ticks=element_blank(),axis.text=element_blank()
,
      legend.title=element_blank(),legend.text=element_text(size=16),
      plot.title=element_text(hjust=0.5,size=16),legend.key.height=unit(0.7,"in"))
dev.off()

#fall ALW differences
jpeg("C:/Users/stor/Documents/Satellites/colorbar_maps/ALW_fall.jpg",height=6,width=8,units
="in",res=300)
states<-map_data("state")
g<-
ggplot(data=states,aes(x=long,y=lat))+geom_polygon(aes(group=group),fill="white",colour="#3
33333",linetype="dashed")+coord_fixed(1.3)+guides(fill=F)
g
g+geom_point(data=regionsfall,aes(x=regionsfall$avglon,y=regionsfall$avglat,

colour=ALW_diff,shape=alwsig),size=4)+guides(shape=F)+scale_shape_manual(values=c(19,1
7))+
  scale_colour_gradientn(colours=matlab.like(22),limits=c(-2.5,2.5),breaks=c(-2.5,-2.0,-1.5,-1.0,-
0.5,0,0.5,1.0,1.5,2.0,2.5))+
  labs(x="",y="",title="")+

theme(panel.background=element_blank(),axis.ticks=element_blank(),axis.text=element_blank()
,
      legend.title=element_blank(),legend.text=element_text(size=16),
      plot.title=element_text(hjust=0.5,size=16),legend.key.height=unit(0.7,"in"))
dev.off()

############################
#Figure 4. Differences in PM2.5#
############################
```

```
regionswin<-
read.csv("C:/Users/amych/Documents/Research/Satellites/regions_allsummers_sca_fixedsites.csv")
regionsspring<-
read.csv("C:/Users/amych/Documents/Research/Satellites/regions_allsprings_sca_fixedsites.csv")
regionssum<-
read.csv("C:/Users/amych/Documents/Research/Satellites/regions_allfalls_sca_fixedsites.csv")
regionsfall<-
read.csv("C:/Users/amych/Documents/Research/Satellites/regions_allwinters_sca_fixedsites.csv")

#PM2.5
regionswin$PM_diff<-regionswin$med_PM25_CLOUD-regionswin$med_PM25_SUN
regionsspring$PM_diff<-regionsspring$med_PM25_CLOUD-regionsspring$med_PM25_SUN
regionssum$PM_diff<-regionssum$med_PM25_CLOUD-regionssum$med_PM25_SUN
regionsfall$PM_diff<-regionsfall$med_PM25_CLOUD-regionsfall$med_PM25_SUN

regionswin$pmsig<-ifelse(regionswin$PM25_scp<0.05,"Y","N")
regionsspring$pmsig<-ifelse(regionsspring$PM25_scp<0.05,"Y","N")
regionssum$pmsig<-ifelse(regionssum$PM25_scp<0.05,"Y","N")
regionsfall$pmsig<-ifelse(regionsfall$PM25_scp<0.05,"Y","N")

jpeg("C:/Users/amych/Documents/Research/Satellites/colorbar_maps/PM_winter.jpg",height=6,
width=8,units="in",res=300)
states<-map_data("state")
g<-
ggplot(data=states,aes(x=long,y=lat))+geom_polygon(aes(group=group),fill="white",colour="bl
ack")+coord_fixed(1.3)+guides(fill=F)
g
g+geom_point(data=regionswin,aes(x=regionswin$avglon,y=regionswin$avglat,

colour=PM_diff,shape=pmsig),size=4)+guides(shape=F)+scale_shape_manual(values=c(19,17))
+
  scale_colour_gradientn(colours=matlab.like(22),limits=c(-3,3),breaks=c(-3,-2,-1,0,1,2,3))+
  labs(x="",y="",title="")+

theme(panel.background=element_blank(),axis.ticks=element_blank(),axis.text=element_blank()
,
      legend.title=element_blank(),legend.text=element_text(size=12),
      plot.title=element_text(hjust=0.5,size=16),legend.key.height=unit(0.7,"in"))
dev.off()

jpeg("C:/Users/amych/Documents/Research/Satellites/colorbar_maps/PM_spring.jpg",height=6,
width=8,units="in",res=300)
states<-map_data("state")
```

```
g<-
ggplot(data=states,aes(x=long,y=lat))+geom_polygon(aes(group=group),fill="white",colour="bl
ack")+coord_fixed(1.3)+guides(fill=F)
g
g+geom_point(data=regionsspring,aes(x=regionsspring$avglon,y=regionsspring$avglat,

colour=PM_diff,shape=pmsig),size=4)+guides(shape=F)+scale_shape_manual(values=c(19,17))
+
  scale_colour_gradientn(colours=matlab.like(22),limits=c(-3,3),breaks=c(-3,-2,-1,0,1,2,3))+
  labs(x="",y="",title="")+

theme(panel.background=element_blank(),axis.ticks=element_blank(),axis.text=element_blank()
,
      legend.title=element_blank(),legend.text=element_text(size=12),
      plot.title=element_text(hjust=0.5,size=16),legend.key.height=unit(0.7,"in"))
dev.off()

jpeg("C:/Users/amych/Documents/Research/Satellites/colorbar_maps/PM_summer.jpg",height=
6,width=8,units="in",res=300)
states<-map_data("state")
g<-
ggplot(data=states,aes(x=long,y=lat))+geom_polygon(aes(group=group),fill="white",colour="bl
ack")+coord_fixed(1.3)+guides(fill=F)
g
g+geom_point(data=regionssum,aes(x=regionssum$avglon,y=regionssum$avglat,

colour=PM_diff,shape=pmsig),size=4)+guides(shape=F)+scale_shape_manual(values=c(19,17))
+
  scale_colour_gradientn(colours=matlab.like(22),limits=c(-3,3),breaks=c(-3,-2,-1,0,1,2,3))+
  labs(x="",y="",title="")+

theme(panel.background=element_blank(),axis.ticks=element_blank(),axis.text=element_blank()
,
      legend.title=element_blank(),legend.text=element_text(size=12),
      plot.title=element_text(hjust=0.5,size=16),legend.key.height=unit(0.7,"in"))
dev.off()

jpeg("C:/Users/amych/Documents/Research/Satellites/colorbar_maps/PM_fall.jpg",height=6,wid
th=8,units="in",res=300)
states<-map_data("state")
g<-
ggplot(data=states,aes(x=long,y=lat))+geom_polygon(aes(group=group),fill="white",colour="bl
ack")+coord_fixed(1.3)+guides(fill=F)
g
g+geom_point(data=regionsfall,aes(x=regionsfall$avglon,y=regionsfall$avglat,
```

```
colour=PM_diff,shape=pmsig),size=4)+guides(shape=F)+scale_shape_manual(values=c(19,17))
+
  scale_colour_gradientn(colours=matlab.like(22),limits=c(-3,3),breaks=c(-3,-2,-1,0,1,2,3))+
  labs(x="",y="",title="")+

theme(panel.background=element_blank(),axis.ticks=element_blank(),axis.text=element_blank()
,
      legend.title=element_blank(),legend.text=element_text(size=12),
      plot.title=element_text(hjust=0.5,size=16),legend.key.height=unit(0.7,"in"))
dev.off()

#significant and insignificant legend
jpeg("C:/Users/amych/Documents/Research/Satellites/colorbar_maps/significance_legend.jpg",h
eight=4,width=4,units="in",res=300)
plot(NULL)
legend("center",legend=c("Significiant","Not
Significant"),pch=c(2,1),col="black",cex=1.75,ncol=1)
dev.off()

#########################
#Figure 5. Differences in SO4#
#########################
regionswin$SO4_diff<-regionswin$med_SO4_CLOUD-regionswin$med_SO4_SUN
regionsspring$SO4_diff<-regionsspring$med_SO4_CLOUD-regionsspring$med_SO4_SUN
regionssum$SO4_diff<-regionssum$med_SO4_CLOUD-regionssum$med_SO4_SUN
regionsfall$SO4_diff<-regionsfall$med_SO4_CLOUD-regionsfall$med_SO4_SUN

regionswin$so4sig<-ifelse(regionswin$SO4_scp<0.05,"Y","N")
regionsspring$so4sig<-ifelse(regionsspring$SO4_scp<0.05,"Y","N")
regionssum$so4sig<-ifelse(regionssum$SO4_scp<0.05,"Y","N")
regionsfall$so4sig<-ifelse(regionsfall$SO4_scp<0.05,"Y","N")

jpeg("C:/Users/amych/Documents/Research/Satellites/colorbar_maps/SO4_winter.jpg",height=6,
width=8,units="in",res=300)
states<-map_data("state")
g<-
ggplot(data=states,aes(x=long,y=lat))+geom_polygon(aes(group=group),fill="white",colour="bl
ack")+coord_fixed(1.3)+guides(fill=F)
g
g+geom_point(data=regionswin,aes(x=regionswin$avglon,y=regionswin$avglat,

colour=SO4_diff,shape=so4sig),size=4)+guides(shape=F)+scale_shape_manual(values=c(19,17)
)+
  scale_colour_gradientn(colours=matlab.like(22),limits=c(-0.7,0.7),breaks=c(-0.7,-
0.35,0,0.35,0.7))+
```

```
  labs(x="",y="",title="")+

theme(panel.background=element_blank(),axis.ticks=element_blank(),axis.text=element_blank()
,
      legend.title=element_blank(),legend.text=element_text(size=12),
      plot.title=element_text(hjust=0.5,size=16),legend.key.height=unit(0.7,"in"))
dev.off()

jpeg("C:/Users/amych/Documents/Research/Satellites/colorbar_maps/SO4_spring.jpg",height=6,
width=8,units="in",res=300)
states<-map_data("state")
g<-
ggplot(data=states,aes(x=long,y=lat))+geom_polygon(aes(group=group),fill="white",colour="bl
ack")+coord_fixed(1.3)+guides(fill=F)
g
g+geom_point(data=regionsspring,aes(x=regionsspring$avglon,y=regionsspring$avglat,

colour=SO4_diff,shape=so4sig),size=4)+guides(shape=F)+scale_shape_manual(values=c(19,17)
)+
  scale_colour_gradientn(colours=matlab.like(22),limits=c(-0.7,0.7),breaks=c(-0.7,-
0.35,0,0.35,0.7))+
  labs(x="",y="",title="")+

theme(panel.background=element_blank(),axis.ticks=element_blank(),axis.text=element_blank()
,
      legend.title=element_blank(),legend.text=element_text(size=12),
      plot.title=element_text(hjust=0.5,size=16),legend.key.height=unit(0.7,"in"))
dev.off()

jpeg("C:/Users/amych/Documents/Research/Satellites/colorbar_maps/SO4_summer.jpg",height=
6,width=8,units="in",res=300)
states<-map_data("state")
g<-
ggplot(data=states,aes(x=long,y=lat))+geom_polygon(aes(group=group),fill="white",colour="bl
ack")+coord_fixed(1.3)+guides(fill=F)
g
g+geom_point(data=regionssum,aes(x=regionssum$avglon,y=regionssum$avglat,

colour=SO4_diff,shape=so4sig),size=4)+guides(shape=F)+scale_shape_manual(values=c(19,17)
)+
  scale_colour_gradientn(colours=matlab.like(22),limits=c(-0.7,0.7),breaks=c(-0.7,-
0.35,0,0.35,0.7))+
  labs(x="",y="",title="")+

theme(panel.background=element_blank(),axis.ticks=element_blank(),axis.text=element_blank()
,
```

```
      legend.title=element_blank(),legend.text=element_text(size=12),
      plot.title=element_text(hjust=0.5,size=16),legend.key.height=unit(0.7,"in"))
dev.off()

jpeg("C:/Users/amych/Documents/Research/Satellites/colorbar_maps/SO4_fall.jpg",height=6,wi
dth=8,units="in",res=300)
states<-map_data("state")
g<-
ggplot(data=states,aes(x=long,y=lat))+geom_polygon(aes(group=group),fill="white",colour="bl
ack")+coord_fixed(1.3)+guides(fill=F)
g
g+geom_point(data=regionsfall,aes(x=regionsfall$avglon,y=regionsfall$avglat,

colour=SO4_diff,shape=so4sig),size=4)+guides(shape=F)+scale_shape_manual(values=c(19,17)
)+
  scale_colour_gradientn(colours=matlab.like(22),limits=c(-0.7,0.7),breaks=c(-0.7,-
0.35,0,0.35,0.7))+
  labs(x="",y="",title="")+

theme(panel.background=element_blank(),axis.ticks=element_blank(),axis.text=element_blank()
,
      legend.title=element_blank(),legend.text=element_text(size=12),
      plot.title=element_text(hjust=0.5,size=16),legend.key.height=unit(0.7,"in"))
dev.off()

##########################
#Figure 6. Differences in NO3#
##########################
regionswin$NO3_diff<-regionswin$med_NO3_CLOUD-regionswin$med_NO3_SUN
regionsspring$NO3_diff<-regionsspring$med_NO3_CLOUD-regionsspring$med_NO3_SUN
regionssum$NO3_diff<-regionssum$med_NO3_CLOUD-regionssum$med_NO3_SUN
regionsfall$NO3_diff<-regionsfall$med_NO3_CLOUD-regionsfall$med_NO3_SUN

regionswin$no3sig<-ifelse(regionswin$NO3_scp<0.05,"Y","N")
regionsspring$no3sig<-ifelse(regionsspring$NO3_scp<0.05,"Y","N")
regionssum$no3sig<-ifelse(regionssum$NO3_scp<0.05,"Y","N")
regionsfall$no3sig<-ifelse(regionsfall$NO3_scp<0.05,"Y","N")

jpeg("C:/Users/amych/Documents/Research/Satellites/colorbar_maps/NO3_winter.jpg",height=6
,width=8,units="in",res=300)
states<-map_data("state")
g<-
ggplot(data=states,aes(x=long,y=lat))+geom_polygon(aes(group=group),fill="white",colour="bl
ack")+coord_fixed(1.3)+guides(fill=F)
g
g+geom_point(data=regionswin,aes(x=regionswin$avglon,y=regionswin$avglat,
```

```
colour=NO3_diff,shape=no3sig),size=4)+guides(shape=F)+scale_shape_manual(values=c(19,17
))+
  scale_colour_gradientn(colours=blue2red(22),limits=c(-0.4,0.4),breaks=c(-0.4,-0.2,0,0.2,0.4))+
  labs(x="",y="",title="")+

theme(panel.background=element_blank(),axis.ticks=element_blank(),axis.text=element_blank()
,
      legend.title=element_blank(),legend.text=element_text(size=12),
      plot.title=element_text(hjust=0.5,size=16),legend.key.height=unit(0.7,"in"))
dev.off()
#star and triangle made in powerpoint

jpeg("C:/Users/amych/Documents/Research/Satellites/colorbar_maps/NO3_spring.jpg",height=6
,width=8,units="in",res=300)
states<-map_data("state")
g<-
ggplot(data=states,aes(x=long,y=lat))+geom_polygon(aes(group=group),fill="white",colour="bl
ack")+coord_fixed(1.3)+guides(fill=F)
g
g+geom_point(data=regionsspring,aes(x=regionsspring$avglon,y=regionsspring$avglat,

colour=NO3_diff,shape=no3sig),size=4)+guides(shape=F)+scale_shape_manual(values=c(19,17
))+
  scale_colour_gradientn(colours=blue2red(22),limits=c(-0.4,0.4),breaks=c(-0.4,-0.2,0,0.2,0.4))+
  labs(x="",y="",title="")+

theme(panel.background=element_blank(),axis.ticks=element_blank(),axis.text=element_blank()
,
      legend.title=element_blank(),legend.text=element_text(size=12),
      plot.title=element_text(hjust=0.5,size=16),legend.key.height=unit(0.7,"in"))
dev.off()

jpeg("C:/Users/amych/Documents/Research/Satellites/colorbar_maps/NO3_summer.jpg",height
=6,width=8,units="in",res=300)
states<-map_data("state")
g<-
ggplot(data=states,aes(x=long,y=lat))+geom_polygon(aes(group=group),fill="white",colour="bl
ack")+coord_fixed(1.3)+guides(fill=F)
g
g+geom_point(data=regionssum,aes(x=regionssum$avglon,y=regionssum$avglat,

colour=NO3_diff,shape=no3sig),size=4)+guides(shape=F)+scale_shape_manual(values=c(19,17
))+
  scale_colour_gradientn(colours=blue2red(22),limits=c(-0.4,0.4),breaks=c(-0.4,-0.2,0,0.2,0.4))+
  labs(x="",y="",title="")+
```

```
theme(panel.background=element_blank(),axis.ticks=element_blank(),axis.text=element_blank()
,
      legend.title=element_blank(),legend.text=element_text(size=12),
      plot.title=element_text(hjust=0.5,size=16),legend.key.height=unit(0.7,"in"))
dev.off()

jpeg("C:/Users/amych/Documents/Research/Satellites/colorbar_maps/NO3_fall.jpg",height=6,wi
dth=8,units="in",res=300)
states<-map_data("state")
g<-
ggplot(data=states,aes(x=long,y=lat))+geom_polygon(aes(group=group),fill="white",colour="bl
ack")+coord_fixed(1.3)+guides(fill=F)
g
g+geom_point(data=regionsfall,aes(x=regionsfall$avglon,y=regionsfall$avglat,

colour=NO3_diff,shape=no3sig),size=4)+guides(shape=F)+scale_shape_manual(values=c(19,17
))+
  scale_colour_gradientn(colours=blue2red(22),limits=c(-0.4,0.4),breaks=c(-0.4,-0.2,0,0.2,0.4))+
  labs(x="",y="",title="")+

theme(panel.background=element_blank(),axis.ticks=element_blank(),axis.text=element_blank()
,
      legend.title=element_blank(),legend.text=element_text(size=12),
      plot.title=element_text(hjust=0.5,size=16),legend.key.height=unit(0.7,"in"))
dev.off()

############################
#Figure 7. Differences in TOC#
############################
regionswin$TOC_diff<-regionswin$med_TOC_CLOUD-regionswin$med_TOC_SUN
regionsspring$TOC_diff<-regionsspring$med_TOC_CLOUD-regionsspring$med_TOC_SUN
regionssum$TOC_diff<-regionssum$med_TOC_CLOUD-regionssum$med_TOC_SUN
regionsfall$TOC_diff<-regionsfall$med_TOC_CLOUD-regionsfall$med_TOC_SUN

regionswin$tocsig<-ifelse(regionswin$TOC_scp<0.05,"Y","N")
regionsspring$tocsig<-ifelse(regionsspring$TOC_scp<0.05,"Y","N")
regionssum$tocsig<-ifelse(regionssum$TOC_scp<0.05,"Y","N")
regionsfall$tocsig<-ifelse(regionsfall$TOC_scp<0.05,"Y","N")

jpeg("C:/Users/amych/Documents/Research/Satellites/colorbar_maps/TOC_winter.jpg",height=6
,width=8,units="in",res=300)
states<-map_data("state")
g<-
ggplot(data=states,aes(x=long,y=lat))+geom_polygon(aes(group=group),fill="white",colour="bl
ack")+coord_fixed(1.3)+guides(fill=F)
```

```
g
g+geom_point(data=regionswin,aes(x=regionswin$avglon,y=regionswin$avglat,

colour=TOC_diff,shape=tocsig),size=4)+guides(shape=F)+scale_shape_manual(values=c(19,17)
)+
  scale_colour_gradientn(colours=matlab.like(22),limits=c(-0.51,0.5),breaks=c(-0.5,-
0.25,0,0.25,0.5))+
  labs(x="",y="",title="")+

theme(panel.background=element_blank(),axis.ticks=element_blank(),axis.text=element_blank()
,
      legend.title=element_blank(),legend.text=element_text(size=12),
      plot.title=element_text(hjust=0.5,size=16),legend.key.height=unit(0.7,"in"))
dev.off()

jpeg("C:/Users/amych/Documents/Research/Satellites/colorbar_maps/TOC_spring.jpg",height=6
,width=8,units="in",res=300)
states<-map_data("state")
g<-
ggplot(data=states,aes(x=long,y=lat))+geom_polygon(aes(group=group),fill="white",colour="bl
ack")+coord_fixed(1.3)+guides(fill=F)
g
g+geom_point(data=regionsspring,aes(x=regionsspring$avglon,y=regionsspring$avglat,

colour=TOC_diff,shape=tocsig),size=4)+guides(shape=F)+scale_shape_manual(values=c(19,17)
)+
  scale_colour_gradientn(colours=matlab.like(22),limits=c(-0.51,0.5),breaks=c(-0.5,-
0.25,0,0.25,0.5))+
  labs(x="",y="",title="")+

theme(panel.background=element_blank(),axis.ticks=element_blank(),axis.text=element_blank()
,
      legend.title=element_blank(),legend.text=element_text(size=12),
      plot.title=element_text(hjust=0.5,size=16),legend.key.height=unit(0.7,"in"))
dev.off()

jpeg("C:/Users/amych/Documents/Research/Satellites/colorbar_maps/TOC_summer.jpg",height
=6,width=8,units="in",res=300)
states<-map_data("state")
g<-
ggplot(data=states,aes(x=long,y=lat))+geom_polygon(aes(group=group),fill="white",colour="bl
ack")+coord_fixed(1.3)+guides(fill=F)
g
g+geom_point(data=regionssum,aes(x=regionssum$avglon,y=regionssum$avglat,
```

```
colour=TOC_diff,shape=tocsig),size=4)+guides(shape=F)+scale_shape_manual(values=c(19,17)
)+
  scale_colour_gradientn(colours=matlab.like(22),limits=c(-0.51,0.5),breaks=c(-0.5,-
0.25,0,0.25,0.5))+
  labs(x="",y="",title="")+

theme(panel.background=element_blank(),axis.ticks=element_blank(),axis.text=element_blank()
,
      legend.title=element_blank(),legend.text=element_text(size=12),
      plot.title=element_text(hjust=0.5,size=16),legend.key.height=unit(0.7,"in"))
dev.off()

jpeg("C:/Users/amych/Documents/Research/Satellites/colorbar_maps/TOC_fall.jpg",height=6,wi
dth=8,units="in",res=300)
states<-map_data("state")
g<-
ggplot(data=states,aes(x=long,y=lat))+geom_polygon(aes(group=group),fill="white",colour="bl
ack")+coord_fixed(1.3)+guides(fill=F)
g
g+geom_point(data=regionsfall,aes(x=regionsfall$avglon,y=regionsfall$avglat,

colour=TOC_diff,shape=tocsig),size=4)+guides(shape=F)+scale_shape_manual(values=c(19,17)
)+
  scale_colour_gradientn(colours=matlab.like(22),limits=c(-0.51,0.5),breaks=c(-0.5,-
0.25,0,0.25,0.5))+
  labs(x="",y="",title="")+

theme(panel.background=element_blank(),axis.ticks=element_blank(),axis.text=element_blank()
,
      legend.title=element_blank(),legend.text=element_text(size=12),
      plot.title=element_text(hjust=0.5,size=16),legend.key.height=unit(0.7,"in"))
dev.off()

############################
#Figure 8. Mid South box plots#
############################
midsouth<-
subset(allyears,SiteCode=="CHER1"|SiteCode=="HEGL1"|SiteCode=="ELLI1"|SiteCode=="W
IMO1"|SiteCode=="UPBU1"|SiteCode=="CACR1"|SiteCode=="SIKE1")
midsouthsun<-subset(midsouth,CLOUDY==0)
midsouthcloud<-subset(midsouth,CLOUDY==1)

midsouthsummersun<-subset(midsouthsun,Month==6|Month==7|Month==8)
midsouthsummercloud<-subset(midsouthcloud,Month==6|Month==7|Month==8)
midsouthwintersun<-subset(midsouthsun,Month==12|Month==1|Month==2)
```

```
midsouthwintercloud<-subset(midsouthcloud,Month==12|Month==1|Month==2)
midsouthspringsun<-subset(midsouthsun,Month==3|Month==4|Month==5)
midsouthspringcloud<-subset(midsouthcloud,Month==3|Month==4|Month==5)
midsouthfallsun<-subset(midsouthsun,Month==9|Month==10|Month==11)
midsouthfallcloud<-subset(midsouthcloud,Month==9|Month==10|Month==11)

midsouthsummer<-subset(midsouth,Month==6|Month==7|Month==8)
midsouthwinter<-subset(midsouth,Month==12|Month==1|Month==2)
midsouthspring<-subset(midsouth,Month==3|Month==4|Month==5)
midsouthfall<-subset(midsouth,Month==9|Month==10|Month==11)

#####
#SO4#
#####

#winter
jpeg("C:/Users/amych/Documents/Research/Satellites/nearSGP/MidSouth_winter_SO4.jpg",heig
ht=6,width=6,units="in",res=300)
boxplot(midsouthwintersun$SO4,midsouthwintercloud$SO4,las=1,cex.axis=3,ylim=c(0,6),

na.action=na.exclude,medcol="black",col=c("gold3","deepskyblue3"),outline=F,yaxt="n",xaxt="
n",varwidth=T)
axis(side=2,at=seq(0,6,by=2),line=-0.8,cex.axis=3,tick=F,las=1)
title("MidSouth Winter",line=1,cex.main=2)
axis(side=1,at=seq(1,2,by=1),labels=c("Clear Sky","Cloudy"),line=0.5,cex.axis=2.75,tick=F)
dev.off()

#spring
jpeg("C:/Users/amych/Documents/Research/Satellites/nearSGP/MidSouth_spring_SO4.jpg",heig
ht=6,width=6,units="in",res=300)
boxplot(midsouthspringsun$SO4,midsouthspringcloud$SO4,las=1,cex.axis=3,ylim=c(0,6),

na.action=na.exclude,medcol="black",col=c("gold3","deepskyblue3"),outline=F,yaxt="n",xaxt="
n",varwidth=T)
axis(side=2,at=seq(0,6,by=2),line=-0.8,cex.axis=3,tick=F,las=1)
title("MidSouth Spring",line=1,cex.main=2)
axis(side=1,at=seq(1,2,by=1),labels=c("Clear Sky","Cloudy"),line=0.5,cex.axis=2.75,tick=F)
dev.off()

#summer
jpeg("C:/Users/amych/Documents/Research/Satellites/nearSGP/MidSouth_summer_SO4.jpg",he
ight=6,width=6,units="in",res=300)
boxplot(midsouthsummersun$SO4,midsouthsummercloud$SO4,las=1,cex.axis=3,ylim=c(0,6),

na.action=na.exclude,medcol="black",col=c("gold3","deepskyblue3"),outline=F,yaxt="n",xaxt="
n",varwidth=T)
```

```
axis(side=2,at=seq(0,6,by=2),line=-0.8,cex.axis=3,tick=F,las=1)
title("MidSouth Summer",line=1,cex.main=2)
axis(side=1,at=seq(1,2,by=1),labels=c("Clear Sky","Cloudy"),line=0.5,cex.axis=2.75,tick=F)
dev.off()

#fall
jpeg("C:/Users/amych/Documents/Research/Satellites/nearSGP/MidSouth_fall_SO4.jpg",height
=6,width=6,units="in",res=300)
boxplot(midsouthfallsun$SO4,midsouthfallcloud$SO4,las=1,cex.axis=3,ylim=c(0,6),

na.action=na.exclude,medcol="black",col=c("gold3","deepskyblue3"),outline=F,yaxt="n",xaxt="
n",varwidth=T)
axis(side=2,at=seq(0,6,by=2),line=-0.8,cex.axis=3,tick=F,las=1)
title("MidSouth Fall",line=1,cex.main=2)
axis(side=1,at=seq(1,2,by=1),labels=c("Clear Sky","Cloudy"),line=0.5,cex.axis=2.75,tick=F)
dev.off()

#####
#NO3#
#####

#winter
jpeg("C:/Users/stor/Documents/Satellites/allsites
data/regions/boxplots/MidSouth_winter_NO3.jpg",height=6,width=6,units="in",res=300)
boxplot(midsouthwintersun$NO3,midsouthwintercloud$NO3,las=1,cex.axis=3,ylim=c(0,6),

na.action=na.exclude,medcol="black",col=c("gold3","deepskyblue3"),outline=F,yaxt="n",xaxt="
n",varwidth=T)
axis(side=2,at=seq(0,6,by=2),line=-0.8,cex.axis=3,tick=F,las=1)
title("MidSouth Winter",line=1,cex.main=2)
axis(side=1,at=seq(1,2,by=1),labels=c("Clear Sky","Cloudy"),line=0.5,cex.axis=2.75,tick=F)
dev.off()

#spring
jpeg("C:/Users/stor/Documents/Satellites/allsites
data/regions/boxplots/MidSouth_spring_NO3.jpg",height=6,width=6,units="in",res=300)
boxplot(midsouthspringsun$NO3,midsouthspringcloud$NO3,las=1,cex.axis=3,ylim=c(0,6),

na.action=na.exclude,medcol="black",col=c("gold3","deepskyblue3"),outline=F,yaxt="n",xaxt="
n",varwidth=T)
axis(side=2,at=seq(0,6,by=2),line=-0.8,cex.axis=3,tick=F,las=1)
title("MidSouth Spring",line=1,cex.main=2)
axis(side=1,at=seq(1,2,by=1),labels=c("Clear Sky","Cloudy"),line=0.5,cex.axis=2.75,tick=F)
dev.off()

#summer
```

```
jpeg("C:/Users/stor/Documents/Satellites/allsites
data/regions/boxplots/MidSouth_summer_NO3.jpg",height=6,width=6,units="in",res=300)
boxplot(midsouthsummersun$NO3,midsouthsummercloud$NO3,las=1,cex.axis=3,ylim=c(0,6),

na.action=na.exclude,medcol="black",col=c("gold3","deepskyblue3"),outline=F,yaxt="n",xaxt="
n",varwidth=T)
axis(side=2,at=seq(0,6,by=2),line=-0.8,cex.axis=3,tick=F,las=1)
title("MidSouth Summer",line=1,cex.main=2)
axis(side=1,at=seq(1,2,by=1),labels=c("Clear Sky","Cloudy"),line=0.5,cex.axis=2.75,tick=F)
dev.off()

#fall
jpeg("C:/Users/stor/Documents/Satellites/allsites
data/regions/boxplots/MidSouth_fall_NO3.jpg",height=6,width=6,units="in",res=300)
boxplot(midsouthfallsun$NO3,midsouthfallcloud$NO3,las=1,cex.axis=3,ylim=c(0,6),

na.action=na.exclude,medcol="black",col=c("gold3","deepskyblue3"),outline=F,yaxt="n",xaxt="
n",varwidth=T)
axis(side=2,at=seq(0,6,by=2),line=-0.8,cex.axis=3,tick=F,las=1)
title("MidSouth Fall",line=1,cex.main=2)
axis(side=1,at=seq(1,2,by=1),labels=c("Clear Sky","Cloudy"),line=0.5,cex.axis=2.75,tick=F)
dev.off()

####
#RH#
####

#winter
jpeg("C:/Users/stor/Documents/Satellites/allsites
data/regions/boxplots/MidSouth_winter_RH.jpg",height=6,width=6,units="in",res=300)
boxplot(midsouthwintersun$RH,midsouthwintercloud$RH,las=1,cex.axis=3,ylim=c(0,1),

na.action=na.exclude,medcol="black",col=c("gold3","deepskyblue3"),outline=F,yaxt="n",xaxt="
n",varwidth=T)
axis(side=2,at=seq(0,1,by=0.2),line=-0.8,cex.axis=3,tick=F,las=1)
title("MidSouth Winter",line=1,cex.main=2)
axis(side=1,at=seq(1,2,by=1),labels=c("Clear Sky","Cloudy"),line=0.5,cex.axis=2.75,tick=F)
dev.off()

#spring
jpeg("C:/Users/stor/Documents/Satellites/allsites
data/regions/boxplots/MidSouth_spring_RH.jpg",height=6,width=6,units="in",res=300)
boxplot(midsouthspringsun$RH,midsouthspringcloud$RH,las=1,cex.axis=3,ylim=c(0,1),

na.action=na.exclude,medcol="black",col=c("gold3","deepskyblue3"),outline=F,yaxt="n",xaxt="
n",varwidth=T)
```

```
axis(side=2,at=seq(0,1,by=0.2),line=-0.8,cex.axis=3,tick=F,las=1)
title("MidSouth Spring",line=1,cex.main=2)
axis(side=1,at=seq(1,2,by=1),labels=c("Clear Sky","Cloudy"),line=0.5,cex.axis=2.75,tick=F)
dev.off()

#summer
jpeg("C:/Users/stor/Documents/Satellites/allsites
data/regions/boxplots/MidSouth_summer_RH.jpg",height=6,width=6,units="in",res=300)
boxplot(midsouthsummersun$RH,midsouthsummercloud$RH,las=1,cex.axis=3,ylim=c(0,1),

na.action=na.exclude,medcol="black",col=c("gold3","deepskyblue3"),outline=F,yaxt="n",xaxt="
n",varwidth=T)
axis(side=2,at=seq(0,1,by=0.2),line=-0.8,cex.axis=3,tick=F,las=1)
title("MidSouth Summer",line=1,cex.main=2)
axis(side=1,at=seq(1,2,by=1),labels=c("Clear Sky","Cloudy"),line=0.5,cex.axis=2.75,tick=F)
dev.off()

#fall
jpeg("C:/Users/stor/Documents/Satellites/allsites
data/regions/boxplots/MidSouth_fall_RH.jpg",height=6,width=6,units="in",res=300)
boxplot(midsouthfallsun$RH,midsouthfallcloud$RH,las=1,cex.axis=3,ylim=c(0,1),

na.action=na.exclude,medcol="black",col=c("gold3","deepskyblue3"),outline=F,yaxt="n",xaxt="
n",varwidth=T)
axis(side=2,at=seq(0,1,by=0.2),line=-0.8,cex.axis=3,tick=F,las=1)
title("MidSouth Fall",line=1,cex.main=2)
axis(side=1,at=seq(1,2,by=1),labels=c("Clear Sky","Cloudy"),line=0.5,cex.axis=2.75,tick=F)
dev.off()


#######
#PM2.5#
#######

#winter
jpeg("C:/Users/stor/Documents/Satellites/allsites
data/regions/boxplots/MidSouth_winter_PM25.jpg",height=6,width=6,units="in",res=300)
boxplot(midsouthwintersun$MF.Value,midsouthwintercloud$MF.Value,las=1,cex.axis=3,ylim=
c(0,20),

na.action=na.exclude,medcol="black",col=c("gold3","deepskyblue3"),outline=F,yaxt="n",xaxt="
n",varwidth=T)
axis(side=2,at=seq(0,20,by=5),line=-0.8,cex.axis=3,tick=F,las=1)
title("MidSouth Winter",line=1,cex.main=2)
axis(side=1,at=seq(1,2,by=1),labels=c("Clear Sky","Cloudy"),line=0.5,cex.axis=2.75,tick=F)
dev.off()
```

```
#spring
jpeg("C:/Users/stor/Documents/Satellites/allsites
data/regions/boxplots/MidSouth_spring_PM25.jpg",height=6,width=6,units="in",res=300)
boxplot(midsouthspringsun$MF.Value,midsouthspringcloud$MF.Value,las=1,cex.axis=3,ylim=c
(0,20),

na.action=na.exclude,medcol="black",col=c("gold3","deepskyblue3"),outline=F,yaxt="n",xaxt="
n",varwidth=T)
axis(side=2,at=seq(0,20,by=5),line=-0.8,cex.axis=3,tick=F,las=1)
title("MidSouth Spring",line=1,cex.main=2)
axis(side=1,at=seq(1,2,by=1),labels=c("Clear Sky","Cloudy"),line=0.5,cex.axis=2.75,tick=F)
dev.off()

#summer
jpeg("C:/Users/stor/Documents/Satellites/allsites
data/regions/boxplots/MidSouth_summer_PM25.jpg",height=6,width=6,units="in",res=300)
boxplot(midsouthsummersun$MF.Value,midsouthsummercloud$MF.Value,las=1,cex.axis=3,yli
m=c(0,20),

na.action=na.exclude,medcol="black",col=c("gold3","deepskyblue3"),outline=F,yaxt="n",xaxt="
n",varwidth=T)
axis(side=2,at=seq(0,20,by=5),line=-0.8,cex.axis=3,tick=F,las=1)
title("MidSouth Summer",line=1,cex.main=2)
axis(side=1,at=seq(1,2,by=1),labels=c("Clear Sky","Cloudy"),line=0.5,cex.axis=2.75,tick=F)
dev.off()

#fall
jpeg("C:/Users/stor/Documents/Satellites/allsites
data/regions/boxplots/MidSouth_fall_PM25.jpg",height=6,width=6,units="in",res=300)
boxplot(midsouthfallsun$MF.Value,midsouthfallcloud$MF.Value,las=1,cex.axis=3,ylim=c(0,20
),

na.action=na.exclude,medcol="black",col=c("gold3","deepskyblue3"),outline=F,yaxt="n",xaxt="
n",varwidth=T)
axis(side=2,at=seq(0,20,by=5),line=-0.8,cex.axis=3,tick=F,las=1)
title("MidSouth Fall",line=1,cex.main=2)
axis(side=1,at=seq(1,2,by=1),labels=c("Clear Sky","Cloudy"),line=0.5,cex.axis=2.75,tick=F)
dev.off()

#####
#ALW#
#####

#winter
```

```
jpeg("C:/Users/stor/Documents/Satellites/allsites
data/regions/boxplots/MidSouth_winter_ALW3.jpg",height=6,width=6,units="in",res=300)
boxplot(midsouthwintersun$water,midsouthwintercloud$water,las=1,cex.axis=3,ylim=c(0,15),

na.action=na.exclude,medcol="black",col=c("gold3","deepskyblue3","green4"),outline=F,yaxt="
n",xaxt="n",varwidth=T)
axis(side=2,at=seq(0,15,by=5),line=-0.8,cex.axis=3,tick=F,las=1)
title("MidSouth Winter",line=1,cex.main=2)
axis(side=1,at=seq(1,2,by=1),labels=c("Clear Sky","Cloudy"),line=0.5,cex.axis=2.75,tick=F)
dev.off()

#spring
jpeg("C:/Users/stor/Documents/Satellites/allsites
data/regions/boxplots/MidSouth_spring_ALW3.jpg",height=6,width=6,units="in",res=300)
boxplot(midsouthspringsun$water,midsouthspringcloud$water,las=1,cex.axis=3,ylim=c(0,15),

na.action=na.exclude,medcol="black",col=c("gold3","deepskyblue3","green4"),outline=F,yaxt="
n",xaxt="n",varwidth=T)
axis(side=2,at=seq(0,15,by=5),line=-0.8,cex.axis=3,tick=F,las=1)
title("MidSouth Spring",line=1,cex.main=2)
axis(side=1,at=seq(1,2,by=1),labels=c("Clear Sky","Cloudy"),line=0.5,cex.axis=2.75,tick=F)
dev.off()

#summer
jpeg("C:/Users/stor/Documents/Satellites/allsites
data/regions/boxplots/MidSouth_summer_ALW3.jpg",height=6,width=6,units="in",res=300)
boxplot(midsouthsummersun$water,midsouthsummercloud$water,las=1,cex.axis=3,ylim=c(0,15
),

na.action=na.exclude,medcol="black",col=c("gold3","deepskyblue3","green4"),outline=F,yaxt="
n",xaxt="n",varwidth=T)
axis(side=2,at=seq(0,15,by=5),line=-0.8,cex.axis=3,tick=F,las=1)
title("MidSouth Summer",line=1,cex.main=2)
axis(side=1,at=seq(1,2,by=1),labels=c("Clear Sky","Cloudy"),line=0.5,cex.axis=2.75,tick=F)
dev.off()

#fall
jpeg("C:/Users/stor/Documents/Satellites/allsites
data/regions/boxplots/MidSouth_fall_ALW3.jpg",height=6,width=6,units="in",res=300)
boxplot(midsouthfallsun$water,midsouthfallcloud$water,las=1,cex.axis=3,ylim=c(0,15),

na.action=na.exclude,medcol="black",col=c("gold3","deepskyblue3","green4"),outline=F,yaxt="
n",xaxt="n",varwidth=T)
axis(side=2,at=seq(0,15,by=5),line=-0.8,cex.axis=3,tick=F,las=1)
title("MidSouth Fall",line=1,cex.main=2)
axis(side=1,at=seq(1,2,by=1),labels=c("Clear Sky","Cloudy"),line=0.5,cex.axis=2.75,tick=F)
```

```
dev.off()
```

```
#Supporting Information for Chapter 3

################################
#Figure S1. Site and region locations#
################################
allyears<-read.csv("C:/Users/stor/Documents/Satellites/allyears_updated_withcations.csv")
allyears<-
read.csv("C:/Users/amych/Documents/Research/Satellites/allyears_updated_withcations.csv")
allyears$MF.Value<-ifelse(allyears$MF.Value<0,NA,allyears$MF.Value)
allyears$SO4<-ifelse(allyears$SO4<0,NA,allyears$SO4)
allyears$NO3<-ifelse(allyears$NO3<0,NA,allyears$NO3)
allyears$water<-ifelse(allyears$water<0,NA,allyears$water)
allyears$OC1f.Value<-ifelse(allyears$OC1f.Value<0,NA,allyears$OC1f.Value)
allyears$OC2f.Value<-ifelse(allyears$OC2f.Value<0,NA,allyears$OC2f.Value)
allyears$OC3f.Value<-ifelse(allyears$OC3f.Value<0,NA,allyears$OC3f.Value)
allyears$OC4f.Value<-ifelse(allyears$OC4f.Value<0,NA,allyears$OC4f.Value)
allyears$OPf.Value<-ifelse(allyears$OPf.Value<0,NA,allyears$OPf.Value)
allyears$OCtot<-ifelse(allyears$OCtot<0,NA,allyears$OCtot)

attach(allyears)

northwest<-
allyears[SiteCode=="MAKA1"|SiteCode=="MAKA2"|SiteCode=="OLYM1"|SiteCode=="LYN
D1"|SiteCode=="NOCA1"|SiteCode=="PASA1"|SiteCode=="SNPA1"|SiteCode=="MORA1"|Si
teCode=="WHPA1",]
#columgorge<-allyears[SiteCode=="COGO1"|SiteCode=="CORI1",]
ornorcal<-
allyears[SiteCode=="MOHO1"|SiteCode=="THSI1"|SiteCode=="KALM1"|SiteCode=="CRLA1
"|SiteCode=="REDW1"|SiteCode=="LABE1"|SiteCode=="TRIN1"|SiteCode=="LAVO1"|SiteC
ode=="BLIS1",]
cacoast<-allyears[SiteCode=="PORE1"|SiteCode=="PINN1"|SiteCode=="RAFA1",]
sierranv<-
allyears[SiteCode=="SOLA1"|SiteCode=="YOSE1"|SiteCode=="KAIS1"|SiteCode=="SEQU1"|
SiteCode=="DOME1"|SiteCode=="HOOV1",]
socal<-
allyears[SiteCode=="SAGA1"|SiteCode=="SAGO1"|SiteCode=="JOSH1"|SiteCode=="AGTI1",
]
hellscyn<-
allyears[SiteCode=="STAR1"|SiteCode=="HECA1"|SiteCode=="SALM1"|SiteCode=="SAWT1
"|SiteCode=="SCOV1"|SiteCode=="CRMO1",]
grbasin<-allyears[SiteCode=="JARB1"|SiteCode=="GRBA1",]
norrockies<-
allyears[SiteCode=="CABI1"|SiteCode=="GLAC1"|SiteCode=="FLAT1"|SiteCode=="MONT1
"|SiteCode=="GAMO1"|SiteCode=="SULA1"|SiteCode=="YELL1"|SiteCode=="NOAB1"|Site
Code=="BRID1"|SiteCode=="BOLA2",]
```

```
coplateau<-
allyears[SiteCode=="ARCH1"|SiteCode=="CAPI1"|SiteCode=="ZION1"|SiteCode=="BRCA1"|
SiteCode=="CANY1"|SiteCode=="WEMI1"|SiteCode=="MEVE1"|SiteCode=="ZICA1"|SiteCo
de=="INGA1"|SiteCode=="GRCA1"|SiteCode=="GRCA2"|SiteCode=="SAPE1"|SiteCode=="B
AND1"|SiteCode=="MEAD1",]
mogplateau<-
allyears[SiteCode=="SYCA1"|SiteCode=="HILL1"|SiteCode=="IKBA1"|SiteCode=="PEFO1"|
SiteCode=="SIAN1"|SiteCode=="TONT1"|SiteCode=="QUVA1"|SiteCode=="BALD1"|SiteCo
de=="BOAP1"|SiteCode=="WHIT1"|SiteCode=="GICL1"|SiteCode=="SAAN1",]
soaz<-
allyears[SiteCode=="ORPI1"|SiteCode=="SAWE1"|SiteCode=="SAGU1"|SiteCode=="DOUG1
"|SiteCode=="CHIR1",]
norgrpln<-
allyears[SiteCode=="MELA1"|SiteCode=="ULBE1"|SiteCode=="LOST1"|SiteCode=="FOPE1"
|SiteCode=="THRO1"|SiteCode=="NOCH1"|SiteCode=="CLPE1"|SiteCode=="THBA1"|SiteCo
de=="WICA1"|SiteCode=="BADL1",]
cenrockies<-
allyears[SiteCode=="BRLA1"|SiteCode=="MOZI1"|SiteCode=="STPE1"|SiteCode=="RMHQ1
"|SiteCode=="ROMO1"|SiteCode=="WHRI1"|SiteCode=="GRSA1"|SiteCode=="SHMI1"|SiteC
ode=="WHPE1",]
wtexas<-allyears[SiteCode=="SACR1"|SiteCode=="GUMO1"|SiteCode=="BIBE1",]
cengrpln<-
allyears[SiteCode=="CRES1"|SiteCode=="NEBR1"|SiteCode=="BLMO1"|SiteCode=="GRRI1"
|SiteCode=="OMAH1"|SiteCode=="VILA1"|SiteCode=="LASU1"|SiteCode=="LASU2"|SiteCo
de=="BOND1"|SiteCode=="CEBL1"|SiteCode=="SAFO1"|SiteCode=="TALL1"|SiteCode=="E
LDO1",]
midsouth<-
allyears[SiteCode=="CHER1"|SiteCode=="HEGL1"|SiteCode=="ELLI1"|SiteCode=="WIMO1"
|SiteCode=="UPBU1"|SiteCode=="CACR1"|SiteCode=="SIKE1",]
bndywaters<-
allyears[SiteCode=="VOYA1"|SiteCode=="VOYA2"|SiteCode=="BOWA1"|SiteCode=="ISRO
1"|SiteCode=="ISLE1"|SiteCode=="SENE1",]
ohriver<-
allyears[SiteCode=="MING1"|SiteCode=="CADI1"|SiteCode=="MACA1"|SiteCode=="LIVO1"
|SiteCode=="QUCI1"|SiteCode=="MKGO1",]
appalachia<-
allyears[SiteCode=="SIPS1"|SiteCode=="COHU1"|SiteCode=="GRSM1"|SiteCode=="SHRO1"
|SiteCode=="LIGO1"|SiteCode=="DOSO1"|SiteCode=="FRRE1"|SiteCode=="AREN1"|SiteCo
de=="SHEN1"|SiteCode=="JART1"|SiteCode=="JEFF1",]
southeast<-
allyears[SiteCode=="BRIS1"|SiteCode=="BRET1"|SiteCode=="OKEF1"|SiteCode=="ROMA1"
|SiteCode=="SAMA1"|SiteCode=="CHAS1"|SiteCode=="EVER1",]
ecoast<-allyears[SiteCode=="SWAN1"|SiteCode=="BRIG1",]
northeast<-
allyears[SiteCode=="PRIS1"|SiteCode=="MOOS1"|SiteCode=="PEND1"|SiteCode=="OLTO1"|
SiteCode=="ACAD1"|SiteCode=="CABA1"|SiteCode=="BRMA1"|SiteCode=="GRGU1"|SiteC
```

```
ode=="PNRF1"|SiteCode=="PACK1"|SiteCode=="LOND1"|SiteCode=="CACO1"|SiteCode=="
QURE1"|SiteCode=="LYBR1"|SiteCode=="MAVI1"|SiteCode=="MOMO1"|SiteCode=="COHI
1"|SiteCode=="ADPI1",]

#first, all sites
library(maps)

jpeg("C:/Users/stor/Documents/Satellites/paper
plots/allsites_map_color.jpg",height=4,width=6,units="in",res=300)
map("state", interior = FALSE, lwd=1,col="gray20")
map("state", boundary = FALSE, lty = 2, add = TRUE,col="gray50")
points(unique(northwest$lon),unique(northwest$lat),col="steelblue3",pch=16,cex=0.75)
points(unique(ecoast$lon),unique(ecoast$lat),col="seagreen4",pch=16,cex=0.75)
points(unique(ohriver$lon),unique(ohriver$lat),col="peru",pch=16,cex=0.75)
points(unique(appalachia$lon),unique(appalachia$lat),col="orchid3",pch=16,cex=0.75)
points(unique(southeast$lon),unique(southeast$lat),col="sienna4",pch=16,cex=0.75)
points(unique(midsouth$lon),unique(midsouth$lat),col="mediumblue",pch=16,cex=0.75)
points(unique(cengrpln$lon),unique(cengrpln$lat),col="palegreen4",pch=16,cex=0.75)
points(unique(bndywaters$lon),unique(bndywaters$lat),col="skyblue",pch=16,cex=0.75)
points(unique(norgrpln$lon),unique(norgrpln$lat),col="brown2",pch=16,cex=0.75)
points(unique(cenrockies$lon),unique(cenrockies$lat),col="mediumpurple",pch=16,cex=0.75)
points(unique(coplateau$lon),unique(coplateau$lat),col="lightblue4",pch=16,cex=0.75)
points(unique(mogplateau$lon),unique(mogplateau$lat),col="pink4",pch=16,cex=0.75)
points(unique(wtexas$lon),unique(wtexas$lat),col="mediumturquoise",pch=16,cex=0.75)
points(unique(soaz$lon),unique(soaz$lat),col="darkred",pch=16,cex=0.75)
points(unique(norrockies$lon),unique(norrockies$lat),col="lightgoldenrod4",pch=16,cex=0.75)
points(unique(grbasin$lon),unique(grbasin$lat),col="lightblue",pch=16,cex=0.75)
points(unique(sierranv$lon),unique(sierranv$lat),col="chocolate4",pch=16,cex=0.75)
points(unique(cacoast$lon),unique(cacoast$lat),col="dodgerblue4",pch=16,cex=0.75)
points(unique(ornorcal$lon),unique(ornorcal$lat),col="greenyellow",pch=16,cex=0.75)
points(unique(northeast$lon),unique(northeast$lat),col="midnightblue",pch=16,cex=0.75)
points(unique(socal$lon),unique(socal$lat),col="lightgreen",pch=16,cex=0.75)
points(unique(hellscyn$lon),unique(hellscyn$lat),col="black",pch=16,cex=0.75)
dev.off()

#region average locations, by color
jpeg("C:/Users/stor/Documents/Satellites/paper
plots/allregions_map_color.jpg",height=4,width=6,units="in",res=300)
map("state", interior = FALSE, lwd=1,col="gray20")
map("state", boundary = FALSE, lty = 2, add = TRUE,col="gray50")
points(mean(northwest$lon),mean(northwest$lat),col="steelblue3",pch=16,cex=0.75)
points(mean(ecoast$lon),mean(ecoast$lat),col="seagreen4",pch=16,cex=0.75)
points(mean(ohriver$lon),mean(ohriver$lat),col="peru",pch=16,cex=0.75)
points(mean(appalachia$lon),mean(appalachia$lat),col="orchid3",pch=16,cex=0.75)
points(mean(southeast$lon),mean(southeast$lat),col="sienna4",pch=16,cex=0.75)
points(mean(midsouth$lon),mean(midsouth$lat),col="mediumblue",pch=16,cex=0.75)
```

```
points(mean(cengrpln$lon),mean(cengrpln$lat),col="palegreen4",pch=16,cex=0.75)
points(mean(bndywaters$lon),mean(bndywaters$lat),col="skyblue",pch=16,cex=0.75)
points(mean(norgrpln$lon),mean(norgrpln$lat),col="brown2",pch=16,cex=0.75)
points(mean(cenrockies$lon),mean(cenrockies$lat),col="mediumpurple",pch=16,cex=0.75)
points(mean(coplateau$lon),mean(coplateau$lat),col="lightblue4",pch=16,cex=0.75)
points(mean(mogplateau$lon),mean(mogplateau$lat),col="pink4",pch=16,cex=0.75)
points(mean(wtexas$lon),mean(wtexas$lat),col="mediumturquoise",pch=16,cex=0.75)
points(mean(soaz$lon),mean(soaz$lat),col="darkred",pch=16,cex=0.75)
points(mean(norrockies$lon),mean(norrockies$lat),col="lightgoldenrod4",pch=16,cex=0.75)
points(mean(grbasin$lon),mean(grbasin$lat),col="lightblue",pch=16,cex=0.75)
points(mean(sierranv$lon),mean(sierranv$lat),col="chocolate4",pch=16,cex=0.75)
points(mean(cacoast$lon),mean(cacoast$lat),col="dodgerblue4",pch=16,cex=0.75)
points(mean(ornorcal$lon),mean(ornorcal$lat),col="greenyellow",pch=16,cex=0.75)
points(mean(northeast$lon),mean(northeast$lat),col="midnightblue",pch=16,cex=0.75)
points(mean(socal$lon),mean(socal$lat),col="lightgreen",pch=16,cex=0.75)
points(mean(hellscyn$lon),mean(hellscyn$lat),col="black",pch=16,cex=0.75)

text(mean(northwest$lon),mean(northwest$lat+1),"Northwest",cex=0.75,col="steelblue3")
text(mean(hellscyn$lon),mean(hellscyn$lat+1),"Hells Canyon",cex=0.75,col="black")
text(mean(norrockies$lon),mean(norrockies$lat+1),"Northern
Rockies",cex=0.75,col="lightgoldenrod4")
text(mean(norgrpln$lon+2),mean(norgrpln$lat-1),"Northern Great
Plains",cex=0.75,col="brown2")
text(mean(bndywaters$lon),mean(bndywaters$lat+1),"Boundary
Waters",cex=0.75,col="skyblue")
text(mean(cenrockies$lon+2),mean(cenrockies$lat+1),"Central
Rockies",cex=0.75,col="mediumpurple")
text(mean(cengrpln$lon),mean(cengrpln$lat+1),"Central Great
Plains",cex=0.75,col="palegreen4")
text(mean(northeast$lon),mean(northeast$lat+1),"Northeast",cex=0.75,col="midnightblue")
text(mean(ecoast$lon),mean(ecoast$lat+1),"East Coast",cex=0.75,col="seagreen4")
text(mean(appalachia$lon),mean(appalachia$lat-1),"Appalachia",cex=0.75,col="orchid3")
text(mean(ohriver$lon),mean(ohriver$lat+1),"Ohio River Valley",cex=0.75,col="peru")
text(mean(southeast$lon),mean(southeast$lat+1),"Southeast",cex=0.75,col="sienna4")
text(mean(midsouth$lon),mean(midsouth$lat+1),"Mid South",cex=0.75,col="mediumblue")
text(mean(wtexas$lon+2),mean(wtexas$lat+1),"West Texas",cex=0.75,col="mediumturquoise")
text(mean(mogplateau$lon),mean(mogplateau$lat+1),"Mogollon
Plateau",cex=0.75,col="pink4")
text(mean(soaz$lon),mean(soaz$lat-1),"Southern AZ",cex=0.75,col="darkred")
text(mean(coplateau$lon+2),mean(coplateau$lat-0.75),"Colorado
Plateau",cex=0.75,col="lightblue4")
text(mean(socal$lon-1),mean(socal$lat-1),"Southern CA",cex=0.75,col="lightgreen")
text(mean(sierranv$lon),mean(sierranv$lat+1),"Sierra Nevada",cex=0.75,col="chocolate4")
text(mean(cacoast$lon-1),mean(cacoast$lat-1),"CA Coast",xpd=T,cex=0.75,col="dodgerblue4")
text(mean(grbasin$lon-1),mean(grbasin$lat+1),"Great Basin",cex=0.75,col="lightblue")
```

```
text(mean(ornorcal$lon),mean(ornorcal$lat+1),"Oregon/Northern
CA",xpd=T,cex=0.75,col="greenyellow")
dev.off()

#####################################################
#Figure S2. Comparison of dust and no-dust ALW estimations#
#####################################################
allyears$Month<-as.numeric(allyears$Month)
allyears$year<-as.numeric(allyears$year)

dfrm<-
data.frame(Date=allyears$Date,Month=allyears$Month,year=allyears$year,water=allyears$wate
r,
           water_withcats=allyears$water_withcats,SO4=allyears$SO4,NO3=allyears$NO3,

RH=allyears$RH,TEMP=allyears$TEMP,Na=allyears$NAf.Value,Cl=allyears$CHLf.Value,
           Ca=allyears$CAf.Value,K=allyears$Kf.Value,Na=allyears$NAf.Value)
dfrmmeds<-aggregate(dfrm,by=list(dfrm$Month,dfrm$year),FUN="median",na.rm=T)

tiff("C:/Users/stor/Documents/Satellites/Dust_vs_NoDust_ALW.tif",height=6,width=6,units="in
",res=300)
par(mar=c(5.1,5.1,4.1,2.1))
plot(dfrmmeds$Date,dfrmmeds$water,type="l",ylim=c(0,1.5),lwd=3,las=1,ylab=expression("AL
W"~(mu*g~m^{-3})),cex.axis=1.5,cex.lab=1.5,xlab="")
lines(dfrmmeds$Date,dfrmmeds$water_withcats,col="blue",lwd=3)
legend("topright",legend=c("No Dust","With
Dust"),lwd=3,col=c("black","blue"),cex=1.5,bty="n")
dev.off()

#################################
#Figure S3. ALW mass concentrations#
#################################
library(ggplot2)
library(colorRamps)

northwest<-
allyears[SiteCode=="MAKA1"|SiteCode=="MAKA2"|SiteCode=="OLYM1"|SiteCode=="LYN
D1"|SiteCode=="NOCA1"|SiteCode=="PASA1"|SiteCode=="SNPA1"|SiteCode=="MORA1"|Si
teCode=="WHPA1",]
ornorcal<-
allyears[SiteCode=="MOHO1"|SiteCode=="THSI1"|SiteCode=="KALM1"|SiteCode=="CRLA1
"|SiteCode=="REDW1"|SiteCode=="LABE1"|SiteCode=="TRIN1"|SiteCode=="LAVO1"|SiteC
ode=="BLIS1",]
cacoast<-allyears[SiteCode=="PORE1"|SiteCode=="PINN1"|SiteCode=="RAFA1",]
```

```
sierranv<-
allyears[SiteCode=="SOLA1"|SiteCode=="YOSE1"|SiteCode=="KAIS1"|SiteCode=="SEQU1"|
SiteCode=="DOME1"|SiteCode=="HOOV1",]
socal<-
allyears[SiteCode=="SAGA1"|SiteCode=="SAGO1"|SiteCode=="JOSH1"|SiteCode=="AGTI1",
]
hellscyn<-
allyears[SiteCode=="STAR1"|SiteCode=="HECA1"|SiteCode=="SALM1"|SiteCode=="SAWT1
"|SiteCode=="SCOV1"|SiteCode=="CRMO1",]
grbasin<-allyears[SiteCode=="JARB1"|SiteCode=="GRBA1",]
norrockies<-
allyears[SiteCode=="CABI1"|SiteCode=="GLAC1"|SiteCode=="FLAT1"|SiteCode=="MONT1
"|SiteCode=="GAMO1"|SiteCode=="SULA1"|SiteCode=="YELL1"|SiteCode=="NOAB1"|Site
Code=="BRID1"|SiteCode=="BOLA2",]
coplateau<-
allyears[SiteCode=="ARCH1"|SiteCode=="CAPI1"|SiteCode=="ZION1"|SiteCode=="BRCA1"|
SiteCode=="CANY1"|SiteCode=="WEMI1"|SiteCode=="MEVE1"|SiteCode=="ZICA1"|SiteCo
de=="INGA1"|SiteCode=="GRCA1"|SiteCode=="GRCA2"|SiteCode=="SAPE1"|SiteCode=="B
AND1"|SiteCode=="MEAD1",]
mogplateau<-
allyears[SiteCode=="SYCA1"|SiteCode=="HILL1"|SiteCode=="IKBA1"|SiteCode=="PEFO1"|
SiteCode=="SIAN1"|SiteCode=="TONT1"|SiteCode=="QUVA1"|SiteCode=="BALD1"|SiteCo
de=="BOAP1"|SiteCode=="WHIT1"|SiteCode=="GICL1"|SiteCode=="SAAN1",]
soaz<-
allyears[SiteCode=="ORPI1"|SiteCode=="SAWE1"|SiteCode=="SAGU1"|SiteCode=="DOUG1
"|SiteCode=="CHIR1",]
norgrpln<-
allyears[SiteCode=="MELA1"|SiteCode=="ULBE1"|SiteCode=="LOST1"|SiteCode=="FOPE1"
|SiteCode=="THRO1"|SiteCode=="NOCH1"|SiteCode=="CLPE1"|SiteCode=="THBA1"|SiteCo
de=="WICA1"|SiteCode=="BADL1",]
cenrockies<-
allyears[SiteCode=="BRLA1"|SiteCode=="MOZI1"|SiteCode=="STPE1"|SiteCode=="RMHQ1
"|SiteCode=="ROMO1"|SiteCode=="WHRI1"|SiteCode=="GRSA1"|SiteCode=="SHMI1"|SiteC
ode=="WHPE1",]
wtexas<-allyears[SiteCode=="SACR1"|SiteCode=="GUMO1"|SiteCode=="BIBE1",]
cengrpln<-
allyears[SiteCode=="CRES1"|SiteCode=="NEBR1"|SiteCode=="BLMO1"|SiteCode=="GRRI1"
|SiteCode=="OMAH1"|SiteCode=="VILA1"|SiteCode=="LASU1"|SiteCode=="LASU2"|SiteCo
de=="BOND1"|SiteCode=="CEBL1"|SiteCode=="SAFO1"|SiteCode=="TALL1"|SiteCode=="E
LDO1",]
midsouth<-
allyears[SiteCode=="CHER1"|SiteCode=="HEGL1"|SiteCode=="ELLI1"|SiteCode=="WIMO1"
|SiteCode=="UPBU1"|SiteCode=="CACR1"|SiteCode=="SIKE1",]
bndywaters<-
allyears[SiteCode=="VOYA1"|SiteCode=="VOYA2"|SiteCode=="BOWA1"|SiteCode=="ISRO
1"|SiteCode=="ISLE1"|SiteCode=="SENE1",]
```

```
ohriver<-
allyears[SiteCode=="MING1"|SiteCode=="CADI1"|SiteCode=="MACA1"|SiteCode=="LIVO1"
|SiteCode=="QUCI1"|SiteCode=="MKGO1",]
appalachia<-
allyears[SiteCode=="SIPS1"|SiteCode=="COHU1"|SiteCode=="GRSM1"|SiteCode=="SHRO1"
|SiteCode=="LIGO1"|SiteCode=="DOSO1"|SiteCode=="FRRE1"|SiteCode=="AREN1"|SiteCo
de=="SHEN1"|SiteCode=="JART1"|SiteCode=="JEFF1",]
southeast<-
allyears[SiteCode=="BRIS1"|SiteCode=="BRET1"|SiteCode=="OKEF1"|SiteCode=="ROMA1"
|SiteCode=="SAMA1"|SiteCode=="CHAS1"|SiteCode=="EVER1",]
ecoast<-allyears[SiteCode=="SWAN1"|SiteCode=="BRIG1",]
northeast<-
allyears[SiteCode=="PRIS1"|SiteCode=="MOOS1"|SiteCode=="PEND1"|SiteCode=="OLTO1"|
SiteCode=="ACAD1"|SiteCode=="CABA1"|SiteCode=="BRMA1"|SiteCode=="GRGU1"|SiteC
ode=="PNRF1"|SiteCode=="PACK1"|SiteCode=="LOND1"|SiteCode=="CACO1"|SiteCode=="
QURE1"|SiteCode=="LYBR1"|SiteCode=="MAVI1"|SiteCode=="MOMO1"|SiteCode=="COHI
1"|SiteCode=="ADPI1",]

northwest$avglat<-mean(unique(northwest$lat))
ornorcal$avglat<-mean(unique(ornorcal$lat))
cacoast$avglat<-mean(unique(cacoast$lat))
sierranv$avglat<-mean(unique(sierranv$lat))
socal$avglat<-mean(unique(socal$lat))
hellscyn$avglat<-mean(unique(hellscyn$lat))
grbasin$avglat<-mean(unique(grbasin$lat))
norrockies$avglat<-mean(unique(norrockies$lat))
coplateau$avglat<-mean(unique(coplateau$lat))
mogplateau$avglat<-mean(unique(mogplateau$lat))
soaz$avglat<-mean(unique(soaz$lat))
norgrpln$avglat<-mean(unique(norgrpln$lat))
cenrockies$avglat<-mean(unique(cenrockies$lat))
wtexas$avglat<-mean(unique(wtexas$lat))
cengrpln$avglat<-mean(unique(cengrpln$lat))
midsouth$avglat<-mean(unique(midsouth$lat))
bndywaters$avglat<-mean(unique(bndywaters$lat))
ohriver$avglat<-mean(unique(ohriver$lat))
appalachia$avglat<-mean(unique(appalachia$lat))
southeast$avglat<-mean(unique(southeast$lat))
ecoast$avglat<-mean(unique(ecoast$lat))
northeast$avglat<-mean(unique(northeast$lat))

northwest$avglon<-mean(unique(northwest$lon))
ornorcal$avglon<-mean(unique(ornorcal$lon))
cacoast$avglon<-mean(unique(cacoast$lon))
sierranv$avglon<-mean(unique(sierranv$lon))
socal$avglon<-mean(unique(socal$lon))
```

```
hellscyn$avglon<-mean(unique(hellscyn$lon))
grbasin$avglon<-mean(unique(grbasin$lon))
norrockies$avglon<-mean(unique(norrockies$lon))
coplateau$avglon<-mean(unique(coplateau$lon))
mogplateau$avglon<-mean(unique(mogplateau$lon))
soaz$avglon<-mean(unique(soaz$lon))
norgrpln$avglon<-mean(unique(norgrpln$lon))
cenrockies$avglon<-mean(unique(cenrockies$lon))
wtexas$avglon<-mean(unique(wtexas$lon))
cengrpln$avglon<-mean(unique(cengrpln$lon))
midsouth$avglon<-mean(unique(midsouth$lon))
bndywaters$avglon<-mean(unique(bndywaters$lon))
ohriver$avglon<-mean(unique(ohriver$lon))
appalachia$avglon<-mean(unique(appalachia$lon))
southeast$avglon<-mean(unique(southeast$lon))
ecoast$avglon<-mean(unique(ecoast$lon))
northeast$avglon<-mean(unique(northeast$lon))

northwest$region<-"northwest"
ornorcal$region<-"ornorcal"
cacoast$region<-"cacoast"
sierranv$region<-"sierranv"
socal$region<-"socal"
hellscyn$region<-"hellscyn"
grbasin$region<-"grbasin"
norrockies$region<-"norrockies"
coplateau$region<-"coplateau"
mogplateau$region<-"mogplateau"
soaz$region<-"soaz"
norgrpln$region<-"norgrpln"
cenrockies$region<-"cenrockies"
wtexas$region<-"wtexas"
cengrpln$region<-"cengrpln"
midsouth$region<-"midsouth"
bndywaters$region<-"bndywaters"
ohriver$region<-"ohriver"
appalachia$region<-"appalachia"
southeast$region<-"southeast"
ecoast$region<-"ecoast"
northeast$region<-"northeast"

regions<-rbind(northwest,ornorcal,cacoast,sierranv,socal,hellscyn,grbasin,norrockies,coplateau,

mogplateau,soaz,norgrpln,cenrockies,wtexas,cengrpln,midsouth,bndywaters,ohriver,appalachia,
        southeast,ecoast,northeast)
```

```
regionsdfrm<-
data.frame(lat=regions$lat,lon=regions$lon,water=regions$water,region=regions$region)

regionsdfrmmeans<-aggregate(regionsdfrm,by=list(regions$region),FUN="mean",na.rm=T)

tiff("C:/Users/stor/Documents/Satellites/colorbar_maps/ALW_concentrations.tif",height=6,widt
h=8,units="in",res=300)
states<-map_data("state")
g<-
ggplot(data=states,aes(x=long,y=lat))+geom_polygon(aes(group=group),fill="white",colour="bl
ack")+coord_fixed(1.3)+guides(fill=F)
g
g+geom_point(data=regionsdfrmmeans,aes(x=regionsdfrmmeans$lon,y=regionsdfrmmeans$lat,
                                colour=water),size=4)+guides(shape=F)+
  scale_colour_gradientn(colours=matlab.like(22),limits=c(0,6.5),breaks=c(0,2,4,6))+
  labs(x="",y="",title="")+

theme(panel.background=element_blank(),axis.ticks=element_blank(),axis.text=element_blank()
,
      legend.title=element_blank(),legend.text=element_text(size=12),
      plot.title=element_text(hjust=0.5,size=16),legend.key.height=unit(0.7,"in"))
dev.off()

#box done in powerpoint

##############################
#Figure S4. MODIS cloud fraction#
##############################
cloudfr<-
read.csv("C:/Users/amych/Documents/Research/Satellites/number_per_cloudfrac_winter.csv")
cloudfr<-
read.csv("C:/Users/amych/Documents/Research/Satellites/number_per_cloudfrac_summer.csv")
cloudfr<-
read.csv("C:/Users/amych/Documents/Research/Satellites/number_per_cloudfrac_spring.csv")
cloudfr<-
read.csv("C:/Users/amych/Documents/Research/Satellites/number_per_cloudfrac_fall.csv")

#winter
jpeg("C:/Users/amych/Documents/Research/Satellites/cloudfrac_winter.jpg",height=5,width=6,u
nits="in",res=300)
states<-map_data("state")
g<-
ggplot(data=states,aes(x=long,y=lat))+geom_polygon(aes(group=group),fill="white",colour="bl
ack")+coord_fixed(1.3) #define g to be a drawing of the contiguous US
g
g+geom_point(data=cloudfr,aes(x=cloudfr$avglon,y=cloudfr$avglat,colour=cloudfrac,size=4))+
```

```
scale_colour_gradientn(guide=guide_colorbar(barwidth=1,barheight=12),colours=matlab.like2(22),limits=c(0,1))+
  xlab("")+ylab("")+ggtitle("Cloud Fraction")+

theme(panel.background=element_blank(),axis.ticks=element_blank(),axis.text=element_blank(),
      legend.title=element_blank(),legend.text=element_text(size=12),
      plot.title=element_text(hjust=0.5))+
  guides(size=F)
dev.off()

#summer
jpeg("C:/Users/amych/Documents/Research/Satellites/cloudfrac_summer.jpg",height=5,width=6,units="in",res=300)
states<-map_data("state")
g<-
ggplot(data=states,aes(x=long,y=lat))+geom_polygon(aes(group=group),fill="white",colour="black")+coord_fixed(1.3) #define g to be a drawing of the contiguous US
g
g+geom_point(data=cloudfr,aes(x=cloudfr$avglon,y=cloudfr$avglat,colour=cloudfrac,size=4))+

scale_colour_gradientn(guide=guide_colorbar(barwidth=1,barheight=12),colours=matlab.like2(22),limits=c(0,1))+
  xlab("")+ylab("")+ggtitle("Cloud Fraction")+

theme(panel.background=element_blank(),axis.ticks=element_blank(),axis.text=element_blank(),
      legend.title=element_blank(),legend.text=element_text(size=12),
      plot.title=element_text(hjust=0.5))+
  guides(size=F)
dev.off()

#spring
jpeg("C:/Users/amych/Documents/Research/Satellites/cloudfrac_spring.jpg",height=5,width=6,units="in",res=300)
states<-map_data("state")
g<-
ggplot(data=states,aes(x=long,y=lat))+geom_polygon(aes(group=group),fill="white",colour="black")+coord_fixed(1.3) #define g to be a drawing of the contiguous US
g
g+geom_point(data=cloudfr,aes(x=cloudfr$avglon,y=cloudfr$avglat,colour=cloudfrac,size=4))+

scale_colour_gradientn(guide=guide_colorbar(barwidth=1,barheight=12),colours=matlab.like2(22),limits=c(0,1))+
  xlab("")+ylab("")+ggtitle("Cloud Fraction")+
```

```
theme(panel.background=element_blank(),axis.ticks=element_blank(),axis.text=element_blank()
,
      legend.title=element_blank(),legend.text=element_text(size=12),
      plot.title=element_text(hjust=0.5))+
  guides(size=F)
dev.off()

#fall
jpeg("C:/Users/amych/Documents/Research/Satellites/cloudfrac_fall.jpg",height=5,width=6,unit
s="in",res=300)
states<-map_data("state")
g<-
ggplot(data=states,aes(x=long,y=lat))+geom_polygon(aes(group=group),fill="white",colour="bl
ack")+coord_fixed(1.3) #define g to be a drawing of the contiguous US
g
g+geom_point(data=cloudfr,aes(x=cloudfr$avglon,y=cloudfr$avglat,colour=cloudfrac,size=4))+

scale_colour_gradientn(guide=guide_colorbar(barwidth=1,barheight=12),colours=matlab.like2(2
2),limits=c(0,1))+
  xlab("")+ylab("")+ggtitle("Cloud Fraction")+

theme(panel.background=element_blank(),axis.ticks=element_blank(),axis.text=element_blank()
,
      legend.title=element_blank(),legend.text=element_text(size=12),
      plot.title=element_text(hjust=0.5))+
  guides(size=F)
dev.off()

####################
#Figure S5. Flowchart#
####################

#made in powerpoint

#########################
#Figure S6. Percent matching#
#########################
percs<-read.csv("C:/Users/stor/Documents/Satellites/percent_matching.csv")

jpeg("C:/Users/stor/Documents/Satellites/paper
plots/Percent_Matching.jpg",height=5,width=6,units="in",res=300)
states<-map_data("state")
g<-
ggplot(data=states,aes(x=long,y=lat))+geom_polygon(aes(group=group),fill="white",colour="bl
ack")+coord_fixed(1.3)+guides(fill=F)
```

```
g
g+geom_point(data=percs,aes(x=percs$avglon,y=percs$avglat,colour=avg),size=4)+

scale_colour_gradientn(colours=rev(heat.colors(22)),limits=c(40,100))+labs(x="",y="",title="")
+

theme(panel.background=element_blank(),axis.ticks=element_blank(),axis.text=element_blank()
,legend.title=element_blank(),legend.text=element_text(size=12),plot.title=element_text(hjust=0.
5,size=16))
dev.off()



########################################
#Figure S7. Cloud fraction vs chem constituents#
########################################
meds<-read.csv("C:/Users/stor/Documents/Satellites/regions_allsummers_sca_fixedsites.csv")
meds$cloudfrac<-meds$PM25_CLOUD_n/meds$PM25_ALL_n

meds2<-read.csv("C:/Users/stor/Documents/Satellites/regions_allsprings_sca_fixedsites.csv")
meds2$cloudfrac<-meds2$PM25_CLOUD_n/meds2$PM25_ALL_n

meds3<-read.csv("C:/Users/stor/Documents/Satellites/regions_allfalls_sca_fixedsites.csv")
meds3$cloudfrac<-meds3$PM25_CLOUD_n/meds3$PM25_ALL_n

meds4<-read.csv("C:/Users/stor/Documents/Satellites/regions_allwinters_sca_fixedsites.csv")
meds4$cloudfrac<-meds4$PM25_CLOUD_n/meds4$PM25_ALL_n

#particle chemical components
meds$so4_diff<-meds$med_SO4_CLOUD-meds$med_SO4_SUN
meds$no3_diff<-meds$med_NO3_CLOUD-meds$med_NO3_SUN
meds$alw_diff<-meds$med_ALW_CLOUD-meds$med_ALW_SUN
meds$toc_diff<-meds$med_TOC_CLOUD-meds$med_TOC_SUN

meds2$so4_diff<-meds2$med_SO4_CLOUD-meds2$med_SO4_SUN
meds2$no3_diff<-meds2$med_NO3_CLOUD-meds2$med_NO3_SUN
meds2$alw_diff<-meds2$med_ALW_CLOUD-meds2$med_ALW_SUN
meds2$toc_diff<-meds2$med_TOC_CLOUD-meds2$med_TOC_SUN

meds3$so4_diff<-meds3$med_SO4_CLOUD-meds3$med_SO4_SUN
meds3$no3_diff<-meds3$med_NO3_CLOUD-meds3$med_NO3_SUN
meds3$alw_diff<-meds3$med_ALW_CLOUD-meds3$med_ALW_SUN
meds3$toc_diff<-meds3$med_TOC_CLOUD-meds3$med_TOC_SUN

meds4$so4_diff<-meds4$med_SO4_CLOUD-meds4$med_SO4_SUN
meds4$no3_diff<-meds4$med_NO3_CLOUD-meds4$med_NO3_SUN
```

```
meds4$alw_diff<-meds4$med_ALW_CLOUD-meds4$med_ALW_SUN
meds4$toc_diff<-meds4$med_TOC_CLOUD-meds4$med_TOC_SUN

jpeg("C:/Users/amych/Documents/Research/Satellites/chemconst_cloudfrac_summer2.jpg",heig
ht=6,width=6,units="in", res=300)
par(mar=c(5.1,4.5,4.1,2.1))
plot(meds$cloudfrac,meds$so4_diff,pch=16,col="firebrick2",ylim=c(-
1.5,2),xlim=c(0,1),las=1,cex.axis=2,cex=1.5,ylab="",xlab="")
points(meds$cloudfrac,meds$no3_diff,pch=16,col="mediumblue",ylab="",xlab="",cex=1.5)
points(meds$cloudfrac,meds$alw_diff,pch=16,col="turquoise2",ylab="",xlab="",cex=1.5)
points(meds$cloudfrac,meds$toc_diff,pch=16,col="darkgreen",ylab="",xlab="",cex=1.5)
dev.off()

jpeg("C:/Users/amych/Documents/Research/Satellites/chemconst_cloudfrac_spring2.jpg",height
=6,width=6,units="in", res=300)
par(mar=c(5.1,4.5,4.1,2.1))
plot(meds2$cloudfrac,meds2$so4_diff,pch=16,col="firebrick2",ylim=c(-
1.5,2),xlim=c(0,1),las=1,cex.axis=2,cex=1.5,ylab="",xlab="")
points(meds2$cloudfrac,meds2$no3_diff,pch=16,col="mediumblue",ylab="",xlab="",cex=1.5)
points(meds2$cloudfrac,meds2$alw_diff,pch=16,col="turquoise2",ylab="",xlab="",cex=1.5)
points(meds2$cloudfrac,meds2$toc_diff,pch=16,col="darkgreen",ylab="",xlab="",cex=1.5)
dev.off()

jpeg("C:/Users/amych/Documents/Research/Satellites/chemconst_cloudfrac_fall2.jpg",height=6,
width=6,units="in", res=300)
par(mar=c(5.1,4.5,4.1,2.1))
plot(meds3$cloudfrac,meds3$so4_diff,pch=16,col="firebrick2",ylim=c(-
1.5,2),xlim=c(0,1),las=1,cex.axis=2,cex=1.5,ylab="",xlab="")
points(meds3$cloudfrac,meds3$no3_diff,pch=16,col="mediumblue",ylab="",xlab="",cex=1.5)
points(meds3$cloudfrac,meds3$catalw_diff,pch=16,col="turquoise2",ylab="",xlab="",cex=1.5)
points(meds3$cloudfrac,meds3$toc_diff,pch=16,col="darkgreen",ylab="",xlab="",cex=1.5)
dev.off()

jpeg("C:/Users/amych/Documents/Research/Satellites/chemconst_cloudfrac_winter2.jpg",height
=6,width=6,units="in", res=300)
par(mar=c(5.1,4.5,4.1,2.1))
plot(meds4$cloudfrac,meds4$so4_diff,pch=16,col="firebrick2",ylim=c(-
1.5,2),xlim=c(0,1),las=1,cex.axis=2,cex=1.5,ylab="",xlab="")
points(meds4$cloudfrac,meds4$no3_diff,pch=16,col="mediumblue",ylab="",xlab="",cex=1.5)
points(meds4$cloudfrac,meds4$catalw_diff,pch=16,col="turquoise2",ylab="",xlab="",cex=1.5)
points(meds4$cloudfrac,meds4$toc_diff,pch=16,col="darkgreen",ylab="",xlab="",cex=1.5)
dev.off()

################################
#Figure S8. Cloud fraction vs PM2.5#
################################
```

```
meds<-
read.csv("C:/Users/amych/Documents/Research/Satellites/regions_allsummers_sca_fixedsites.csv")
meds2<-
read.csv("C:/Users/amych/Documents/Research/Satellites/regions_allsprings_sca_fixedsites.csv")
meds3<-
read.csv("C:/Users/amych/Documents/Research/Satellites/regions_allfalls_sca_fixedsites.csv")
meds4<-
read.csv("C:/Users/amych/Documents/Research/Satellites/regions_allwinters_sca_fixedsites.csv")

meds$pm25_diff<-meds$med_PM25_CLOUD-meds$med_PM25_SUN
meds2$pm25_diff<-meds2$med_PM25_CLOUD-meds2$med_PM25_SUN
meds3$pm25_diff<-meds3$med_PM25_CLOUD-meds3$med_PM25_SUN
meds4$pm25_diff<-meds4$med_PM25_CLOUD-meds4$med_PM25_SUN

meds$cloudfrac<-meds$PM25_CLOUD_n/meds$PM25_ALL_n
meds2$cloudfrac<-meds2$PM25_CLOUD_n/meds2$PM25_ALL_n
meds3$cloudfrac<-meds3$PM25_CLOUD_n/meds3$PM25_ALL_n
meds4$cloudfrac<-meds4$PM25_CLOUD_n/meds4$PM25_ALL_n

jpeg("C:/Users/amych/Documents/Research/Satellites/pm25_cloudfrac_winter2.jpg",height=6,width=6,units="in", res=300)
par(mar=c(5.1,4.5,4.1,2.1))
plot(meds4$cloudfrac,meds4$pm25_diff,pch=16,las=1,ylim=c(-
3,3),xlim=c(0,1),cex.axis=2,cex=1.5,
    ylab=expression("Median PM"[2.5]~"Difference"~(mu*g~m^{-3})),xlab="",cex.lab=2)
dev.off()

jpeg("C:/Users/amych/Documents/Research/Satellites/pm25_cloudfrac_summer2.jpg",height=6,
width=6,units="in", res=300)
par(mar=c(5.1,4.5,4.1,2.1))
plot(meds$cloudfrac,meds$pm25_diff,pch=16,las=1,ylim=c(-
3,3),xlim=c(0,1),cex.axis=2,cex=1.5,
    ylab=expression("Median PM"[2.5]~"Difference"~(mu*g~m^{-3})),xlab="",cex.lab=2)
dev.off()

jpeg("C:/Users/amych/Documents/Research/Satellites/pm25_cloudfrac_spring2.jpg",height=6,width=6,units="in", res=300)
par(mar=c(5.1,4.5,4.1,2.1))
plot(meds2$cloudfrac,meds2$pm25_diff,pch=16,las=1,ylim=c(-
3,3),xlim=c(0,1),cex.axis=2,cex=1.5,
    ylab=expression("Median PM"[2.5]~"Difference"~(mu*g~m^{-3})),xlab="",cex.lab=2)
dev.off()
```

```
jpeg("C:/Users/amych/Documents/Research/Satellites/pm25_cloudfrac_fall2.jpg",height=6,widt
h=6,units="in", res=300)
par(mar=c(5.1,4.5,4.1,2.1))
plot(meds3$cloudfrac,meds3$pm25_diff,pch=16,las=1,ylim=c(-
3,3),xlim=c(0,1),cex.axis=2,cex=1.5,
    ylab=expression("Median PM"[2.5]~"Difference"~(mu*g~m^{-3})),xlab="",cex.lab=2)
dev.off()
```

# APPENDIX F

## R CODE FOR CHAPTER 4

```
#Christiansen et al. 2020, ES&T (submitted)
#Main paper figures

#########################################################################
#Figure 1. Decadal % changes in TOC and OC fractions, determined by# Sen's slope & Mann Kendall test#####################################

diffs<-read.csv("C:/Users/amych/Documents/Research/OC Fraction Trends/all_percent_diffs_bestQA.csv")

#TOC
jpeg("C:/Users/amych/Documents/Research/OC Fraction Trends/TOC_slope_perc_map_bigpch.jpg",width=7,height=6,units="in",res=300)
par(xpd=T)
map('state',lty=1,lwd=1,interior=F,col="black")
map("state", boundary = FALSE, lty = 2, add = TRUE,col="black")
points(x=diffs$avglon,y=diffs$avglat,pch=ifelse(diffs$mkt<0.05,16,1),
     cex=ifelse(diffs$tocperc< -0.3,5,ifelse(diffs$tocperc< -0.2,4,ifelse(diffs$tocperc< -0.1,3,2))),
     col=ifelse(diffs$tocperc<0,"mediumblue","firebrick2"),lwd=4)
legend(-114,24.5,legend=c("< -30","-30 to -20","-20 to -10","> -10"),
     pch=c(16,16,16,16),pt.cex=c(5,4,3,2),ncol=2,cex=1.75,y.intersp=1,

col=c("mediumblue","mediumblue","mediumblue","mediumblue"),pt.lwd=3,title=expression("TOC Percent Change (%)"),bty="n")
dev.off()

#OC1
jpeg("C:/Users/amych/Documents/Research/OC Fraction Trends/OC1_slope_perc_map_bigpch.jpg",width=7,height=6,units="in",res=300)
par(xpd=T)
map('state',lty=1,lwd=1,interior=F,col="black")
map("state", boundary = FALSE, lty = 2, add = TRUE,col="black")
points(x=diffs$avglon,y=diffs$avglat,pch=ifelse(diffs$mk1<0.05,16,1),
     cex=ifelse(diffs$oc1perc< -0.1,4,ifelse(diffs$oc1perc< -0.05,3,ifelse(diffs$oc1perc<0,2,2))),
     col=ifelse(diffs$oc1perc<0,"mediumblue","firebrick2"),lwd=4)
legend(-114,24.5,legend=c("< -10","-10 to -5","-5 to 0","> 0"),
     pch=c(16,16,16,16),pt.cex=c(4,3,2,2),ncol=2,cex=1.75,y.intersp=1,
```

```
col=c("mediumblue","mediumblue","mediumblue","firebrick2"),pt.lwd=3,title=expression("OC
Fraction Percent Change (%)"),bty="n")
dev.off()

#OC2
jpeg("C:/Users/amych/Documents/Research/OC Fraction
Trends/OC2_slope_perc_map_bigpch.jpg",width=7,height=6,units="in",res=300)
par(xpd=T)
map('state',lty=1,lwd=1,interior=F,col="black")
map("state", boundary = FALSE, lty = 2, add = TRUE,col="black")
points(x=diffs$avglon,y=diffs$avglat,pch=ifelse(diffs$mk2<0.05,16,1),
      cex=ifelse(diffs$oc2perc< -0.1,4,ifelse(diffs$oc2perc< -0.05,3,ifelse(diffs$oc2perc<0,2,2))),
      col=ifelse(diffs$oc2perc<0,"mediumblue","firebrick2"),lwd=4)
legend(-114,24.5,legend=c("< -10","-10 to -5","-5 to 0","> 0"),
      pch=c(16,16,16,16),pt.cex=c(4,3,2,2),ncol=2,cex=1.75,y.intersp=1,

col=c("mediumblue","mediumblue","mediumblue","firebrick2"),pt.lwd=3,title=expression("OC
Fraction Percent Change (%)"),bty="n")
dev.off()

#OC3
jpeg("C:/Users/amych/Documents/Research/OC Fraction
Trends/OC3_slope_perc_map_bigpch.jpg",width=7,height=6,units="in",res=300)
par(xpd=T)
map('state',lty=1,lwd=1,interior=F,col="black")
map("state", boundary = FALSE, lty = 2, add = TRUE,col="black")
points(x=diffs$avglon,y=diffs$avglat,pch=ifelse(diffs$mk3<0.05,16,1),
      cex=ifelse(diffs$oc3perc< -0.1,4,ifelse(diffs$oc3perc< -0.05,3,ifelse(diffs$oc3perc<0,2,2))),
      col=ifelse(diffs$oc3perc<0,"mediumblue","firebrick2"),lwd=4)
legend(-114,24.5,legend=c("< -10","-10 to -5","-5 to 0","> 0"),
      pch=c(16,16,16,16),pt.cex=c(4,3,2,2),ncol=2,cex=1.75,y.intersp=1,

col=c("mediumblue","mediumblue","mediumblue","firebrick2"),pt.lwd=3,title=expression("OC
Fraction Percent Change (%)"),bty="n")
dev.off()

#OC4
jpeg("C:/Users/amych/Documents/Research/OC Fraction
Trends/OC4_slope_perc_map_bigpch.jpg",width=7,height=6,units="in",res=300)
par(xpd=T)
map('state',lty=1,lwd=1,interior=F,col="black")
map("state", boundary = FALSE, lty = 2, add = TRUE,col="black")
points(x=diffs$avglon,y=diffs$avglat,pch=ifelse(diffs$mk4<0.05,16,1),
      cex=ifelse(diffs$oc4perc< -0.1,4,ifelse(diffs$oc4perc< -0.05,3,ifelse(diffs$oc4perc<0,2,2))),
      col=ifelse(diffs$oc4perc<0,"mediumblue","firebrick2"),lwd=4)
```

```
legend(-114,24.5,legend=c("< -10","-10 to -5","-5 to 0","> 0"),
      pch=c(16,16,16,16),pt.cex=c(4,3,2,2),ncol=2,cex=1.75,y.intersp=1,

col=c("mediumblue","mediumblue","mediumblue","firebrick2"),pt.lwd=3,title=expression("OC
Fraction Percent Change (%)"),bty="n")
dev.off()

#OP
jpeg("C:/Users/amych/Documents/Research/OC Fraction
Trends/OP_slope_perc_map_bigpch.jpg",width=7,height=6,units="in",res=300)
par(xpd=T)
map('state',lty=1,lwd=1,interior=F,col="black")
map("state", boundary = FALSE, lty = 2, add = TRUE,col="black")
points(x=diffs$avglon,y=diffs$avglat,pch=ifelse(diffs$mkp<0.05,16,1),
      cex=ifelse(diffs$opperc< -0.1,4,ifelse(diffs$opperc< -0.05,3,ifelse(diffs$opperc<0,2,2))),
      col=ifelse(diffs$opperc<0,"mediumblue","firebrick2"),lwd=4)
legend(-114,24.5,legend=c("< -10","-10 to -5","-5 to 0","> 0"),
      pch=c(16,16,16,16),pt.cex=c(4,3,2,2),ncol=2,cex=1.75,y.intersp=1,

col=c("mediumblue","mediumblue","mediumblue","firebrick2"),pt.lwd=3,title=expression("OC
Fraction Percent Change (%)"),bty="n")
dev.off()

####################################
#Figure 2. Contributions to TOC over time#
####################################

sds<-read.csv("C:/Users/amych/Documents/Research/OC Fraction
Trends/review/med_stdevs_conus.csv")

jpeg("C:/Users/amych/Documents/Research/OC Fraction
Trends/review/CONUS_OCfraction_withPC_year_rawvalues_errors.jpg",height=6,width=8,unit
s="in",res=300)
par(mar=c(5,6,3,1))
plot(meds3$year,meds3$OCf.Value,type="l",col="darkgreen",ylim=c(0,0.9),lwd=5,xlab="",ylab
="",cex.axis=2,las=1)
points(meds3$year,meds3$OCf.Value,col="darkgreen",cex=1.25,pch=16)
arrows(meds3$year,(meds3$OCf.Value-
sds$setot),meds3$year,(meds3$OCf.Value+sds$setot),length=0.05,angle=90,code=3,
      col=adjustcolor("darkgreen",alpha.f=0.5),lwd=3)
mtext(side=2,line=3.5,expression("[OC]"~(mu*g~m^{-3})),cex=2)
lines(meds3$year,meds3$OC1_QA,type="l",col="olivedrab3",lwd=5,lty=1)
points(meds3$year,meds3$OC1_QA,col="olivedrab3",cex=1.25,pch=16)
arrows(meds3$year,(meds3$OC1_QA-
sds$se1),meds3$year,(meds3$OC1_QA+sds$se1),length=0.05,angle=90,code=3,
      col=adjustcolor("olivedrab3",alpha.f=0.5),lwd=3)
```

```
lines(meds3$year,meds3$OC2_QA,type="l",col="limegreen",lwd=5,lty=1)
points(meds3$year,meds3$OC2_QA,col="limegreen",cex=1.25,pch=16)
arrows(meds3$year,(meds3$OC2_QA-
sds$se2),meds3$year,(meds3$OC2_QA+sds$se2),length=0.05,angle=90,code=3,
      col=adjustcolor("limegreen",alpha.f=0.5),lwd=3)
lines(meds3$year,meds3$OC3_QA,type="l",col="chartreuse3",lwd=5,lty=4)
points(meds3$year,meds3$OC3_QA,col="chartreuse3",cex=1.25,pch=16)
arrows(meds3$year,(meds3$OC3_QA-
sds$se3),meds3$year,(meds3$OC3_QA+sds$se3),length=0.05,angle=90,code=3,
      col=adjustcolor("chartreuse3",alpha.f=0.5),lwd=3)
lines(meds3$year,meds3$OC4_QA,type="l",col="forestgreen",lwd=5,lty=3)
points(meds3$year,meds3$OC4_QA,col="forestgreen",cex=1.25,pch=16)
arrows(meds3$year,(meds3$OC4_QA-
sds$se4),meds3$year,(meds3$OC4_QA+sds$se4),length=0.05,angle=90,code=3,
      col=adjustcolor("forestgreen",alpha.f=0.5),lwd=3)
lines(meds3$year,meds3$OP_QA,type="l",col="black",lwd=5,lty=1)
points(meds3$year,meds3$OP_QA,col="black",cex=1.25,pch=16)
arrows(meds3$year,(meds3$OP_QA-
sds$sep),meds3$year,(meds3$OP_QA+sds$sep),length=0.05,angle=90,code=3,
      col=adjustcolor("black",alpha.f=0.5),lwd=3)
legend("topright",col=c("olivedrab3","limegreen","chartreuse3","forestgreen","darkgreen","blac
k"),
      legend=c("OC1","OC2","OC3","OC4","TOC","PC"),lty=c(1,1,4,3,1,1),
      cex=1.5,ncol=2,bty="n",lwd=c(5,5,5,5,5,5))#,x.intersp=0.3,text.width=500)
dev.off()

sds<-read.csv("C:/Users/amych/Documents/Research/OC Fraction
Trends/review/med_frac_stdevs_conus.csv")

jpeg("C:/Users/amych/Documents/Research/OC Fraction
Trends/review/CONUS_fractional_cont_withPC_yearround_RAW_errors.jpg",height=6,width=
8,units="in",res=300)
par(mar=c(5,6,3,1))
plot(meds3$year,meds3$OC1frac,type="l",col="olivedrab3",ylim=c(0,0.6),lwd=5,xlab="",ylab=
"",cex.axis=2,las=1)
points(meds3$year,meds3$OC1frac,col="olivedrab3",cex=1.25,pch=16)
arrows(meds3$year,(meds3$OC1frac-
sds$se1),meds3$year,(meds3$OC1frac+sds$se1),length=0.05,angle=90,code=3,
      col=adjustcolor("olivedrab3",alpha.f=0.5),lwd=3)
mtext(side=2,line=3.5,expression("Contribution to TOC (%)"),cex=2)
lines(meds3$year,meds3$OC2frac,type="l",col="limegreen",lwd=5,lty=1)
points(meds3$year,meds3$OC2frac,col="limegreen",cex=1.25,pch=16)
arrows(meds3$year,(meds3$OC2frac-
sds$se2),meds3$year,(meds3$OC2frac+sds$se2),length=0.05,angle=90,code=3,
      col=adjustcolor("limegreen",alpha.f=0.5),lwd=3)
lines(meds3$year,meds3$OC3frac,type="l",col="chartreuse3",lwd=5,lty=4)
```

```
points(meds3$year,meds3$OC3frac,col="chartreuse3",cex=1.25,pch=16)
arrows(meds3$year,(meds3$OC3frac-
sds$se3),meds3$year,(meds3$OC3frac+sds$se3),length=0.05,angle=90,code=3,
      col=adjustcolor("chartreuse3",alpha.f=0.5),lwd=3)
lines(meds3$year,meds3$OC4frac,type="l",col="forestgreen",lwd=5,lty=3)
points(meds3$year,meds3$OC4frac,col="forestgreen",cex=1.25,pch=16)
arrows(meds3$year,(meds3$OC4frac-
sds$se4),meds3$year,(meds3$OC4frac+sds$se4),length=0.05,angle=90,code=3,
      col=adjustcolor("forestgreen",alpha.f=0.5),lwd=3)
lines(meds3$year,meds3$OPfrac,type="l",col="black",lwd=5,lty=1)
points(meds3$year,meds3$OPfrac,col="black",cex=1.25,pch=16)
arrows(meds3$year,(meds3$OPfrac-
sds$sep),meds3$year,(meds3$OPfrac+sds$sep),length=0.05,angle=90,code=3,
      col=adjustcolor("black",alpha.f=0.5),lwd=3)
legend("topright",col=c("olivedrab3","limegreen","chartreuse3","forestgreen","black"),
      legend=c("OC1","OC2","OC3","OC4","PC"),lty=c(1,1,4,3,1),
      cex=1.5,ncol=2,bty="n",lwd=c(5,5,5,5,5))#,x.intersp=0.3,text.width=500)
dev.off()

########################################
#Figure 3. GEOS-Chem OA and TOM comparison#
########################################

alldata<-read.csv("C:/Users/amych/Documents/Research/OC Fraction
Trends/alldata_with_geos.csv")
alldata$Date<-as.Date(as.character(alldata$Date),format="%Y-%m-%d")
dfrm<-
data.frame(year=alldata$year,TOM=alldata$TOM,TotalOA=alldata$TotalOA,OCtot=alldata$O
Ctot)
conus2<-aggregate(dfrm,by=list(dfrm$year),FUN="mean",na.rm=T)

#need to calculate standard errors
for(i in 2005:2015){
  cy<-subset(alldata,alldata$year==i)
  setom<-sd(cy$TOM,na.rm=T)/sqrt(length(cy$TOM[!is.na(cy$TOM)]))
  setoa<-sd(cy$TotalOA,na.rm=T)/sqrt(length(cy$TotalOA[!is.na(cy$TotalOA)]))
  year<-unique(cy$year)
  dfrm<-data.frame(year=year,setom=setom,setoa=setoa)
  write.table(dfrm,"C:/Users/amych/Documents/Research/OC Fraction
Trends/review/tom_toa_stdevs_conus.csv",append=T,sep=",",col.names=T)
}

ses<-read.csv("C:/Users/amych/Documents/Research/OC Fraction
Trends/review/tom_toa_stdevs_conus.csv")
```

```
tiff("C:/Users/amych/Documents/Research/OC Fraction
Trends/review/improve_geos_comparison_conus.tif",width=7,height=6,units="in",res=300)
par(mar=c(4,5.5,4,2))
plot(conus2$year,conus2$TOM,type="l",ylim=c(0,2.5),las=1,ylab=expression("Organic Aerosol
Mass"~(mu*g~m^{-3})),
    xlab="",cex.lab=1.5,cex.axis=1.5,lwd=3,col="green4")
points(conus2$year,conus2$TOM,pch=16,cex=1.25,col="green4")
arrows(conus2$year,(conus2$TOM-
ses$setom),conus2$year,(conus2$TOM+ses$setom),length=0.05,angle=90,code=3,
      col=adjustcolor("green4",alpha.f=0.5),lwd=3)
lines(conus2$year,conus2$TotalOA,col="darkgreen",lty=2,lwd=3,ylab="",xlab="")
points(conus2$year,conus2$TotalOA,col="darkgreen",pch=16,cex=1.25)
arrows(conus2$year,(conus2$TotalOA-
ses$setoa),conus2$year,(conus2$TotalOA+ses$setoa),length=0.05,angle=90,code=3,
      col=adjustcolor("darkgreen",alpha.f=0.5),lwd=3)
legend("bottomright",legend=c("IMPROVE TOM","GEOS-Chem
OA"),col=c("green4","darkgreen"),lwd=3,lty=c(1,2),
      cex=1.5,bty="n")
dev.off()


#################################################################
#Figure 4. OM2, ISOAAQ, and ALW comparisons in Appalachia and Great#
Basin#############################################################

alldata<-read.csv("C:/Users/amych/Documents/Research/OC Fraction
Trends/alldata_with_geos.csv")
alldata$Date<-as.Date(as.character(alldata$Date),format="%Y-%m-%d")

#appalachia
app<-subset(alldata,alldata$number==20)
appsum<-subset(app,app$seasonnum==3)
appsum$year<-as.numeric(appsum$year)
a<-
data.frame(year=appsum$year,water=appsum$water,OM2=appsum$OM2,AerMassISOAAQ=ap
psum$AerMassISOAAQ)
appagg<-aggregate(a,by=list(a$year),FUN="median",na.rm=T)

plot(appagg$year,appagg$water,type="l")
plot(appagg$year,appagg$AerMassISOAAQ,type="l")
plot(appagg$year,appagg$OM2,type="l")

jpeg("C:/Users/amych/Documents/Research/OC Fraction
Trends/review/appalachia_isoaaq_om2_alw_pts.jpg",width=9,height=6,units="in",res=300)
par(mar=c(4,5,4,11))
```

```
plot(appagg$year,appagg$water,type="l",col="turquoise3",lwd=3,las=1,cex.axis=1.5,ylab="",xla
b="",axes=F,ylim=c(0,20))
points(appagg$year,appagg$water,pch=16,cex=1.5,col="turquoise3")
box()
axis(side=2,cex.axis=1.5,las=1,col.axis="turquoise3")
axis(side=1,cex.axis=1.5)
mtext(side=2,line=2.5,expression("ALW"~(mu*g~m^{-3})),col="turquoise3",cex=1.5)
par(new=T)
plot(appagg$year,appagg$AerMassISOAAQ,type="l",col="green3",lty=2,lwd=3,axes=F,ylab=""
,xlab="",ylim=c(0,7))
points(appagg$year,appagg$AerMassISOAAQ,pch=16,cex=1.5,col="green3")
axis(side=4,cex.axis=1.5,las=1,col.axis="green3")
mtext(side=4,line=4.5,expression("GEOS-Chem ISOAAQ"~(mu*g~m^{-
3})),cex=1.5,col="green3")
par(new=T)
plot(appagg$year,appagg$OM2,lwd=3,col="darkgreen",lty=4,ylim=c(0,2),axes=F,ylab="",xlab=
"",type="l")
points(appagg$year,appagg$OM2,pch=16,cex=1.5,col="darkgreen")
axis(side=4,line=6,cex.axis=1.5,las=1,col.axis="darkgreen")
mtext(side=4,line=9.5,expression("OM2"~(mu*g~m^{-3})),cex=1.5,col="darkgreen")
legend("topright",legend=c("ALW","ISOAAQ","OM2"),lty=c(1,2,4),col=c("turquoise3","green3
","darkgreen"),lwd=3,cex=1.5,bty="n")
dev.off()

#great basin
grb<-subset(alldata,alldata$number==8)
grbsum<-subset(grb,grb$seasonnum==3)
grbsum$year<-as.numeric(grbsum$year)
d<-
data.frame(year=grbsum$year,water=grbsum$water,OM2=grbsum$OM2,AerMassISOAAQ=grb
sum$AerMassISOAAQ)
grbagg<-aggregate(d,by=list(d$year),FUN="median",na.rm=T)

plot(grbagg$year,grbagg$water,type="l")
plot(grbagg$year,grbagg$AerMassISOAAQ,type="l")
plot(grbagg$year,grbagg$OM2,type="l")

jpeg("C:/Users/amych/Documents/Research/OC Fraction
Trends/review/grbasin_isoaaq_om2_alw_pts.jpg",width=9,height=6,units="in",res=300)
par(mar=c(4,5,4,11))
plot(grbagg$year,grbagg$water,type="l",col="turquoise3",lwd=3,las=1,cex.axis=1.5,ylab="",xla
b="",axes=F,ylim=c(0,0.6))
points(grbagg$year,grbagg$water,pch=16,cex=1.5,col="turquoise3")
box()
axis(side=2,cex.axis=1.5,las=1,col.axis="turquoise3")
axis(side=1,cex.axis=1.5)
```

```
mtext(side=2,line=3,expression("ALW"~(mu*g~m^{-3})),col="turquoise3",cex=1.5)
par(new=T)
plot(grbagg$year,grbagg$AerMassISOAAQ,type="l",col="green3",lty=2,lwd=3,axes=F,ylab="",
xlab="",ylim=c(0,0.3))
points(grbagg$year,grbagg$AerMassISOAAQ,pch=16,cex=1.5,col="green3")
axis(side=4,cex.axis=1.5,las=1,col.axis="green3")
mtext(side=4,line=4.5,expression("GEOS-Chem ISOAAQ"~(mu*g~m^{-
3})),cex=1.5,col="green3")
par(new=T)
plot(grbagg$year,grbagg$OM2,lwd=3,col="darkgreen",lty=4,ylim=c(0,0.5),axes=F,ylab="",xlab
="",type="l")
points(grbagg$year,grbagg$OM2,pch=16,cex=1.5,col="darkgreen")
axis(side=4,line=6,cex.axis=1.5,las=1,col.axis="darkgreen")
mtext(side=4,line=9.5,expression("OM2"~(mu*g~m^{-3})),cex=1.5,col="darkgreen")
legend("topright",legend=c("ALW","ISOAAQ","OM2"),lty=c(1,2,4),col=c("turquoise3","green3
","darkgreen"),lwd=3,cex=1.5,bty="n")
dev.off()
```

#Supporting Information Code for Chapter 4

```
###################################
#Figure S1. Locations of sites and regions#
###################################
jdata<-read.csv("C:/Users/amych/Documents/Research/OC Fraction
Trends/alldata_updated_thru2016.csv")
jdata$Date<-as.Date(as.character(jdata$Date),format="%m/%d/%Y")
jdata$month<-substring(jdata$Date,6,7)
jdata$month<-as.numeric(jdata$month)
jdata$year<-substring(jdata$Date,1,4)
jdata$year<-as.numeric(jdata$year)
jdata$Year<-ifelse(jdata$month=="12",jdata$Year<-as.numeric(jdata$year)+1,jdata$Year<-
jdata$year)
library(zoo)
yq<-as.yearqtr(as.yearmon(jdata$Date,"%Y-%m-%d")+1/12)
jdata$season<-factor(format(yq,"%q"),levels=1:4,labels=c("winter","spring","summer","fall"))
jdata$OC1f.Value<-ifelse(jdata$OC1f.Value<0,NA,jdata$OC1f.Value)
jdata$OC2f.Value<-ifelse(jdata$OC2f.Value<0,NA,jdata$OC2f.Value)
jdata$OC3f.Value<-ifelse(jdata$OC3f.Value<0,NA,jdata$OC3f.Value)
jdata$OC4f.Value<-ifelse(jdata$OC4f.Value<0,NA,jdata$OC4f.Value)
jdata$OPf.Value<-ifelse(jdata$OPf.Value<0,NA,jdata$OPf.Value)
jdata$OCtot<-ifelse(jdata$OCtot<0,NA,jdata$OCtot)
attach(jdata)
#chem clim regions#
#this does not include urban sites since some urban sites do not fall into any regions
northwest<-
jdata[SiteCode=="MAKA1"|SiteCode=="MAKA2"|SiteCode=="OLYM1"|SiteCode=="LYND1
"|SiteCode=="NOCA1"|SiteCode=="PASA1"|SiteCode=="SNPA1"|SiteCode=="MORA1"|Site
Code=="WHPA1",]
columgorge<-jdata[SiteCode=="COGO1"|SiteCode=="CORI1",]
ornorcal<-
jdata[SiteCode=="MOHO1"|SiteCode=="THSI1"|SiteCode=="KALM1"|SiteCode=="CRLA1"|S
iteCode=="REDW1"|SiteCode=="LABE1"|SiteCode=="TRIN1"|SiteCode=="LAVO1"|SiteCod
e=="BLIS1",]
cacoast<-jdata[SiteCode=="PORE1"|SiteCode=="PINN1"|SiteCode=="RAFA1",]
sierranv<-
jdata[SiteCode=="SOLA1"|SiteCode=="YOSE1"|SiteCode=="KAIS1"|SiteCode=="SEQU1"|Sit
eCode=="DOME1"|SiteCode=="HOOV1",]
socal<-
jdata[SiteCode=="SAGA1"|SiteCode=="SAGO1"|SiteCode=="JOSH1"|SiteCode=="AGTI1",]
hellscyn<-
jdata[SiteCode=="STAR1"|SiteCode=="HECA1"|SiteCode=="SALM1"|SiteCode=="SAWT1"|S
iteCode=="SCOV1"|SiteCode=="CRMO1",]
grbasin<-jdata[SiteCode=="JARB1"|SiteCode=="GRBA1",]
```

```
norrockies<-
jdata[SiteCode=="CABI1"|SiteCode=="GLAC1"|SiteCode=="FLAT1"|SiteCode=="MONT1"|Si
teCode=="GAMO1"|SiteCode=="SULA1"|SiteCode=="YELL1"|SiteCode=="NOAB1"|SiteCod
e=="BRID1"|SiteCode=="BOLA2",]
coplateau<-
jdata[SiteCode=="ARCH1"|SiteCode=="CAPI1"|SiteCode=="ZION1"|SiteCode=="BRCA1"|Sit
eCode=="CANY1"|SiteCode=="WEMI1"|SiteCode=="MEVE1"|SiteCode=="ZICA1"|SiteCode
=="INGA1"|SiteCode=="GRCA1"|SiteCode=="GRCA2"|SiteCode=="SAPE1"|SiteCode=="BA
ND1"|SiteCode=="MEAD1",]
mogplateau<-
jdata[SiteCode=="SYCA1"|SiteCode=="HILL1"|SiteCode=="IKBA1"|SiteCode=="PEFO1"|Site
Code=="SIAN1"|SiteCode=="TONT1"|SiteCode=="QUVA1"|SiteCode=="BALD1"|SiteCode=
="BOAP1"|SiteCode=="WHIT1"|SiteCode=="GICL1"|SiteCode=="SAAN1",]
soaz<-
jdata[SiteCode=="ORPI1"|SiteCode=="SAWE1"|SiteCode=="SAGU1"|SiteCode=="DOUG1"|S
iteCode=="CHIR1",]
norgrpln<-
jdata[SiteCode=="MELA1"|SiteCode=="ULBE1"|SiteCode=="LOST1"|SiteCode=="FOPE1"|Si
teCode=="THRO1"|SiteCode=="NOCH1"|SiteCode=="CLPE1"|SiteCode=="THBA1"|SiteCode
=="WICA1"|SiteCode=="BADL1",]
cenrockies<-
jdata[SiteCode=="BRLA1"|SiteCode=="MOZI1"|SiteCode=="STPE1"|SiteCode=="RMHQ1"|Si
teCode=="ROMO1"|SiteCode=="WHRI1"|SiteCode=="GRSA1"|SiteCode=="SHMI1"|SiteCode
=="WHPE1",]
wtexas<-jdata[SiteCode=="SACR1"|SiteCode=="GUMO1"|SiteCode=="BIBE1",]
cengrpln<-
jdata[SiteCode=="CRES1"|SiteCode=="NEBR1"|SiteCode=="BLMO1"|SiteCode=="GRRI1"|Si
teCode=="OMAH1"|SiteCode=="VILA1"|SiteCode=="LASU1"|SiteCode=="LASU2"|SiteCode
=="BOND1"|SiteCode=="CEBL1"|SiteCode=="SAFO1"|SiteCode=="TALL1"|SiteCode=="EL
DO1",]
midsouth<-
jdata[SiteCode=="CHER1"|SiteCode=="HEGL1"|SiteCode=="ELLI1"|SiteCode=="WIMO1"|Si
teCode=="UPBU1"|SiteCode=="CACR1"|SiteCode=="SIKE1",]
bndywaters<-
jdata[SiteCode=="VOYA1"|SiteCode=="VOYA2"|SiteCode=="BOWA1"|SiteCode=="ISRO1"|
SiteCode=="ISLE1"|SiteCode=="SENE1",]
ohriver<-
jdata[SiteCode=="MING1"|SiteCode=="CADI1"|SiteCode=="MACA1"|SiteCode=="LIVO1"|Si
teCode=="QUCI1"|SiteCode=="MKGO1",]
appalachia<-
jdata[SiteCode=="SIPS1"|SiteCode=="COHU1"|SiteCode=="GRSM1"|SiteCode=="SHRO1"|Sit
eCode=="LIGO1"|SiteCode=="DOSO1"|SiteCode=="FRRE1"|SiteCode=="AREN1"|SiteCode=
="SHEN1"|SiteCode=="JART1"|SiteCode=="JEFF1",]
southeast<-
jdata[SiteCode=="BRIS1"|SiteCode=="BRET1"|SiteCode=="OKEF1"|SiteCode=="ROMA1"|Si
teCode=="SAMA1"|SiteCode=="CHAS1"|SiteCode=="EVER1",]
```

```
ecoast<-jdata[SiteCode=="SWAN1"|SiteCode=="BRIG1",]
northeast<-
jdata[SiteCode=="PRIS1"|SiteCode=="MOOS1"|SiteCode=="PEND1"|SiteCode=="OLTO1"|Sit
eCode=="ACAD1"|SiteCode=="CABA1"|SiteCode=="BRMA1"|SiteCode=="GRGU1"|SiteCod
e=="PNRF1"|SiteCode=="PACK1"|SiteCode=="LOND1"|SiteCode=="CACO1"|SiteCode=="Q
URE1"|SiteCode=="LYBR1"|SiteCode=="MAVI1"|SiteCode=="MOMO1"|SiteCode=="COHI1
"|SiteCode=="ADPI1",]
#urbansites<-
jdata[SiteCode=="PUSO1"|SiteCode=="SPOK1"|SiteCode=="FRES1"|SiteCode=="RUBI1"|Site
Code=="PHOE1"|SiteCode=="CHIC1"|SiteCode=="DETR1"|SiteCode=="HOUS1"|SiteCode==
"BIRM1"|SiteCode=="ATLA1"|SiteCode=="WASH1"|SiteCode=="PITT1"|SiteCode=="NEYO
1"|SiteCode=="BALT1",]

northwest$avglat<-mean(unique(northwest$lat),na.rm=T)
columgorge$avglat<-mean(unique(columgorge$lat),na.rm=T)
ornorcal$avglat<-mean(unique(ornorcal$lat),na.rm=T)
cacoast$avglat<-mean(unique(cacoast$lat),na.rm=T)
sierranv$avglat<-mean(unique(sierranv$lat),na.rm=T)
socal$avglat<-mean(unique(socal$lat),na.rm=T)
hellscyn$avglat<-mean(unique(hellscyn$lat),na.rm=T)
grbasin$avglat<-mean(unique(grbasin$lat),na.rm=T)
norrockies$avglat<-mean(unique(norrockies$lat),na.rm=T)
coplateau$avglat<-mean(unique(coplateau$lat),na.rm=T)
mogplateau$avglat<-mean(unique(mogplateau$lat),na.rm=T)
soaz$avglat<-mean(unique(soaz$lat),na.rm=T)
norgrpln$avglat<-mean(unique(norgrpln$lat),na.rm=T)
cenrockies$avglat<-mean(unique(cenrockies$lat),na.rm=T)
wtexas$avglat<-mean(unique(wtexas$lat),na.rm=T)
cengrpln$avglat<-mean(unique(cengrpln$lat),na.rm=T)
midsouth$avglat<-mean(unique(midsouth$lat),na.rm=T)
bndywaters$avglat<-mean(unique(bndywaters$lat),na.rm=T)
ohriver$avglat<-mean(unique(ohriver$lat),na.rm=T)
appalachia$avglat<-mean(unique(appalachia$lat),na.rm=T)
southeast$avglat<-mean(unique(southeast$lat),na.rm=T)
ecoast$avglat<-mean(unique(ecoast$lat),na.rm=T)
northeast$avglat<-mean(unique(northeast$lat),na.rm=T)

northwest$avglon<-mean(unique(northwest$lon),na.rm=T)
columgorge$avglon<-mean(unique(columgorge$lon),na.rm=T)
ornorcal$avglon<-mean(unique(ornorcal$lon),na.rm=T)
cacoast$avglon<-mean(unique(cacoast$lon),na.rm=T)
sierranv$avglon<-mean(unique(sierranv$lon),na.rm=T)
socal$avglon<-mean(unique(socal$lon),na.rm=T)
hellscyn$avglon<-mean(unique(hellscyn$lon),na.rm=T)
grbasin$avglon<-mean(unique(grbasin$lon),na.rm=T)
norrockies$avglon<-mean(unique(norrockies$lon),na.rm=T)
```

```
coplateau$avglon<-mean(unique(coplateau$lon),na.rm=T)
mogplateau$avglon<-mean(unique(mogplateau$lon),na.rm=T)
soaz$avglon<-mean(unique(soaz$lon),na.rm=T)
norgrpln$avglon<-mean(unique(norgrpln$lon),na.rm=T)
cenrockies$avglon<-mean(unique(cenrockies$lon),na.rm=T)
wtexas$avglon<-mean(unique(wtexas$lon),na.rm=T)
cengrpln$avglon<-mean(unique(cengrpln$lon),na.rm=T)
midsouth$avglon<-mean(unique(midsouth$lon),na.rm=T)
bndywaters$avglon<-mean(unique(bndywaters$lon),na.rm=T)
ohriver$avglon<-mean(unique(ohriver$lon),na.rm=T)
appalachia$avglon<-mean(unique(appalachia$lon),na.rm=T)
southeast$avglon<-mean(unique(southeast$lon),na.rm=T)
ecoast$avglon<-mean(unique(ecoast$lon),na.rm=T)
northeast$avglon<-mean(unique(northeast$lon),na.rm=T)

library(maps)
jpeg("C:/Users/amych/Documents/Research/OC Fraction
Trends/review/regions_map_color_nourban_bigpch.jpg",height=4,width=6,units="in",res=300)
par(xpd=T)
map("state", interior = FALSE, lwd=1,col="gray20")
map("state", boundary = FALSE, lty = 2, add = TRUE,col="gray50")
points(mean(northwest$lon,na.rm=T),mean(northwest$lat,na.rm=T),col="steelblue3",pch=16,ce
x=1)
points(mean(columgorge$lon,na.rm=T),mean(columgorge$lat,na.rm=T),col="maroon4",pch=16,
cex=1)
points(mean(ecoast$lon,na.rm=T),mean(ecoast$lat,na.rm=T),col="seagreen4",pch=16,cex=1)
points(mean(ohriver$lon,na.rm=T),mean(ohriver$lat,na.rm=T),col="peru",pch=16,cex=1)
points(mean(appalachia$lon,na.rm=T),mean(appalachia$lat,na.rm=T),col="orchid3",pch=16,cex
=1)
points(mean(southeast$lon,na.rm=T),mean(southeast$lat,na.rm=T),col="sienna4",pch=16,cex=1
)
points(mean(midsouth$lon,na.rm=T),mean(midsouth$lat,na.rm=T),col="mediumblue",pch=16,c
ex=1)
points(mean(cengrpln$lon,na.rm=T),mean(cengrpln$lat,na.rm=T),col="palegreen4",pch=16,cex
=1)
points(mean(bndywaters$lon,na.rm=T),mean(bndywaters$lat,na.rm=T),col="skyblue",pch=16,c
ex=1)
points(mean(norgrpln$lon,na.rm=T),mean(norgrpln$lat,na.rm=T),col="brown2",pch=16,cex=1)
points(mean(cenrockies$lon,na.rm=T),mean(cenrockies$lat,na.rm=T),col="mediumpurple",pch=
16,cex=1)
points(mean(coplateau$lon,na.rm=T),mean(coplateau$lat,na.rm=T),col="lightblue4",pch=16,cex
=1)
points(mean(mogplateau$lon,na.rm=T),mean(mogplateau$lat,na.rm=T),col="pink4",pch=16,cex
=1)
points(mean(wtexas$lon,na.rm=T),mean(wtexas$lat,na.rm=T),col="mediumturquoise",pch=16,c
ex=1)
```

```
points(mean(soaz$lon,na.rm=T),mean(soaz$lat,na.rm=T),col="darkred",pch=16,cex=1)
points(mean(norrockies$lon,na.rm=T),mean(norrockies$lat,na.rm=T),col="lightgoldenrod4",pch
=16,cex=1)
points(mean(grbasin$lon,na.rm=T),mean(grbasin$lat,na.rm=T),col="lightblue",pch=16,cex=1)
points(mean(sierranv$lon,na.rm=T),mean(sierranv$lat,na.rm=T),col="chocolate4",pch=16,cex=
1)
points(mean(cacoast$lon,na.rm=T),mean(cacoast$lat,na.rm=T),col="dodgerblue4",pch=16,cex=
1)
points(mean(ornorcal$lon,na.rm=T),mean(ornorcal$lat,na.rm=T),col="greenyellow",pch=16,cex
=1)
points(mean(northeast$lon,na.rm=T),mean(northeast$lat,na.rm=T),col="midnightblue",pch=16,c
ex=1)
points(mean(socal$lon,na.rm=T),mean(socal$lat,na.rm=T),col="lightgreen",pch=16,cex=1)
points(mean(hellscyn$lon,na.rm=T),mean(hellscyn$lat,na.rm=T),col="black",pch=16,cex=1)
#points(unique(urbansites$lon,na.rm=T),unique(urbansites$lat,na.rm=T),col="firebrick2",pch=1
8,cex=1)
text(mean(northwest$lon,na.rm=T),mean(northwest$lat,na.rm=T)+1,"Northwest",cex=0.75,col=
"steelblue3")
text(mean(columgorge$lon,na.rm=T),mean(columgorge$lat,na.rm=T)+1,"Columbia River
Gorge",cex=0.75,col="maroon4")
text(mean(hellscyn$lon,na.rm=T),mean(hellscyn$lat,na.rm=T)+1,"Hells
Canyon",cex=0.75,col="black")
text(mean(norrockies$lon,na.rm=T),mean(norrockies$lat,na.rm=T)+1.25,"Northern
Rockies",cex=0.75,col="lightgoldenrod4")
text(mean(norgrpln$lon,na.rm=T)+2,mean(norgrpln$lat,na.rm=T)-1,"Northern Great
Plains",cex=0.75,col="brown2")
text(mean(bndywaters$lon,na.rm=T),mean(bndywaters$lat+1),"Boundary
Waters",cex=0.75,col="skyblue")
text(mean(cenrockies$lon,na.rm=T)+2,mean(cenrockies$lat,na.rm=T)+1,"Central
Rockies",cex=0.75,col="mediumpurple")
text(mean(cengrpln$lon,na.rm=T),mean(cengrpln$lat,na.rm=T)+1,"Central Great
Plains",cex=0.75,col="palegreen4")
text(mean(northeast$lon,na.rm=T),mean(northeast$lat,na.rm=T)+1,"Northeast",cex=0.75,col="
midnightblue")
text(mean(ecoast$lon,na.rm=T),mean(ecoast$lat,na.rm=T)+1,"East
Coast",cex=0.75,col="seagreen4")
text(mean(appalachia$lon,na.rm=T),mean(appalachia$lat,na.rm=T)-
1,"Appalachia",cex=0.75,col="orchid3")
text(mean(ohriver$lon,na.rm=T),mean(ohriver$lat,na.rm=T)+1,"Ohio River
Valley",cex=0.75,col="peru")
text(mean(southeast$lon,na.rm=T),mean(southeast$lat,na.rm=T)+1,"Southeast",cex=0.75,col="s
ienna4")
text(mean(midsouth$lon,na.rm=T),mean(midsouth$lat,na.rm=T)+1,"Mid
South",cex=0.75,col="mediumblue")
text(mean(wtexas$lon,na.rm=T)+2,mean(wtexas$lat,na.rm=T)+1,"West
Texas",cex=0.75,col="mediumturquoise")
```

```
text(mean(mogplateau$lon,na.rm=T),mean(mogplateau$lat,na.rm=T)+1,"Mogollon
Plateau",cex=0.75,col="pink4")
text(mean(soaz$lon,na.rm=T),mean(soaz$lat,na.rm=T)-1,"Southern
AZ",cex=0.75,col="darkred")
text(mean(coplateau$lon,na.rm=T)+2,mean(coplateau$lat,na.rm=T)-1,"Colorado
Plateau",cex=0.75,col="lightblue4")
text(mean(socal$lon,na.rm=T)-1,mean(socal$lat,na.rm=T)-1,"Southern
CA",cex=0.75,col="lightgreen")
text(mean(sierranv$lon,na.rm=T),mean(sierranv$lat,na.rm=T)+1,"Sierra
Nevada",cex=0.75,col="chocolate4")
text(mean(cacoast$lon,na.rm=T)-1,mean(cacoast$lat,na.rm=T)-1,"CA
Coast",xpd=T,cex=0.75,col="dodgerblue4")
text(mean(grbasin$lon,na.rm=T)-1,mean(grbasin$lat,na.rm=T)+1,"Great
Basin",cex=0.75,col="lightblue")
text(mean(ornorcal$lon,na.rm=T),mean(ornorcal$lat,na.rm=T)+1,"Oregon/Northern
CA",xpd=T,cex=0.75,col="greenyellow")
dev.off()

jpeg("C:/Users/amych/Documents/Research/OC Fraction
Trends/review/sites_map_color_nourban_bigpch.jpg",height=4,width=6,units="in",res=300)
map("state", interior = FALSE, lwd=1,col="gray20")
map("state", boundary = FALSE, lty = 2, add = TRUE,col="gray50")
points(unique(northwest$lon),unique(northwest$lat),col="steelblue3",pch=16,cex=1.25)
points(unique(columgorge$lon),unique(columgorge$lat),col="maroon4",pch=16,cex=1.25)
points(unique(ecoast$lon),unique(ecoast$lat),col="seagreen4",pch=16,cex=1.25)
points(unique(ohriver$lon),unique(ohriver$lat),col="peru",pch=16,cex=1.25)
points(unique(appalachia$lon),unique(appalachia$lat),col="orchid3",pch=16,cex=1.25)
points(unique(southeast$lon),unique(southeast$lat),col="sienna4",pch=16,cex=1.25)
points(unique(midsouth$lon),unique(midsouth$lat),col="mediumblue",pch=16,cex=1.25)
points(unique(cengrpln$lon),unique(cengrpln$lat),col="palegreen4",pch=16,cex=1.25)
points(unique(bndywaters$lon),unique(bndywaters$lat),col="skyblue",pch=16,cex=1.25)
points(unique(norgrpln$lon),unique(norgrpln$lat),col="brown2",pch=16,cex=1.25)
points(unique(cenrockies$lon),unique(cenrockies$lat),col="mediumpurple",pch=16,cex=1.25)
points(unique(coplateau$lon),unique(coplateau$lat),col="lightblue4",pch=16,cex=1.25)
points(unique(mogplateau$lon),unique(mogplateau$lat),col="pink4",pch=16,cex=1.25)
points(unique(wtexas$lon),unique(wtexas$lat),col="mediumturquoise",pch=16,cex=1.25)
points(unique(soaz$lon),unique(soaz$lat),col="darkred",pch=16,cex=1.25)
points(unique(norrockies$lon),unique(norrockies$lat),col="lightgoldenrod4",pch=16,cex=1.25)
points(unique(grbasin$lon),unique(grbasin$lat),col="lightblue",pch=16,cex=1.25)
points(unique(sierranv$lon),unique(sierranv$lat),col="chocolate4",pch=16,cex=1.25)
points(unique(cacoast$lon),unique(cacoast$lat),col="dodgerblue4",pch=16,cex=1.25)
points(unique(ornorcal$lon),unique(ornorcal$lat),col="greenyellow",pch=16,cex=1.25)
points(unique(northeast$lon),unique(northeast$lat),col="midnightblue",pch=16,cex=1.25)
points(unique(socal$lon),unique(socal$lat),col="lightgreen",pch=16,cex=1.25)
points(unique(hellscyn$lon),unique(hellscyn$lat),col="black",pch=16,cex=1.25)
```

```
#points(unique(urbansites$lon,na.rm=T),unique(urbansites$lat,na.rm=T),col="firebrick2",pch=1
8,cex=1)
dev.off()

########################################
#Figure S2. Decadal trends in copper, iron, sea salt#
########################################
metals<-
read.table("C:/Users/amych/Downloads/202031793313478L0wO02.txt",header=T,sep=",")
metals$Date<-as.Date(as.character(metals$Date),format="%m/%d/%Y")
metals$month<-as.numeric(substring(metals$Date,6,7))
metals$year<-as.numeric(substring(metals$Date,1,4))
metals$CUf.Value<-ifelse(metals$CUf.Value<0,NA,metals$CUf.Value)
metals$FEf.Value<-ifelse(metals$FEf.Value<0,NA,metals$FEf.Value)
metals$SeaSaltf.Value<-ifelse(metals$SeaSaltf.Value<0,NA,metals$SeaSaltf.Value)
metalsavg<-aggregate(metals,by=list(metals$year),FUN="mean",na.rm=T)

tiff("C:/Users/amych/Documents/Research/OC Fraction
Trends/review/interfering_concs.tif",width=7,height=6,units="in",res=300)
par(mar=c(4,6,3,2))
plot(metalsavg$year,metalsavg$CUf.Value,type="l",ylim=c(0,0.2),col="brown4",lwd=3,lty=1,
    ylab="",xlab="",las=1,cex.axis=1.5,cex.lab=1.5)
mtext(side=2,line=3.5,expression("Concentration"~(mu*g~m^{-3})),cex=1.5)
lines(metalsavg$year,metalsavg$FEf.Value,col="firebrick2",lwd=3,lty=3)
lines(metalsavg$year,metalsavg$SeaSaltf.Value,col="turquoise3",lwd=3,lty=2)
legend("topright",legend=c("Copper","Iron","Sea
Salt"),lty=c(1,3,2),col=c("brown4","firebrick2","turquoise3"),
      lwd=3,cex=1.5,bty="n")
dev.off()

################################
#Figure S3. OM:OC ratios over time#
################################
regions4<-read.csv("C:/Users/amych/Downloads/all_combined_data.csv")
regions4$Date<-as.Date(as.character(regions4$Date),format="%Y-%m-%d")
omocseas<-aggregate(regions4,by=list(regions4$month,regions4$year),FUN="mean",na.rm=T)

tiff("C:/Users/amych/Documents/Research/OC Fraction
Trends/review/om_oc_time.tif",height=6,width=7,units="in",res=300)
i<-order(omocseas$Date)
par(mar=c(3,5,4,3))
plot(omocseas$Date[i],omocseas$om.oc[i],type="l",ylim=c(0,5),ylab="OM:OC",xlab="",cex.lab
=1.5,cex.axis=1.5,lwd=3,las=1)
dev.off()
```

```
##########################################
#Figure S4. Absolute decadal OC fraction changes#
##########################################
#basically need to multiply sen's slope trend (ug/m3/yr) by 11 yrs to get ug/m3/decade
diffs<-read.csv("C:/Users/amych/Documents/Research/OC Fraction
Trends/all_percent_diffs_bestQA.csv")
diffs$tocd<-(diffs$sst*11)
diffs$oc1d<-(diffs$ss1*11)
diffs$oc2d<-(diffs$ss2*11)
diffs$oc3d<-(diffs$ss3*11)
diffs$oc4d<-(diffs$ss4*11)
diffs$opd<-(diffs$ssp*11)

#TOC abs diffs
jpeg("C:/Users/amych/Documents/Research/OC Fraction
Trends/review/TOC_absdiffs_dec.jpg",width=7,height=6,units="in",res=300)
par(xpd=T)
map('state',lty=1,lwd=1,interior=F,col="black")
map("state", boundary = FALSE, lty = 2, add = TRUE,col="black")
points(x=diffs$avglon,y=diffs$avglat,pch=ifelse(diffs$mkt<0.05,16,1),
      cex=ifelse(diffs$tocd< -0.4,5.5,ifelse(diffs$tocd< -0.3,4.5,ifelse(diffs$tocd< -
0.2,3.5,ifelse(diffs$tocd< -0.1,2.5,1.5)))),
      col=ifelse(diffs$tocd<0,"mediumblue","firebrick2"),lwd=4)
legend(-127.5,24.5,legend=c("< -0.4","-0.4 to -0.3","-0.3 to -0.2","-0.2 to -0.1","-0.1 to 0"),
      pch=c(16,16,16,16,16),pt.cex=c(5.5,4.5,3.5,2.5,1.5),ncol=3,cex=1.75,y.intersp=1.1,

col=c("mediumblue","mediumblue","mediumblue","mediumblue","mediumblue"),pt.lwd=3,title
=expression("TOC Change"~(mu*g~m^{-3})),bty="n")
dev.off()

#OC1 abs diffs
jpeg("C:/Users/amych/Documents/Research/OC Fraction
Trends/review/OC1_absdiffs_dec.jpg",width=7,height=6,units="in",res=300)
par(xpd=T)
map('state',lty=1,lwd=1,interior=F,col="black")
map("state", boundary = FALSE, lty = 2, add = TRUE,col="black")
points(x=diffs$avglon,y=diffs$avglat,pch=ifelse(diffs$mk1<0.05,16,1),
      cex=ifelse(diffs$oc1d< -0.2,5.5,ifelse(diffs$oc1d< -0.15,4.5,ifelse(diffs$oc1d< -
0.1,3.5,ifelse(diffs$oc1d< -0.05,2.5,ifelse(diffs$oc1d< 0,1.5,1.5))))),
      col=ifelse(diffs$oc1d<0,"mediumblue","firebrick2"),lwd=4)
legend(-127.5,24.5,legend=c("< -0.2","-0.2 to -0.15","-0.15 to -0.1","-0.1 to -0.05","-0.05 to
0","> 0"),
      pch=c(16,16,16,16,16,16),pt.cex=c(5.5,4.5,3.5,2.5,1.5,1.5),ncol=3,cex=1.75,y.intersp=1.1,

col=c("mediumblue","mediumblue","mediumblue","mediumblue","mediumblue","firebrick2"),p
t.lwd=3,title=expression("OC Change"~(mu*g~m^{-3})),bty="n")
```

```
dev.off()

#OC2 abs diffs
jpeg("C:/Users/amych/Documents/Research/OC Fraction
Trends/review/OC2_absdiffs_dec.jpg",width=7,height=6,units="in",res=300)
par(xpd=T)
map('state',lty=1,lwd=1,interior=F,col="black")
map("state", boundary = FALSE, lty = 2, add = TRUE,col="black")
points(x=diffs$avglon,y=diffs$avglat,pch=ifelse(diffs$mk2<0.05,16,1),
      cex=ifelse(diffs$oc2d< -0.2,5.5,ifelse(diffs$oc2d< -0.15,4.5,ifelse(diffs$oc2d< -
0.1,3.5,ifelse(diffs$oc2d< -0.05,2.5,ifelse(diffs$oc2d< 0,1.5,1.5))))),
      col=ifelse(diffs$oc2d<0,"mediumblue","firebrick2"),lwd=4)
legend(-127.5,24.5,legend=c("< -0.2","-0.2 to -0.15","-0.15 to -0.1","-0.1 to -0.05","-0.05 to
0","> 0"),
      pch=c(16,16,16,16,16,16),pt.cex=c(5.5,4.5,3.5,2.5,1.5,1.5),ncol=3,cex=1.75,y.intersp=1.1,

col=c("mediumblue","mediumblue","mediumblue","mediumblue","mediumblue","firebrick2"),p
t.lwd=3,title=expression("OC Change"~(mu*g~m^{-3})),bty="n")
dev.off()

#OC3 abs diffs
jpeg("C:/Users/amych/Documents/Research/OC Fraction
Trends/review/OC3_absdiffs_dec.jpg",width=7,height=6,units="in",res=300)
par(xpd=T)
map('state',lty=1,lwd=1,interior=F,col="black")
map("state", boundary = FALSE, lty = 2, add = TRUE,col="black")
points(x=diffs$avglon,y=diffs$avglat,pch=ifelse(diffs$mk3<0.05,16,1),
      cex=ifelse(diffs$oc3d< -0.2,5.5,ifelse(diffs$oc3d< -0.15,4.5,ifelse(diffs$oc3d< -
0.1,3.5,ifelse(diffs$oc3d< -0.05,2.5,ifelse(diffs$oc3d< 0,1.5,1.5))))),
      col=ifelse(diffs$oc3d<0,"mediumblue","firebrick2"),lwd=4)
legend(-127.5,24.5,legend=c("< -0.2","-0.2 to -0.15","-0.15 to -0.1","-0.1 to -0.05","-0.05 to
0","> 0"),
      pch=c(16,16,16,16,16,16),pt.cex=c(5.5,4.5,3.5,2.5,1.5,1.5),ncol=3,cex=1.75,y.intersp=1.1,

col=c("mediumblue","mediumblue","mediumblue","mediumblue","mediumblue","firebrick2"),p
t.lwd=3,title=expression("OC Change"~(mu*g~m^{-3})),bty="n")
dev.off()

#OC4 abs diffs
jpeg("C:/Users/amych/Documents/Research/OC Fraction
Trends/review/OC4_absdiffs_dec.jpg",width=7,height=6,units="in",res=300)
par(xpd=T)
map('state',lty=1,lwd=1,interior=F,col="black")
map("state", boundary = FALSE, lty = 2, add = TRUE,col="black")
points(x=diffs$avglon,y=diffs$avglat,pch=ifelse(diffs$mk4<0.05,16,1),
```

```
      cex=ifelse(diffs$oc4d< -0.2,5.5,ifelse(diffs$oc4d< -0.15,4.5,ifelse(diffs$oc4d< -
0.1,3.5,ifelse(diffs$oc4d< -0.05,2.5,ifelse(diffs$oc4d< 0,1.5,1.5)))),
      col=ifelse(diffs$oc4d<0,"mediumblue","firebrick2"),lwd=4)
legend(-127.5,24.5,legend=c("< -0.2","-0.2 to -0.15","-0.15 to -0.1","-0.1 to -0.05","-0.05 to
0","> 0"),
      pch=c(16,16,16,16,16,16),pt.cex=c(5.5,4.5,3.5,2.5,1.5,1.5),ncol=3,cex=1.75,y.intersp=1.1,

col=c("mediumblue","mediumblue","mediumblue","mediumblue","mediumblue","firebrick2"),p
t.lwd=3,title=expression("OC Change"~(mu*g~m^{-3})),bty="n")
dev.off()

#PC abs diffs
jpeg("C:/Users/amych/Documents/Research/OC Fraction
Trends/review/PC_absdiffs_dec.jpg",width=7,height=6,units="in",res=300)
par(xpd=T)
map('state',lty=1,lwd=1,interior=F,col="black")
map("state", boundary = FALSE, lty = 2, add = TRUE,col="black")
points(x=diffs$avglon,y=diffs$avglat,pch=ifelse(diffs$mkp<0.05,16,1),
      cex=ifelse(diffs$opd< -0.2,5.5,ifelse(diffs$opd< -0.15,4.5,ifelse(diffs$opd< -
0.1,3.5,ifelse(diffs$opd< -0.05,2.5,ifelse(diffs$opd< 0,1.5,1.5)))),
      col=ifelse(diffs$opd<0,"mediumblue","firebrick2"),lwd=4)
legend(-127.5,24.5,legend=c("< -0.2","-0.2 to -0.15","-0.15 to -0.1","-0.1 to -0.05","-0.05 to
0","> 0"),
      pch=c(16,16,16,16,16,16),pt.cex=c(5.5,4.5,3.5,2.5,1.5,1.5),ncol=3,cex=1.75,y.intersp=1.1,

col=c("mediumblue","mediumblue","mediumblue","mediumblue","mediumblue","firebrick2"),p
t.lwd=3,title=expression("OC Change"~(mu*g~m^{-3})),bty="n")
dev.off()

##################################
#Figure S5. Decadal % change in ALW#
##################################
diffs2<-read.csv("C:/Users/stor/Documents/OC Fraction Trends/review/water_sen_percent.csv")

#map!
jpeg("C:/Users/stor/Documents/OC Fraction
Trends/review/water_perc_peryear_allseason.jpg",width=7,height=6,units="in",res=300)
states<-map_data("state")
g<-
ggplot(data=states,aes(x=long,y=lat))+geom_polygon(aes(group=group),fill="white",colour="bl
ack")+coord_fixed(1.3)+guides(fill=F)
g
g+geom_point(data=diffs2,aes(x=diffs2$avglon,y=diffs2$avglat,
                    colour=waterperc),size=4)+guides(shape=F)+
  scale_colour_gradientn(colours=rev(matlab.like(23)),limits=c(-1,0),breaks=c(-1,-0.75,-0.5,-
0.25,0))+
```

```
  labs(x="",y="",title="")+

theme(panel.background=element_blank(),axis.ticks=element_blank(),axis.text=element_blank()
,
      legend.title=element_blank(),legend.text=element_text(size=16),
      plot.title=element_text(hjust=0.5,size=16),legend.key.height=unit(0.7,"in"))
dev.off()


#Figure S6. Decadal % change in PC
diffs<-read.csv("C:/Users/stor/Documents/OC Fraction Trends/all_percent_diffs.csv")
#map
library(ggplot2)
library(colorRamps)
library(RColorBrewer)

jpeg("C:/Users/stor/Documents/OC Fraction
Trends/review/pc_perc_peryear_allseason.jpg",width=7,height=6,units="in",res=300)
states<-map_data("state")
g<-
ggplot(data=states,aes(x=long,y=lat))+geom_polygon(aes(group=group),fill="white",colour="bl
ack")+coord_fixed(1.3)+guides(fill=F)
g
g+geom_point(data=diffs,aes(x=diffs$avglon,y=diffs$avglat,
                    colour=opperc),size=4)+guides(shape=F)+
  scale_colour_gradientn(colours=rev(matlab.like(23)),limits=c(-0.2,0),breaks=c(-0.2,-0.15,-0.1,-
0.05,0))+
  labs(x="",y="",title="")+

theme(panel.background=element_blank(),axis.ticks=element_blank(),axis.text=element_blank()
,
      legend.title=element_blank(),legend.text=element_text(size=16),
      plot.title=element_text(hjust=0.5,size=16),legend.key.height=unit(0.7,"in"))
dev.off()

##########################################################
#Figure S7. OC fraction changes in Appalachia with uncertainties#
##########################################################
ocdat<-read.csv("C:/Users/amych/Documents/Research/OC Fraction Trends/OC_bestQA.csv")
ocdat$Date<-as.Date(as.character(ocdat$Date),format="%Y-%m-%d")
ocdat2<-
data.frame(SiteCode=ocdat$SiteCode,Date=ocdat$Date,month=ocdat$month,year=ocdat$year,

OC1_QA=ocdat$OC1_QA,OC2_QA=ocdat$OC2_QA,OC3_QA=ocdat$OC3_QA,OC4_QA=oc
dat$OC4_QA,
              OP_QA=ocdat$OP_QA,OCtot=ocdat$OCf.Value,
```

```
        oc1_low=ocdat$oc1_low,oc1_high=ocdat$oc1_high,oc2_low=ocdat$oc2_low,

oc2_high=ocdat$oc2_high,oc3_low=ocdat$oc3_low,oc3_high=ocdat$oc3_high,oc4_low=ocdat$
oc4_low,
        oc4_high=ocdat$oc4_high,op_low=ocdat$op_low,op_high=ocdat$op_high)
ocdat3<-aggregate(ocdat2,by=list(ocdat2$SiteCode,ocdat2$Date),FUN="mean",na.rm=T)
ocdat3$SiteCode<-ocdat3$Group.1
ocdat3$Date<-ocdat3$Group.2
ocdat3$Group.1<-NULL
ocdat3$Group.2<-NULL

#appalachia
attach(ocdat3)
appalachia<-
ocdat3[SiteCode=="SIPS1"|SiteCode=="COHU1"|SiteCode=="GRSM1"|SiteCode=="SHRO1"|
SiteCode=="LIGO1"|SiteCode=="DOSO1"|SiteCode=="FRRE1"|SiteCode=="AREN1"|SiteCod
e=="SHEN1"|SiteCode=="JART1"|SiteCode=="JEFF1",]
appalachia$SiteCode<-NULL
appmon<-
aggregate(appalachia,by=list(appalachia$month,appalachia$year),FUN="median",na.rm=T)

jpeg("C:/Users/amych/Documents/Research/OC Fraction
Trends/review/app_month_oc1_uncerts.jpg",width=7,height=6,units="in",res=300)
par(mar=c(4,6,4,2))
plot(appmon$Date,appmon$OC1_QA,type="l",col="black",ylim=c(0,1),las=1,ylab="",xlab="",c
ex.axis=2)
mtext(side=2,line=3.5,cex=2,expression("OC1"~(mu*g~m^{-3})))
polygon(c(appmon$Date,rev(appmon$Date)),c(appmon$oc1_high,rev(appmon$oc1_low)),col="
gray80",border="gray80")
lines(appmon$Date,appmon$OC1_QA,col="black",lwd=2)
dev.off()

jpeg("C:/Users/amych/Documents/Research/OC Fraction
Trends/review/app_month_oc2_uncerts.jpg",width=7,height=6,units="in",res=300)
par(mar=c(4,6,4,2))
plot(appmon$Date,appmon$OC2_QA,type="l",col="black",ylim=c(0,1),las=1,ylab="",xlab="",c
ex.axis=2)
mtext(side=2,line=3.5,cex=2,expression("OC2"~(mu*g~m^{-3})))
polygon(c(appmon$Date,rev(appmon$Date)),c(appmon$oc2_high,rev(appmon$oc2_low)),col="
gray80",border="gray80")
lines(appmon$Date,appmon$OC2_QA,col="black",lwd=2)
dev.off()

jpeg("C:/Users/amych/Documents/Research/OC Fraction
Trends/review/app_month_oc3_uncerts.jpg",width=7,height=6,units="in",res=300)
par(mar=c(4,6,4,2))
```

```
plot(appmon$Date,appmon$OC3_QA,type="l",col="black",ylim=c(0,1),las=1,ylab="",xlab="",cex.axis=2)
mtext(side=2,line=3.5,cex=2,expression("OC3"~(mu*g~m^{-3})))
polygon(c(appmon$Date,rev(appmon$Date)),c(appmon$oc3_high,rev(appmon$oc3_low)),col="gray80",border="gray80")
lines(appmon$Date,appmon$OC3_QA,col="black",lwd=2)
dev.off()

jpeg("C:/Users/amych/Documents/Research/OC Fraction Trends/review/app_month_oc4_uncerts.jpg",width=7,height=6,units="in",res=300)
par(mar=c(4,6,4,2))
plot(appmon$Date,appmon$OC4_QA,type="l",col="black",ylim=c(0,1),las=1,ylab="",xlab="",cex.axis=2)
mtext(side=2,line=3.5,cex=2,expression("OC4"~(mu*g~m^{-3})))
polygon(c(appmon$Date,rev(appmon$Date)),c(appmon$oc4_high,rev(appmon$oc4_low)),col="gray80",border="gray80")
lines(appmon$Date,appmon$OC4_QA,col="black",lwd=2)
dev.off()

jpeg("C:/Users/amych/Documents/Research/OC Fraction Trends/review/app_month_op_uncerts.jpg",width=7,height=6,units="in",res=300)
par(mar=c(4,6,4,2))
plot(appmon$Date,appmon$OP_QA,type="l",col="black",ylim=c(0,1),las=1,ylab="",xlab="",cex.axis=2)
mtext(side=2,line=3.5,cex=2,expression("PC"~(mu*g~m^{-3})))
polygon(c(appmon$Date,rev(appmon$Date)),c(appmon$op_high,rev(appmon$op_low)),col="gray80",border="gray80")
lines(appmon$Date,appmon$OP_QA,col="black",lwd=2)
dev.off()

########################################
#Figure S8. Decadal % changes in OC3 by season#
########################################
spe<-read.csv("C:/Users/amych/Documents/Research/OC Fraction Trends/review/OC3_senssloped_byseason.csv")
spe$oc3perc100<-spe$oc3perc*100

spewinter<-subset(spe,spe$seasonnum==1)
spespring<-subset(spe,spe$seasonnum==2)
spesummer<-subset(spe,spe$seasonnum==3)
spefall<-subset(spe,spe$seasonnum==4)

library(ggplot2)
library(colorRamps)
library(RColorBrewer)
```

```
spewinter$oc3sig<-ifelse(spewinter$pOC3<0.05,"Y","N")
spespring$oc3sig<-ifelse(spespring$pOC3<0.05,"Y","N")
spesummer$oc3sig<-ifelse(spesummer$pOC3<0.05,"Y","N")
spefall$oc3sig<-ifelse(spefall$pOC3<0.05,"Y","N")

jpeg("C:/Users/amych/Documents/Research/OC Fraction
Trends/review/OC3_changes_winter.jpg",width=7,height=6,units="in",res=300)
states<-map_data("state")
g<-
ggplot(data=states,aes(x=long,y=lat))+geom_polygon(aes(group=group),fill="white",colour="#3
33333",linetype="dashed")+coord_fixed(1.3)+guides(fill=F)
g
g+geom_point(data=spewinter,aes(x=spewinter$avglon,y=spewinter$avglat,

colour=oc3perc100,shape=spewinter$oc3sig,stroke=2),size=4)+guides(shape=F)+scale_shape_
manual(values=c(1,19))+
  scale_colour_gradientn(colours=blue2red(23),limits=c(-60,60),breaks=c(-60,-30,0,30,60))+
  labs(x="",y="",title="")+

theme(panel.background=element_blank(),axis.ticks=element_blank(),axis.text=element_blank()
,
      legend.title=element_blank(),legend.text=element_text(size=16),
      plot.title=element_text(hjust=0.5,size=16),legend.key.height=unit(0.7,"in"))
dev.off()

jpeg("C:/Users/amych/Documents/Research/OC Fraction
Trends/review/OC3_changes_spring.jpg",width=7,height=6,units="in",res=300)
states<-map_data("state")
g<-
ggplot(data=states,aes(x=long,y=lat))+geom_polygon(aes(group=group),fill="white",colour="#3
33333",linetype="dashed")+coord_fixed(1.3)+guides(fill=F)
g
g+geom_point(data=spespring,aes(x=spespring$avglon,y=spespring$avglat,

colour=oc3perc100,shape=spespring$oc3sig,stroke=2),size=4)+guides(shape=F)+scale_shape_m
anual(values=c(1,19))+
  scale_colour_gradientn(colours=blue2red(23),limits=c(-60,60),breaks=c(-60,-30,0,30,60))+
  labs(x="",y="",title="")+

theme(panel.background=element_blank(),axis.ticks=element_blank(),axis.text=element_blank()
,
      legend.title=element_blank(),legend.text=element_text(size=16),
      plot.title=element_text(hjust=0.5,size=16),legend.key.height=unit(0.7,"in"))
dev.off()
```

```
jpeg("C:/Users/amych/Documents/Research/OC Fraction
Trends/review/OC3_changes_summer.jpg",width=7,height=6,units="in",res=300)
states<-map_data("state")
g<-
ggplot(data=states,aes(x=long,y=lat))+geom_polygon(aes(group=group),fill="white",colour="#3
33333",linetype="dashed")+coord_fixed(1.3)+guides(fill=F)
g
g+geom_point(data=spesummer,aes(x=spesummer$avglon,y=spesummer$avglat,

colour=oc3perc100,shape=spesummer$oc3sig,stroke=2),size=4)+guides(shape=F)+scale_shape_
manual(values=c(1,19))+
  scale_colour_gradientn(colours=blue2red(23),limits=c(-60,60),breaks=c(-60,-30,0,30,60))+
  labs(x="",y="",title="")+

theme(panel.background=element_blank(),axis.ticks=element_blank(),axis.text=element_blank()
,
      legend.title=element_blank(),legend.text=element_text(size=16),
      plot.title=element_text(hjust=0.5,size=16),legend.key.height=unit(0.7,"in"))
dev.off()

jpeg("C:/Users/amych/Documents/Research/OC Fraction
Trends/review/OC3_changes_fall.jpg",width=7,height=6,units="in",res=300)
states<-map_data("state")
g<-
ggplot(data=states,aes(x=long,y=lat))+geom_polygon(aes(group=group),fill="white",colour="#3
33333",linetype="dashed")+coord_fixed(1.3)+guides(fill=F)
g
g+geom_point(data=spefall,aes(x=spefall$avglon,y=spefall$avglat,

colour=oc3perc100,shape=spefall$oc3sig,stroke=2),size=4)+guides(shape=F)+scale_shape_man
ual(values=c(1,19))+
  scale_colour_gradientn(colours=blue2red(23),limits=c(-60,60),breaks=c(-60,-30,0,30,60))+
  labs(x="",y="",title="")+

theme(panel.background=element_blank(),axis.ticks=element_blank(),axis.text=element_blank()
,
      legend.title=element_blank(),legend.text=element_text(size=16),
      plot.title=element_text(hjust=0.5,size=16),legend.key.height=unit(0.7,"in"))
dev.off()

#####################################################
#Figure S9. Correlations between ISOAAQ and OM fractions#
#####################################################
cors<-read.csv("C:/Users/amych/Downloads/Median_Allregions_new_OM_correlations_R.csv")
ps<-read.csv("C:/Users/amych/Downloads/Median_Allregions_new_OM_correlations_p.csv")
```

```
corssummer<-subset(cors,cors$seasonnum==3)
pssummer<-subset(ps,ps$seasonnum==3)

library(ggplot2)
library(colorRamps)
library(RColorBrewer)

corssummer$om1sig<-ifelse(pssummer$OM1vISOAAQ<0.05,"Y","N")
corssummer$om2sig<-ifelse(pssummer$OM2vISOAAQ<0.05,"Y","N")
corssummer$om3sig<-ifelse(pssummer$OM3vISOAAQ<0.05,"Y","N")
corssummer$om4sig<-ifelse(pssummer$OM4vISOAAQ<0.05,"Y","N")
corssummer$tomsig<-ifelse(pssummer$TOMvISOAAQ<0.05,"Y","N")

jpeg("C:/Users/amych/Documents/Research/OC Fraction
Trends/review/isoaaq_OM1_cors_summer.jpg",width=7,height=6,units="in",res=300)
states<-map_data("state")
g<-
ggplot(data=states,aes(x=long,y=lat))+geom_polygon(aes(group=group),fill="white",colour="#3
33333",linetype="dashed")+coord_fixed(1.3)+guides(fill=F)
g
g+geom_point(data=corssummer,aes(x=corssummer$avglon,y=corssummer$avglat,

colour=OM1vISOAAQ,shape=corssummer$om1sig,stroke=2),size=4)+guides(shape=F)+scale_s
hape_manual(values=c(1,19))+
  scale_colour_gradientn(colours=matlab.like(23),limits=c(-0.9,0.9),breaks=c(-0.9,-0.6,-
0.3,0,0.3,0.6,0.9))+
  labs(x="",y="",title="")+

theme(panel.background=element_blank(),axis.ticks=element_blank(),axis.text=element_blank()
,
      legend.title=element_blank(),legend.text=element_text(size=16),
      plot.title=element_text(hjust=0.5,size=16),legend.key.height=unit(0.7,"in"))
dev.off()

jpeg("C:/Users/amych/Documents/Research/OC Fraction
Trends/review/isoaaq_OM2_cors_summer.jpg",width=7,height=6,units="in",res=300)
states<-map_data("state")
g<-
ggplot(data=states,aes(x=long,y=lat))+geom_polygon(aes(group=group),fill="white",colour="#3
33333",linetype="dashed")+coord_fixed(1.3)+guides(fill=F)
g
g+geom_point(data=corssummer,aes(x=corssummer$avglon,y=corssummer$avglat,

colour=OM2vISOAAQ,shape=corssummer$om2sig,stroke=2),size=4)+guides(shape=F)+scale_s
hape_manual(values=c(1,19))+
```

```
  scale_colour_gradientn(colours=matlab.like(23),limits=c(-0.9,0.9),breaks=c(-0.9,-0.6,-
0.3,0,0.3,0.6,0.9))+
  labs(x="",y="",title="")+

theme(panel.background=element_blank(),axis.ticks=element_blank(),axis.text=element_blank()
,
        legend.title=element_blank(),legend.text=element_text(size=16),
        plot.title=element_text(hjust=0.5,size=16),legend.key.height=unit(0.7,"in"))
dev.off()

jpeg("C:/Users/amych/Documents/Research/OC Fraction
Trends/review/isoaaq_OM3_cors_summer.jpg",width=7,height=6,units="in",res=300)
states<-map_data("state")
g<-
ggplot(data=states,aes(x=long,y=lat))+geom_polygon(aes(group=group),fill="white",colour="#3
33333",linetype="dashed")+coord_fixed(1.3)+guides(fill=F)
g
g+geom_point(data=corssummer,aes(x=corssummer$avglon,y=corssummer$avglat,

colour=OM3vISOAAQ,shape=corssummer$om3sig,stroke=2),size=4)+guides(shape=F)+scale_s
hape_manual(values=c(1,19))+
  scale_colour_gradientn(colours=matlab.like(23),limits=c(-0.9,0.9),breaks=c(-0.9,-0.6,-
0.3,0,0.3,0.6,0.9))+
  labs(x="",y="",title="")+

theme(panel.background=element_blank(),axis.ticks=element_blank(),axis.text=element_blank()
,
        legend.title=element_blank(),legend.text=element_text(size=16),
        plot.title=element_text(hjust=0.5,size=16),legend.key.height=unit(0.7,"in"))
dev.off()

jpeg("C:/Users/amych/Documents/Research/OC Fraction
Trends/review/isoaaq_OM4_cors_summer.jpg",width=7,height=6,units="in",res=300)
states<-map_data("state")
g<-
ggplot(data=states,aes(x=long,y=lat))+geom_polygon(aes(group=group),fill="white",colour="#3
33333",linetype="dashed")+coord_fixed(1.3)+guides(fill=F)
g
g+geom_point(data=corssummer,aes(x=corssummer$avglon,y=corssummer$avglat,

colour=OM4vISOAAQ,shape=corssummer$om4sig,stroke=2),size=4)+guides(shape=F)+scale_s
hape_manual(values=c(1,19))+
  scale_colour_gradientn(colours=matlab.like(23),limits=c(-0.9,0.9),breaks=c(-0.9,-0.6,-
0.3,0,0.3,0.6,0.9))+
  labs(x="",y="",title="")+
```

```
theme(panel.background=element_blank(),axis.ticks=element_blank(),axis.text=element_blank()
,
      legend.title=element_blank(),legend.text=element_text(size=16),
      plot.title=element_text(hjust=0.5,size=16),legend.key.height=unit(0.7,"in"))
dev.off()

jpeg("C:/Users/amych/Documents/Research/OC Fraction
Trends/review/isoaaq_TOM_cors_summer.jpg",width=7,height=6,units="in",res=300)
states<-map_data("state")
g<-
ggplot(data=states,aes(x=long,y=lat))+geom_polygon(aes(group=group),fill="white",colour="#3
33333",linetype="dashed")+coord_fixed(1.3)+guides(fill=F)
g
g+geom_point(data=corssummer,aes(x=corssummer$avglon,y=corssummer$avglat,

colour=TOMvISOAAQ,shape=corssummer$tomsig,stroke=2),size=4)+guides(shape=F)+scale_s
hape_manual(values=c(1,19))+
  scale_colour_gradientn(colours=matlab.like(23),limits=c(-0.9,0.9),breaks=c(-0.9,-0.6,-
0.3,0,0.3,0.6,0.9))+
  labs(x="",y="",title="")+

theme(panel.background=element_blank(),axis.ticks=element_blank(),axis.text=element_blank()
,
      legend.title=element_blank(),legend.text=element_text(size=16),
      plot.title=element_text(hjust=0.5,size=16),legend.key.height=unit(0.7,"in"))
dev.off()

##############################################
#Figure S10. Decadal % change in ISOAAQ by season#
##############################################
spe<-read.csv("C:/Users/stor/Documents/OC Fraction Trends/review/Median_geos-
chem_sensslopes.csv")
spe$isoaaqperc100<-spe$isoaaqperc*100

spewinter<-subset(spe,spe$seasonnum==1)
spespring<-subset(spe,spe$seasonnum==2)
spesummer<-subset(spe,spe$seasonnum==3)
spefall<-subset(spe,spe$seasonnum==4)

library(ggplot2)
library(colorRamps)
library(RColorBrewer)

spewinter$isosig<-ifelse(spewinter$pISOAAQ<0.05,"Y","N")
spespring$isosig<-ifelse(spespring$pISOAAQ<0.05,"Y","N")
```

```
spesummer$isosig<-ifelse(spesummer$pISOAAQ<0.05,"Y","N")
spefall$isosig<-ifelse(spefall$pISOAAQ<0.05,"Y","N")

jpeg("C:/Users/amych/Documents/Research/OC Fraction
Trends/review/isoaaq_decreases_winter.jpg",width=7,height=6,units="in",res=300)
states<-map_data("state")
g<-
ggplot(data=states,aes(x=long,y=lat))+geom_polygon(aes(group=group),fill="white",colour="#3
33333",linetype="dashed")+coord_fixed(1.3)+guides(fill=F)
g
g+geom_point(data=spewinter,aes(x=spewinter$avglon,y=spewinter$avglat,

colour=isoaaqperc100,shape=spewinter$isosig,stroke=2),size=4)+guides(shape=F)+scale_shape
_manual(values=c(1,19))+
  scale_colour_gradientn(colours=blue2red(23),limits=c(-200,200),breaks=c(-200,-150,-100,-
50,0,50,100,150,200))+
  labs(x="",y="",title="")+

theme(panel.background=element_blank(),axis.ticks=element_blank(),axis.text=element_blank()
,
      legend.title=element_blank(),legend.text=element_text(size=16),
      plot.title=element_text(hjust=0.5,size=16),legend.key.height=unit(0.7,"in"))
dev.off()

jpeg("C:/Users/amych/Documents/Research/OC Fraction
Trends/review/isoaaq_decreases_spring.jpg",width=7,height=6,units="in",res=300)
states<-map_data("state")
g<-
ggplot(data=states,aes(x=long,y=lat))+geom_polygon(aes(group=group),fill="white",colour="#3
33333",linetype="dashed")+coord_fixed(1.3)+guides(fill=F)
g
g+geom_point(data=spespring,aes(x=spespring$avglon,y=spespring$avglat,

colour=isoaaqperc100,shape=spespring$isosig,stroke=2),size=4)+guides(shape=F)+scale_shape
_manual(values=c(1,19))+
  scale_colour_gradientn(colours=blue2red(23),limits=c(-200,200),breaks=c(-200,-150,-100,-
50,0,50,100,150,200))+
  labs(x="",y="",title="")+

theme(panel.background=element_blank(),axis.ticks=element_blank(),axis.text=element_blank()
,
      legend.title=element_blank(),legend.text=element_text(size=16),
      plot.title=element_text(hjust=0.5,size=16),legend.key.height=unit(0.7,"in"))
dev.off()
```

```
jpeg("C:/Users/amych/Documents/Research/OC Fraction
Trends/review/isoaaq_decreases_summer.jpg",width=7,height=6,units="in",res=300)
states<-map_data("state")
g<-
ggplot(data=states,aes(x=long,y=lat))+geom_polygon(aes(group=group),fill="white",colour="#3
33333",linetype="dashed")+coord_fixed(1.3)+guides(fill=F)
g
g+geom_point(data=spesummer,aes(x=spesummer$avglon,y=spesummer$avglat,

colour=isoaaqperc100,shape=spesummer$isosig,stroke=2),size=4)+guides(shape=F)+scale_shap
e_manual(values=c(1,19))+
  scale_colour_gradientn(colours=blue2red(23),limits=c(-200,200),breaks=c(-200,-150,-100,-
50,0,50,100,150,200))+
  labs(x="",y="",title="")+

theme(panel.background=element_blank(),axis.ticks=element_blank(),axis.text=element_blank()
,
      legend.title=element_blank(),legend.text=element_text(size=16),
      plot.title=element_text(hjust=0.5,size=16),legend.key.height=unit(0.7,"in"))
dev.off()

jpeg("C:/Users/amych/Documents/Research/OC Fraction
Trends/review/isoaaq_decreases_fall.jpg",width=7,height=6,units="in",res=300)
states<-map_data("state")
g<-
ggplot(data=states,aes(x=long,y=lat))+geom_polygon(aes(group=group),fill="white",colour="#3
33333",linetype="dashed")+coord_fixed(1.3)+guides(fill=F)
g
g+geom_point(data=spefall,aes(x=spefall$avglon,y=spefall$avglat,

colour=isoaaqperc100,shape=spefall$isosig,stroke=2),size=4)+guides(shape=F)+scale_shape_m
anual(values=c(1,19))+
  scale_colour_gradientn(colours=blue2red(23),limits=c(-200,200),breaks=c(-200,-150,-100,-
50,0,50,100,150,200))+
  labs(x="",y="",title="")+

theme(panel.background=element_blank(),axis.ticks=element_blank(),axis.text=element_blank()
,
      legend.title=element_blank(),legend.text=element_text(size=16),
      plot.title=element_text(hjust=0.5,size=16),legend.key.height=unit(0.7,"in"))
dev.off()

#####################################################
#Figure S11. Decadal trends in increasing GEOS-Chem species#
#####################################################
```

```
alldata<-read.csv("C:/Users/amych/Documents/Research/OC Fraction
Trends/alldata_with_geos.csv")
alldata$Date<-as.Date(as.character(alldata$Date),format="%Y-%m-%d")
dfrm<-
data.frame(year=alldata$year,water=alldata$water,geos_water=alldata$Chem_WaterSav,OM2=a
lldata$OM2,OM3=alldata$OM3,

SO4=alldata$SO4,geos_so4=alldata$AerMassSO4,opoa=alldata$AerMassOPOA,seasonnum=all
data$seasonnum,

Date=alldata$Date,asoa=alldata$AerMassASOA,tsoa=alldata$AerMassTSOA,poa=alldata$Aer
MassPOA)
conus<-aggregate(dfrm,by=list(dfrm$seasonnum,dfrm$year),FUN="median",na.rm=T)
conus2<-aggregate(dfrm,by=list(dfrm$year),FUN="median",na.rm=T)

jpeg("C:/Users/amych/Documents/Research/OC Fraction
Trends/review/OPOA_increases_byseason.jpg",width=7,height=6,units="in",res=300)
par(mar=c(4,5.5,4,2.5))
plot(conus$Date,conus$opoa,type="l",lwd=3,col="darkgreen",las=1,cex.axis=1.5,xlab="",
    ylab="",cex.lab=1.5,ylim=c(0,2))
mtext(side=2,line=3.5,expression("GEOS-Chem OPOA"~(mu*g~m^{-3})),cex=1.5)
dev.off()

jpeg("C:/Users/amych/Documents/Research/OC Fraction
Trends/review/TSOA_increases_byseason.jpg",width=7,height=6,units="in",res=300)
par(mar=c(4,5.5,4,2.5))
plot(conus$Date,conus$tsoa,type="l",lwd=3,col="darkgreen",las=1,cex.axis=1.5,xlab="",
    ylab="",cex.lab=1.5,ylim=c(0,1))
mtext(side=2,line=3.5,expression("GEOS-Chem TSOA"~(mu*g~m^{-3})),cex=1.5)
dev.off()

jpeg("C:/Users/amych/Documents/Research/OC Fraction
Trends/review/ASOA_increases_byseason.jpg",width=7,height=6,units="in",res=300)
par(mar=c(4,5.5,4,2.5))
plot(conus$Date,conus$asoa,type="l",lwd=3,col="darkgreen",las=1,cex.axis=1.5,xlab="",
    ylab="",cex.lab=1.5,ylim=c(0,0.1))
mtext(side=2,line=3.5,expression("GEOS-Chem ASOA"~(mu*g~m^{-3})),cex=1.5)
dev.off()

jpeg("C:/Users/amych/Documents/Research/OC Fraction
Trends/review/POA_increases_byseason.jpg",width=7,height=6,units="in",res=300)
par(mar=c(4,5.5,4,2.5))
plot(conus$Date,conus$poa,type="l",lwd=3,col="darkgreen",las=1,cex.axis=1.5,xlab="",
    ylab="",cex.lab=1.5,ylim=c(0,0.1))
mtext(side=2,line=3.5,expression("GEOS-Chem POA"~(mu*g~m^{-3})),cex=1.5)
dev.off()
```

```
##############################################
#Figure S12. OM3 and OPOA correlation in all seasons#
##############################################
cors<-read.csv("C:/Users/amych/Downloads/Median_Allregions_new_OM_correlations_R.csv")
ps<-read.csv("C:/Users/amych/Downloads/Median_Allregions_new_OM_correlations_p.csv")

corswinter<-subset(cors,cors$seasonnum==1)
pswinter<-subset(ps,ps$seasonnum==1)
corsspring<-subset(cors,cors$seasonnum==2)
psspring<-subset(ps,ps$seasonnum==2)
corssummer<-subset(cors,cors$seasonnum==3)
pssummer<-subset(ps,ps$seasonnum==3)
corsfall<-subset(cors,cors$seasonnum==4)
psfall<-subset(ps,ps$seasonnum==4)

corswinter$om3sig<-ifelse(pswinter$OM3vOPOA<0.05,"Y","N")
corsspring$om3sig<-ifelse(psspring$OM3vOPOA<0.05,"Y","N")
corssummer$om3sig<-ifelse(pssummer$OM3vOPOA<0.05,"Y","N")
corsfall$om3sig<-ifelse(psfall$OM3vOPOA<0.05,"Y","N")

jpeg("C:/Users/amych/Documents/Research/OC Fraction
Trends/review/opoa_om3_cors_winter.jpg",width=7,height=6,units="in",res=300)
states<-map_data("state")
g<-
ggplot(data=states,aes(x=long,y=lat))+geom_polygon(aes(group=group),fill="white",colour="#3
33333",linetype="dashed")+coord_fixed(1.3)+guides(fill=F)
g
g+geom_point(data=corswinter,aes(x=corswinter$avglon,y=corswinter$avglat,

colour=OM3vOPOA,shape=corswinter$om3sig,stroke=2),size=4)+guides(shape=F)+scale_shap
e_manual(values=c(1,19))+
  scale_colour_gradientn(colours=matlab.like(23),limits=c(-0.9,0.9),breaks=c(-0.9,-0.6,-
0.3,0,0.3,0.6,0.9))+
  labs(x="",y="",title="")+

theme(panel.background=element_blank(),axis.ticks=element_blank(),axis.text=element_blank()
,
      legend.title=element_blank(),legend.text=element_text(size=16),
      plot.title=element_text(hjust=0.5,size=16),legend.key.height=unit(0.7,"in"))
dev.off()

jpeg("C:/Users/amych/Documents/Research/OC Fraction
Trends/review/opoa_om3_cors_spring.jpg",width=7,height=6,units="in",res=300)
states<-map_data("state")
```

```
g<-
ggplot(data=states,aes(x=long,y=lat))+geom_polygon(aes(group=group),fill="white",colour="#3
33333",linetype="dashed")+coord_fixed(1.3)+guides(fill=F)
g
g+geom_point(data=corsspring,aes(x=corsspring$avglon,y=corsspring$avglat,

colour=OM3vOPOA,shape=corsspring$om3sig,stroke=2),size=4)+guides(shape=F)+scale_shap
e_manual(values=c(1,19))+
  scale_colour_gradientn(colours=matlab.like(23),limits=c(-0.9,0.9),breaks=c(-0.9,-0.6,-
0.3,0,0.3,0.6,0.9))+
  labs(x="",y="",title="")+

theme(panel.background=element_blank(),axis.ticks=element_blank(),axis.text=element_blank()
,
      legend.title=element_blank(),legend.text=element_text(size=16),
      plot.title=element_text(hjust=0.5,size=16),legend.key.height=unit(0.7,"in"))
dev.off()

jpeg("C:/Users/amych/Documents/Research/OC Fraction
Trends/review/opoa_om3_cors_summer.jpg",width=7,height=6,units="in",res=300)
states<-map_data("state")
g<-
ggplot(data=states,aes(x=long,y=lat))+geom_polygon(aes(group=group),fill="white",colour="#3
33333",linetype="dashed")+coord_fixed(1.3)+guides(fill=F)
g
g+geom_point(data=corssummer,aes(x=corssummer$avglon,y=corssummer$avglat,

colour=OM3vOPOA,shape=corssummer$om3sig,stroke=2),size=4)+guides(shape=F)+scale_sha
pe_manual(values=c(1,19))+
  scale_colour_gradientn(colours=matlab.like(23),limits=c(-0.9,0.9),breaks=c(-0.9,-0.6,-
0.3,0,0.3,0.6,0.9))+
  labs(x="",y="",title="")+

theme(panel.background=element_blank(),axis.ticks=element_blank(),axis.text=element_blank()
,
      legend.title=element_blank(),legend.text=element_text(size=16),
      plot.title=element_text(hjust=0.5,size=16),legend.key.height=unit(0.7,"in"))
dev.off()

jpeg("C:/Users/amych/Documents/Research/OC Fraction
Trends/review/opoa_om3_cors_fall.jpg",width=7,height=6,units="in",res=300)
states<-map_data("state")
g<-
ggplot(data=states,aes(x=long,y=lat))+geom_polygon(aes(group=group),fill="white",colour="#3
33333",linetype="dashed")+coord_fixed(1.3)+guides(fill=F)
g
```

```
g+geom_point(data=corsfall,aes(x=corsfall$avglon,y=corsfall$avglat,

colour=OM3vOPOA,shape=corsfall$om3sig,stroke=2),size=4)+guides(shape=F)+scale_shape_
manual(values=c(1,19))+
  scale_colour_gradientn(colours=matlab.like(23),limits=c(-0.9,0.9),breaks=c(-0.9,-0.6,-
0.3,0,0.3,0.6,0.9))+
  labs(x="",y="",title="")+

theme(panel.background=element_blank(),axis.ticks=element_blank(),axis.text=element_blank()
,
      legend.title=element_blank(),legend.text=element_text(size=16),
      plot.title=element_text(hjust=0.5,size=16),legend.key.height=unit(0.7,"in"))
dev.off()

####################################
#Figure S13. OPOA and OM3 time series#
####################################
alldata<-read.csv("C:/Users/amych/Documents/Research/OC Fraction
Trends/alldata_with_geos.csv")
alldata$Date<-as.Date(as.character(alldata$Date),format="%Y-%m-%d")
dfrm<-
data.frame(year=alldata$year,water=alldata$water,geos_water=alldata$Chem_WaterSav,OM2=a
lldata$OM2,OM3=alldata$OM3,

SO4=alldata$SO4,geos_so4=alldata$AerMassSO4,opoa=alldata$AerMassOPOA,seasonnum=all
data$seasonnum,

Date=alldata$Date,asoa=alldata$AerMassASOA,tsoa=alldata$AerMassTSOA,poa=alldata$Aer
MassPOA)
conus<-aggregate(dfrm,by=list(dfrm$seasonnum,dfrm$year),FUN="median",na.rm=T)

tiff("C:/Users/amych/Documents/Research/OC Fraction
Trends/review/OPOA_and_OM3_conus.tif",width=7,height=6,units="in",res=300)
par(mar=c(4,5.5,4,6))
plot(conus$Date,conus$opoa,type="l",lwd=3,col="darkgreen",las=1,cex.axis=1.5,xlab="",
    ylab="",cex.lab=1.5,ylim=c(0,2))
par(new=T)
plot(conus$Date,conus$OM3,type="l",lty=4,col="green3",lwd=3,axes=F,ylab="",xlab="",ylim=
c(0,0.9))
axis(side=4,las=1,cex.axis=1.5)
mtext(side=4,line=3.75,expression("OM3"~(mu*g~m^{-3})),cex=1.5)
mtext(side=2,line=3,expression("GEOS-Chem OPOA"~(mu*g~m^{-3})),cex=1.5)
legend("topleft",legend=c("OPOA","OM3"),col=c("darkgreen","green3"),lty=c(1,4),lwd=3,bty=
"n",cex=1.5)
dev.off()
```